DECOMPOSITION OF MULTI-COMPONENT MEASUREMENTS INTO P AND S WAVES

PROEFSCHRIFT

ter verkrijging van de graad van doctor
aan de Technische Universiteit Delft,
op gezag van de Rector Magnificus,
prof.drs. P.A. Schenck,
in het openbaar te verdedigen
ten overstaan van een commissie,
aangewezen door het College van Dekanen
op maandag 29 juni 1992 te 10.00 uur door

PHILIPPE CHARLES HERRMANN

geboren te Suresnes (Frankrijk)
Geofysisch ingenieur

Dit proefschrift is goedgekeurd door de promotor
prof.dr.ir. A.J. BERKHOUT.
Toegevoegd promotor
dr.ir. C.P.A. WAPENAAR.

CIP-DATA KONINKLIJKE BIBLIOTHEEK, DEN HAAG

Herrmann, Philippe Charles
Decomposition of multi-component measurements into P and S waves / Philippe Herrmann
[S.l. : s.n.] (Zoetermeer : Gebotekst). – Ill.
Thesis Delft. – With ref. – With summary in Dutch
ISBN 90–9005197–X
Subject headings: vector waves / wavefield decomposition.

printed in The Netherlands by: N.K.B. Offset bv, Bleiswijk

à Isabelle,

This thesis is the result of a CIFRE convention between the CGG (Compagnie Générale de Géophysique) and the Laboratory of Seismics and Acoustics of the Delft University. First of all I want to thank Mr DIET who has given me for five years the opportunity to improve my education and to write my thesis in the best circumstances of working. Then, I want to thank Professor BERKHOUT who allowed me to work in his laboratory, to be involved in the DELPHI project and to take part in meetings all over the world where I learnt the latest advances in seismics. This work could not have been done without the careful patience and the continuous help from Doctor WAPENAAR; his advices, suggestions and preliminary work were of great help; thanks for all Kees!

I can not say how much Cees DE BRUIN and Greg HAIMÉ comforted me when I was too homesick; I am grateful and thankful for their friendship and their kind regards. I will never forget all the help, all the nice time and joys I was given by the whole DELPHI team: Cees DE BRUIN, Jan Willem DE BRUIJN, Henk COX, Johan DE HAAS, Greg HAIMÉ, Walter RIETVELD, Eric VERSCHUUR and Kees WAPENAAR.

I would like to thank my CGG colleagues Laurence BOISSY, Guillaume CAMBOIS, Jean DUVAL, Serge GLUCK, Pierre LANFRANCHI, Antonio PICA, Robert SOUBARAS, Irene HUARD, Mr POSTIC and Xiao Ming ZHANG for their daily encouragements they provided me during the writing of the thesis.

I have a special regard for Véronique who helped me to make this text more readable, my whole family and family-in-law for their encouragements and last but not least the cheerful hereness of my beloved wife, Isabelle.

CHAPTER 1

RECORDING AND PROCESSING OF MULTI-COMPONENT DATA

1.1 RECORDING OF MULTI-COMPONENT DATA

Seismic wave motion, although often treated as a scalar phenomenon, is actually a vector phenomenon since particle motions should be represented by vectors. Three component detectors are then necessary to define precisely the received wavefield, and three component sources are necessary to determine the earth's response to any excitation, cf *Figure 1.1.1*. Using single-component sources and receivers, means that we only aim at one of the nine components of the total wavefield, with the underlying assumption that this component is sufficient to derive the properties of the subsurface.

Dealing with multi-component seismic data instead of conventional single-component data, implies handling extra information. To take full benefit of this increase of information about the subsurface, seismic processing must be vector oriented. The change from single- to multi-component seismic data does not only involve methodology changes in the data processing but also in the data acquisition. Multi-component data acquisition adds complexity to most field recording procedures, including geophone planting, flagging, surveying and cabling. The source and receiver orientation are of particular concern for anisotropy analysis and wavefield decomposition. The calibration for source and receiver components is important, channel imbalances can introduce significant errors in further processing.

In elastic media any particle motion associated to wave propagation is a combination of three different wave-types, cf *Figure 1.1.2a*. In an isotropic medium the three possible wave-types

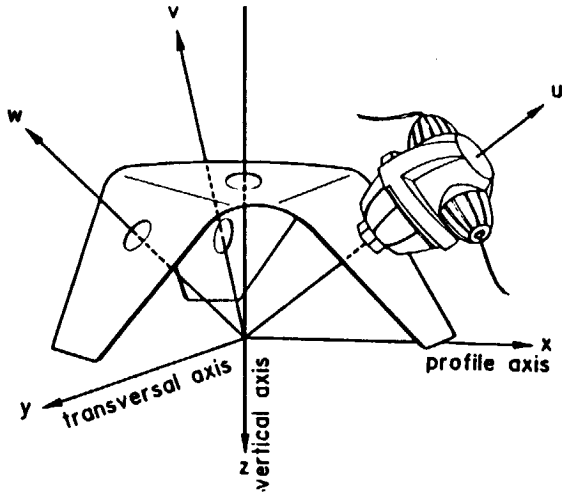

Figure 1.1.1a

To measure precisely the received vector wavefield, it is necessary to record it along three independent directions. Given the fact that vertical and horizontal geophones have different conceptions and sensitivities and are often set independently-implying different couplings-, it is preferable to use a special sensor called triphone. Introduced by Soviet geophysicists, the triphone consists of three geophones mounted rigidly on the same support with the same coupling and sensitivities (from Cliet and Dubesset, 1984).

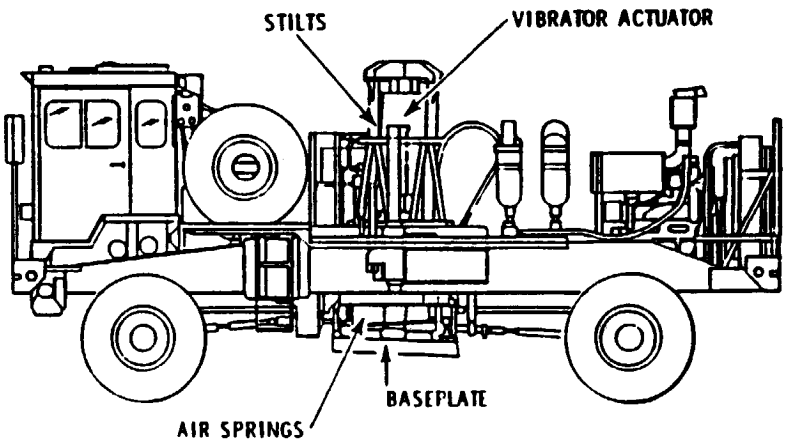

Figure 1.1.1b

To determine the earth's response to any type of vector source wavefield, three-component sources are required. In the case of surface sources we can use vibroseis trucks that may apply normal and tangential tractions to the earth's surface. The above picture represents a vibroseis truck that imposes a normal traction to the earth's surface (from Baeten, 1989).

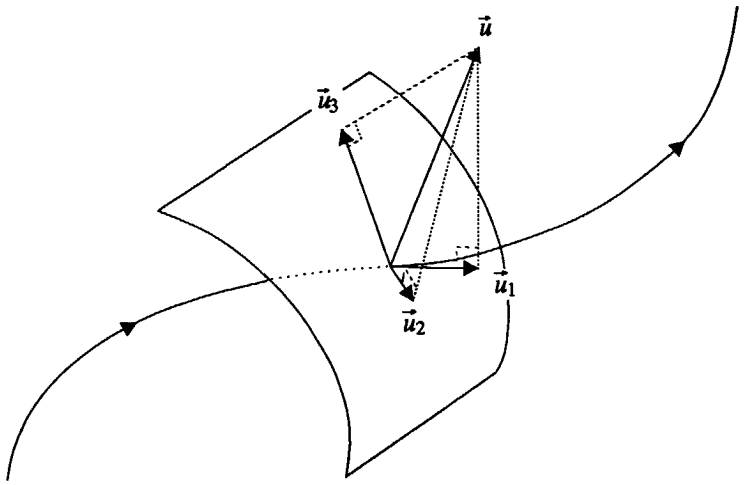

Figure 1.1.2a

The particle wave motion $\vec{u}$ associated to a wavefield, propagating in an elastic medium, can be decomposed into three wave-types, having respectively the particle wave motions $\vec{u}_1$, $\vec{u}_2$, $\vec{u}_3$ ($\vec{u} = \vec{u}_1+\vec{u}_2+\vec{u}_3$). The polarization and the phase velocity of these three wave-types give information about the elastic parameters and the density of the elastic medium.

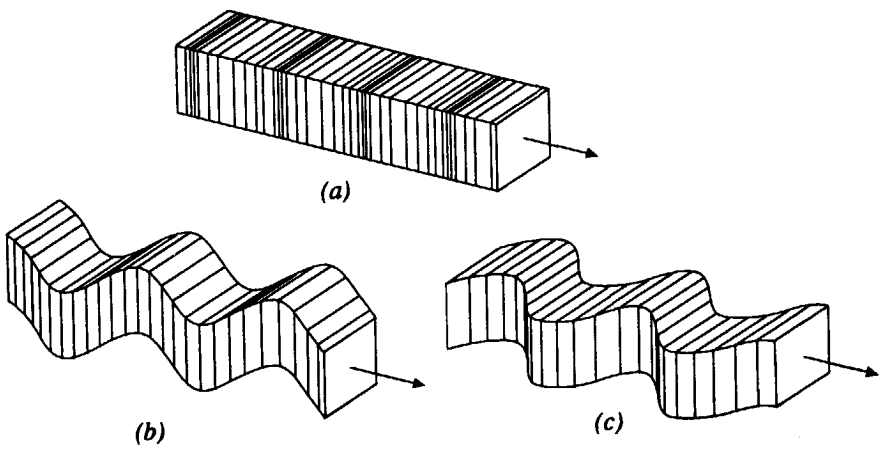

Figure 1.1.2b

In an isotropic medium the three wave-types correspond to two distinct mechanical behaviours. The first wave-type has a compressional mode of propagation, the second and third one have a shear mode of propagation. (a) volume variation of a solid medium submitted to a compressional wave, (b,c) vertical and horizontal shape variation of a solid medium submitted to a shear wave.

are the compressional (*P*) and the two shear (*S*) wave-types, see *Figure 1.1.2b*. The polarization, the amplitude and the propagation velocity of these three wave-types give information about the elastic parameters and the density of the medium. In an anisotropic medium, we speak of to quasi-*P* and -*S* waves; the polarization and the propagating velocity as a function of the direction of propagation may also give information about the fractures and stress conditions in the subsurface. We may also mention that the propagation velocity of the compressional waves depends on both the rock properties and on the pore fill; the propagation velocity of the shear waves mainly depends on the rock properties. For more interesting information we refer to a special issue on vector waves of the Leading Edge, November 1990, Vol 9, N°11. From the above remarks it may be appreciated how important a correct wave-type decomposition is for the determination of the physical properties of the medium through which the waves have propagated. To go one step further, Berkhout and Wapenaar (1989) showed that this type of wavefield decomposition simplifies the initial vector oriented processing into parallel scalar oriented processing schemes.

1.2 PROCESSING OF MULTI-COMPONENT DATA

A straightforward wave-type decomposition algorithm that can be applied to multi-component data is described in *Figure 1.2*. It consists composed of three steps: the first step (denoted by step *I*) consists of a plane wave decomposition of multi-component data, initially in the space frequency domain. This plane wave decomposition by Fourier transformation requires a range of detector positions when applied at the receiver side and requires a range of source positions when applied at the source side. Step *I* is typically a multi-channel process. The plane wave decomposition of the data, which corresponds to a wavefield decomposition per wave of distinct horizontal slowness (surface seismics) or vertical slowness (borehole seismics), is done to make the wave-type decomposition, in step *II*, *unique* and *stable*. Indeed, knowing the *P* and *S* wave velocities (here we assume that the velocities are constant all along the sources and the receivers) we can easily determine for each plane wave the polarization vectors of each wave-type. From the linear relations that exist between the polarization vectors, the amplitude of each wave-type and the measured elastic wavefield quantities (particle velocities and, optionally stresses) we can easily separate in a unique and stable way the distinct wave-types that constitute the plane wave. In the last step of this algorithm, step *III*, the decomposed plane waves are transformed back to the space domain. So far we have assumed that the medium is laterally homogeneous along the sources and the receivers. In the case of lateral velocity variations, the wavefield decomposition is applied in the space frequency domain. Steps *I*, *II* and *III* together are then replaced by convolutional products of the multi-component data with space dependent decomposition operators. In the following of this thesis we decide in favour of this algorithm because of its stability and the uniqness of its output, independent of the data complexity.

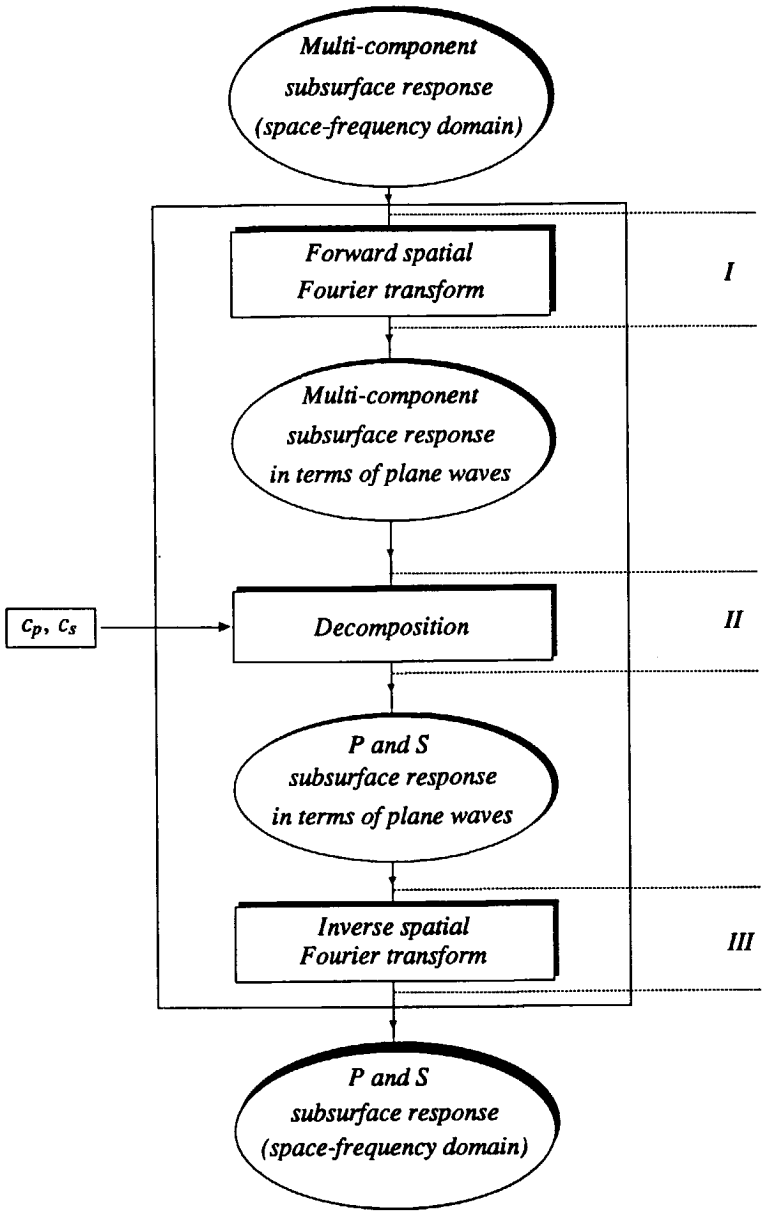

Figure 1.2

Wavefield decomposition algorithm applied to multi-component data. This algorithm is chosen for its stability and the uniqness of its output independent of the data complexity. Here we assume that the medium is laterally homogeneous along the sources and the receivers. In the case of lateral velocity variations the wavefield decomposition is applied in the space-frequency domain and the steps I, II and III together are replaced by convolutional products of the multi-component data with space dependent decomposition operators.

When the complexity of the data decreases alternative versions of this algorithm are possible, but these have a limited validity of application and require a preinterpretation of the data. Cliet and Dubesset (1984) propose to separate the distinct wave-types using a single detector position (single channel approach). They assume that over a time window the recorded wavefield only consists of two incident plane waves with known angles of incidence. Then the plane wave decomposition, step *I*, is not necessary and we can directly apply the wave-type decomposition to the data contained in the selected window. The first disadvantage of this method lies in its oversimplification of the seismic data. The second disadvantage is that the angles of incidence have to be known. This is a problem in the case of interfering arrivals or in the case the recording site interacts with the incident waves (traction free surface). The decomposition is then not unique as it depends on the values that are chosen for the angles of incidence. The third disadvantage is the instability if the two incident plane waves have nearly parallel polarization vectors (e.g. a plane P wave with angle of incidence θ_p has the same polarization as an incident plane S wave of angle of incidence $\theta_s = \theta_p + 90^o$). As a consequence, single channel decomposition methods are not recommended.

In the case the wavefield can be well approximated by a small number n (e.g. $n=4$) of plane waves at each detector position, Leaney (1990) proposes a parametric inversion of the data. His method consists of fitting the data with n plane waves, the output of the parametric inversion being the amplitude and slowness of each of them. The parametric inversion can be done over n detector positions, instead of all the detector positons as required by the Fourier transforms. This method is advantageous in the case of laterally variant medium at the source and receiver side; it has been successfully illustrated for near and medium offset VSP. The parametric inversion can be substituted in step *I* of the general algorithm presented in ***Figure 1.2***. A serious disadvantage of this method is the need of a preinterpretation of the data. Moreover, its costs increase with the data complexity.

We would like to mention the pioneering work of Dankbaar (1985) as well as Devaney and Oristaglio (1986). Dankbaar is the first author in the open literature who has applied the algorithm represented in *Figure 1.2* to decompose 2D elastic wavefields recorded by multi-component detectors on a traction free surface that is laterally homogeneous. Devaney and Oristaglio have applied this algorithm to decompose 2D elastic wavefields recorded by multi-component detectors along a VSP well, assuming a homogeneous medium as well.

Using a more general approach, we propose to decompose *3D* elastic wavefields at the *receiver* as well as at the *source side* in surface and borehole seismics. The elastic medium may be *anisotropic* and *inhomogeneous*. We will show that the algorithm in *Figure 1.2* should be applied twice, once along the receiver coordinate and once along the source coordinate. Moreover, we will show that this application should occur by spatial *convolution*.

1.3 WAVEFIELD DECOMPOSITION OF SURFACE SEISMIC DATA

To get a good physical understanding of the decomposition procedure, we present the main processing steps and their effects on the data with the aid of some illustrations. Let us consider the 2-D model presented in *Figure 1.3*, which consists of a single isotropic homogeneous layer overlaying an infinite isotropic homogeneous half space and bounded by a traction free earth surface. When vertical (τ_{zz}) or horizontal (τ_{xz}) traction sources are applied on the earth's surface, see *Figure 1.3.1*, downgoing compressional (P) and shear (S) waves are generated. They propagate into the layer and are reflected and converted at the layer interface between the layer and the lower half space. These waves propagate then upward and generate vertical (v_z) and horizontal (v_x) particle velocities at the traction free surface. Due to the traction free surface all the upgoing waves are reflected or converted at the earth's surface and are emitted back into the medium. Thus generating a series of surface related multiples that are not represented in these Figures. *Figure 1.3.1* illustrates how the P and S wave-types are mixed at the source as well as at the receiver side.

The *wavefield decomposition at the receiver side* consists of decomposing the wavefield recorded by the particle velocity detectors into its *upgoing* compressional and shear wave constituents. Applying this process on the two original shot records, we obtain two new shot records represented in *Figure 1.3.2*. Here again the surface related multiples are not represented. One can immediately observe that the wavefield decomposition at the receiver side simplifies the shot record without loss of information. The decomposition at the receiver side is a multi-channel process, it involves several adjacent multi-component detector positions.

The *wavefield decomposition at the source side* consists of decomposing the wavefield emitted by the traction sources into its compressional and its shear wave constituents. Similar to the decomposition at the receiver side, the decomposition at the source side is a multi-channel process; it involves several adjacent source positions. Hence the data must be reordered per common detector gather, see *Figure 1.3.3*. As can be seen from this figure, in the common detector gather the simulated detector only records one type of upgoing wave, the sources still emit both wave-types. The wavefield separation at the source side consists in decomposing the wavefield emitted by the traction sources into its downgoing compressional and shear wave constituents. For this process multi-component sources are necessary. Applying the decomposition at the source side to the two detector gathers we obtain two new detector gathers represented in *Figure 1.3.4*. One can observe that the wavefield decomposition at the source side simplifies the common detector gathers without losing information.

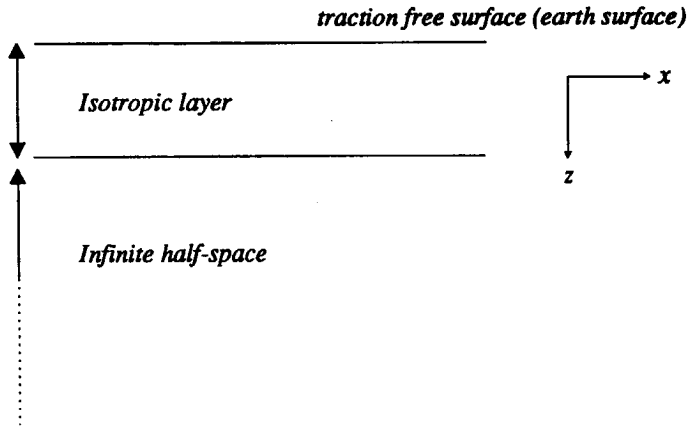

Figure 1.3

Subsurface model used to illustrate the different processing steps involved in the decomposition of the wavefield at the source and receiver side into their different wave-types.

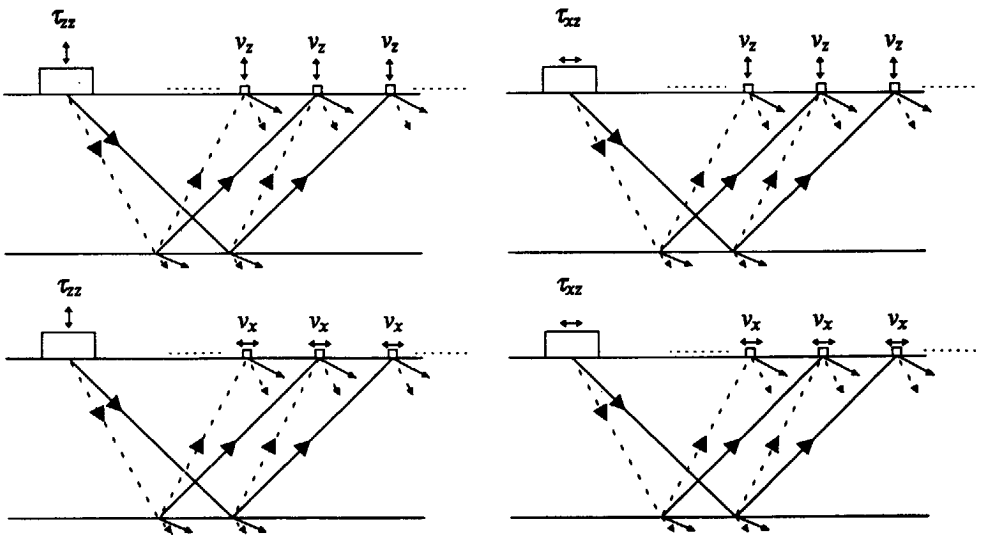

Figure 1.3.1

If traction sources are applied at the earth's surface, downgoing P and S waves are emitted. Similarly, if particle velocity detectors measure the wavefield at the earth surface, both the compressional and the shear wave-types are recorded without distinction. Compressional waves are solid lines, shear waves are dotted lines.

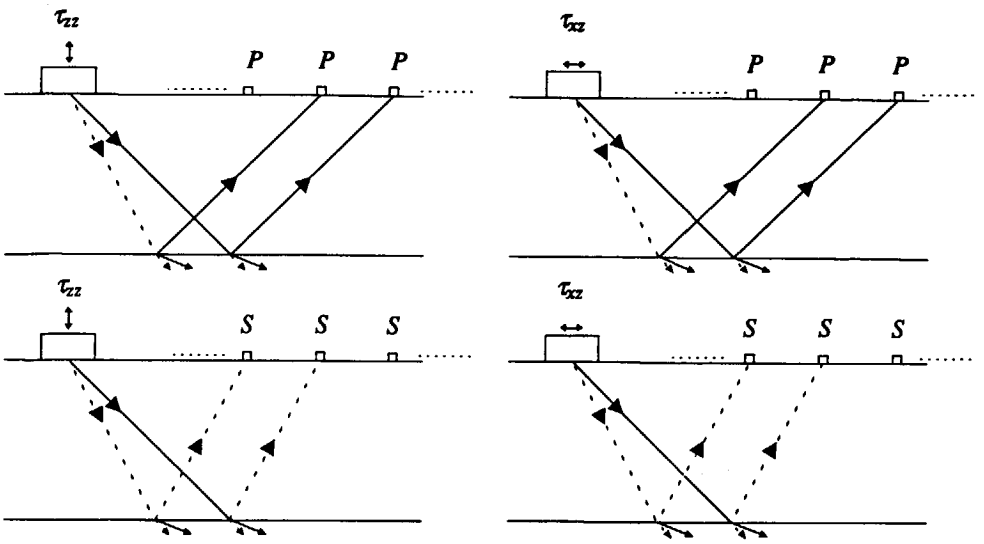

Figure 1.3.2

The wavefield decomposition applied to a shot record at the receiver side has the effect of replacing the original particle velocity detectors (sensitive to both P and S waves) by simulated pure P and S wave detectors. There is no loss of information.

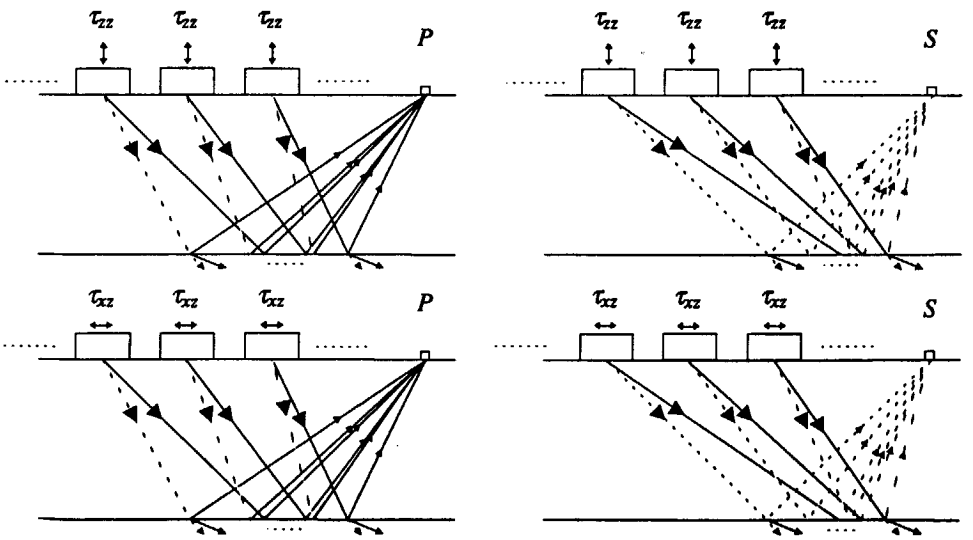

Figure 1.3.3

The decomposition at the source side is also a multi-channel process. For this process the data have to be reorganized into common detector gathers.

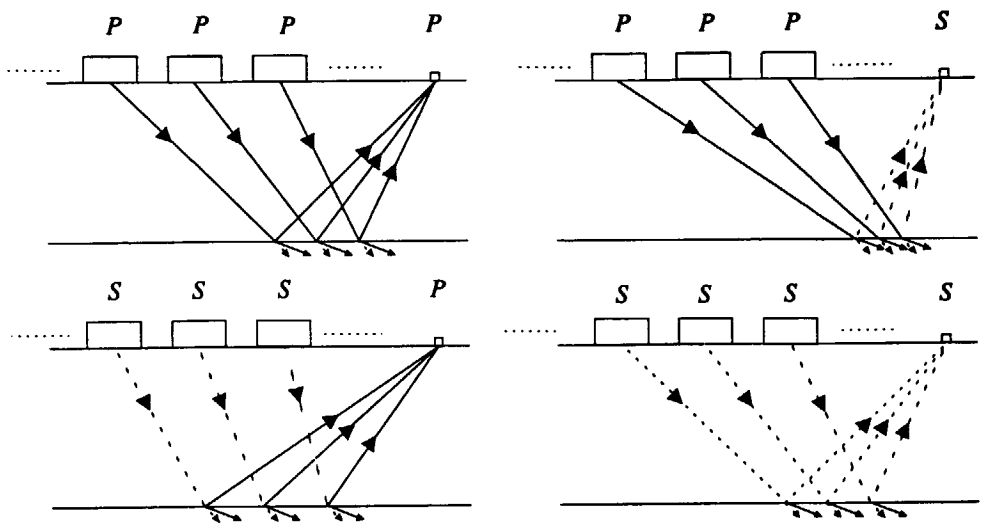

Figure 1.3.4

The wavefield decomposition at the source side applied on a common detector gather has the effect of replacing the original traction sources (that emit both downgoing P and S waves) by simulated pure P and S wave sources. There is no loss of information.

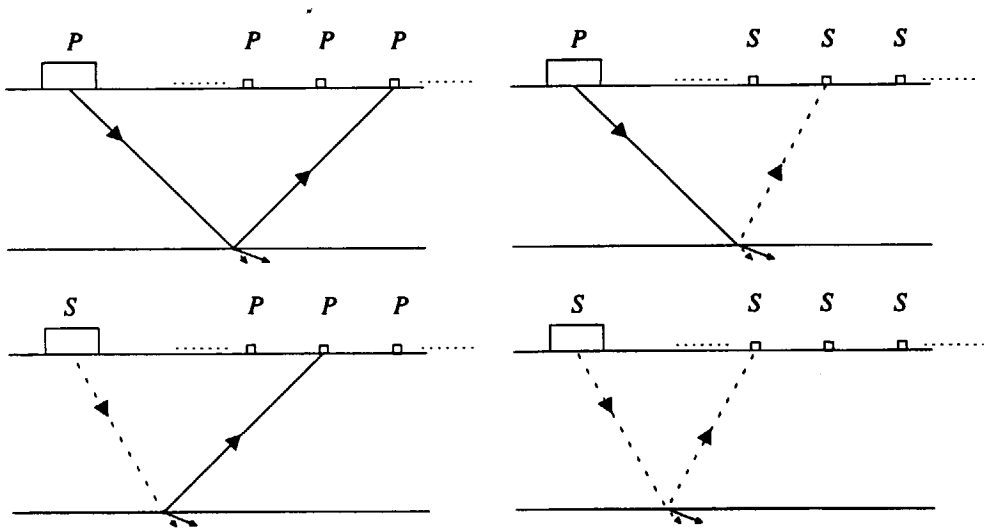

Figure 1.3.5

Shot gathers after wavefield decomposition at the receiver and source side.

Reorganizing the decomposed common detector gathers into shot records, see *Figure 1.3.5*, and comparing them to the original ones, see *Figure 1.3.1*, we observe that the wavefield decomposition of surface seismic data is no more than a data reorganization per wave-type at the source and receiver side. Starting from these decomposed data panels, further processing like migration and angle dependent imaging, simplifies to scalar processing, which is similar in its formalism to the one traditionally used within the acoustic approximation. The philosophy on the inversion of multi-component data is developed in the *DELPHI* project (*DEL*ft *PH*ilosophy on *I*nversion) at the Delft laboratory of Seismics and Acoustics, see Berkhout and Wapenaar (1988).

1.4 WAVEFIELD DECOMPOSITION OF VSP DATA

Before entering in the theoretical considerations of chapter 5, we would like to show what will be the effect of the wavefield decomposition at the receiver side on VSP data with the aid of some illustrations.

Consider the simple 2-D model depicted in *Figure 1.4.1*, a buried source in an isotropic homogeneous layer overlaying a half space. The source emits compressional as well as shear waves, that are reflected and converted at the layer interface. The horizontal and vertical particle velocity detectors, clamped in the borehole, record the two wave-types. The decomposition at the receiver side consists in this case of decomposing the elastic wavefield recorded by the particle velocity detectors into its compressional and shear wave constituents. Applying this procedure to the original shot record we obtain a new shot record as represented in *Figure 1.4.2*. The wavefield decomposition of VSP data is no more than a data reorganization per wave-type at the receiver side. The decomposition at the receiver side is a multi-channel process, it involves several adjacent multi-component detector positions. In the case several multi-component sources have been used, a wavefield decomposition at the source side is also possible.

1.5 OUTLINE OF THE THESIS

This thesis is divided in two main parts; chapters 2, 3 and 4 are dedicated to wavefield decomposition of surface seismic data and chapter 5 is dedicated to the wavefield decomposition of VSP data. The important notions about wave propagation in elastic media are introduced for the first study; we will directly use these results for the wavefield decomposition of VSP data.

Surface seismic data

The decomposition at the receiver side consists of separating the three upgoing wave-types at

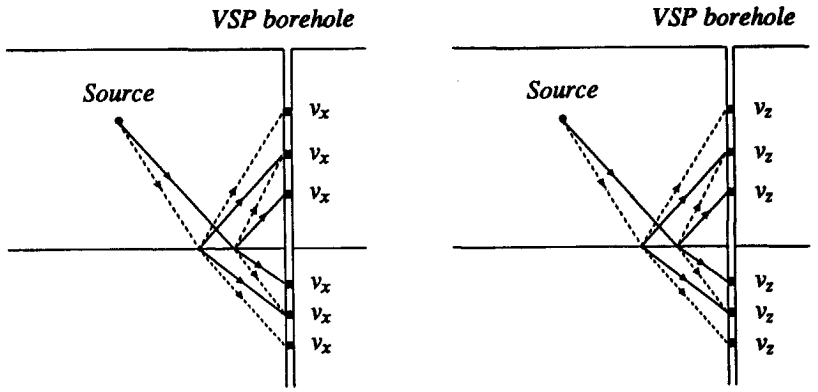

Figure 1.4.1

Simple subsurface model used to illustrate the effects of the wavefield decomposition at the receiver side, applied to VSP multi-component data. When particle velocity detectors measure the elastic wavefield along the VSP borehole, both the compressional and the shear wave-types are recorded without distinction. Compressional waves are solid lines, shear waves are dotted lines.

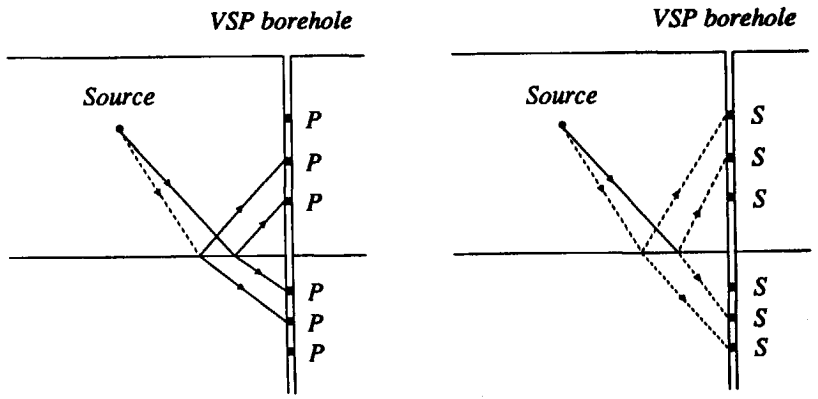

Figure 1.4.2

The wavefield decomposition at the receiver side, applied to VSP multi-component data, has the effect of replacing the original particle velocity detectors (sensitive to both P and S waves) by simulated pure P and S detectors. There is no loss of information.

the traction free surface (the earth's surface) from the particle velocities, taking into account the influence of the acquisition surface on the incident wavefield. Similarly, for the decomposition at the source side we want to be able to separate the three downgoing wave-types generated by the source. Here we see the following question arising: how can a distinction be made between upgoing and downgoing waves if the wavefield is only measured on a horizontal surface. The answer to this question is studied in chapter 2 for anisotropic elastic media. In this chapter we will see how the wavefield known at a horizontal surface (the three particle velocity and the three traction components) can be decomposed into its three upgoing and three downgoing wave-types. In chapter 2 we will also study how the wavefield components can be extrapolated from one depth level to another, and how they are affected by vertical variations in the density and in the elastic parameters of the medium. Information is also given about the wave-types emitted in an isotropic medium by the following sources: explosion, force and moment sources. Chapter 2 introduces all the basic physical quantities and relations that will be used in the remainder of this thesis; it can be skipped by readers already familiar with such considerations.

Using the results developed in chapter 2, we show in chapter 3 how a 3×3 component surface seismic survey (an areal distribution of three component sources and detectors) described in terms of traction sources and particle velocity detectors, may be decomposed at the source and receiver side. Chapter 3 is dedicated to the theoretical justification of the wavefield decomposition of surface seismic data presented in section 1.3. The process will be illustrated on simulated data for an isotropic medium with lateral variations in the subsurface. We will also see that the data handling involved in the wavefield decomposition of surface seismic data is similar to the data handling in full pre-stack migration. To do a correct wavefield decomposition of surface seismic data we need to know the near surface elastic and density parameters. As these parameters are not always well defined, part of this chapter will be dedicated to a sensitivity analysis of the method to these input parameters. The last tackled item will be the influence of a stack of thin near surface low velocity layers on the emitted and received seismic wavefields. This situation is often met in practice and may have significant effects.

In chapter 3 we assume an areal distribution of sources and detectors. The system of coordinates chosen for such a situation is the Cartesian one, which implies a plane wave decomposition of the data. However, it generally occurs in practice that the seismic survey is only carried out along a line direction and not over the whole surface. For such situations we show in chapter 4 that it is preferrable to replace the Cartesian system of coordinates by the cylindrical one, which implies a cylindrical wave decomposition of the data. If the wavefield is only recorded for a given azimuth, it is only possible to precisely recognize the different cylindrical wave types if and only if the wavefield exhibits a specific type of azimuthal symmetry. As for such situations the cylindrical wave decomposition of the data involves Hankel transforms, we present two algorithms that enable to compute them efficiently .

Finally, in chapter 5 we present how the elastic wavefield measured by multi-component detectors along a VSP borehole, can be decomposed at the receiver side into its one-way P and S wave-type components. We will study the decomposition at the receiver side for a 2D as well as for a 3D seismic wavefield propagating in an isotropic and in an anisotropic medium. The procedure will be illustrated on simulated and on field data.

CHAPTER 2

ELASTIC WAVE EQUATIONS

2.1 INTRODUCTION

The wavefield decomposition procedure presented in this thesis is fully based on the relations between the ***two-way*** and the ***one-way*** wavefield components in an elastic medium. A two-way wavefield component is a physical quantity that describes the *total* wavefield, in terms of the particle velocity or the stress. A one-way wavefield component, is a physical quantity that describes the part of the wavefield propagating in the positive direction (increasing coordinate values) or in the negative direction (decreasing coordinate values) of a chosen coordinate axis. In surface seismics, we choose this coordinate axis to be the z- axis. A one-way wavefield description consists then in making a distinction between: wavefield quantities associated to waves propagating in the increasing z value direction (+, downgoing waves), and the wavefield quantities associated to waves propagating in the decreasing z value direction (-, upgoing waves), see *Figure 2.1a*. In borehole seismic, we choose the coordinate axis to be the r- axis (cylindrical coordinates with the origin at the source). A one-way wavefield description consists then in making a distinction between: wavefield quantities associated to waves propagating in the increasing r value direction (+, expanding waves), and wavefield quantities associated to waves propagating in the decreasing r value direction (-, converging waves), see *Figure 2.1b*. In section 2.2 we illustrate the distinction that exists between a two-way and a one-way wavefield description.

In order to understand the meaning of the notation and of the equations used in the following chapters, we start from the two basic equations governing the wave propagation in an elastic medium (i.e. the linearized equation of motion and the constitutive relation), to derive and to

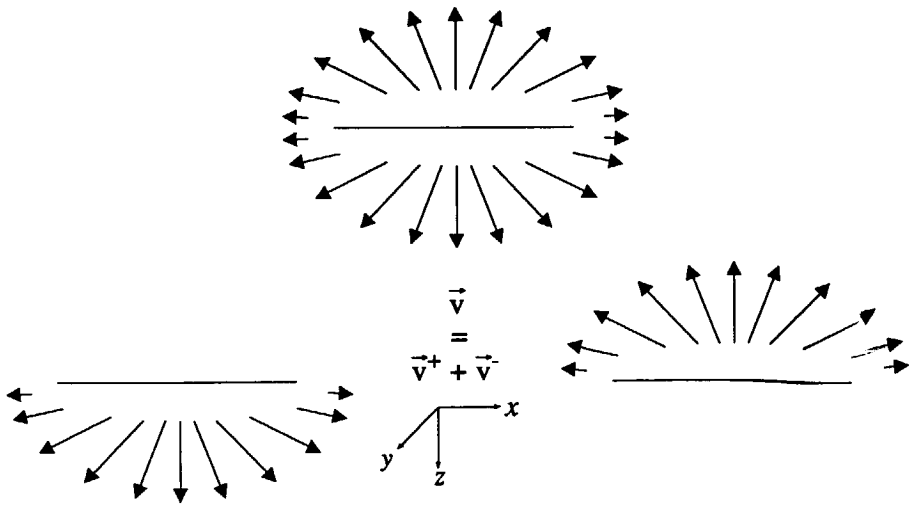

Figure 2.1a

In surface seismics, the two-way particle velocity vector $\vec{v}$ describes the particle velocity field of the total wavefield. The one-way particle velocity vector $\vec{v}^{+}$ describes the particle velocity field of the downgoing (increasing z values) part of the total wavefield. The one-way particle velocity vector $\vec{v}^{-}$ describes the particle velocity field of the upgoing (decreasing z values) part of the total wavefield.

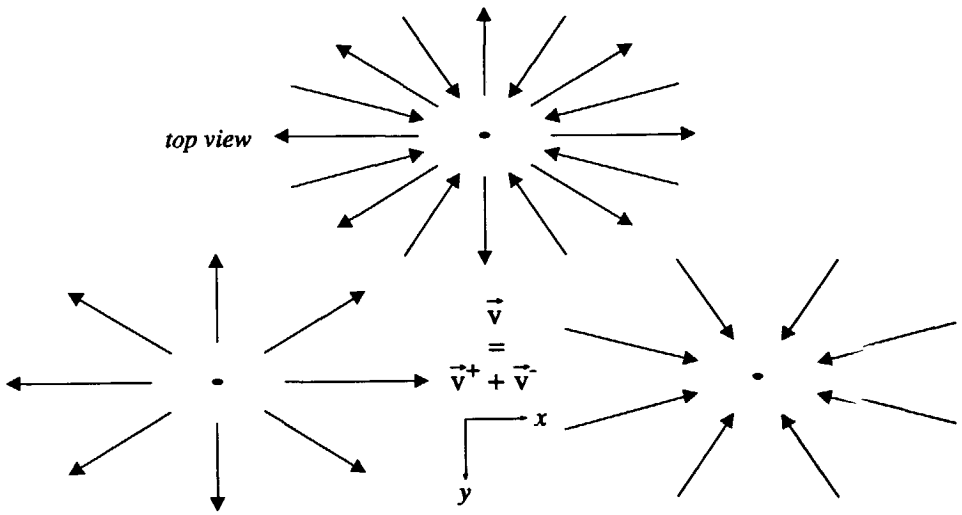

Figure 2.1b

In borehole seismics, the two-way particle velocity vector $\vec{v}$ describes the particle velocity field of the total wavefield. The one-way particle velocity vector $\vec{v}^{+}$ describes the particle velocity field of the expanding (increasing r value) part of the total wavefield. The one-way particle velocity vector $\vec{v}^{-}$ describes the particle velocity field of the converging (decreasing r value) part of the total wavefield.

Table 2.1 *Elastic wavefield quantities and their SI units*

symbol	[SI - unit]	quantity
τ_{ij}	[Pa]	stress tensor component
d_{pq}	[s^{-1}]	deformation rate tensor [$d_{pq} = (\partial_p v_q + \partial_q v_p) / 2$].
v_i	[$m.s^{-1}$]	particle velocity component along the i axis.
f_i	[$N.m^{-3}$]	volume density of body force source along the i axis.
h_{pq}	[1]	deformation tensor [$h_{pq} = (\partial_p u_q + \partial_q u_p) / 2$].
σ_{ij}	[Pa]	stress source tensor component [$\sigma_{ij} = C_{ijpq}\, h_{pq}$]
C_{ijpq}	[Pa]	stiffness tensor.
λ,μ	[Pa]	Lamé coefficients of an isotropic elastic medium.
K_C	[Pa]	constrained compression modulus [$K_C = \lambda+2\mu$].
ρ	[$kg.m^{-3}$]	volume density of mass.
k_i	[$rad.m^{-1}$]	wavevector component along the *i* axis.
ω	[$rad.s^{-1}$]	circular frequency.

Table 2.2 *Mathematical symbols and their SI units*

symbol	[SI - unit]	quantity
∂_i	[m^{-1}]	partial space differential operator.
∂_t	[s^{-1}]	partial time differential operator.
δ_{ij}	[1]	Kronecker tensor.

explain step by step the different relations and quantities used throughout this monograph. To underline the fact that the wavefield decomposition procedure presented here can be applied to any elastic medium, all the equations are derived for an arbitrary anisotropic medium.

We have made use of several textbooks for writing this chapter. We would like to mention Musgrave (1970), Achenbach (1973) and Aki and Richards (1980) for their completeness and clarity; they provide an excellent introduction to the study of wave propagation in an elastic medium. Also the book of Wapenaar and Berkhout (1989) is unique for its complete overview of the two-way and one-way wavefield properties in an acoustic or elastic medium.

As far as the notation used throughout this text is concerned, we make use of Einstein's summation convention for repeated indices. Repeated Latin indices imply a summation over *1*, *2* and *3* or, equivalently over x, y and z. Repeated Greek indices imply a summation from *1* to *2* or, equivalently over x and y..

2.2 ELASTIC WAVE EQUATIONS IN THE SPACE-TIME DOMAIN

The wave propagation in an elastic medium can be described by two fundamental equations, the linearized equation of motion :

$$\partial_t \tau_{ij} - \rho\, \partial_t v_i = -f_i\,, \qquad (2.2.1a)$$

derived from the generalized Newton's law, and the constitutive relation :

$$\partial_t \tau_{ij} - C_{ijpq}\, d_{pq} = -\partial_t \sigma_{ij}\,, \qquad (2.2.1b)$$

which is a generalization of Hooke's law. Using the stiffness tensor symmetry property :

$$C_{ijpq} = C_{ijqp}\,, \qquad (2.2.1c)$$

and the deformation rate equation :

$$d_{pq} = \frac{1}{2}\left(\partial_p v_q + \partial_q v_p\right), \qquad (2.2.1d)$$

the constitutive relation can be rewritten as follows :

$$\partial_t \tau_{ij} - C_{ijpq}\, \partial_q v_p = -\partial_t \sigma_{ij}\,. \qquad (2.2.1e)$$

The meaning and the *SI* units of the symbols used in expressions *(2.2.1)* are summarized in *Table 2.1*. The derivation of these equations can be found in Aki and Richards (1980) chapter 2. We regard the elastic medium as time invariant. Therefore the stiffness and the density only depend on the space coordinates. Equation *(2.2.1a)* relates the total stress field that acts on the outer faces of an elementary cube and the acceleration of the cube due to the body forces to

which the cube is submitted. Equation *(2.2.1b)* relates the time variation of the stress field to the deformation rate via the stiffness tensor which contains the elastic properties of the medium.

Equations *(2.2.1)* can be rewritten in a more compact way using a vector notation (Woodhouse, 1974) :

$$\partial_j \vec{\tau}_j - \rho\, \partial_t \vec{v} = -\vec{f}\,, \qquad (2.2.2a)$$

and

$$\partial_t \vec{\tau}_j - C_{jq}\, \partial_q \vec{v} = -\partial_t \vec{\sigma}_j\,, \qquad (2.2.2b)$$

with,

$$\vec{\tau}_j = (\tau_{xj}\,, \tau_{yj}\,, \tau_{zj})^T\,,$$
$$\vec{v} = (v_x\,, v_y\,, v_z)^T\,,$$
$$\vec{f} = (f_x\,, f_y\,, f_z)^T\,,$$
$$\vec{\sigma}_j = (\sigma_{xj}\,, \sigma_{yj}\,, \sigma_{zj})^T\,,$$

where T denotes transposition, and

$$C_{jq} = \begin{pmatrix} C_{1j\,1q} & C_{1j\,2q} & C_{1j\,3q} \\ C_{2j\,1q} & C_{2j\,2q} & C_{2j\,3q} \\ C_{3j\,1q} & C_{3j\,2q} & C_{3j\,3q} \end{pmatrix}. \qquad (2.2.2c)$$

Expressions *(2.2)* are fundamental, in fact as we will see in section 2.4 they can be rewritten in the wavenumber-frequency domain, simplifying the space and time derivatives to simple multiplication products. The study of the wave propagation in a linear elastic medium simplifies then to a problem which involves matrix and vector products. We can then take benefit of the powerful linear algebra theories to study the laws that govern the wave propagation.

After this presentation of the fundamental equations *(2.2)*, we may illustrate with some Figures the difference that exists between a two-way and a one-way wavefield description. Equations *(2.2)* can be used to simulate how waves propagate in an elastic medium. The simulation programs are of great importance to gain a better understanding of the physical phenomena that may occur in such a medium. Let us consider the simple model of *Figure 2.2a*. It consists of an upper isotropic homogeneous half-space overlying a lower isotropic homogeneous half space. As we will see later, isotropic media are characterized by the velocity of propagation of the compressional waves (c_p), the velocity of propagation of the shear waves (c_s) and the mass density (ρ), see *Figure 2.2a* for the values chosen for this example. Using a modeling program, we have simulated the particle velocity field at a distance of *200m* above the interface generated by an explosion source located at a distance of *400m* above the interface. *Figure 2.2b* represents the lateral space and time variations of the horizontal and vertical components of the two-way particle velocity vertor ($\vec{v}$). They describe the total wavefield. *Figure 2.2c* represents

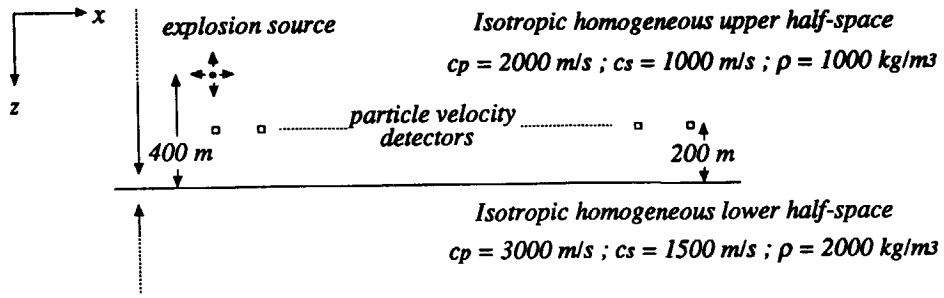

Figure 2.2a

The model we consider consists of two elastic isotropic half-spaces in contact. Using a simulation program we can determine the horizontal and vertical particle velocity field (at a distance of 200 m above the interface) generated by an explosion point source located at a distance of 400 m above the interface. This example will enable to illustrate the difference that exists between a two-way and a one-way description of the wavefield.

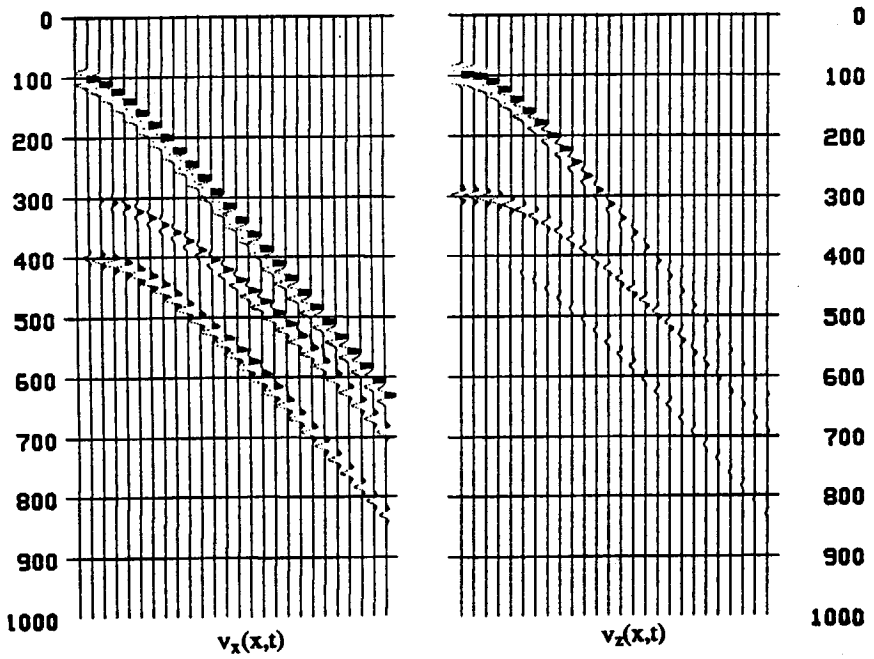

Figure 2.2b

Space and time variations of the horizontal and vertical particle velocity components recorded by the particle velocity detectors. These seismic sections describe the total wavefield: it contains the downgoing source wavefield as well as the upgoing reflected wavefield. We have a two-way representation of the seismic wavefield.

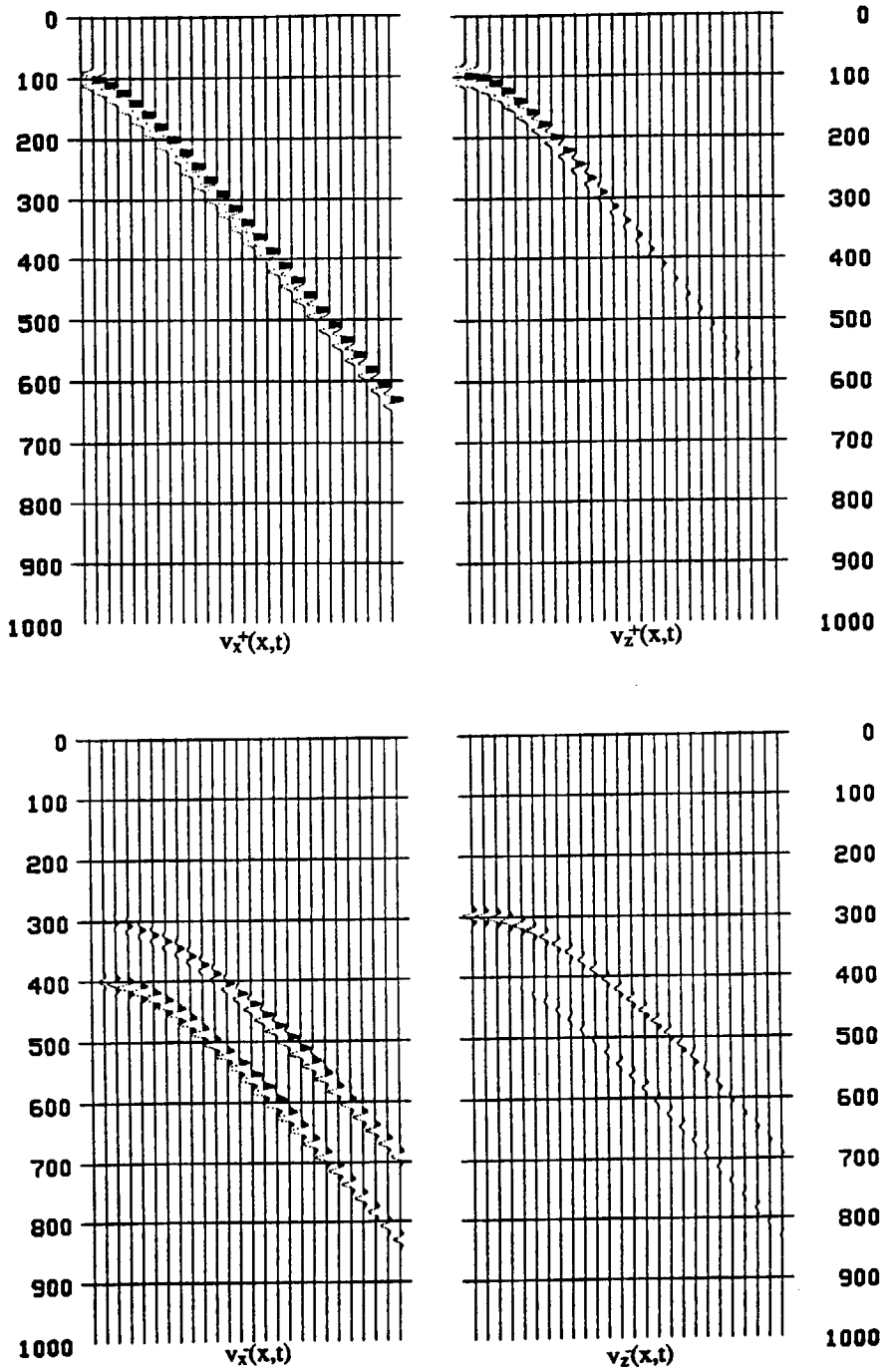

Figure 2.2c

Space and time variations of the horizontal and vertical particle velocity components associated to the downgoing(+) and to the upgoing (-) waves. We have a one-way representation of the seismic wavefield.

the lateral space and time variations of the horizontal and vertical components of the one-way particle velocity vector ($\vec{v}^{+}$) generated by the downgoing source wavefield, and of the one-way particle velocity vector ($\vec{v}^{-}$) generated by the upgoing reflected wavefield. We have $\vec{v} = \vec{v}^{+} + \vec{v}^{-}$. Similar figures can be made for the stress tensor components, we also have $\vec{\tau}_j = \vec{\tau}_j^{+} + \vec{\tau}_j^{-}$.

In seismics we measure the two-way components of the seismic wavefield as the total wavefield is measured. In this thesis we show how seismic data described in terms of two-way components may be described in terms of one-way components. For all the advantages of such a data transformation we refer to Berkhout and Wapenaar (1989).

2.3 THE TRANSFORM DOMAIN

The transformation from the space-time domain to the wavenumber-frequency domain corresponds to a spectral decomposition achieved by using Fourier transforms. The temporal Fourier transformation of a function h*(x,y,z,t)* from the space-time to the space-frequency domain is defined as:

$$h(x, y, z, \omega) = \int_{-\infty}^{+\infty} \mathrm{h}(x, y, z, t)\, e^{-j\omega t}\, dt\,, \qquad (2.3.1a)$$

and its inverse as,

$$\mathrm{h}(x, y, z, t) = \frac{1}{2\pi} \int_{-\infty}^{+\infty} h(x, y, z, \omega)\, e^{+j\omega t}\, d\omega\,. \qquad (2.3.1b)$$

In the following we will assume that h*(x,y,z,t)* is a real function so that :

$$h(x, y, z, -\omega) = h^{*}(x, y, z, \omega)\,, \qquad (2.3.2)$$

where (*) denotes complex conjugation. From *(2.3.2)* we note that negative frequency components do not provide independent information with respect to the positive frequency components. Therefore in the following we will only consider positive frequencies, $\omega \geq 0$, and the inverse temporal Fourier transformation can then be reformulated as :

$$\mathrm{h}(x, y, z, t) = \frac{1}{\pi} Real \left\{ \int_{0}^{+\infty} h(x, y, z, \omega)\, e^{j\omega t}\, d\omega \right\}. \qquad (2.3.3)$$

From *(2.3.3)* we deduce that there is a correspondence between the partial time derivative of the function h and the complex multiplication of the function *h* with $j\omega$:

$$\partial_t\, \mathrm{h}(x, y, z, t) \Leftrightarrow j\omega\, h(x, y, z, \omega)\,. \qquad (2.3.4)$$

The double Fourier transformation of the complex function $h(x, y, z, \omega)$ from the space-frequency to the wavenumber-frequency domain is defined as :

$$\tilde{h}(k_x, k_y, z, \omega) = \int_{-\infty}^{+\infty}\int h(x, y, z, \omega)\, e^{j(k_x x + k_y y)}\, dx\, dy\,, \qquad (2.3.5a)$$

and its inverse as :

$$h(x, y, z, \omega) = \frac{1}{4\pi^2}\int_{-\infty}^{+\infty}\int \tilde{h}(k_x, k_y, z, \omega)\, e^{-j(k_x x + k_y y)}\, dk_x dk_y\,. \qquad (2.3.5b)$$

From *(2.3.5b)* we deduce that there is a correspondence between the partial space derivative of the function h and the complex multiplication of the function $\tilde{h}$ with $-jk_\alpha$:

$$\partial_x h(x, y, z, \omega) \Leftrightarrow -jk_x \tilde{h}(k_x, k_y, z, \omega)\,, \qquad (2.3.6a)$$

$$\partial_y h(x, y, z, \omega) \Leftrightarrow -jk_y \tilde{h}(k_x, k_y, z, \omega)\,, \qquad (2.3.6b)$$

Combining equations *(2.3.1a)* and *(2.3.5a)* we have the triple Fourier transformation from the space-time to the wavenumber-frequency domain, according to :

$$\tilde{h}(k_x, k_y, z, \omega) = \int_{-\infty}^{-\infty}\int\int \mathrm{h}(x, y, z, t)\, e^{-j(\omega t - k_x x - k_y y)}\, dt\, dx\, dy\,, \qquad (2.3.7)$$

and its inverse, combining *(2.3.1b)* and *(2.3.5b)*:

$$\mathrm{h}(x, y, z, t) = \frac{1}{4\pi^3}\, Real\left\{\int_0^{+\infty}\left[\int_{-\infty}^{+\infty}\int \tilde{h}(k_x, k_y, z, \omega)\, e^{j(\omega t - k_x x - k_y y)}\, dk_x\, dk_y\right] d\omega\right\}, \qquad (2.3.8)$$

When h stands for an elastic wavefield component in a *homogeneous medium*, equation *(2.3.8)* indicates that the triple inverse Fourier transformation corresponds to a composition of the elastic wavefield from monochromatic plane waves, see *Figure 2.3*.

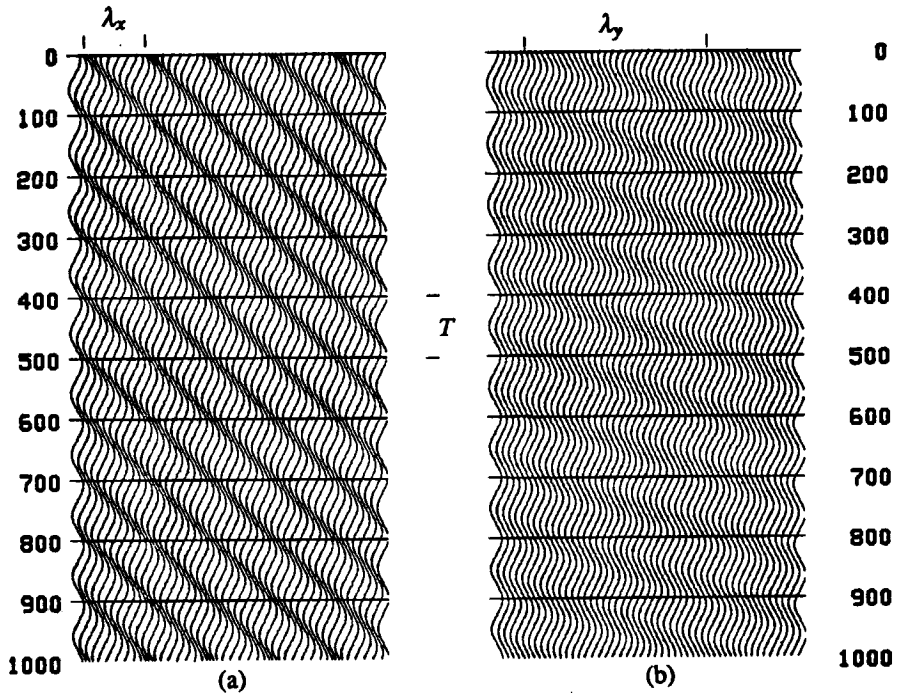

Figure 2.3

The triple Fourier transformation $\tilde{h}(k_x, k_y, z, \omega)$ of the function $h(x, y, z, t)$ corresponds to a decomposition of the elastic wavefield into monochromatic plane waves of period $T=2\pi/\omega$, of apparent horizontal wavelength λ_x ($\lambda_x = 2\pi / k_x$) along the x direction and of apparent horizontal wavelength λ_y ($\lambda_y = 2\pi / k_y$) along the y direction.

(a) projection on the plane (x,0,t) of a monochromatic plane wave of period T and of apparent wavelength λ_x along the x direction.

(b) projection on the plane (y,0,t) of a monochromatic plane wave of period T and of apparent wavelength λ_y along the y direction.

2.4 ELASTIC WAVE EQUATIONS IN A HOMOGENEOUS MEDIUM

In section *2.2* we introduced the equations verified by the two-way elastic wavefield components. Looking at these equations we see that there is an interaction between all the six components, which makes difficult the understanding of the wave phenomena they govern. For some situations like a homogeneous or a laterally homogeneous medium these equations simplify, thus simplifying by the same way the understanding of the physical behaviour they govern.

For the illustration let us consider a homogeneous source free medium. As the medium is source free the right hand side of equations *(2.2.2a,b)* is zero and we can write :

$$\partial_j \vec{\tau}_j = \rho\, \partial_t \vec{v} \,, \qquad (2.4.1a)$$

$$\partial_t \vec{\tau}_j - C_{jq}\, \partial_q \vec{v} = \vec{0} \,. \qquad (2.4.1b)$$

From *(2.4.1b)* we deduce an other equation :

$$\partial_t \partial_j \vec{\tau}_j - C_{jq}\, \partial_j \partial_q \vec{v} = \vec{0} \,, \qquad (2.4.1c)$$

here we have used the fact that the medium is homogeneous *($\partial_j C_{jq} = 0$)*. The combination of equations *(2.4.1a)* and *(2.4.1c)* leads to the wave equation verified by the two-way particle velocity vector in an homogeneous medium (we took into account that the medium is time invariant *($\partial_t \rho = 0$)*):

$$\rho\, \partial_t^2 \vec{v} - C_{jq}\, \partial_j\, \partial_q \vec{v} = \vec{0} \,. \qquad (2.4.2a)$$

Writing the two-way particle velocity vector as the sum of its one-way components:

$$\vec{v} = \vec{v}^{+} + \vec{v}^{-} \,, \qquad (2.4.2b)$$

we can show that equation *(2.4.2a)* is verified independently by $\vec{v}^{+}$ and $\vec{v}^{-}$. We have:

$$\rho\, \partial_t^2 \vec{v}^{\pm} - C_{jq}\, \partial_j\, \partial_q \vec{v}^{\pm} = \vec{0} \,. \qquad (2.4.2c)$$

To simplify the proof, we consider the 1D acoustic situation. Equation *(2.4.2a)* reads then:

$$\rho\, \partial_t^2 \vec{v} - K \partial_x^2 \vec{v} = \vec{0} \,, \qquad (2.4.3a)$$

with K the compression modulus. The relation between $\vec{v}$ and $\vec{v}^{\pm}$ is of the form:

$$\vec{v}(x,t) = \vec{v}^{+}(x - ct) + \vec{v}^{-}(x + ct) \,, \qquad (2.4.3b)$$

with c the propagating velocity of the wave: $c^2 = K/\rho$. We can easily verify that $\vec{v}^{+}$ and $\vec{v}^{-}$ are independent solutions of *(2.4.3a)*. *In a homogeneous source free medium the one-way wavefield vectors do not interact, they can be treated separately. The wavefield does not need to be treated in its totality, we can split the problem in two subproblems.* To show that it is not the case in an inhomogeneous 1D medium, we consider the wave equation in such a medium:

$$\rho\, \partial_t^2 \vec{v} - \partial_x (K . \partial_x \vec{v}) = \vec{0} \,. \qquad (2.4.4)$$

We can easily verify that for an inhomogeneous medium, $\vec{v}^{+}$ and $\vec{v}^{-}$ are not independent solutions of *(2.4.4)*. *In an inhomogeneous source free medium the one-way wavefield vectors interact with each other.* We will come back to this for a more general situation in section 2.6

2.5 ELASTIC WAVE EQUATIONS IN A LATERALLY HOMOGENEOUS MEDIUM

Let us now consider a more complicated medium. A medium vertically inhomogeneous and laterally homogeneous, which means that:

$$\partial_x C_{ijpq} = \partial_y C_{ijpq} = 0 , \qquad (2.5a)$$

and

$$\partial_x \rho = \partial_y \rho = 0 . \qquad (2.5b)$$

As far as such media are concerned, working in the wavenumber-frequency domain reduces the elastic wave study to a problem of linear algebra. The simplification of the problem enables to focus our attention on the properties of the physical phenemenon governed by the wave equation.

Applying the forward triple Fourier transform *(2.3.7)* from the space-time to the wavenumber-frequency domain to equations *(2.2.2a,b)*, we obtain :

$$\frac{\partial}{\partial z} \vec{\vec{\tau}}_z = j\rho\omega \vec{\vec{v}} + jk_\alpha \vec{\vec{\tau}}_\alpha - \vec{\vec{f}} , \qquad (2.5.1a)$$

and

$$C_{j3} \frac{\partial}{\partial z} \vec{\vec{v}} = jk_\beta C_{j\beta} \vec{\vec{v}} + j\omega \vec{\vec{\tau}}_j + j\omega \vec{\vec{\sigma}}_j . \qquad (2.5.1b)$$

We used conditions *(2.5)* for the derivation of the transformed equations *(2.5.1)*. We also used relations *(2.3.6)* and *(2.3.4)* for the transformation of the partial space and time derivatives. Equations *(2.5.1)* can be further simplified by expressing the partial z derivative of the velocity and stress vectors as functions of $\vec{\vec{v}}$ and $\vec{\vec{\tau}}_z$ only, by elimination of $\vec{\vec{\tau}}_x$ and $\vec{\vec{\tau}}_y$. From *(2.5.1b)* we obtain :

$$\frac{\partial}{\partial z} \vec{\vec{v}} = [C_{33}]^{-1} \left[jk_\beta C_{3\beta} \vec{\vec{v}} + j\omega \vec{\vec{\tau}}_z + j\omega \vec{\vec{\sigma}}_z \right] , \qquad (2.5.2a)$$

and from *(2.5.1a)* ,

$$\frac{\partial}{\partial z} \vec{\vec{\tau}}_z = j\rho\omega \vec{\vec{v}} + jk_\alpha \left[-\frac{1}{\omega} k_\beta C_{\alpha\beta} \vec{\vec{v}} + \frac{1}{j\omega} C_{\alpha 3} \frac{\partial}{\partial z} \vec{\vec{v}} - \vec{\vec{\sigma}}_\alpha \right] - \vec{\vec{f}} . \qquad (2.5.2b)$$

The combination of *(2.5.2b)* with *(2.5.2a)* leads to :

$$\frac{\partial}{\partial z}\vec{\tilde{\tau}}_z = j\rho\omega\vec{\tilde{v}} + \frac{1}{j\omega}k_\alpha k_\beta\left[C_{\alpha\beta} - C_{\alpha 3}C_{33}^{-1}C_{3\beta}\right]\vec{\tilde{v}} + jk_\alpha\left[C_{\alpha 3}C_{33}^{-1}(\vec{\tilde{\tau}}_z + \vec{\tilde{\sigma}}_z) - \vec{\tilde{\sigma}}_\alpha\right] - \vec{\tilde{f}}\,. \qquad (2.5.2c)$$

Equations *(2.5.2a)* and *(2.5.2c)* can be combined in one equation according to :

$$\frac{\partial}{\partial z}\vec{\tilde{Q}} = \tilde{A}_1\vec{\tilde{Q}} + \vec{\tilde{S}}\,, \qquad (2.5.3a)$$

where the two-way wavefield vector $\vec{\tilde{Q}}$ is defined according to :

$$\vec{\tilde{Q}} = \begin{pmatrix} \vec{\tilde{v}} \\ \vec{\tilde{\tau}}_z \end{pmatrix}^T, \qquad (2.5.3b)$$

and the first order differential operator $\tilde{A}_1$ as :

$$\tilde{A}_1 = \begin{pmatrix} \tilde{A}_{11} & \tilde{A}_{12} \\ \tilde{A}_{21} & \tilde{A}_{22} \end{pmatrix}, \qquad (2.5.3c)$$

with,

$$\tilde{A}_{11} = jk_\beta C_{33}^{-1}C_{3\beta}\,, \qquad (2.5.3d)$$

$$\tilde{A}_{12} = j\omega C_{33}^{-1}\,, \qquad (2.5.3e)$$

$$\tilde{A}_{21} = j\omega\rho I + \frac{1}{j\omega}k_\alpha k_\beta\left[C_{\alpha\beta} - C_{\alpha 3}C_{33}^{-1}C_{3\beta}\right], \qquad (2.5.3f)$$

$$\tilde{A}_{22} = jk_\alpha C_{\alpha 3}C_{33}^{-1}\,, \qquad (2.5.3g)$$

and finally, the source vector $\vec{\tilde{S}}$ is defined according to :

$$\vec{\tilde{S}} = \begin{pmatrix} \vec{\tilde{s}}_1 \\ \vec{\tilde{s}}_2 \end{pmatrix}, \qquad (2.5.3h)$$

with ,

$$\vec{\tilde{s}}_1 = \tilde{A}_{12}\vec{\tilde{\sigma}}_z\,, \qquad (2.5.3i)$$

and

$$\vec{\tilde{s}}_2 = \tilde{A}_{22}\vec{\tilde{\sigma}}_z - jk_\alpha\vec{\tilde{\sigma}}_\alpha - \vec{\tilde{f}}\,. \qquad (2.5.3j)$$

Matrix differential equations of the type *(2.5.3a)* (often without source term), which describe the wavefield variation along a given direction, are frequently used in the seismic literature. Equation *(2.5.3a)* is essential in the derivation of the two-way extrapolation operator $\tilde{U}$ which enables to extrapolate the two-way wavefield components from one depth level to an other one. Assuming the stiffness and density functions are continuous functions of the variable z, we can expand the two-way wavefield vector, $\vec{\tilde{Q}}(z)$, in a Taylor series :

$$\vec{\vec{Q}}(z) = \sum_{m=0}^{+\infty} \frac{(z-z_0)^m}{m!} \frac{\partial^m}{\partial z^m} \vec{\vec{Q}}(z)|_{z_0} . \qquad (2.5.4a)$$

Following Wapenaar and Berkhout (1989, p82), the solution of equation *(2.5.3a)* reads :

$$\vec{\vec{Q}}(z) = \tilde{U}(z, z_0)\, \vec{\vec{Q}}(z_0) + \int_{z_0}^{z} \tilde{U}(z, z')\, \vec{\vec{S}}(z')\, dz' , \qquad (2.5.4b)$$

where the two-way extrapolation operator $\tilde{U}$ is defined according to :

$$\tilde{U}(z, z_0) = \sum_{m=0}^{+\infty} \frac{(z-z_0)^m}{m!} \tilde{A}_m(z_0) , \qquad (2.5.4c)$$

with $\tilde{A}_m$ defined recursively :

$$\tilde{A}_{m+1}(z_0) = \frac{\partial}{\partial z} \tilde{A}_m(z)|_{z_0} + \tilde{A}_m(z_0)\tilde{A}_1(z_0) , \qquad (2.5.4d)$$

and

$$\tilde{A}_0(z_0) = \tilde{I} . \qquad (2.5.4e)$$

In the case the medium is homogeneous between depth levels z and z_0, the two-way extrapolation operator $\tilde{U}$ simplifies to :

$$\tilde{U}(z, z_0) = exp(\tilde{A}_1 \Delta z) , \qquad (2.5.4f)$$

with,

$$\Delta z = z - z_0 .$$

The solution *(2.5.4b)* is fundamental; for any laterally invariant anisotropic medium it enables to extrapolate the two-way wavefield vector $\vec{\vec{Q}}$ known at depth level z_0 to any depth level z. The solution *(2.5.4b)* takes into account the stiffness and density vertical gradients as well as the added wavefield at z related to all sources between z_0 and z. The two-way extrapolation operator $\tilde{U}$, also called propagation matrix, has several properties. The most interesting ones are :

$$[\tilde{U}(z, z_0)]^{-1} = \tilde{U}(z_0, z) , \qquad (2.5.4g)$$

and

$$\tilde{U}(z, z_0) = \tilde{U}(z, z_i)\ \tilde{U}(z_i, z_0) . \qquad (2.5.4h)$$

For the illustration, we give the expression of the first order differential operator $\tilde{A}_1$ for an isotropic medium. In such a medium (Aki and Richards, 1980, p23) the following relation holds for the stiffness tensor :

$$C_{ijpq} = \lambda\,\delta_{ij}\delta_{pq} + \mu\,(\delta_{ip}\delta_{jq} + \delta_{iq}\delta_{jp})\,. \qquad (2.5.5)$$

From expressions *(2.5.3defg)* we derive the following matrices :

$$\tilde{A}_{11} = \begin{pmatrix} 0 & 0 & jk_x \\ 0 & 0 & jk_y \\ \left(\frac{\lambda}{\lambda+2\mu}\right)jk_x & \left(\frac{\lambda}{\lambda+2\mu}\right)jk_y & 0 \end{pmatrix}, \qquad (2.5.6a)$$

$$\tilde{A}_{12} = \begin{pmatrix} \frac{j\omega}{\mu} & 0 & 0 \\ 0 & \frac{j\omega}{\mu} & 0 \\ 0 & 0 & \frac{j\omega}{(\lambda+2\mu)} \end{pmatrix}, \qquad (2.5.6b)$$

$$\tilde{A}_{21} = \begin{pmatrix} j\omega\rho + \frac{1}{j\omega}(\eta_1 k_x^2 + \mu\, k_y^2) & \frac{1}{j\omega}\eta_2\, k_x k_y & 0 \\ \frac{1}{j\omega}\eta_2\, k_x k_y & j\omega\rho + \frac{1}{j\omega}(\mu k_x^2 + \eta_1 k_y^2) & 0 \\ 0 & 0 & j\omega\rho \end{pmatrix}, \qquad (2.5.6c)$$

$$\tilde{A}_{22} = \begin{pmatrix} 0 & 0 & \left(\frac{\lambda}{\lambda+2\mu}\right)jk_x \\ 0 & 0 & \left(\frac{\lambda}{\lambda+2\mu}\right)jk_y \\ jk_x & jk_y & 0 \end{pmatrix}, \qquad (2.5.6d)$$

with,

$$\eta_1 = 4\mu\left(\frac{\lambda+\mu}{\lambda+2\mu}\right), \qquad (2.5.6e)$$

and

$$\eta_2 = \mu\left(\frac{3\lambda+2\mu}{\lambda+2\mu}\right). \qquad (2.5.6f)$$

The following observation can be made: the first order differential operator $\tilde{A}_1$ *(2.5.3a)* is not a 6×6 *diagonal* matrix. Thus, expression *(2.5.4c)* clearly indicates that the two-way wavefield vector components are interrelated between depth levels z_0 and z, even for the simple situation

of an homogeneous source free medium. It is therefore interesting to look for an other wavefield vector $\vec{\vec{P}}$ whose components would propagate independently of each other, at least in a homogeneous source free medium. In such a medium the wavefield vector $\vec{\vec{P}}$ should then verify an equation like *(2.5.3a)* with a *diagonal* differential operator $\tilde{\boldsymbol{B}}_1$ in the place of $\tilde{\boldsymbol{A}}_1$. Each component of the wavefield vector $\vec{\vec{P}}$ will then correspond to a mode of propagation propagating independently of the others in a homogeneous source free medium. In the following, the components of the wavefield vector $\vec{\vec{P}}$ will be called ***normal modes*** and $\vec{\vec{P}}$ the ***normal mode wavefield vector.***

2.6 NORMAL MODES OF PROPAGATION IN A LATERALLY HOMOGENEOUS ELASTIC MEDIUM

We go back to the general anisotropic situation. The derivation of the normal mode wavefield vector $\vec{\vec{P}}$ is based on the eigenvalue decomposition of the matrix $\tilde{\boldsymbol{A}}_1$:

$$\tilde{\boldsymbol{A}}_1 = \tilde{\boldsymbol{L}}\,\tilde{\boldsymbol{\Lambda}}\,\tilde{\boldsymbol{L}}^{-1}\,, \tag{2.6.1a}$$

where $\tilde{\boldsymbol{\Lambda}}$ is the 6×6 diagonal matrix which contains the 6 eigenvalues of the matrix $\tilde{\boldsymbol{A}}_1$:

$$\tilde{\boldsymbol{\Lambda}} = \begin{pmatrix} \tilde{\boldsymbol{\Lambda}}^{+} & 0 \\ 0 & \tilde{\boldsymbol{\Lambda}}^{-} \end{pmatrix}, \tag{2.6.1b}$$

with,

$$\tilde{\boldsymbol{\Lambda}}^{\pm} = \begin{pmatrix} -jk_{z_1}^{\pm} & 0 & 0 \\ 0 & -jk_{z_2}^{\pm} & 0 \\ 0 & 0 & -jk_{z_3}^{\pm} \end{pmatrix}. \tag{2.6.1c}$$

$\tilde{\boldsymbol{L}}$ is the 6×6 matrix whose columns contain the eigenvectors of matrix $\tilde{\boldsymbol{A}}_1$:

$$\tilde{\boldsymbol{L}} = \begin{pmatrix} \tilde{\boldsymbol{L}}_1^{+} & \tilde{\boldsymbol{L}}_1^{-} \\ \tilde{\boldsymbol{L}}_2^{+} & \tilde{\boldsymbol{L}}_2^{-} \end{pmatrix}. \tag{2.6.1d}$$

The normal wavefield vector $\vec{\vec{P}}$ we are looking for, can be introduced as follows :

$$\vec{\vec{Q}} = \tilde{\boldsymbol{L}}\,\vec{\vec{P}}\,, \tag{2.6.2a}$$

or equivalently,

$$\vec{\vec{P}} = \tilde{\boldsymbol{M}}\,\vec{\vec{Q}}\,, \tag{2.6.2b}$$

with,

$$\widetilde{M} = \widetilde{L}^{-1} = \begin{pmatrix} \widetilde{M}_1^{+} & \widetilde{M}_2^{+} \\ \widetilde{M}_1^{-} & \widetilde{M}_2^{-} \end{pmatrix}, \tag{2.6.2c}$$

and

$$\vec{\vec{P}} = \begin{pmatrix} \vec{\vec{p}}^{+} \\ \vec{\vec{p}}^{-} \end{pmatrix}. \tag{2.6.2d}$$

The matrix $\widetilde{L}$ is called the composition operator, and the matrix $\widetilde{M}$ is called the decomposition operator. $\widetilde{M}$ and $\widetilde{L}$ enable to switch between the two-way and the normal mode wavefield vectors. The columns of the matrix $\widetilde{L}$ contain the two-way wavefield components associated to a single normal mode wavefield component. In particular, the columns of the submatrices $\widetilde{L}_1^{\pm}$ contain the polarization vectors of the downgoing (+) and upgoing (-) normal waves for horizontal wavenumber k_x and k_y. Similarly, the columns of the matrix $\widetilde{M}$ contain the normal mode wavefield decomposition of a single two-way wavefield component. Expression *(2.6.2d)* corresponds to a separation of the normal modes based on their direction of propagation, $\vec{\vec{p}}^{+}$: downgoing normal waves, $\vec{\vec{p}}^{-}$: upgoing normal waves, from which we deduce that $\vec{\vec{P}}$ is a one-way normal mode wavefield vector.

The combination of *(2.5.3a)* with *(2.6.1a)* leads to the equation :

$$\frac{\partial}{\partial z}(\widetilde{L}\,\vec{\vec{P}}) = \widetilde{L}\,\widetilde{\Lambda}\,\vec{\vec{P}} + \vec{\vec{S}}, \tag{2.6.3a}$$

or equivalently ,

$$\frac{\partial}{\partial z}\vec{\vec{P}} = \widetilde{B}_1\vec{\vec{P}} + \vec{\vec{S}}', \tag{2.6.3b}$$

with,

$$\widetilde{B}_1 = \widetilde{\Lambda} - \widetilde{M}\frac{\partial}{\partial z}\widetilde{L}, \tag{2.6.3c}$$

and

$$\vec{\vec{S}}' = \widetilde{M}\,\vec{\vec{S}} = \begin{pmatrix} \vec{\vec{s}}'^{+} \\ \vec{\vec{s}}'^{-} \end{pmatrix}, \tag{2.6.3d}$$

with,

$$\vec{s}'^{\pm} = M_{\alpha}^{\pm}\vec{s}_{\alpha}. \tag{2.6.3e}$$

Equation *(2.6.3b)*, constitutes the one-way normal wave equation in the wavenumber-frequency domain, verified by the normal modes components in a laterally homogeneous medium. Equation *(2.6.3b)* is similar to *(2.5.3a)*, hence following the same reasoning as for the two-way wavefield vector $\vec{\vec{Q}}(z)$, the general solution of *(2.6.3b)* reads :

$$\vec{\tilde{P}}(z) = \tilde{W}(z, z_0)\,\vec{\tilde{P}}(z_0) + \int_{z_0}^{z} \tilde{W}(z, z')\,\vec{\tilde{S}}(z')\,dz' , \qquad (2.6.4a)$$

where the one-way normal mode extrapolation operator $\tilde{W}$ is defined as :

$$\tilde{W}(z, z_0) = \sum_{m=0}^{+\infty} \frac{(z-z_0)^m}{m!}\,\tilde{B}_m(z_0) , \qquad (2.6.4b)$$

with $\tilde{B}_m$ defined recursively :

$$\tilde{B}_{m+1}(z_0) = \frac{\partial}{\partial z}\tilde{B}_m(z)|_{z_0} + \tilde{B}_m(z_0)\,\tilde{B}_1(z_0) , \qquad (2.6.4c)$$

and

$$\tilde{B}_0(z_0) = \tilde{I} . \qquad (2.6.4d)$$

The two-way extrapolation operator, $\tilde{U}(z, z_0)$, is related to the one-way normal mode extrapolation operator, $\tilde{W}(z, z_0)$, according to :

$$\tilde{U}(z, z_0) = \tilde{L}(z)\,\tilde{W}(z, z_0)\,\tilde{M}(z_0) . \qquad (2.6.4e)$$

We can easily check that the wavefield vector $\vec{\tilde{P}}$ really constitutes the wavefield vector we were looking for. As a matter of fact, in a laterally and vertically homogeneous medium the one-way normal mode extrapolation operator gets simplified into :

$$\tilde{W}(z, z_0) = exp\left(\tilde{B}_1\,\Delta z\right) = exp\left(\tilde{\Lambda}\,\Delta z\right) , \qquad (2.6.4f)$$

or equivalently,

$$\tilde{W}(z, z_0) = \begin{pmatrix} \tilde{W}^{+}(z, z_0) & 0 \\ 0 & \tilde{W}^{-}(z, z_0) \end{pmatrix} , \qquad (2.6.4g)$$

with

$$\tilde{W}^{\pm}(z, z_0) = \begin{pmatrix} e^{-jk_{z3}^{\pm}(z-z_0)} & 0 & 0 \\ 0 & e^{-jk_{z3}^{\pm}(z-z_0)} & 0 \\ 0 & 0 & e^{-jk_{z3}^{\pm}(z-z_0)} \end{pmatrix} . \qquad (2.6.4h)$$

As expected for this special situation the one-way normal mode extrapolation operator $\tilde{W}$ simplifies into a 6×6 diagonal matrix. Which means that the components of the one-way normal mode wavefield vector $\vec{\tilde{P}}$ propagate independently of each other. The three components of $\vec{\tilde{p}}^{+}$ ($\vec{\tilde{p}}^{-}$) related to the eigenvalues k_{zi}^{+} (k_{zi}^{-}) correspond to downgoing (upgoing) waves. Going back to equation *(2.6.3b)*, we see that in a vertically inhomogeneous medium, the differential

operator $\tilde{\boldsymbol{B}}_1$ is no more diagonal, implying an interaction between the upgoing and downgoing normal waves :

$$\frac{\partial}{\partial z}\vec{\tilde{p}}^{+} = \tilde{\Lambda}^{+}\vec{\tilde{p}}^{+} - \tilde{\boldsymbol{M}}_{\alpha}^{+}\left[\left(\frac{\partial}{\partial z}\tilde{\boldsymbol{L}}_{\alpha}^{+}\right)\vec{\tilde{p}}^{+} + \left(\frac{\partial}{\partial z}\tilde{\boldsymbol{L}}_{\alpha}^{-}\right)\vec{\tilde{p}}^{-}\right] + \vec{\tilde{s}}'^{+}, \tag{2.6.4i}$$

$$\frac{\partial}{\partial z}\vec{\tilde{p}}^{-} = \tilde{\Lambda}^{-}\vec{\tilde{p}}^{-} - \tilde{\boldsymbol{M}}_{\alpha}^{-}\left[\left(\frac{\partial}{\partial z}\tilde{\boldsymbol{L}}_{\alpha}^{+}\right)\vec{\tilde{p}}^{+} + \left(\frac{\partial}{\partial z}\tilde{\boldsymbol{L}}_{\alpha}^{-}\right)\vec{\tilde{p}}^{-}\right] + \vec{\tilde{s}}'^{-}. \tag{2.6.4j}$$

From the above developments we can determine the variations in depth of the one-way particle velocity components. Knowing that :

$$\vec{\tilde{v}}^{\pm} = \tilde{\boldsymbol{L}}_1^{\pm}\vec{\tilde{p}}^{\pm}(z), \tag{2.6.4k}$$

we deduce that in a homogeneous medium :

$$\frac{\partial}{\partial z}\vec{\tilde{v}}^{\pm}(z) = \tilde{\boldsymbol{L}}_1^{\pm}(z)\,\tilde{\Lambda}^{\pm}(z)\left[\tilde{\boldsymbol{L}}_1^{\pm}(z)\right]^{-1}\vec{\tilde{v}}^{\pm}(z) + \tilde{\boldsymbol{L}}_1^{\pm}(z)\,\vec{\tilde{s}}'^{\pm}(z). \tag{2.6.4l}$$

As expected, the particle velocity field associated to the upgoing waves propagates independently of the particle velocity field associated to the downgoing waves. Due to the fact that the matrices $\tilde{\boldsymbol{L}}_1^{\pm}(z)$ are full 3×3 matrices, we clearly see that the three components of the vectors $\vec{\tilde{v}}^{\pm}$ are interrelated. A similar result could be given for the traction vector $\vec{\tilde{\tau}}_z^{\pm}$.

Although the normal modes behaviour is somewhat difficult to explain for the general anisotropic situation, for the special case of an isotropic medium it is simple; it is the subject of the next section. Remark: since $\tilde{\boldsymbol{M}} = \left[\tilde{\boldsymbol{L}}\right]^{-1}$ (see equation *2.6.2c*) it can be easily checked that the components of the decomposition operator $\tilde{\boldsymbol{M}}$ are related to the components of the composition operator $\tilde{\boldsymbol{L}}$ according to :

$$\tilde{\boldsymbol{M}}_1^{\pm} = \left[\tilde{\boldsymbol{L}}_1^{\pm} - \tilde{\boldsymbol{L}}_1^{\mp}(\tilde{\boldsymbol{L}}_2^{\mp})^{-1}\tilde{\boldsymbol{L}}_2^{\pm}\right]^{-1}, \tag{2.6.5a}$$

$$\tilde{\boldsymbol{M}}_2^{\pm} = \left[\tilde{\boldsymbol{L}}_2^{\pm} - \tilde{\boldsymbol{L}}_2^{\mp}(\tilde{\boldsymbol{L}}_1^{\mp})^{-1}\tilde{\boldsymbol{L}}_1^{\pm}\right]^{-1}. \tag{2.6.5b}$$

Vice versa the composition operator components are related to the decomposition operator components according to :

$$\tilde{\boldsymbol{L}}_1^{\pm} = \left[\tilde{\boldsymbol{M}}_1^{\pm} - \tilde{\boldsymbol{M}}_2^{\pm}(\tilde{\boldsymbol{M}}_2^{\mp})^{-1}\tilde{\boldsymbol{M}}_1^{\mp}\right]^{-1}, \tag{2.6.5c}$$

$$\tilde{\boldsymbol{L}}_2^{\pm} = \left[\tilde{\boldsymbol{M}}_2^{\pm} - \tilde{\boldsymbol{M}}_1^{\pm}(\tilde{\boldsymbol{M}}_1^{\mp})^{-1}\tilde{\boldsymbol{M}}_2^{\mp}\right]^{-1}. \tag{2.6.5d}$$

2.7 NORMAL MODES OF PROPAGATION IN AN ISOTROPIC MEDIUM : P AND S WAVES

In this section, we study the normal modes of propagation that can take place in an isotropic medium. Starting from the linearized equation of motion *(2.2.2a)* and the constitutive relation *(2.2.2b)*, it is possible to show that in a homogeneous isotropic source free medium, the compressional and shear waves propagate independently of each other.

The combination of *(2.2.2a)* and *(2.2.2b)* leads to the two-way wave equation for the particle velocity components:

$$\partial_j \left(C_{jq}\, \partial_q \vec{v}\right) - \rho\, \partial_t^2 \vec{v} = -\partial_t \left(\vec{f} - \partial_j \vec{\sigma}_j\right) . \qquad (2.7.1a)$$

Using *(2.5.5)* for the expression of the stiffness tensor in an isotropic medium, the above equation simplifies into :

$$\vec{\nabla}(K_c\, \vec{\nabla}.\vec{v}) - \vec{\nabla} \times (\mu\, \vec{\nabla}\times\vec{v}) - \rho\, \partial_t^2 \vec{v} + 2\left[(\vec{\nabla}\mu.\vec{\nabla})\vec{v} - (\vec{\nabla}\mu)(\vec{\nabla}.\vec{v}) + \vec{\nabla}\mu \times (\vec{\nabla}\times\vec{v})\right] = -\partial_t \left(\vec{f} - \partial_j \vec{\sigma}_j\right) . \qquad (2.7.1b)$$

with K_c the constrained compression modulus ,

$$K_c = \lambda + 2\mu . \qquad (2.7.1c)$$

In a homogeneous source free medium, equation *(2.7.1b)* simplifies to :

$$K_c\, \vec{\nabla}(\vec{\nabla}.\vec{v}) - \mu\vec{\nabla} \times \vec{\nabla} \times \vec{v} - \rho\, \partial_t^2 \vec{v} = \vec{0} . \qquad (2.7.1d)$$

The velocity vector can be decomposed in a compressional and shear component (Achenbach 1973, p65) by introducing the scalar potential ϕ and the vector potential $\vec{\Psi}$ related to $\vec{v}$ according to:

$$\vec{v} = \vec{v}_p + \vec{v}_s , \qquad (2.7.2a)$$

with,

$$\vec{v}_p = \vec{\nabla}\, \phi ,$$
$$\vec{v}_s = \vec{\nabla} \times \vec{\Psi} ,$$
$$\vec{\Psi} = (\Psi_x , \Psi_y , \Psi_z)^T . \qquad (2.7.2b)$$

It is important to point out that although the vector $\vec{\Psi}$ has three components only two are independent. Indeed, since the particle velocity vector $\vec{v}$ has three independent components whereas expression *(2.7.2a)* involves four variables, a relation must exist between the components of vector $\vec{\Psi}$. Later in this section we discuss various possible relations .

As :

$$\vec{\nabla}.\vec{v} = \vec{\nabla}.(\vec{v}_p+\vec{v}_s) = \vec{\nabla}.\vec{v}_p \ , \qquad (2.7.2c)$$

$\vec{v}_p$ represents the compressional part of the particle velocity field. An elementary cube submitted to a particle velocity field $\vec{v}_p$ will change its volume but not its shape. Similarly, as :

$$\vec{\nabla}\times\vec{v} = \vec{\nabla}\times(\vec{v}_p+\vec{v}_s) = \vec{\nabla}\times\vec{v}_s \ , \qquad (2.7.2d)$$

$\vec{v}_s$ represents the shearing part of the particle velocity field. An elementary cube submitted to a particle velocity field $\vec{v}_s$ will change its shape but not its volume.

Rewriting *(2.7.1d)*, taking into account the decomposition *(2.7.2a)*, the following equation is obtained:

$$K_c \vec{\nabla}(\nabla^2\phi - \frac{\rho}{K_c}\partial_t^2\phi) + \mu \vec{\nabla}\times(-\vec{\nabla}\times\vec{\nabla}\times\vec{\psi} - \frac{\rho}{\mu}\partial_t^2\vec{\psi}) = \vec{0} \ . \qquad (2.7.3a)$$

The two-way wave equation *(2.7.3a)* remains unchanged by adding the term $\vec{\nabla}(\vec{\nabla}.\vec{\psi})$ in the second pair of brackets as $\vec{\nabla}\times\vec{\nabla}(\vec{\nabla}.\vec{\psi}) = \vec{0}$. Equation *(2.7.3a)* is then equivalent to :

$$K_c \vec{\nabla}(\nabla^2\phi - \frac{\rho}{K_c}\partial_t^2\phi) + \mu \vec{\nabla}\times(\nabla^2\vec{\psi} - \frac{\rho}{\mu}\partial_t^2\vec{\psi}) = \vec{0} \ , \qquad (2.7.3b)$$

where the following vectorial equality has been used :

$$-\vec{\nabla}\times\vec{\nabla}\times\vec{\psi} + \vec{\nabla}(\vec{\nabla}.\vec{\psi}) = \nabla^2\vec{\psi} \ . \qquad (2.7.3c)$$

Equation *(2.7.3b)* admits two natural solutions :

$$\nabla^2\phi - \frac{\rho}{K_c}\partial_t^2\phi = 0 \ , \qquad (2.7.4a)$$

and

$$\nabla^2\vec{\psi} - \frac{\rho}{\mu}\partial_t^2\vec{\psi} = \vec{0} \ . \qquad (2.7.4b)$$

Equations *(2.7.4)* are typical wave equations and clearly indicate that in a homogeneous isotropic source free medium the compressional part of the wavefield propagates independently of the shearing part. Conclusion: *in an isotropic medium the normal modes of propagation are the compressional and the shear modes*. The compressional waves, also called longitudinal or *P* waves, propagate with a velocity c_p:

$$c_p = \sqrt{\frac{K_c}{\rho}} = \sqrt{\frac{\lambda+2\mu}{\rho}} \ . \qquad (2.7.5a)$$

For plane waves, the *P* wave particle velocity vector $\vec{v}_p$ is normal to the wave front or, equivalently, parallel to the direction of propagation. The shear waves, also called transversal or *S* waves, propagate with a velocity c_s:

$$c_s = \sqrt{\frac{\mu}{\rho}} \,. \qquad (2.7.5b)$$

For plane waves, the S wave particle velocity vector $\vec{v}_s$ is tangent to the wave front or, equivalently, normal to the direction of propagation. Note that $c_P > c_S$, meaning that P-waves propagate faster than S-waves. *Figure 1.1.2b* displays the volume and shape variations of a solid column submitted to a P or S wavefield.

In order to determine the solutions of the differential equations *(2.7.4)* we transform them from the space-time to the wavenumber-frequency domain. In the wavenumber-frequency domain they read :

$$\frac{\partial^2}{\partial z^2} \tilde{\phi} = - k_{z,p}^2 \tilde{\phi} \,, \qquad (2.7.6a)$$

with ,

$$k_{z,p}^2 = k_p^2 - k_x^2 - k_y^2 \quad , \quad k_p = \frac{\omega}{c_p} \,, \qquad (2.7.6b)$$

and

$$\frac{\partial^2}{\partial z^2} \tilde{\vec{\psi}} = - k_{z,s}^2 \tilde{\vec{\psi}} \,, \qquad (2.7.6c)$$

with,

$$k_{z,s}^2 = k_s^2 - k_x^2 - k_y^2 \quad , \quad k_s = \frac{\omega}{c_s} \,. \qquad (2.7.6d)$$

Expressions *(2.7.6b,d)* are called dispersion relations. For a monochromatic plane wave the dispersion relations establish the relation that exists between the wavelength λ and the apparent horizontal (λ_x, λ_y) and vertical (λ_z) wavelengths, see *Figure 2.7.1*. For the most general anisotropic situation they read :

$$\frac{1}{\lambda_x^2} + \frac{1}{\lambda_y^2} + \frac{1}{\lambda_z^2} = \frac{1}{\lambda^2 (\lambda_x, \lambda_y, \lambda_z)} \quad \Leftrightarrow \quad k_x^2 + k_y^2 + k_z^2 = k^2(k_x, k_y, k_z) \,. \qquad (2.7.6e)$$

In an isotropic medium the wavelength does not depend on the direction of propagation, we then have :

$$\frac{1}{\lambda_x^2} + \frac{1}{\lambda_y^2} + \frac{1}{\lambda_z^2} = \frac{1}{\lambda^2} \quad \Leftrightarrow \quad k_x^2 + k_y^2 + k_z^2 = k^2 \,, \qquad (2.7.6f)$$

where k may stand for k_p or k_s.

Equation *(2.7.6a)* admits the following solution for the compressional waves :

$$\tilde{\phi} = \tilde{\phi}^+ + \tilde{\phi}^- \,, \qquad (2.7.7a)$$

with,

$$\tilde{\phi}^{\pm} = \tilde{\phi}_0^{\pm} \, e^{\mp j k_{z,p} z} \,. \qquad (2.7.7b)$$

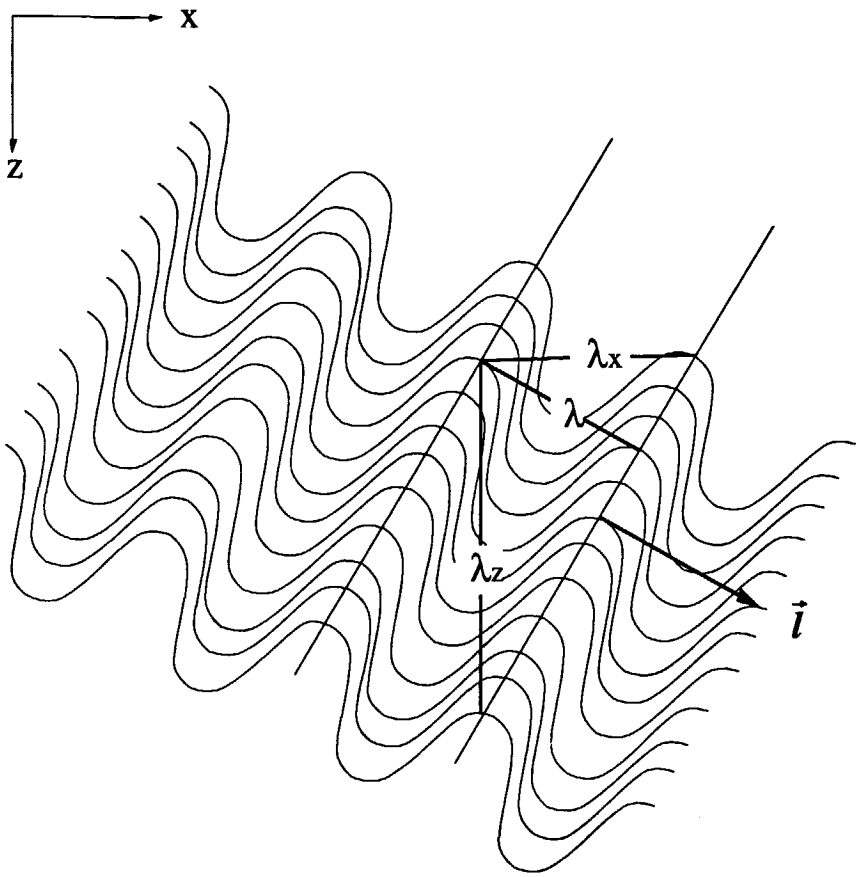

Figure 2.7.1

The dispersion relations establish for a monochromatic plane wave the relation that exists between the wavelength λ and the apparent horizontal (λ_x, λ_y) and vertical (λ_z) wavelengths. The above picture illustrates the relation for the 2D case ($1/\lambda_y=0$).

and

$$k_{z,p} = \sqrt{k_p^2 - k_x^2 - k_y^2}\,, \qquad \text{when} \qquad k_p^2 - k_x^2 - k_y^2 \geq 0\,, \tag{2.7.7c}$$

$$k_{z,p} = -j\sqrt{-(k_p^2 - k_x^2 - k_y^2)}\,, \qquad \text{when} \qquad k_p^2 - k_x^2 - k_y^2 < 0\,. \tag{2.7.7d}$$

Equation *(2.7.6c)* admits the following solution for the shear waves

$$\vec{\tilde{\psi}} = \vec{\tilde{\psi}}^{+} + \vec{\tilde{\psi}}^{-}\,, \tag{2.7.7e}$$

with,

$$\tilde{\tilde{\psi}}^{\pm} = \tilde{\tilde{\psi}}_0^{\pm}\, e^{\mp j\, k_{z,s}\, z}\,, \tag{2.7.7f}$$

and

$$k_{z,s} = \sqrt{k_s^2 - k_x^2 - k_y^2}\,, \qquad \text{when} \qquad k_s^2 - k_x^2 - k_y^2 \geq 0\,, \tag{2.7.7g}$$

$$k_{z,s} = -j\sqrt{-(k_s^2 - k_x^2 - k_y^2)}\,, \qquad \text{when} \qquad k_s^2 - k_x^2 - k_y^2 < 0\,, \tag{2.7.7h}$$

The wave splitting *(2.7.7a,e)* corresponds to a separation of the total P and S wavefield into an upgoing (-) and downgoing (+) part. Using the notation introduced in the previous section we define the one-way normal mode wavefield vector $\vec{\tilde{p}}^{\pm}$ according to :

$$\vec{\tilde{p}}^{\pm} = (\tilde{\phi}^{\pm}, \tilde{\psi}_1^{\pm}, \tilde{\psi}_2^{\pm})^T\,. \tag{2.7.8a}$$

As expected, in a homogeneous isotropic source free medium, the one-way normal wavefield vector $\vec{\tilde{P}} = \begin{pmatrix} \vec{\tilde{p}}^{+} \\ \vec{\tilde{p}}^{-} \end{pmatrix}$ satifies the following differential equation :

$$\frac{\partial}{\partial z}\vec{\tilde{P}} = \tilde{\Lambda}\,\vec{\tilde{P}}\,, \tag{2.7.8b}$$

with the diagonal first order differential operator $\tilde{\Lambda}$,

$$\tilde{\Lambda} = \begin{pmatrix} \tilde{\Lambda}^{+} & 0 \\ 0 & \tilde{\Lambda}^{-} \end{pmatrix}, \tag{2.7.8c}$$

and

$$\tilde{\Lambda}^{\pm} = \begin{pmatrix} \mp jk_{z,p} & 0 & 0 \\ 0 & \mp jk_{z,s} & 0 \\ 0 & 0 & \mp jk_{z,s} \end{pmatrix}. \tag{2.7.8d}$$

As two eigenvalues are identical, i.e. $k_{z_2}^{\pm} = k_{z_3}^{\pm} = \pm\, k_{z,s}$, the wavefield decomposition into S waves is not unique.

Here the first order differential operator $\tilde{\Lambda}$ has been derived from the two-way particle velocity equation *(2.7.1d)*. An other way to obtain the matrix $\tilde{\Lambda}$ consists in calculating eigenvalues and eigenvectors of the matrix $\tilde{A}_1$, as explained in section 2.6.

For the isotropic situation we have found that :

$$k_{zi}^{+} = -\,k_{zi}^{-}\,, \tag{2.7.9}$$

This relation can not be generalized to an arbitrary anisotropic medium, but only to the one with a horizontal plane of symmetry. We have also seen that in an isotropic homogeneous source free medium the compressional part of the wavefield $\vec{v}_p$ propagates faster than and independently of the shearing part $\vec{v}_s$. In an anisotropic medium this is not necessarily the case, the normal modes of propagation can combine the compressional as well as the shearing part of the two-way wavefield.

To conclude this section, we give for the isotropic situation, the expressions of the composition ($\tilde{L}$) and decomposition ($\tilde{M}$) matrices for two different definitions of the *S* wave vector potential $\vec{\Psi}$. In the following, according to Wapenaar and Berkhout (1989,p49) we slightly change the *P* and *S* wave potentials definition according to:

$$\vec{v} = -\frac{1}{j\rho\omega}(\vec{\nabla}\phi + \vec{\nabla}\times\vec{\psi}) . \qquad (2.7.10a)$$

Note that for the limiting case of an ideal fluid, the *P* wave potential ϕ as defined in *(2.7.10a)* is identical to the acoustic pressure p :

$$\vec{v} = -\frac{1}{j\rho\omega}\vec{\nabla}p . \qquad (2.7.10b)$$

The analytic expression for the composition matrix is easy determined when we combine the particle velocity-potential relation *(2.7.2a)* with the stress-strain equation. On the other hand the analytic derivation of the decomposition matrix, the inverse of the composition matrix, greatly simplifies due to the symmetry of the composition operator. Here we only give the final results in the wavenumber-frequency domain. In the first case, we write the *S* wave particle velocity vector according to :

$$\vec{\tilde{v}}_s = -\frac{1}{j\rho\omega}\vec{\tilde{\nabla}}\times\vec{\tilde{\psi}} = -\frac{1}{j\rho\omega}\vec{\tilde{\nabla}}\times\begin{pmatrix}\tilde{\psi}_x\\ \tilde{\psi}_y\\ \tilde{\psi}_z\end{pmatrix} \qquad (2.7.11a)$$

with,

$$\vec{\tilde{\nabla}}.\vec{\tilde{\psi}} = 0 , \qquad (2.7.11b)$$

($\vec{\tilde{\nabla}}$ is the nabla operator in the wavenumber domain : $\vec{\tilde{\nabla}} = \left(-jk_x, -jk_y, \frac{\partial}{\partial z}\right)^T$), which implies that :

$$\frac{\partial}{\partial z}\tilde{\psi}_z = jk_x\tilde{\psi}_x + jk_y\tilde{\psi}_y . \qquad (2.7.11c)$$

This choice for the $\vec{\tilde{\psi}}$ vector has the advantage of making the velocity decomposition *(2.7.2a)* consistent with the Helmholtz decomposition of a vector, see Achenbach (1973,p88). The following relations hold :

$$\tilde{\phi} = \frac{jK_c}{\omega}\vec{\tilde{\nabla}}.\vec{\tilde{v}} , \qquad (2.7.11d)$$

and

$$\vec{\tilde{\psi}} = -\frac{j\mu}{\omega}\vec{\tilde{\nabla}}\times\vec{\tilde{v}} , \qquad (2.7.11e)$$

The normal mode wavefield vector $\vec{\tilde{P}}$ can then be defined as follows:

$$\vec{\tilde{P}}^{\pm} = (\tilde{\phi}^{\pm}, \tilde{\psi}_x^{\pm}, \tilde{\psi}_y^{\pm})^T , \qquad (2.7.11f)$$

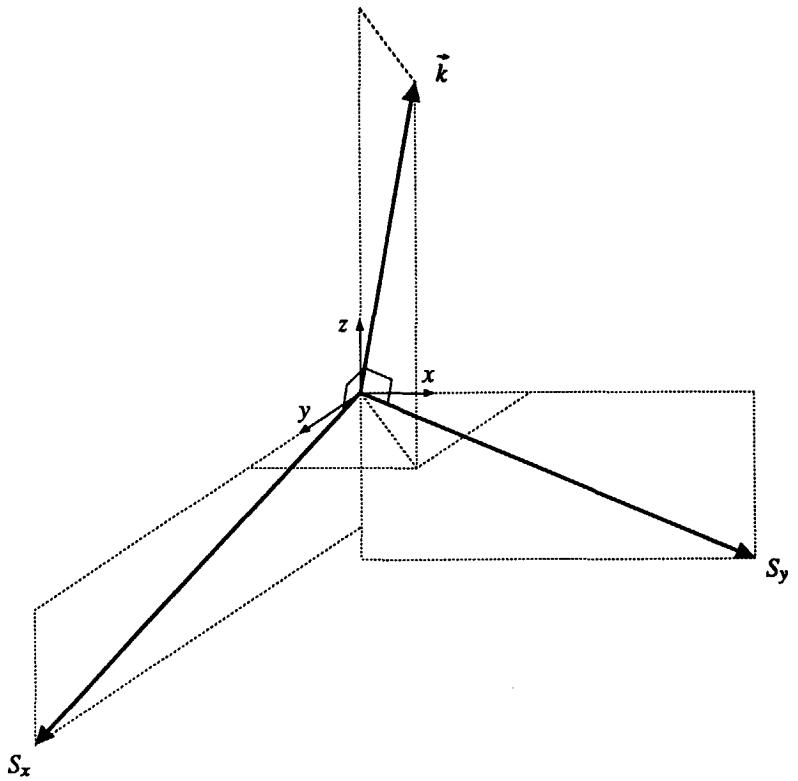

Figure 2.7.2

For an plane S wave of wave vector $\vec{k}$, this figure represents the relative orientation of the wavevector with the S_x and S_y polarization vectors.

with,

$\tilde{\psi}_x$: potential for S_x waves polarized in the (y,z) plane,
$\tilde{\psi}_y$: potential for S_y waves polarized in the (x,z) plane, see *Figure 2.7.2*

This choice for the S wave vector potential implies the following expressions for the composition ($\tilde{L}$) and decomposition ($\tilde{M}$) matrices :

$$\tilde{L}_1^{\pm} = \frac{1}{\omega\rho}\begin{pmatrix} k_x & \mp\frac{k_x k_y}{k_{z,s}} & \mp\frac{(k_s^2-k_x^2)}{k_{z,s}} \\ k_y & \pm\frac{(k_s^2-k_y^2)}{k_{z,s}} & \pm\frac{k_x k_y}{k_{z,s}} \\ \pm k_{z,p} & -k_y & k_x \end{pmatrix}, \qquad (2.7.11g)$$

$$\tilde{L}_2^{\pm} = \frac{1}{k_s^2}\begin{pmatrix} \mp 2k_x k_{z,p} & 2k_x k_y & (k_s^2 - 2k_x^2) \\ \mp 2k_y k_{z,p} & -(k_s^2 - 2k_y^2) & -2k_x k_y \\ -(k_s^2 - 2k_x^2 - 2k_y^2) & \pm 2k_y k_{z,s} & \mp 2k_x k_{z,s} \end{pmatrix}, \qquad (2.7.11h)$$

$$\tilde{M}_1^{\pm} = \frac{\mu}{2\omega}\begin{pmatrix} 2k_x & 2k_y & \pm\dfrac{(k_s^2 - 2k_x^2 - 2k_y^2)}{k_{z,p}} \\ \mp\dfrac{k_x k_y}{k_{z,s}} & \pm\dfrac{(k_s^2 - k_x^2 - 2k_y^2)}{k_{z,s}} & -2k_y \\ \mp\dfrac{(k_s^2 - 2k_x^2 - k_y^2)}{k_{z,s}} & \pm\dfrac{k_x k_y}{k_{z,s}} & 2k_x \end{pmatrix}, \qquad (2.7.11i)$$

$$\tilde{M}_2^{\pm} = \frac{1}{2}\begin{pmatrix} \mp\dfrac{k_x}{k_{z,p}} & \mp\dfrac{k_y}{k_{z,p}} & -1 \\ 0 & -1 & \pm\dfrac{k_y}{k_{z,s}} \\ 1 & 0 & \mp\dfrac{k_x}{k_{z,s}} \end{pmatrix}. \qquad (2.7.11j)$$

One can see from expressions *(2.7.11ghij)* that the operators $\tilde{L}$ and $\tilde{M}$ are stable except for horizontally propagating P ($k_{z,p}=0$) and S ($k_{z,s}=0$) plane waves. This implies that horizontally propagating waves can not be split into up or downgoing waves.

As a second case, we write the S wave particle velocity vector according to:

$$\vec{\tilde{v}}_s = -\frac{1}{j\rho\omega}\vec{\nabla} \times \left[-\vec{\nabla} \times \vec{\tilde{\psi}} + \vec{\tilde{\zeta}} \right], \qquad (2.7.12a)$$

with ,

$$\vec{\tilde{\psi}} = (0, 0, \tilde{\psi})^T, \qquad (2.7.12b)$$

and

$$\vec{\tilde{\zeta}} = (0, 0, \tilde{\zeta})^T. \qquad (2.7.12c)$$

The S waves related to the $\vec{\tilde{\psi}}$ and $\vec{\tilde{\zeta}}$ vector potentials are called S_v and S_h waves, respectively. For an S plane wave with wave vector $\vec{k}$, *Figure 2.7.3* represents the polarization vectors of the S_v and of the S_h waves. Note that the S_h wave polarization vector does not have components along the vertical axis; the S_h waves are polarized in the horizontal plane. This choice for the S wave vector potential is useful in the case of a horizontally layered medium, as for such a situation the S_h waves are decoupled from the P and S_v waves at any depth level.

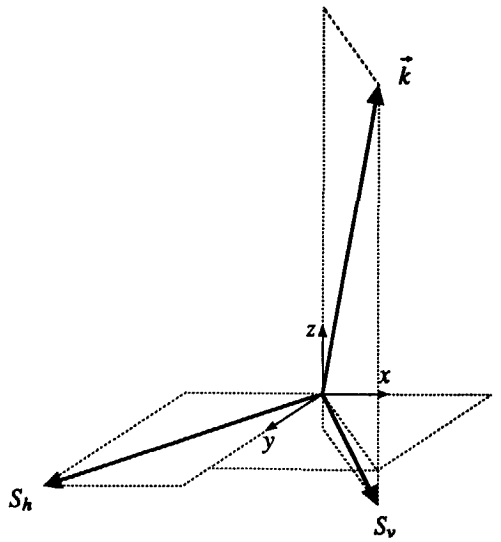

Figure 2.7.3

For an plane S wave of wavevector $\vec{k}$, this figure represents the relative orientation of the wavevector with the S_h and S_v polarization vectors. The S_h wave polarization vector does not havea component along the z direction, contrary to the P and S_v waves. In a horizontally layered medium the S_h waves are decoupled from the P and S_v waves.

Unfortunately the S wavefield splitting into S_v and S_h waves is undefined for vertically propagating S plane waves. This ambiguity can be seen from two points of view. Looking at *Figure 2.7.3*, we see that for vertically propagating S plane waves, the S_v and S_h waves share the same (horizontal) polarization plane, it is then not possible to distinguish them. The ambiguity can also be seen from an other point of view. In the wavenumber frequency domain we have :

$$-j\rho\omega\,\vec{\tilde{v}}_s(k_x, k_y, z, \omega) = -\vec{\nabla}\times\vec{\nabla}\times\vec{\tilde{\psi}} + \vec{\nabla}\times\vec{\tilde{\zeta}},$$

$$-j\rho\omega\,\vec{\tilde{v}}_s(k_x, k_y, z, \omega) = \left(-jk_y\,\tilde{\zeta} + jk_x\frac{\partial}{\partial z}\tilde{\psi},\; jk_x\,\tilde{\zeta} + jk_y\frac{\partial}{\partial z}\tilde{\psi},\; -\left(k_x^2+k_y^2\right)\tilde{\psi}\right)^T. \qquad (2.7.12d)$$

For vertically propagating S plane waves ($k_x = k_y = 0$) and finite potentials $\tilde{\psi}$ and $\tilde{\zeta}$ we have :

$$\vec{\tilde{v}}_s(0, 0, z, \omega) = \vec{0}\,. \qquad (2.7.12e)$$

Which means that with definition *(2.7.12a)* for the S wavefield vector potential, vertically propagating S plane waves do not generate a particle velocity field. This is physically unacceptable and it makes the wavefield decomposition for $\vec{\tilde{v}}_s \neq 0$ unstable. To overcome the instability we can define scaled vector potentials : $\vec{\tilde{\psi}}_s$ and $\vec{\tilde{\zeta}}_s$, related to the vector potentials $\vec{\tilde{\psi}}$ and $\vec{\tilde{\zeta}}$ according to $\vec{\tilde{\psi}}_s = k_r\,\vec{\tilde{\psi}}$ and $\vec{\tilde{\zeta}}_s = k_r\,\vec{\tilde{\zeta}}$, with $k_r^2 = k_x^2 + k_y^2$. With this new definition for the S wavefield vector potentials, a vertically propagating S plane wave generates a non-zero

particle velocity field. The wavefield decomposition for such waves is now stable, but there is still the ambiguity as $\vec{\tilde{v}}_s$ is now discontinuous at $k_x=k_y=0$. In the following, we derive the expression of the composition ($\tilde{L}$) and decomposition ($\tilde{M}$) matrices for the scaled S wavefield vector potential. We define the one-way normal mode wavefield vector $\vec{\tilde{P}}$ according to :

$$\vec{\tilde{p}}^{\pm} = (\tilde{\phi}^{\pm}, \tilde{\psi}_s^{\pm}, \tilde{\zeta}_s^{\pm})^T . \qquad (2.7.13a)$$

This choice for the S wavefield vector potential implies the following expression for the composition ($\tilde{L}$) and decomposition ($\tilde{M}$) matrices :

$$\tilde{L}_1^{\pm} = \frac{1}{\rho\omega}\begin{pmatrix} k_x & \pm\frac{jk_xk_{z,s}}{k_r} & \frac{k_y}{k_r} \\ k_y & \pm\frac{jk_yk_{z,s}}{k_r} & \frac{-k_x}{k_r} \\ \pm k_{z,p} & -jk_r & 0 \end{pmatrix}, \qquad (2.7.13b)$$

$$\tilde{L}_2^{\pm} = \frac{1}{k_s^2}\begin{pmatrix} \mp 2k_xk_{z,p} & -jk_x\frac{k_s^2 - 2k_r^2}{k_r} & \mp\frac{k_yk_{z,s}}{k_r} \\ \mp 2k_yk_{z,p} & -jk_y\frac{k_s^2 - 2k_r^2}{k_r} & \pm\frac{k_xk_{z,s}}{k_r} \\ -k_s^2 + 2k_r^2 & \pm 2jk_{z,s}k_r & 0 \end{pmatrix}, \qquad (2.7.13c)$$

$$\tilde{M}_1^{\pm} = \frac{\mu}{\omega}\begin{pmatrix} k_x & k_y & \pm\frac{(k_s^2 - 2k_r^2)}{2k_{z,p}} \\ \mp\frac{jk_x}{2k_{z,s}}\frac{(k_s^2 - 2k_r^2)}{k_r} & \mp\frac{jk_y}{2k_{z,s}}\frac{(k_s^2 - 2k_r^2)}{k_r} & jk_r \\ \frac{k_yk_s^2}{2k_r} & \frac{-k_xk_s^2}{2k_r} & 0 \end{pmatrix}, \qquad (2.7.13d)$$

$$\tilde{M}_2^{\pm} = \frac{1}{2}\begin{pmatrix} \mp\frac{k_x}{k_{z,p}} & \mp\frac{k_y}{k_{z,p}} & -1 \\ \frac{jk_x}{k_r} & \frac{jk_y}{k_r} & \mp\frac{jk_r}{k_{z,s}} \\ \mp\frac{k_yk_s^2}{k_{z,s}k_r} & \pm\frac{k_xk_s^2}{k_{z,s}k_r} & 0 \end{pmatrix}. \qquad (2.7.13e)$$

Note that the following relations exist between the composition and decomposition operators:

$$\left(\tilde{L}_1^{\pm}\right)^T = \tilde{T}^{\pm}\tilde{M}_2^{\pm}, \qquad (2.7.13f)$$

$$\left(\tilde{L}_2^{\pm}\right)^T = \tilde{T}^{\pm}\tilde{M}_1^{\pm}, \qquad (2.7.13g)$$

with,

$$\tilde{\vec{T}}^{\pm} = \frac{2}{\rho\omega}\begin{pmatrix} \mp k_{z,p} & 0 & 0 \\ 0 & \pm k_{z,s} & 0 \\ 0 & 0 & \mp\frac{k_{z,s}}{k_s^2} \end{pmatrix}. \qquad (2.7.13h)$$

Looking at the expression of the composition and decomposition operators we see that they are only unstable for horizontally propagating P and S plane waves. The operator instability for vertically propagating S plane waves ($k_x = k_y = 0$) has been replaced by an operator discontinuity (due to the square root function k_r). This discontinuity has the disadvantage of producing long operators in the space domain. Other S wavefield vector potential definitions are possible but definitions *(2.7.11a)* and *(2.7.12a)* will be frequently used in the remainder of this thesis.

2.8 NORMAL MODES INTERACTION AND BOUNDARY CONDITIONS

In the previous sections we saw that in any homogeneous anisotropic medium, there exist three normal modes of propagation. In section 2.6 we also saw that in a laterally homogeneous medium with a continuous vertical gradient in the elastic parameters there is an interaction between the upgoing and downgoing normal modes; the interaction being governed by equations *(2.6.4i,j)*. In this section we study the normal modes interaction for some specific boundary conditions like the traction free or the rigid surface. We also study the normal modes interaction in the case of a vertical discontinuity in the elastic or density parameters.

Traction free surface

A surface is traction free, when this surface does not support tractions (e.g. the earth's surface). If the surface is a horizontal plane at z_0, the traction free boundary condition can be formulated in terms of two-way components according to:

$$\tilde{\vec{\tau}}_z(z_0) = \vec{0}\,. \qquad (2.8.1a)$$

The substitution of the above condition into *(2.6.2a)* leads to :

$$\tilde{L}_2^{+}(z_0)\,\tilde{\vec{p}}^{+}(z_0) + \tilde{L}_2^{-}(z_0)\,\tilde{\vec{p}}^{-}(z_0) = \vec{0}\,, \qquad (2.8.1b)$$

which clearly indicates that at a traction free surface downgoing and upgoing normal waves interact with each other. Consider an upgoing wave reaching the traction free surface, the

downgoing waves generated at z_0 in order to fulfill equation *(2.8.1b)* are related to the incident one via a reflection matrix $\tilde{\boldsymbol{R}}_{fr}^{-}(z_0)$. We have :

$$\vec{\tilde{p}}^{+}(z_0) = \tilde{\boldsymbol{R}}_{fr}^{-}(z_0)\,\vec{\tilde{p}}^{-}(z_0)\,. \qquad (2.8.1c)$$

The expression of the reflection matrix is found by replacing *(2.8.1c)* in *(2.8.1b)*, we obtain:

$$\tilde{\boldsymbol{R}}_{fr}^{-}(z_0) = -\left[\tilde{\boldsymbol{L}}_2^{+}(z_0)\right]^{-1}\tilde{\boldsymbol{L}}_2^{-}(z_0)\,. \qquad (2.8.1d)$$

An other expression can be found for $\tilde{\boldsymbol{R}}_{fr}^{-}(z_0)$: knowing that equation *(2.8.1a)* is verified at z_0 we derive from *(2.6.2b)* that :

$$\vec{\tilde{p}}^{\pm}(z_0) = \tilde{\boldsymbol{M}}_1^{\pm}(z_0)\,\vec{\tilde{v}}\,(z_0)\,, \qquad (2.8.1e)$$

from which we deduce that we must have :

$$\tilde{\boldsymbol{R}}_{fr}^{-}(z_0) = \tilde{\boldsymbol{M}}_1^{+}(z_0)\left[\tilde{\boldsymbol{M}}_1^{-}(z_0)\right]^{-1}. \qquad (2.8.1f)$$

$\tilde{\boldsymbol{R}}_{fr}^{-}(z_0)$ is a full 3×3 matrix, hence wave conversions occur at the traction free surface. It is interesting to point out that $\tilde{\boldsymbol{R}}_{fr}^{-}(z_0)$ is singular when :

$$det\left(\tilde{\boldsymbol{L}}_2^{+}(z_0)\right) = 0\,, \qquad (2.8.1g)$$

or equivalently,

$$det\left(\tilde{\boldsymbol{M}}_1^{-}(z_0)\right) = 0\,. \qquad (2.8.1h)$$

This singularity means that the traction free boundary condition can be fulfilled for some particular "downgoing" evanescent plane waves without the need of "upgoing" waves, as equations :

$$\vec{\tilde{\tau}}_z\,(z_0) = \tilde{\boldsymbol{L}}_2^{+}(z_0)\,\vec{\tilde{p}}^{+}(z_0) = \vec{0}\,, \qquad (2.8.1i)$$

and

$$\vec{\tilde{p}}^{-}(z_0) = \tilde{\boldsymbol{M}}_1^{-}(z_0)\,\vec{\tilde{v}}\,(z_0) = \vec{0}\,, \qquad (2.8.1j)$$

admit non trivial solutions. The wavenumbers by which equations *(2.8.1gh)* are verified are called Rayleigh poles, their contribution in the space-time domain constitute the Rayleigh waves.

To illustrate the effects of a traction free surface on the incident upgoing waves, we consider the model depicted in *Figure 2.8.1a*. It consists of a homogeneous isotropic lower half-space bounded by a traction free surface. A line of particle velocity detectors is buried at a depth of *200m* and a pure *P* wave point source is located at a depth of *400m*. *Figure 2.8.1b* represents the recorded particle velocity field. We can recognize the source upgoing *P* wavefield, as well as the reflected *P* and converted *S* waves. Note the angle of incidence dependency of the reflection matrix ($\boldsymbol{R}_{fr}$) .

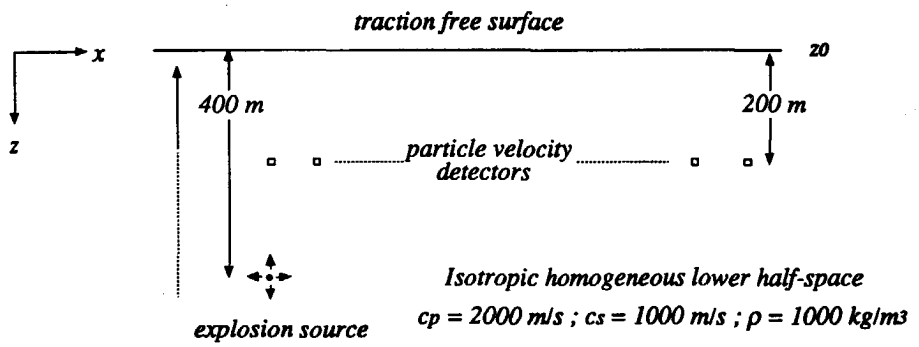

Figure 2.8.1a

The above model is used to illustrate the effect of a traction free surface on an upgoing incident P wavefield. The model consists of an homogeneous isotropic lower half-space bounded by a traction free surface. A line of detectors is buried at a depth of 200m and a pure P wave point source is located at a depth of 400m.

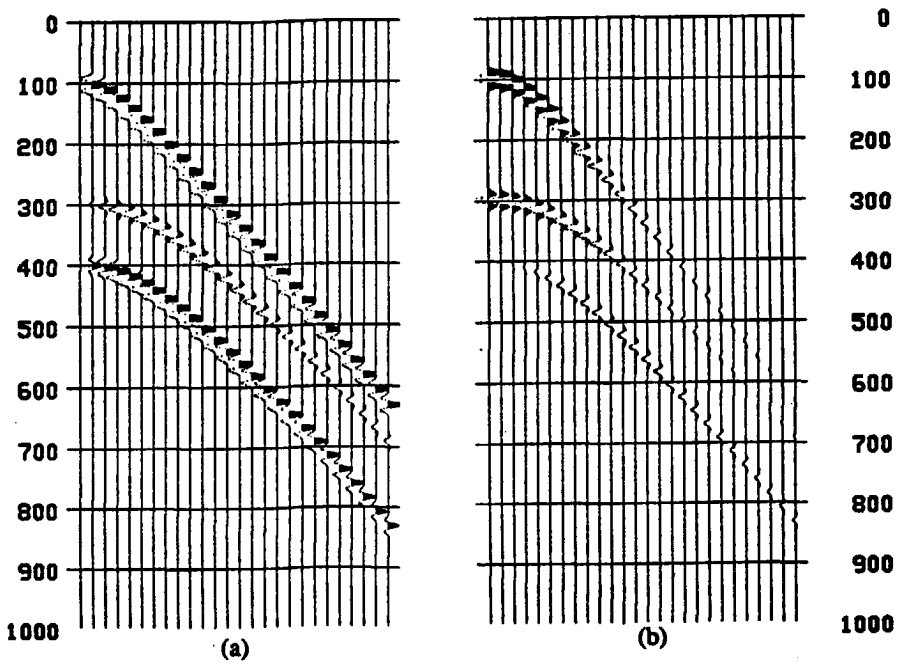

Figure 2.8.1b

Space and time variations of the horizontal (a) and vertical (b) particle velocity field. We can recognize the upgoing P source wavefield, as well as the downgoing reflected P and converted S waves.

Rigid surface

A surface is rigid, when this surface does not support particle displacements. If the surface is a horizontal plane at z_0, the rigid surface boundary condition can be formulated in terms of two-way components according to :

$$\vec{\tilde{v}}(z_0) = \vec{0} . \qquad (2.8.2a)$$

The substitution of the above condition into *(2.6.2a)* leads to :

$$\tilde{L}_1^+(z_0)\,\vec{\tilde{p}}^+(z_0) + \tilde{L}_1^-(z_0)\,\vec{\tilde{p}}^-(z_0) = \vec{0} , \qquad (2.8.2b)$$

which clearly indicates that downgoing and upgoing normal waves interact with each other at a rigid surface. Following the same reasoning as for the traction free boundary condition, we find that an upgoing wavefield reaching the rigid surface generates a downgoing wavefield, related to the incident one via a reflection matrix $\tilde{R}_{rd}^-$:

$$\vec{\tilde{p}}^+(z_0) = \tilde{R}_{rd}^-(z_0)\,\vec{\tilde{p}}^-(z_0) , \qquad (2.8.2c)$$

with,

$$\tilde{R}_{rd}^-(z_0) = -\left(\tilde{L}_1^+(z_0)\right)^{-1} \tilde{L}_1^-(z_0) , \qquad (2.8.2d)$$

or equivalently,

$$\tilde{R}_{rd}^-(z_0) = \tilde{M}_2^+(z_0)\left(\tilde{M}_2^-(z_0)\right)^{-1} . \qquad (2.8.2e)$$

$\tilde{R}_{rd}^-$ is.a full 3×3 matrix, hence wave conversions occur at the rigid surface It is interesting to point out that the inverse of matrices $\tilde{L}_1^+(z_0)$ and $\tilde{M}_2^-(z_0)$ are never singular for real k_x, k_y and ω values.

Two elastic media in contact
(vertical discontinuity in the elastic and density parameters)

When two distinct solid elastic media are in contact at depth level z_1, see *Figure 2.8.2a*, there is a discontinuity in the physical parameters between depth levels $z_1 - \varepsilon$ and $z_1 + \varepsilon$. As the differential operator $\tilde{A}_1$ is not continuous at z_1, the Taylor series expension *(2.5.4a)* and the two-way extrapolation operator $\tilde{U}$ defined in *(2.5.4c)* do not hold. Due to this discontinuity , the two-way extrapolation operator $\tilde{U}$, as defined by *(2.5.4c)* is not valid to extrapolate the wavefield across the discontinuity. As the differential operator $\tilde{A}_1$is not continuous at z_1, the Taylor expension *(2.5.4a)* does not hold. To pass the critical depth level z_1, we invoke that the two-way wavefield components must be continuous at z_1, which can be expressed :

$$\lim_{\varepsilon \to 0^+} \vec{\tilde{Q}}(z_1+\varepsilon) = \lim_{\varepsilon \to 0^+} \vec{\tilde{Q}}(z_1-\varepsilon) . \qquad (2.8.3)$$

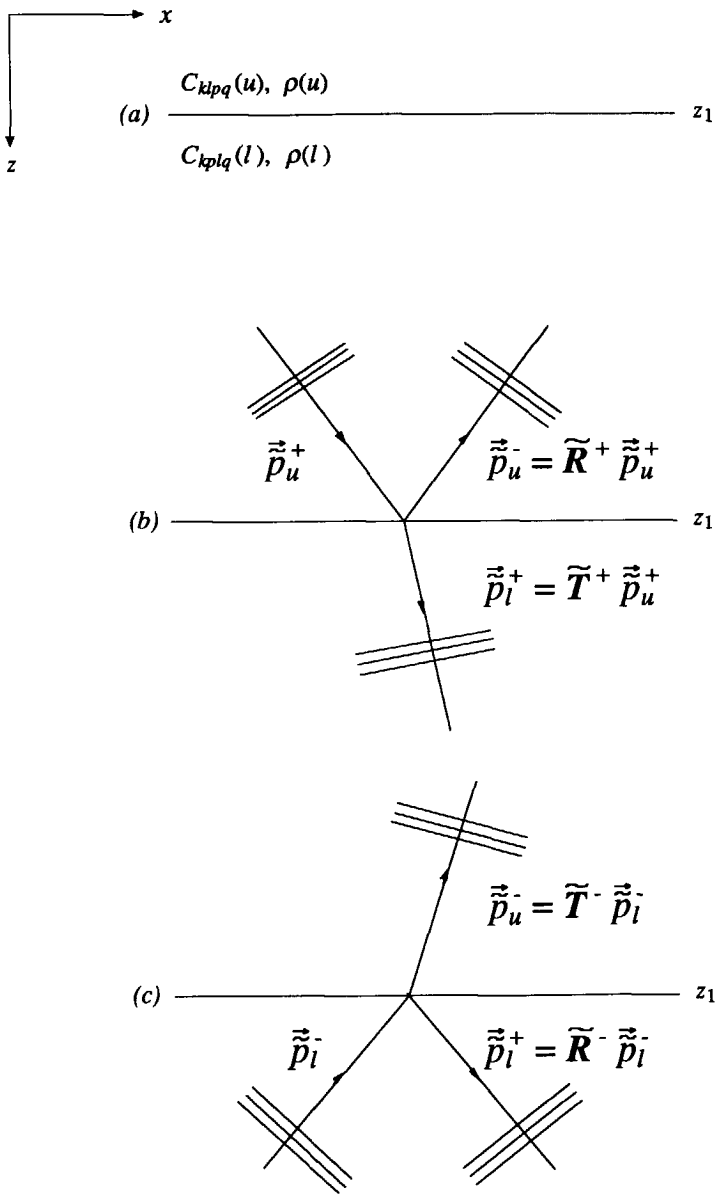

Figure 2.8

If the elastic medium is discontinuous at depth level z1, we can not use the Taylor series expension of the two-way wavefield vector to extrapolate it through z1. To pass the critical depth level z1, we invoke that the two-way wavefield components must be continuous at z1. From this condition of continuity we deduce the reflection and transmission matrices that describe the effect of the discontinuity on any incident normal wave-type.

From the two-way boundary condition of continuity *(2.8.3)* we may deduce its counterpart that apply on the normal one-way wavefield components in terms of reflection and transmission matrices.

The first studied situation is the interaction between a downgoing plane wave $\vec{\tilde{p}}_u^{+}$ coming from the *upper* medium and the discontinuity at z_1 (see Figure 2.8b). This downgoing wave generates a reflected upgoing wavefield, $\vec{\tilde{p}}_u^{-}$, in the *upper* medium and a transmitted downgoing wavefield, $\vec{\tilde{p}}_l^{+}$, in the *lower* medium. The reflected and transmitted waves are related to the incident wave through the reflection ($\tilde{\boldsymbol{R}}^{+}(z_1)$) and transmission ($\tilde{\boldsymbol{T}}^{+}(z_1)$) matrices, according to :

$$\vec{\tilde{p}}_u^{-}(z_1) = \tilde{\boldsymbol{R}}^{+}(z_1)\,\vec{\tilde{p}}_u^{+}(z_1)\,, \qquad (2.8.4a)$$

and

$$\vec{\tilde{p}}_l^{+}(z_1) = \tilde{\boldsymbol{T}}^{+}(z_1)\,\vec{\tilde{p}}_u^{+}(z_1)\,. \qquad (2.8.4b)$$

Applying for this situation the boundary condition of continuity *(2.8.3)*, we obtain :

$$\tilde{\boldsymbol{L}}_u \begin{pmatrix} \vec{\tilde{p}}_u^{+}(z_1) \\ \vec{\tilde{p}}_u^{-}(z_1) \end{pmatrix} = \tilde{\boldsymbol{L}}_l \begin{pmatrix} \vec{\tilde{p}}_l^{+}(z_1) \\ 0 \end{pmatrix}, \qquad (2.8.4c)$$

$\tilde{\boldsymbol{L}}_u$ being the composition operator for the *upper* medium and $\tilde{\boldsymbol{L}}_l$ the composition operator for the *lower* medium. Substituting *(2.8.4ab)* into *(2.8.4c)* and knowing that this equation must hold for any downgoing normal wavefield vector $\vec{\tilde{p}}_u^{+}(z_1)$ we obtain :

$$\tilde{\boldsymbol{L}}_u \begin{pmatrix} \tilde{\boldsymbol{I}} \\ \tilde{\boldsymbol{R}}^{+}(z_1) \end{pmatrix} = \tilde{\boldsymbol{L}}_l \begin{pmatrix} \tilde{\boldsymbol{T}}^{+}(z_1) \\ 0 \end{pmatrix}, \qquad (2.8.4d)$$

from which we deduce that :

$$\tilde{\boldsymbol{T}}^{+}(z_1) = \left[\tilde{\boldsymbol{M}}^{+}_{\alpha,u}\,\tilde{\boldsymbol{L}}^{+}_{\alpha,l}\right]^{-1}, \qquad (2.8.4e)$$

and

$$\tilde{\boldsymbol{R}}^{+}(z_1)\left[\tilde{\boldsymbol{T}}^{+}(z_1)\right]^{-1} = \tilde{\boldsymbol{M}}^{-}_{\alpha,u}\,\tilde{\boldsymbol{L}}^{+}_{\alpha,l}\,, \qquad (2.8.4f)$$

or equivalently,

$$\tilde{\boldsymbol{R}}^{+}(z_1) = \left[\tilde{\boldsymbol{M}}^{-}_{\alpha,u}\,\tilde{\boldsymbol{L}}^{+}_{\alpha,l}\right]\left[\tilde{\boldsymbol{M}}^{+}_{\alpha,u}\,\tilde{\boldsymbol{L}}^{+}_{\alpha,l}\right]^{-1}. \qquad (2.8.4g)$$

As the reflection and transmission matrices are not diagonal, wave conversions will occur at z_1. For the illustration we consider the model represented in *Figure 2.8.3a*. It consist of two homogeneous isotropic half-spaces in contact. *Figure 2.8.3b,c* represent the particle velocity field measured above and below z_1. In *2.8.3b* we can recognize the downgoing source wavefield (we used a pure *P* wave point source), as well as the upgoing reflected *P* and *S* waves. In *Figure 2.8.3c* we can recognize the downgoing transmitted *P* and *S* waves. Note the angle of incidence dependency of the reflection and transmission matrices.

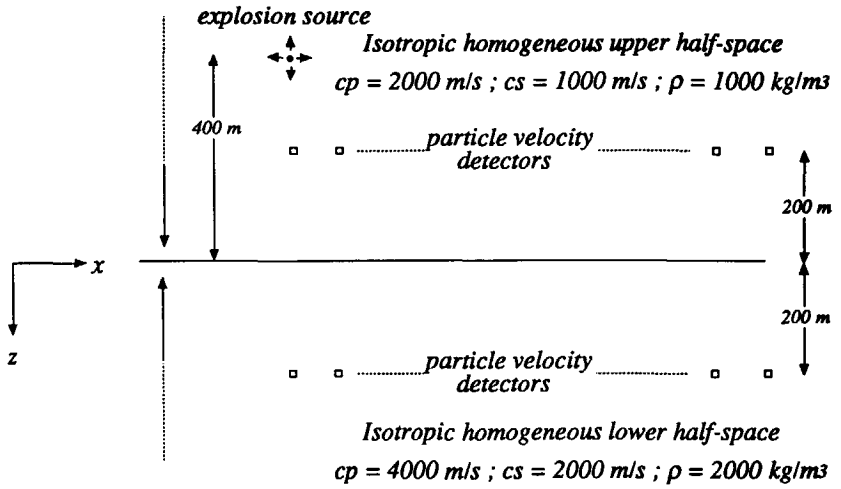

Figure 2.8.3a

The above model is used to illustrate the effects of a vertical discontinuity in the elastic and density parameters on a downgoing incident P wavefield. The model consists of two isotropic half-spaces in contact. A pure P wave point source is located at a distance of 400m above the discontinuity and two lines of detectors record the particle velocity field. A first line is located at a distance of 200m above the interface and a second one at a distance of 200m below the interface.

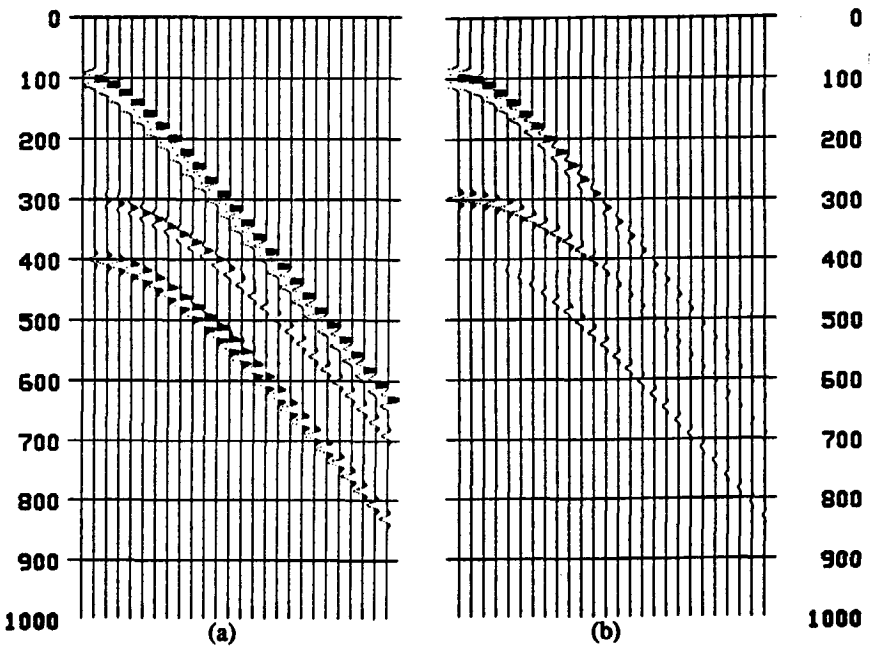

Figure 2.8.3b

Lateral space and time variations of the horizontal (a) and vertical (b) particle velocity field recorded by the line of detectors located above the discontinuity

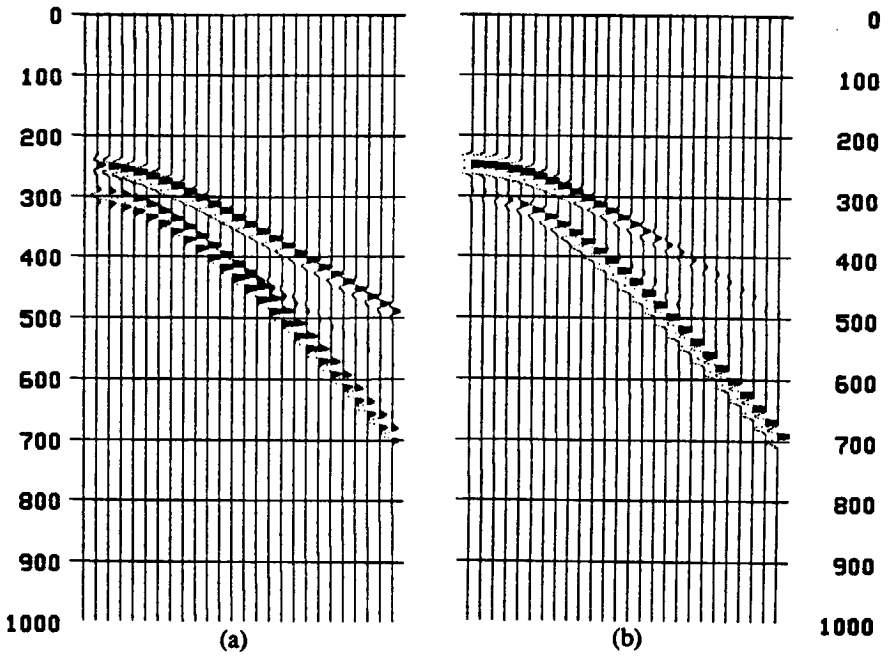

Figure 2.8.3c

Lateral space and time variations of the horizontal (a) and vertical (b) particle velocity field recorded by the line of detectors located below the discontinuity

The second studied situation is the interaction between upgoing plane wave $\vec{\tilde{p}}_l^-$ coming from the *lower* medium and the discontinuity at z_1 (see *Figure 2.8.2c*). This upgoing wave generates a reflected downgoing wavefield, $\vec{\tilde{p}}_l^+$, in the *lower* medium and an upgoing transmitted wave, $\vec{\tilde{p}}_u^-$, in the *upper* medium. The reflected and transmitted wavefields are related to the incident one through the reflection ($\tilde{R}^-(z_1)$) and transmission ($\tilde{T}^-(z_1)$) matrix, according to :

$$\vec{\tilde{p}}_l^+(z_1) = \tilde{R}^-(z_1)\,\vec{\tilde{p}}_l^-(z_1)\,, \qquad (2.8.5a)$$

and

$$\vec{\tilde{p}}_u^-(z_1) = \tilde{T}^-(z_1)\,\vec{\tilde{p}}_l^-(z_1)\,. \qquad (2.8.5b)$$

Following the same reasoning as the one previously developed, we obtain the following results :

$$\tilde{T}^-(z_1) = \left[\tilde{M}^-_{\alpha,l}\,\tilde{L}^-_{\alpha,u}\right]^{-1}, \qquad (2.8.5c)$$

and

$$\tilde{R}^-(z_1)\left[\tilde{T}^-(z_1)\right]^{-1} = \tilde{M}^+_{\alpha,l}\,\tilde{L}^-_{\alpha,u}\,, \qquad (2.8.5d)$$

or equivalently ,

$$\tilde{\boldsymbol{R}}^{-}(z_1) = \left[\tilde{\boldsymbol{M}}^{+}_{\alpha,l}\,\tilde{\boldsymbol{L}}^{-}_{\alpha,u}\right]\left[\tilde{\boldsymbol{M}}^{-}_{\alpha,l}\,\tilde{\boldsymbol{L}}^{-}_{\alpha,u}\right]^{-1} . \qquad (2.8.5e)$$

The transmission and reflection matrices may not be defined for some plane waves, i.e., when the matrix product $\tilde{\boldsymbol{M}}^{\pm}_{\alpha,l}\,\tilde{\boldsymbol{L}}^{\pm}_{\alpha,u}$ is not invertible. The wavenumbers corresponding to these plane waves are called Stoneley poles and their contribution in the space-time domain constitutes the Stoneley waves. Such waves are surface waves propagating at the interface z_1, they are neither transmitted nor reflected.

In order to go one step further in the determination of relations between the reflection and transmission matrices, we consider the following situation : a downgoing plane wave, $\vec{\tilde{p}}^{+}_{u}$, coming from the *upper* medium and an upgoing plane wave, $\vec{\tilde{p}}^{-}_{l}$, coming from the *lower* medium. The boundary condition of wavefield continuity at z_1 can be written as follows :

$$\tilde{\boldsymbol{L}}_u \begin{pmatrix} \vec{\tilde{d}}^{+}_{u}(z_1) \\ \vec{\tilde{d}}^{-}_{u}(z_1) \end{pmatrix} = \tilde{\boldsymbol{L}}_l \begin{pmatrix} \vec{\tilde{d}}^{+}_{l}(z_1) \\ \vec{\tilde{d}}^{-}_{l}(z_1) \end{pmatrix}, \qquad (2.8.6a)$$

with,

$$\vec{\tilde{d}}^{+}_{u}(z_1) = \vec{\tilde{p}}^{+}_{u}(z_1) , \qquad (2.8.6b)$$

$$\vec{\tilde{d}}^{-}_{u}(z_1) = \tilde{\boldsymbol{R}}^{+}(z_1)\,\vec{\tilde{p}}^{+}_{u}(z_1) + \tilde{\boldsymbol{T}}^{-}(z_1)\,\vec{\tilde{p}}^{-}_{l}(z_1) , \qquad (2.8.6c)$$

$$\vec{\tilde{d}}^{+}_{l}(z_1) = \tilde{\boldsymbol{T}}^{+}(z_1)\,\vec{\tilde{p}}^{+}_{u}(z_1) + \tilde{\boldsymbol{R}}^{-}(z_1)\,\vec{\tilde{p}}^{-}_{l}(z_1) , \qquad (2.8.6d)$$

$$\vec{\tilde{d}}^{-}_{l}(z_1) = \vec{\tilde{p}}^{-}_{l}(z_1) . \qquad (2.8.6e)$$

Equation *(2.8.6a)* can be rewritten as :

$$\begin{pmatrix} \vec{\tilde{d}}^{+}_{u}(z_1) \\ \vec{\tilde{d}}^{-}_{u}(z_1) \end{pmatrix} = \tilde{\boldsymbol{M}}_u\,\tilde{\boldsymbol{L}}_l \begin{pmatrix} \vec{\tilde{d}}^{+}_{l}(z_1) \\ \vec{\tilde{d}}^{-}_{l}(z_1) \end{pmatrix}, \qquad (2.8.6f)$$

or using *(2.8.4e,f)*,

$$\begin{pmatrix} \vec{\tilde{d}}^{+}_{u}(z_1) \\ \vec{\tilde{d}}^{-}_{u}(z_1) \end{pmatrix} = \begin{pmatrix} \left[\tilde{\boldsymbol{T}}^{+}\right]^{-1} & \tilde{\boldsymbol{M}}^{+}_{\alpha,u}\,\tilde{\boldsymbol{L}}^{-}_{\alpha,l} \\ \tilde{\boldsymbol{R}}^{+}\left[\tilde{\boldsymbol{T}}^{+}\right]^{-1} & \tilde{\boldsymbol{M}}^{-}_{\alpha,u}\,\tilde{\boldsymbol{L}}^{-}_{\alpha,l} \end{pmatrix} \begin{pmatrix} \vec{\tilde{d}}^{+}_{l}(z_1) \\ \vec{\tilde{d}}^{-}_{l}(z_1) \end{pmatrix} . \qquad (2.8.6g)$$

From which we deduce that:

$$\tilde{\boldsymbol{M}}^{+}_{\alpha,u}\,\tilde{\boldsymbol{L}}^{-}_{\alpha,l} = -\left[\tilde{\boldsymbol{T}}^{+}\right]^{-1}\tilde{\boldsymbol{R}}^{-} , \qquad (2.8.6h)$$

and

$$\tilde{\boldsymbol{M}}^{-}_{\alpha,u}\,\tilde{\boldsymbol{L}}^{-}_{\alpha,l} = \tilde{\boldsymbol{T}}^{-} - \tilde{\boldsymbol{R}}^{+}\left[\tilde{\boldsymbol{T}}^{+}\right]^{-1}\tilde{\boldsymbol{R}}^{-} . \qquad (2.8.6i)$$

Similarly, equation *(2.8.6a)* can be rewritten as :

$$\begin{pmatrix} \vec{\tilde{d}}^{+}_{l}(z_1) \\ \vec{\tilde{d}}^{-}_{l}(z_1) \end{pmatrix} = \tilde{\boldsymbol{M}}_l\,\tilde{\boldsymbol{L}}_u \begin{pmatrix} \vec{\tilde{d}}^{+}_{u}(z_1) \\ \vec{\tilde{d}}^{-}_{u}(z_1) \end{pmatrix}, \qquad (2.8.6j)$$

or using *(2.8.5,cd)*,

$$\begin{pmatrix} \vec{\vec{d}}_l^{+}(z_1) \\ \vec{\vec{d}}_l^{-}(z_1) \end{pmatrix} = \begin{pmatrix} \tilde{M}_{\alpha,l}^{+} \tilde{L}_{\alpha,u}^{+} & \tilde{R}^{-}\left[\tilde{T}^{-}\right]^{-1} \\ \tilde{M}_{\alpha,l}^{-} \tilde{L}_{\alpha,u}^{+} & \left[\tilde{T}^{-}\right]^{-1} \end{pmatrix} \begin{pmatrix} \vec{\vec{d}}_u^{+}(z_1) \\ \vec{\vec{d}}_u^{-}(z_1) \end{pmatrix}. \qquad (2.8.6k)$$

From which we deduce that:

$$\tilde{M}_{\alpha,l}^{+} \tilde{L}_{\alpha,u}^{+} = \tilde{T}^{+} - \tilde{R}^{-}\left[\tilde{T}^{-}\right]^{-1}\tilde{R}^{+}, \qquad (2.8.6l)$$

and

$$\tilde{M}_{\alpha,l}^{-} \tilde{L}_{\alpha,u}^{+} = -\left[\tilde{T}^{-}\right]^{-1}\tilde{R}^{+}, \qquad (2.8.6m)$$

The relations obtained in this section can be summarized as follows :

$$\tilde{M}_u \tilde{L}_l = \begin{pmatrix} \left[\tilde{T}^{+}\right]^{-1} & -\left[\tilde{T}^{+}\right]^{-1}\tilde{R}^{-} \\ \tilde{R}^{+}\left[\tilde{T}^{+}\right]^{-1} & \tilde{T}^{-} - \tilde{R}^{+}\left[\tilde{T}^{+}\right]^{-1}\tilde{R}^{-} \end{pmatrix}, \qquad (2.8.6n)$$

and

$$\tilde{M}_l \tilde{L}_u = \begin{pmatrix} \tilde{T}^{+} - \tilde{R}^{-}\left[\tilde{T}^{-}\right]^{-1} R^{+} & \tilde{R}^{-}\left[T^{-}\right]^{-1} \\ -\left[\tilde{T}^{-}\right]^{-1}\tilde{R}^{+} & \left[\tilde{T}^{-}\right]^{-1} \end{pmatrix}. \qquad (2.8.6o)$$

Equations *(2.8.6no)* are used in chapter 3.

2.9 COMPRESSIONAL AND SHEAR WAVE SOURCES

A source must be applied in the medium to initialize the elastic wavefield. The source used is most often mechanical and expressed in terms of forces or deformation applied to a part of the solid. In this section we study the amplitude and phase of the upgoing and downgoing normal waves emitted in a homogeneous medium by sources located at depth level z_s. More complicated sources, with a depth extension, can be simulated from the previous response by applying the principle of superposition as we work with linearized equations. We consider source functions of the type :

$$\vec{\vec{f}} = \vec{\vec{f}}_0(k_x, k_y, \omega)\, \delta(z-z_s), \qquad (2.9.1a)$$

and

$$\vec{\vec{\sigma}}_i = \vec{\vec{\sigma}}_{0i}(k_x, k_y, \omega)\, \delta(z-z_s). \qquad (2.9.1b)$$

We start with the normal mode one-way wave equation in a homogeneous medium *(2.6.3b)* :

$$\frac{\partial}{\partial z}\vec{\vec{P}} = \tilde{\Lambda}\vec{\vec{P}} + \vec{\vec{S}}', \qquad (2.9.2a)$$

where the normal mode source vector $\vec{\vec{S}}'$ is related to the two-way source vector $\vec{\vec{S}}$ via the decomposition operator $\tilde{M}$ (see *2.6.3d)*

$$\vec{\vec{S}}' = \tilde{M}\,\vec{\vec{S}}. \qquad (2.9.2b)$$

The two-way source vector $\vec{\vec{S}}$ is related to the force $\vec{\vec{f}}$ and stress sources $\vec{\vec{\sigma}}_i$ according to (see *2.5.3ij*) :

$$\vec{\vec{S}} = \begin{pmatrix} \tilde{A}_{12}\,\vec{\vec{\sigma}}_z \\ \tilde{A}_{22}\,\vec{\vec{\sigma}}_z - jk_\alpha \vec{\vec{\sigma}}_\alpha - \vec{\vec{f}} \end{pmatrix}. \qquad (2.9.2c)$$

The combination of *(2.9.2b)* with *(2.9.2c)* leads to the following result :

$$\vec{\vec{S}}' = \begin{pmatrix} \vec{\vec{s}}'^{+} \\ \vec{\vec{s}}'^{-} \end{pmatrix}, \qquad (2.9.2d)$$

$$\vec{\vec{s}}'^{\pm} = \vec{\vec{s}}_0'^{\pm}\,\delta(z-z_s)\,, \qquad (2.9.2e)$$

and

$$\vec{\vec{s}}_0'^{\pm} = \tilde{\Lambda}^{\pm}\,\tilde{M}_2^{\pm}\,\vec{\vec{\sigma}}_{0z} - \tilde{M}_2^{\pm}\left[\, jk_\alpha \vec{\vec{\sigma}}_{0\alpha} + \vec{\vec{f}}_0 \,\right], \qquad (2.9.2f)$$

where we used expression *(2.6.1a)*. Equation *(2.9.2f)* gives us the expressions of the upgoing and downgoing normal waves generated by a force or deformation source. To know how these waves propagate in the homogeneous medium we solve the differential equation *(2.9.2a)*. The following solutions are obtained :

$$\vec{\vec{p}}^{+}(z) = +exp\left(\tilde{\Lambda}^{+}(z-z_s)\right)\vec{\vec{s}}_0'^{+}\,H(z-z_s)\,, \qquad (2.9.3a)$$

$$\vec{\vec{p}}^{-}(z) = -exp\left(\tilde{\Lambda}^{-}(z-z_s)\right)\vec{\vec{s}}_0'^{-}\,H(z_s-z)\,, \qquad (2.9.3b)$$

with $H(z)$ the Heaviside unit step function ,

$$H(z) = 0 \qquad z < 0 \qquad (2.9.3c)$$

$$H(0) = 1/2 \qquad (2.9.3d)$$

$$H(z) = 1 \qquad z > 0 \qquad (2.9.3e)$$

These results are valid for an arbitrary anisotropic homogeneous medium. In the following we give the expression of the P and S waves emitted by, respectively, an explosion, a moment and a force source in an isotropic homogeneous medium.

Explosion source

An explosion point source is a point of expansion. it can be represented with the deformation source tensor. In the space-frequency domain we have :

$$h_{ij} = \frac{V_0(\omega)}{3}\,\delta_{ij}\,\delta(x)\,\delta(y)\,\delta(z)\,, \qquad (2.9.4a)$$

or, in the wavenumber-frequency domain :

$$\tilde{h}_{ij} = \frac{V_0(\omega)}{3}\,\delta_{ij}\,\delta(z)\,. \qquad (2.9.4b)$$

The tensor $\tilde{h}_{ij}$ corresponds to a point of volume injection of strengh $V_0(\omega)$, localized at the origin *(x=0, y=0, z=0)*. In an isotropic medium, the stress tensor associated to this deformation reads :

$$\tilde{\sigma}_{ij} = (\lambda + \frac{2}{3}\mu) V_0(\omega)\, \delta_{ij}\, \delta(z)\,. \qquad (2.9.4c)$$

Setting the volume density of body forces $\vec{\vec{f}}$ to zero in *(2.9.2c)* and using expression *(2.7.11j)* for the matrix $\tilde{M}_2^{\pm}$, we find from equation *(2.9.2f)* the expression of the normal wave source vector $\vec{\vec{s}}_0'^{\pm}$:

$$\vec{\vec{s}}_0'^{\pm} = \frac{j}{6}\frac{k_p^2}{k_{z,p}} V_0(\omega)\,(1,\, 0,\, 0)^T\,. \qquad (2.9.4d)$$

An explosion source in an isotropic homogeneous elastic medium only generates *P* waves. In a more accurate way we can even say that it is a monopole *P* wave source.

moment source

A moment source is a distribution of body force sources that generate a moment of given rotation axis. For the illustration we consider a moment source localized at the origin with a vertical rotation axis. The associated force distribution reads in the space-frequency domain :

$$\vec{f} = M_0(\omega)\, \vec{\nabla} \times \big(0,\, 0,\, \delta(x)\, \delta(y)\, \delta(z)\big)^T\,, \qquad (2.9.5a)$$

or, in the wavenumber-frequency domain :

$$\vec{\vec{f}} = M_0(\omega)\, \vec{\vec{\nabla}} \times \big(0,\, 0,\, \delta(z)\big)\,, \qquad (2.9.5b)$$

$M_0(\omega)$ is the moment strengh. Setting the stress source tensor $\vec{\vec{\sigma}}_j$ to $\vec{0}$ in *(2.9.2f)*, the following expression holds for the normal wave source vector $\vec{\vec{s}}_0'^{\pm}$:

$$\vec{\vec{s}}_0'^{\pm} = \frac{j}{2} M_0(\omega)\,(0,\, k_x,\, k_y)^T\,. \qquad (2.9.4e)$$

A moment source in an isotropic homogeneous elastic medium only generates S waves.

Force source

Finally we consider a vertical body force point source of strength $f_0(\omega)$ localized at the origin :

$$\vec{f} = f_0(\omega)\,\big(0,\, 0,\, \delta(x)\, \delta(y)\, \delta(z)\big)^T\,, \qquad (2.9.5a)$$

Setting the stress source tensor to zero in *(2.9.2f)*, the following expression holds for the normal wave source vector $\vec{\vec{s}}_0'^{\pm}$:

$$\vec{\vec{s}}_0'^{\pm} = -\frac{1}{2} f_0(\omega) \left(-1,\, \pm\frac{k_y}{k_{z,s}},\, \mp\frac{k_x}{k_{z,s}}\right)^T\,. \qquad (2.9.5b)$$

A vertically oriented body force source emits both P and S waves.

CHAPTER 3

ONE-WAY WAVEFIELD DECOMPOSITION OF SURFACE SEISMIC DATA

3.1 INTRODUCTION

Multi-component sources emit three distinct wave-types with an amplitude that depends on the direction of propagation. Similarly, multi-component particle velocity detectors record without distinction all the upgoing and downgoing wave-types with a sensitivity that depends on the angle of incidence of the wavefield. In this chapter we show (using the equations of the wave propagation) how multi-component sources can be combined to simulate sources that only emit one wave-type. Similarly we also show how multi-component detectors can be combined to simulate detectors that are only sensitive to one wave-type (upgoing or downgoing). This chapter constitutes the theoretical justification of the wavefield decomposition of surface seismic data presented in section 1.3.

3.2 FORWARD MODEL OF MULTICOMPONENT SEISMIC DATA

Before we discuss the decomposition scheme we present a forward model of multi-component seismic data. The formulation we give here, is the same as the one developed in the article "*Decomposition of multi-component seismic data* ", see Wapenaar et al.,1990. We can show step by step that this forward model is obtained by applying a number of simple matrix manipulations to the primary one-way responses of the subsurface. An important consequence

is that decomposition of multicomponent seismic data may be accomplished by applying the same matrix manipulations in reverse order.

First we consider the forward model of the primary response of an elastic subsurface bounded by a reflection-free surface at z_0. With reference to *Figure 3.2.1a* we write:

$$\vec{p}^{-}(z_0) = \boldsymbol{X}(z_0)\vec{p}^{+}(z_0)\,, \qquad (3.2.1)$$

Here vector $\vec{p}^{+}(z_0)$ represents a 3D monochromatic downgoing elastic wavefield at z_0 (the matrix/vector notation for discretized wavefields is explained in Appendix 3A). This one-way wavefield propagates into the 3D subsurface $z>z_0$, is partly reflected by the inhomogeneities that can exist below this depth level and propagates back to the surface. The 3D upgoing wavefield arriving at the surface z_0 is denoted by $\vec{p}^{-}(z_0)$. According to *(3.2.1)* the primary one-way response matrix $\boldsymbol{X}(z_0)$ describes the relationship between the downgoing and upgoing one-way wavefields at z_0. To give a clear physical meaning to the one-way wave vector components we consider an isotropic homogeneous upper half-space, the derived equations staying of course valid for any anisotropic homogeneous upper half-space.

For an isotropic homogeneous upper half-space the one-way wavefield vectors $\vec{p}^{+}(z_0)$ and $\vec{p}^{-}(z_0)$ contain three sub-vectors, according to:

$$\vec{p}^{\pm}(z_0) = \begin{pmatrix} \vec{\phi}^{\pm}(z_0) \\ \vec{\psi}_1^{\pm}(z_0) \\ \vec{\psi}_2^{\pm}(z_0) \end{pmatrix}, \qquad (3.2.2a)$$

whereas the response matrix $\boldsymbol{X}(z_0)$ contains nine sub-matrices, according to :

$$\boldsymbol{X}(z_0) = \begin{pmatrix} \boldsymbol{X}_{\phi,\phi}(z_0) & \boldsymbol{X}_{\phi,\psi_1}(z_0) & \boldsymbol{X}_{\phi,\psi_2}(z_0) \\ \boldsymbol{X}_{\psi_1,\phi}(z_0) & \boldsymbol{X}_{\psi_1,\psi_1}(z_0) & \boldsymbol{X}_{\psi_1,\psi_2}(z_0) \\ \boldsymbol{X}_{\psi_2,\phi}(z_0) & \boldsymbol{X}_{\psi_2,\psi_1}(z_0) & \boldsymbol{X}_{\psi_2,\psi_2}(z_0) \end{pmatrix}, \qquad (3.2.2b)$$

Vectors $\vec{\phi}^{+}(z_0)$ and $\vec{\phi}^{-}(z_0)$ represent the potentials for the 3D monochromatic downgoing and upgoing compressional (P) waves at depth level z_0; vectors $\vec{\psi}_1^{+}(z_0)$, $\vec{\psi}_2^{+}(z_0)$ and $\vec{\psi}_1^{-}(z_0)$, $\vec{\psi}_2^{-}(z_0)$ represent the potentials for the downgoing and upgoing first and second shear (S_1,S_2) wave types at z_0. Any of the sub-matrices in *(3.2.2b)* represents a primary response of the elastic subsurface. For example, matrix $\boldsymbol{X}_{\phi,\psi_2}(z_0)$ describes the relationship between downgoing S_2 waves and upgoing P-waves at z_0. The one-way forward model *(3.2.1)* is visualized by the block diagram of *Figure 3.2.1b*.

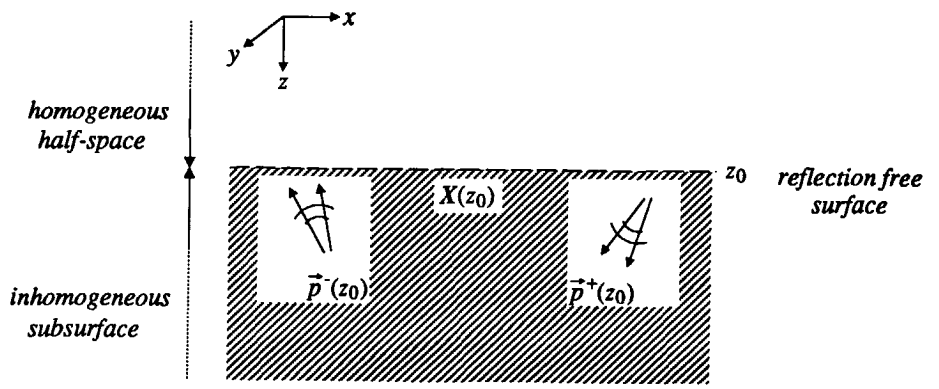

Figure 3.2.1a

The primary one-way response matrix $X(z_0)$ describes the relationship between primary downgoing and upgoing wavefields at the reflection free surface z_0.

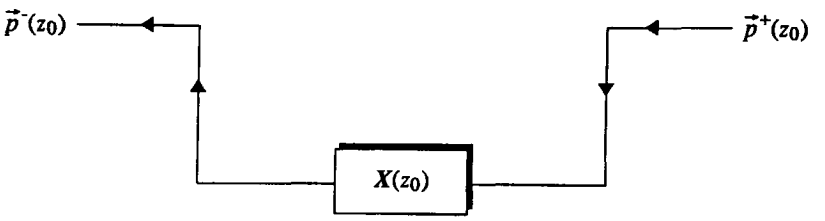

Figure 3.2.1b

One-way forward model of the primary response of an elastic subsurface bounded by a reflection free surface at z_0.

So far we have assumed that surface z_0 is reflection free. However in practical surface seismic situations, surface z_0 represents the Earth's traction free surface which is a perfect reflector for the upgoing waves $\vec{p}^{-}(z_0)$. Therefore in the forward model *(3.2.1)* we should write for the total downgoing wavefield at z_0:

$$\vec{p}^{+}(z_0) = \vec{p}_r^{+}(z_0) + \vec{p}_s^{+}(z_0) \,. \qquad (3.2.3a)$$

Here vector $\vec{p}_r^{+}(z_0)$ is the downgoing reflected wavefield at z_0, according to :

$$\vec{p}_r^{+}(z_0) = \boldsymbol{R}_{fr}^{-}(z_0)\, \vec{p}^{-}(z_0) \,, \qquad (3.2.3b)$$

where matrix $\boldsymbol{R}_{fr}^{-}(z_0)$ describes the reflectivity (including conversion) of the Earth's traction free surface for upgoing waves as has been described in *(2.8.1d)*. The relationship between $\vec{p}_s^{+}(z_0)$ and the seismic source at z_0 is discussed later.

Upon substitution of *(3.2.3ab)* into the forward model *(3.2.1)* we obtain the following implicit expression for the upgoing wavefield at z_0 :

$$\vec{p}^{-}(z_0) = \boldsymbol{X}(z_0)\left[\boldsymbol{R}_{fr}^{-}(z_0)\, \vec{p}^{-}(z_0) + \vec{p}_s^{+}(z_0)\right] , \qquad (3.2.4a)$$

see *Figure 3.2.2a* and *Figure 3.2.2b*. This expression can be rewritten explicitly, according to :

$$\vec{p}^{-}(z_0) = \boldsymbol{X}_{fr}(z_0)\, \vec{p}_s^{+}(z_0) \,, \qquad (3.2.4b)$$

where the free surface one-way response matrix $\boldsymbol{X}_{fr}(z_0)$is defined as :

$$\boldsymbol{X}_{fr}(z_0) = \left[\boldsymbol{I} - \boldsymbol{X}(z_0)\boldsymbol{R}_{fr}^{-}(z_0)\right]^{-1}\boldsymbol{X}(z_0) \,, \qquad (3.2.4c)$$

or, rewriting the inverse matrix as a series expansion ,

$$\boldsymbol{X}_{fr}(z_0) = \left[\boldsymbol{I} + \sum_{m=1}^{\infty}\left(\boldsymbol{X}(z_0)\boldsymbol{R}_{fr}^{-}(z_0)\right)^{m}\right]\boldsymbol{X}(z_0) \,. \qquad (3.2.4d)$$

The latter expression clearly shows that the free surface generates an infinite number of multiple reflections and conversions. This result is equivalent with the acoustic multiple series derived by Berkhout (1982).

Next we discuss the relationship between the one-way wavefields in the forward model *(3.2.4)* and the two-way seismic data. In analogy with *(2.6.2a)*, the general relationship between two-way and one-way elastic wavefields reads:

$$\begin{pmatrix} \vec{v}(z) \\ \vec{\tau}_z(z) \end{pmatrix} = \begin{pmatrix} \boldsymbol{L}_1^{+}(z) & \boldsymbol{L}_1^{-}(z) \\ \boldsymbol{L}_2^{+}(z) & \boldsymbol{L}_2^{-}(z) \end{pmatrix} \begin{pmatrix} \vec{p}^{+}(z) \\ \vec{p}^{-}(z) \end{pmatrix} , \qquad (3.2.5a)$$

where the three-component velocity and traction vectors $\vec{v}(z)$ and $\vec{\tau}_z(z)$ are defined according to:

$$\vec{v}(z) = \begin{pmatrix} \vec{v}_x(z) \\ \vec{v}_y(z) \\ \vec{v}_z(z) \end{pmatrix} , \qquad (3.2.5b)$$

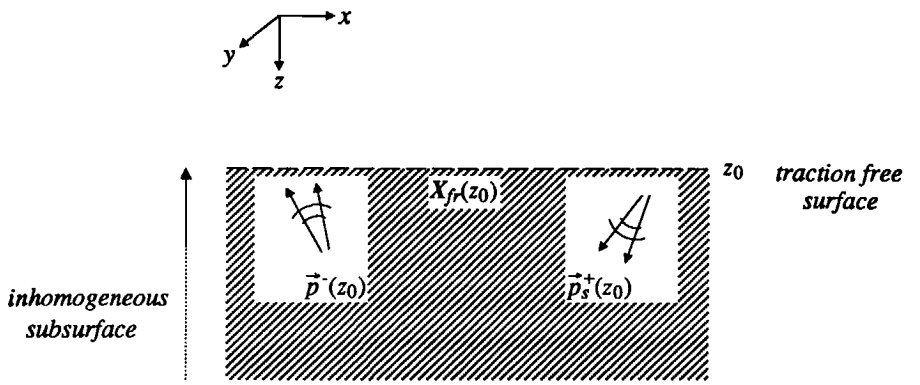

Figure 3.2.2a

The one-way response matrix $X_{fr}(z_0)$ for the traction free surface describes the relationship between the reflected upgoing and downgoing source wavefields at the traction free surface z_0.

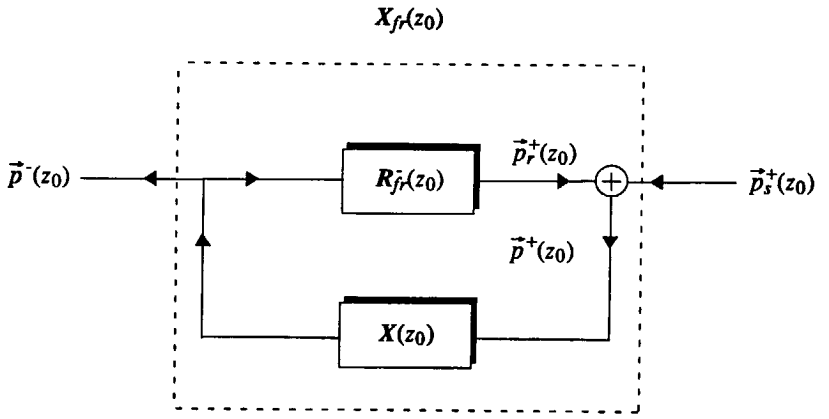

Figure 3.2.2b

One-way forward model, including surface-related multiple reflections and conversions.

and

$$\vec{\tau}_z(z) = \begin{pmatrix} \vec{\tau}_{xz}(z) \\ \vec{\tau}_{yz}(z) \\ \vec{\tau}_{zz}(z) \end{pmatrix}. \qquad (3.2.5c)$$

In the following we restrict ourselves, for an easier comprehension, to the situation where the sources and receivers are at the free surface see *Figure 3.2.3*. When the source is located at z_0, it only generates downgoing waves $\vec{p}_s^{+}(z_0)$in the subsurface.

Replacing *(3.2.3a)* in *(3.2.5a)* we obtain :

$$\vec{v}(z_0) = \boldsymbol{L}_1^{+}(z_0)\left[\vec{p}_r^{+}(z_0) + \vec{p}_s^{+}(z_0)\right] + \boldsymbol{L}_1^{-}(z_0)\vec{p}^{-}(z_0)\,, \qquad (3.2.6a)$$

and

$$\vec{\tau}_z(z_0) = \boldsymbol{L}_2^{+}(z_0)\left[\vec{p}_r^{+}(z_0) + \vec{p}_s^{+}(z_0)\right] + \boldsymbol{L}_2^{-}(z_0)\vec{p}^{-}(z_0)\,. \qquad (3.2.6b)$$

Substituting *(3.2.3b)* in *(3.2.6ab)* we can write :

$$\vec{v}(z_0) = \vec{v}_r(z_0) + \vec{v}_s(z_0)\,, \qquad (3.2.6c)$$

and

$$\vec{\tau}_z(z_0) = \vec{\tau}_{z,r}(z_0) + \vec{\tau}_{z,s}(z_0)\,, \qquad (3.2.6d)$$

with,

$$\vec{v}_r(z_0) = \left[\boldsymbol{L}_1^{+}(z_0)\boldsymbol{R}_{fr}^{-}(z_0) + \boldsymbol{L}_1^{-}(z_0)\right]\vec{p}^{-}(z_0), \qquad (3.2.6e)$$

$$\vec{v}_s(z_0) = \boldsymbol{L}_1^{+}(z_0)\,\vec{p}_s^{+}(z_0)\,, \qquad (3.2.6f)$$

$$\vec{\tau}_{z,r}(z_0) = \left[\boldsymbol{L}_2^{+}(z_0)\boldsymbol{R}_{fr}^{-}(z_0) + \boldsymbol{L}_2^{-}(z_0)\right]\vec{p}^{-}(z_0)\,, \qquad (3.2.6g)$$

$$\vec{\tau}_{z,s}(z_0) = \boldsymbol{L}_2^{+}(z_0)\vec{p}_s^{+}(z_0)\,. \qquad (3.2.6h)$$

Equation *(3.2.6c)* corresponds to a separation of the total particle velocity field at z_0 in a part $\vec{v}_s(z_0)$, directly generated at the surface by the source, and in a part $\vec{v}_r(z_0)$, generated at the traction free acquisition surface by the upgoing reflected waves $\vec{p}^{-}(z_0)$. $\vec{v}_s(z_0)$ corresponds to the direct waves; in the case of a surface source it contains the direct *P* and *S* waves as well as the non-dispersive Rayleigh surface waves. In the case of a homogeneous subsurface $\vec{v}_r(z_0)$ equals $\vec{0}$, the particle velocity field simplifies then to the direct waves. Similarly equation *(3.2.6d)* corresponds to a separation of the traction vector at z_0 in a part $\vec{\tau}_{z,s}(z_0)$, due to the applied traction source, and in a part $\vec{\tau}_{z,r}(z_0)$, generated by the upgoing reflected wavefield reaching the surface. As we consider a traction free acquisition surface we have:

$$\vec{\tau}_{z,r}(z_0) = \vec{0}\,. \qquad (3.2.6i)$$

The combination of *(3.2.6g)* with *(3.2.6i)* leads to the following expression for $\boldsymbol{R}_{fr}^{-}(z_0)$:

$$\boldsymbol{R}_{fr}^{-}(z_0) = -\left[\boldsymbol{L}_2^{+}(z_0)\right]^{-1}\boldsymbol{L}_2^{-}(z_0)\,, \qquad (3.2.6j)$$

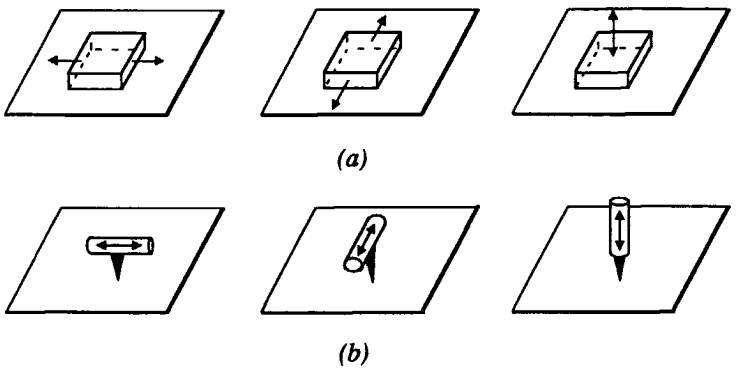

Figure 3.2.3

Multicomponent data acquisition

a) Three differently oriented seismic vibrators imposing tractions along the x-, y- and z-direction to the earth's surface.

b) Three differently oriented geophones, measuring the x-, y- and z- components of the particle velocity at the earth's surface.

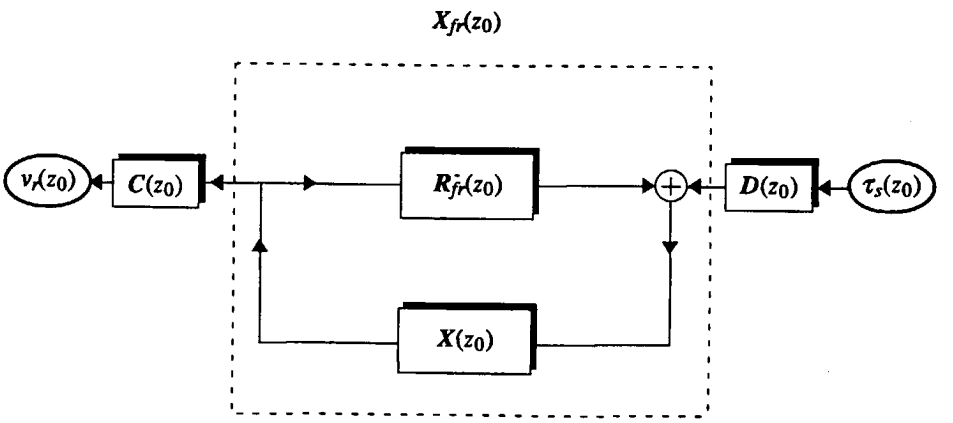

Figure 3.2.4

Forward model for multicomponent seismic data (the direct waves are ignored).

which is in agreement with the result *(2.8.1d)*.

We define a source-decomposition operator $\boldsymbol{D}(z_0)$, which describes the relationship between the traction source vector $\vec{\tau}_{z,s}(z_0)$at the traction free surface and the downgoing source wave vector $\vec{p}_s^{+}(z_0)$ according to :

$$\vec{p}_s^{+}(z_0) = \boldsymbol{D}(z_0)\,\vec{\tau}_{z,s}(z_0)\,. \qquad (3.2.7a)$$

Combining *(3.2.7a)* with *(3.2.6h)*, the source-decomposition operator reads :

$$\boldsymbol{D}(z_0) = \left[\boldsymbol{L}_2^{+}(z_0)\right]^{-1}. \qquad (3.2.7b)$$

We also define a receiver-composition operator $\boldsymbol{C}(z_0)$ which describes the particle velocities generated at the traction free surface $\vec{v}_r(z_0)$, by the upgoing wavefield $\vec{p}^{-}(z_0)$, according to :

$$\vec{v}_r(z_0) = \boldsymbol{C}(z_0)\,\vec{p}^{-}(z_0)\,. \qquad (3.2.8a)$$

Combining *(3.2.8a)* with *(3.2.6e)* and *(3.2.6j)*, the receiver-composition operator reads :

$$\boldsymbol{C}(z_0) = -\,\boldsymbol{L}_1^{+}(z_0)\left[\boldsymbol{L}_2^{+}(z_0)\right]^{-1}\boldsymbol{L}_2^{-}(z_0) + \boldsymbol{L}_1^{-}(z_0)\,, \qquad (3.2.8b)$$

or according to *(2.6.5a)*,

$$\boldsymbol{C}(z_0) = \left[\boldsymbol{M}_1^{-}(z_0)\right]^{-1}. \qquad (3.2.8c)$$

Note that the one-way forward model *(3.2.4b)* may be elegantly combined with the decomposition and composition operators *(3.2.7a)* and *(3.2.8a)* yielding:

$$\vec{v}(z_0) = \boldsymbol{C}(z_0)\boldsymbol{X}_{fr}(z_0)\boldsymbol{D}(z_0)\,\vec{\tau}_{z,s}(z_0) + \vec{v}_s(z_0)\,, \qquad (3.2.9a)$$

or suppressing the direct wave from the data :

$$\vec{v}_r(z_0) = \boldsymbol{C}(z_0)\boldsymbol{X}_{fr}(z_0)\boldsymbol{D}(z_0)\,\vec{\tau}_{z,s}(z_0)\,, \qquad (3.2.9b)$$

see also *Figure 3.2.4*. From right to left *(3.2.9b)* contains a source vector (describing the traction distribution of a seismic vibrator at the free surface), a decomposition matrix (transforming the traction into downgoing one-way waves), a one-way response matrix (describing the response of the subsurface, including multiple reflections and conversions related to the free surface), and a composition matrix (transforming the upgoing one-way waves into velocities at the traction free surface). We may conclude that *(3.2.9b)* is the forward model of one (monochromatic) multicomponent shot record, ignoring direct waves. For a point source of tensile stress (vertical vibrator), vector $\vec{\tau}_{zz,s}(z_0)$ contains only one non-zero element, its value representing the source signature $s(\omega)$. Similarly, for a point source of shearing stress (a horizontal vibrator), one of the vectors $\vec{\tau}_{xz,s}(z_0)$ or $\vec{\tau}_{yz,s}(z_0)$ contains only one non-zero element, its value representing $s(\omega)$. When the vibrators are not ideal point sources, the source vector contains the stress distribution at z_0. The forward model for one shot record can be extended easily to a forward model for a complete seismic survey. Ideally, in the elastic

situation three independent seismic experiments should be carried out for each source position by applying three differently oriented seismic vibrators. For a *3×3* component seismic survey the extended forward model reads.

$$\boldsymbol{V}_r(z_0) = \boldsymbol{C}(z_0)\, \boldsymbol{X}_{fr}(z_0)\, \boldsymbol{D}(z_0)\, \boldsymbol{\mathcal{T}}_{z,s}(z_0)\,. \tag{3.2.10a}$$

Here the columns of the data matrix $\boldsymbol{V}_r(z_0)$ contain the different data vectors $\vec{v}_r(z_0)$. The columns of the source matrix $\boldsymbol{\mathcal{T}}_{z,s}(z_0)$ contain the corresponding source vectors $\vec{\tau}_{z,s}(z_0)$. When use is made of independent horizontal and vertical vibrators (*Figure 3.3*) then the source vectors can be ordered in such a way that the source matrix can be written as:

$$\boldsymbol{\mathcal{T}}_{z,s}(z_0) = \begin{pmatrix} \mathcal{T}_{xz,s}(z_0) & 0 & 0 \\ 0 & \mathcal{T}_{yz,s}(z_0) & 0 \\ 0 & 0 & \mathcal{T}_{zz,s}(z_0) \end{pmatrix}. \tag{3.2.10b}$$

Moreover, for identical point sources this expression may be further simplified to:

$$\boldsymbol{\mathcal{T}}_{z,s}(z_0) = s(\omega)\, \boldsymbol{I}\,. \tag{3.2.10c}$$

Now *(3.2.10a)* may be replaced by :

$$\boldsymbol{V}_r(z_0) = \boldsymbol{C}(z_0)\, \boldsymbol{X}^s_{fr}(z_0)\, \boldsymbol{D}(z_0)\,, \tag{3.2.11a}$$

with,

$$\boldsymbol{X}^s_{fr}(z_0) = s(\omega)\, \boldsymbol{X}_{fr}(z_0)\,, \tag{3.2.11b}$$

and

$$\boldsymbol{V}_r(z_0) = \begin{pmatrix} V_{x,x}(z_0) & V_{x,y}(z_0) & V_{x,z}(z_0) \\ V_{y,x}(z_0) & V_{y,y}(z_0) & V_{y,z}(z_0) \\ V_{z,x}(z_0) & V_{z,y}(z_0) & V_{z,z}(z_0) \end{pmatrix}. \tag{3.2.11c}$$

Here any of the submatrices $\boldsymbol{V}_{i,j}(z_0)$ for $i=x,y,z$ and $j=x,y,z$ represents a (monochromatic) single-component seismic survey, carried out with geophones oriented in the i- direction and vibrators oriented in the j- direction. The purpose of this section was to present how a two-way seismic experiment can be written as a sequence of basic one-way operations thus providing a starting point for a systematic discussion of the surface-related processing scheme.

3.3 DECOMPOSITION OF SURFACE SEISMIC DATA

Assume that a *3×3* component seismic survey has been carried out. When the different vibrators are oriented in arbitrary directions, then mutually perpendicular vibrators should be simulated by applying a weighted summation of the different responses. A similar remark can be made for the geophones (Cliet and Dubesset,1984). Before the decomposition can be carried out, the direct waves $\vec{v}_s(z_0)$, should be removed from the data. We do not discuss this procedure, a good reference is Beresford-Smith and Rango (1989) and Mc Mechan (1991). By

applying a Fourier transform to each trace, the data are decomposed into monochromatic seismic surveys. Any of those monochromatic surveys satisfies the forward model described in the previous section. Our starting point for the discussion of the elastic decomposition scheme is *(3.2.11a)*, which is the forward model of a monochromatic multi-experiment multi-offset multi-component seismic data, excluding the direct waves. Assuming that the source signature $s(\omega)$ is unknown, the scaled free one-way response matrix can be obtained from the seismic data $\boldsymbol{V}_r(z_0)$ by inverting *(3.2.11a)* yielding:

$$\boldsymbol{X}^s_{fr}(z_0) = [\boldsymbol{C}(z_0)]^{-1}\, \boldsymbol{V}_r(z_0)\, [\boldsymbol{D}(z_0)]^{-1}\,, \tag{3.3.1a}$$

where,

$$[\boldsymbol{D}(z_0)]^{-1} = \boldsymbol{L}^+_2(z_0)\,, \tag{3.3.1b}$$

and

$$[\boldsymbol{C}(z_0)]^{-1} = \boldsymbol{M}^-_1(z_0)\,. \tag{3.3.1c}$$

The decomposition of the two-way seismic data into normal one-way wave responses may be carried out by applying the matrix operator $[\boldsymbol{C}(z_0)]^{-1}$ and $[\boldsymbol{D}(z_0)]^{-1}$ to the data matrix, see *Figure 3.3.1*. Note that $[\boldsymbol{C}(z_0)]^{-1}\boldsymbol{V}_r(z_0)$ describes a lateral deconvolution process along the columns (i.e, the monochromatic common shot records) of matrix $\boldsymbol{V}_r(z_0)$. This accounts for the decomposition of the received wavefields into upgoing one-way waves. We name this process "*decomposition at the receiver side*" and accordingly $[\boldsymbol{C}(z_0)]^{-1}$ "*decomposition operator at the receiver side*". Similarly, $\boldsymbol{V}_r(z_0)[\boldsymbol{D}(z_0)]^{-1}$ describes a lateral deconvolution process along the rows (i.e the monochromatic common receiver records) of matrix $\boldsymbol{V}_r(z_0)$. This accounts for the composition of the emitted wavefields into downgoing one-way waves. We name this process "*composition at the source side*" and accordingly $[\boldsymbol{D}(z_0)]^{-1}$ "*composition operator at the source side*". In the case of an homogeneous medium at the source and receiver side these operations can be done in the wavenumber domain, convolutions are replaced by multiplications.

Note the important similarity of the wavefield decomposition *(3.3.1a)* with Berkhout's formulation of prestack inverse wavefield extrapolation, which is the nucleus of prestack migration (Berkhout,1982). Hence, the practical implementation of a decomposition scheme is very similar to the practical implementation of a prestack migration scheme. Like prestack migration, decomposition as formulated by *(3.3.1a)* fully accounts for lateral variations of the medium parameters.

In analogy with *(3.2.2b)* the decomposed data matrix $\boldsymbol{X}^s_{fr}(z_0)$ may be written as :

$$\boldsymbol{X}^s_{fr}(z_0) = \begin{pmatrix} X_{\phi,\phi}(z_0) & X_{\phi,\psi_1}(z_0) & X_{\phi,\psi_2}(z_0) \\ X_{\psi_1,\phi}(z_0) & X_{\psi_1,\psi_1}(z_0) & X_{\psi_1,\psi_2}(z_0) \\ X_{\psi_2,\phi}(z_0) & X_{\psi_2,\psi_1}(z_0) & X_{\psi_2,\psi_2}(z_0) \end{pmatrix}^{(s)}_{fr}\,. \tag{3.3.2}$$

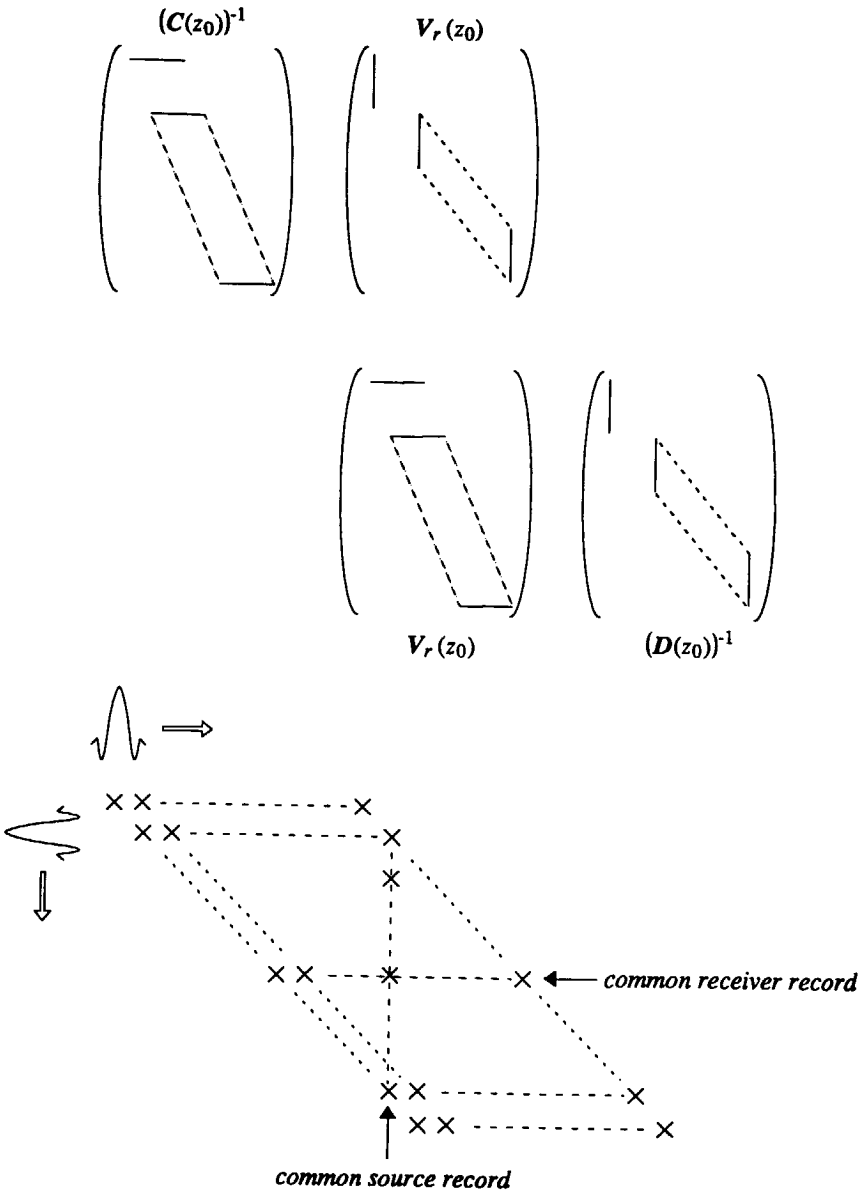

Figure 3.3.1

According to (3.3.1a), decomposition into normal one-way responses involves lateral deconvolution processes along the receivers in each common shot record and along the sources in each common receiver record. Note that the same principle holds for prestack inverse wavefield extrapolation, as applied in depth migration.

Any of the submatrices simulates a (monochromatic) single-component one-way seismic survey at the free surface. Matrices $\left(X_{\phi,\phi}(z_0)\right)_{fr}^{(s)}$ and $\left(X_{\phi,\psi_\alpha}(z_0)\right)_{fr}^{(s)}$ for $\alpha=1,2$ represent seismic surveys in terms of received upgoing P-waves related to sources in terms of downgoing S_1- or S_2- waves. Similarly, matrices $\left(X_{\psi_\beta,\phi}(z_0)\right)_{fr}^{(s)}$ and $\left(X_{\psi_\beta,\psi_\alpha}(z_0)\right)_{fr}^{(s)}$ for $\beta=1,2$ and $\alpha=1,2$ represent seismic surveys in terms of received upgoing S_1- or S_2- waves related to sources in terms of downgoing P-waves or downgoing S_1- or S_2- waves. In *Figure 3.3.2a* the situation is shown for one element of matrix $\left(X_{\phi,\phi}(z_0)\right)_{fr}^{(s)}$. Similarly, in *Figure 3.3.2b,c,d* the situation is shown for the corresponding elements in matrices $\left(X_{\psi_y,\phi}(z_0)\right)_{fr}^{(s)}$, $\left(X_{\phi,\psi_y}(z_0)\right)_{fr}^{(s)}$ and $\left(X_{\psi_y,\psi_y}(z_0)\right)_{fr}^{(s)}$, respectively.

We illustrate the elastic decomposition procedure with a 2D example. For the subsurface configuration shown in *Figure 3.3.3* we generated 128 multi-component seismic shot records by finite-difference modeling (Kelly et al.,1976; Haimé,1987). We used vertical and horizontal vibrators as well as vertical and horizontal geophones at the free surface z_0. *Figure 3.3.4* shows the source and receiver configuration used for this experiment. One multicomponent shot record is shown in the space-time domain in *Figure 3.3.5*. In the case we use a vertical traction source $\tau_{zz,s}$ and vertical particle velocity detectors v_z, we call the data panel recorded with such a configuration a pseudo P-P panel. For vertically propagating waves this source only emits P waves and the detectors only record P waves. As this is only true for vertically propagating waves we have a pseudo P-P data panel. *Figure 3.3.6* shows the same multi-component shot record after removal of the direct wave. All multicomponent shot records are transformed from the time domain to the frequency domain, yielding a data matrix $\boldsymbol{V}_r(z_0)$ for each frequency in the seismic band ($5\text{Hz} < f=(\omega/2\pi) < 80$ Hz). Next we apply the decomposition at the receiver side (*Figure3.3.7*) followed by the decomposition at the source side (*Figure3.3.8*). *Figure 3.3.8* represents one multicomponent shot record after full decomposition. Note that the spurious events, indicated by the arrows in *Figure 3.3.6* have vanished completely. After the decomposition has been carried out, the scaled multicomponent one-way response matrix at the traction free surface $\boldsymbol{X}_{fr}^{(s)}(z_0)$, is available for all frequencies in the seismic band. This response matrix contains significant multiple reflections and conversions related to the free surface, see *Figure 3.12*. They can be removed following the multiple elimination scheme proposed by Berkhout (1982) and Verschuur et al. (1990), yielding the primary one-way response $\boldsymbol{X}(z_0)$ of the subsurface, see *Figure 3.3.9*.and *Figure 3.3.10*. The proposed decomposition procedure is valid for any inhomogeneous anisotropic subsurface. An interesting aspect of this procedure is that no knowledge of the subsurface is required, the subsurface may have any degree of complexity. In the decomposition algorithm *(3.3.1a)* the matrices $\boldsymbol{C}(z_0)$ and $\boldsymbol{D}(z_0)$ are fully determined by the medium parameters at the free surface. For the anisotropic situation they can be computed numerically, for the isotropic situation we have their analytic solution. In the next section we discuss in details the physical meaning and the properties of the decomposition operators at the source and receiver side.

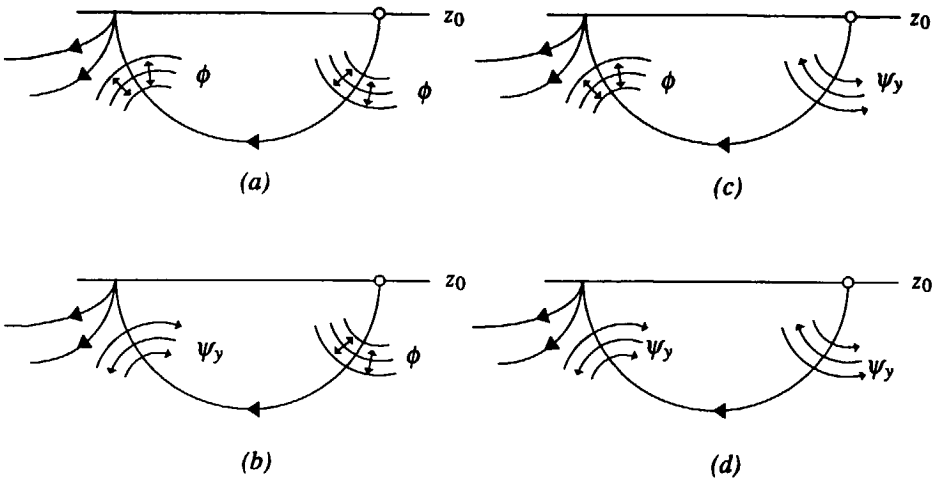

Figure 3.3.2

2D visualization of decomposed data at a free surface z_0.

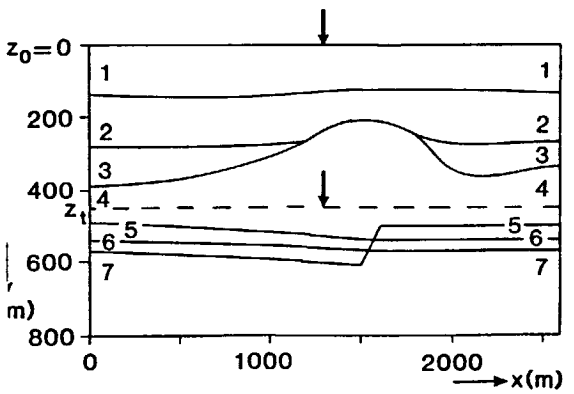

Layer	Cp(m/s)	Cs(m/s)	ρ(kg/m³)
1	2400	1400	1000
2	3000	2000	1600
3	3000	2000	2100
4	4100	2200	2200
5	3700	2000	2300
6	4200	2400	2000
7	3500	2100	1800

Figure 3.3.3

2D inhomogeneous elastic subsurface. The multicomponent vibrators and geophones are located at the free surface $z_0 = 0m$.

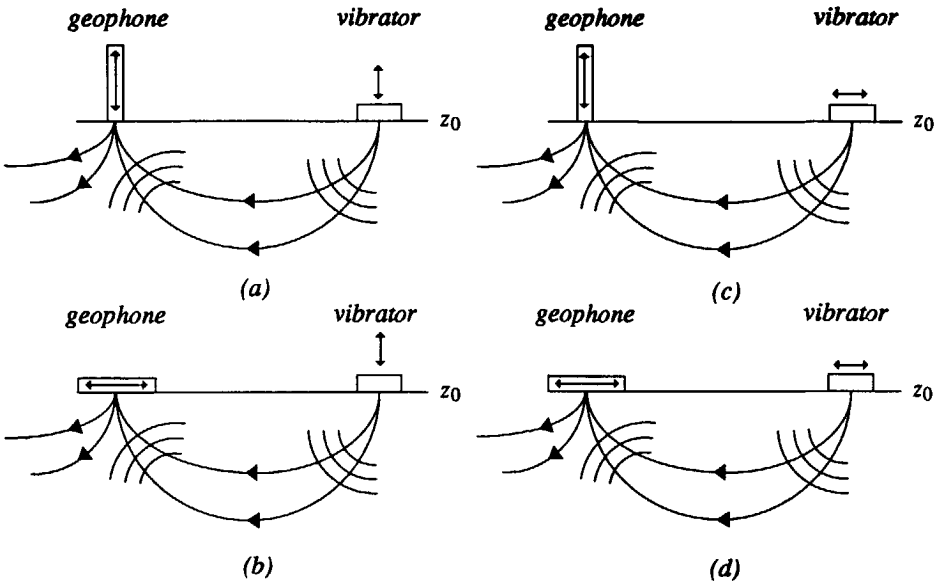

Figure 3.3.4

2D visualization of multicomponent data acquisition at a traction free surface z0. The double raypaths symbolically represent P- and S- waves

3.4 WAVEFIELD DETECTION IN SURFACE SEISMICS

The decomposition operator at the receiver side enables to obtain the upgoing normal one-way wavefield components reaching the traction free surface from the measured particle velocities. Thus, the inverse of this operator enables to study the conditions of detection of the elastic wavefield by particle velocity detectors in surface seismics. Expression *(3.2.8a)* establishes that the particle velocity detectors sensitivity to upgoing normal one-way plane waves is described by the receiver-composition operator $C(z_0)$. In the wavenumber-frequency domain we have :

$$\vec{\tilde{v}}_r(z_0) = \tilde{C}(z_0)\,\vec{\tilde{p}}^{-}(z_0)\,, \qquad (3.4.1a)$$

with,

$$\tilde{C}(z_0) = \left[\tilde{M}_1^{-}(z_0)\right]^{-1}\,, \qquad (3.4.1b)$$

or using *(2.6.5a)* and *(2.8.1d)*,

$$\tilde{C}(z_0) = \tilde{L}_1^{-}(z_0) + \tilde{L}_1^{+}(z_0)\,\tilde{R}_{fr}^{-}(z_0). \qquad (3.4.1c)$$

The last expression makes clear that the receiver-composition operator takes into account the

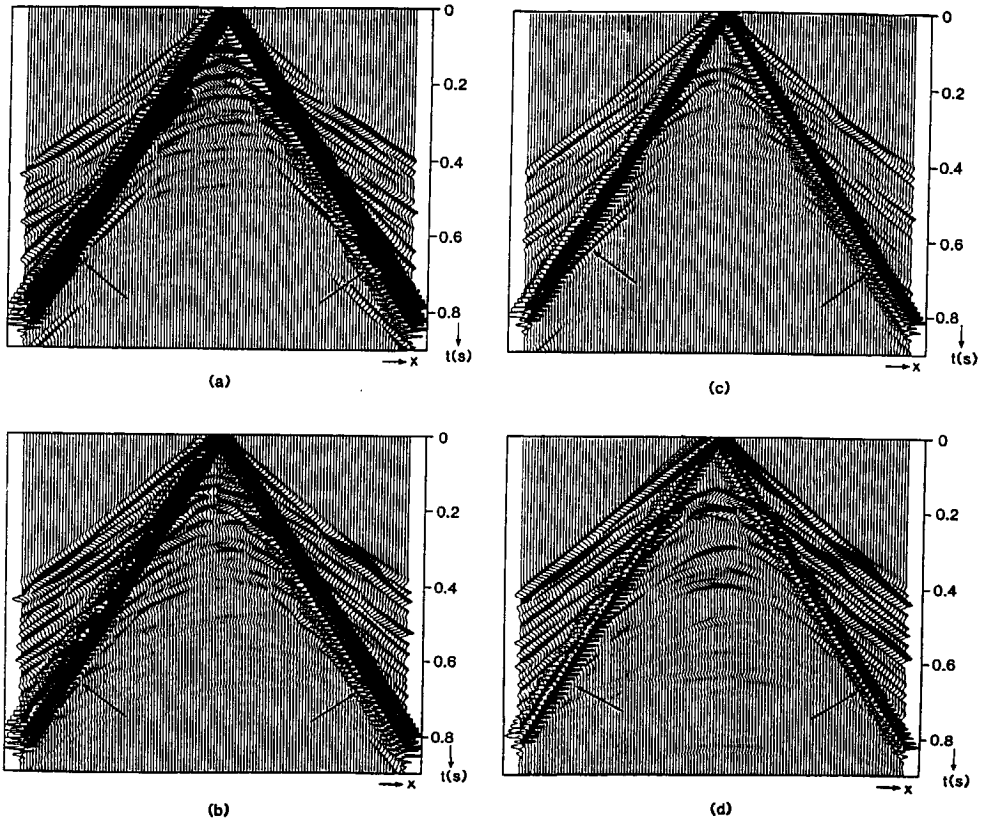

Figure 3.3.5

Multicomponent shot record. The source position is indicated by the arrow in Figure 3.3.3
a) pseudo P receiver-pseudo P source *c) pseudo P receiver-pseudo S_y source*
b) pseudo S_y receiver-pseudo P source *d) pseudo S_y receiver-pseudo S_y source*
The arrows indicate the ground-roll, being non dispersive here as the near surface medium is homogeneous. The amplitude of the ground-roll is much higher that the one of the body waves for three reasons:

-The ground roll consists of evanescent horizontally propagating P and S waves, its geometrical spreading is less than that of body waves.

-Traction sources applied on a traction free surface generate high amplitude Rayleigh waves.

-The sensitivity of the particle velocity detectors put on a traction free surface is high for waves propagating with the horizontal slowness of the Rayleigh waves.

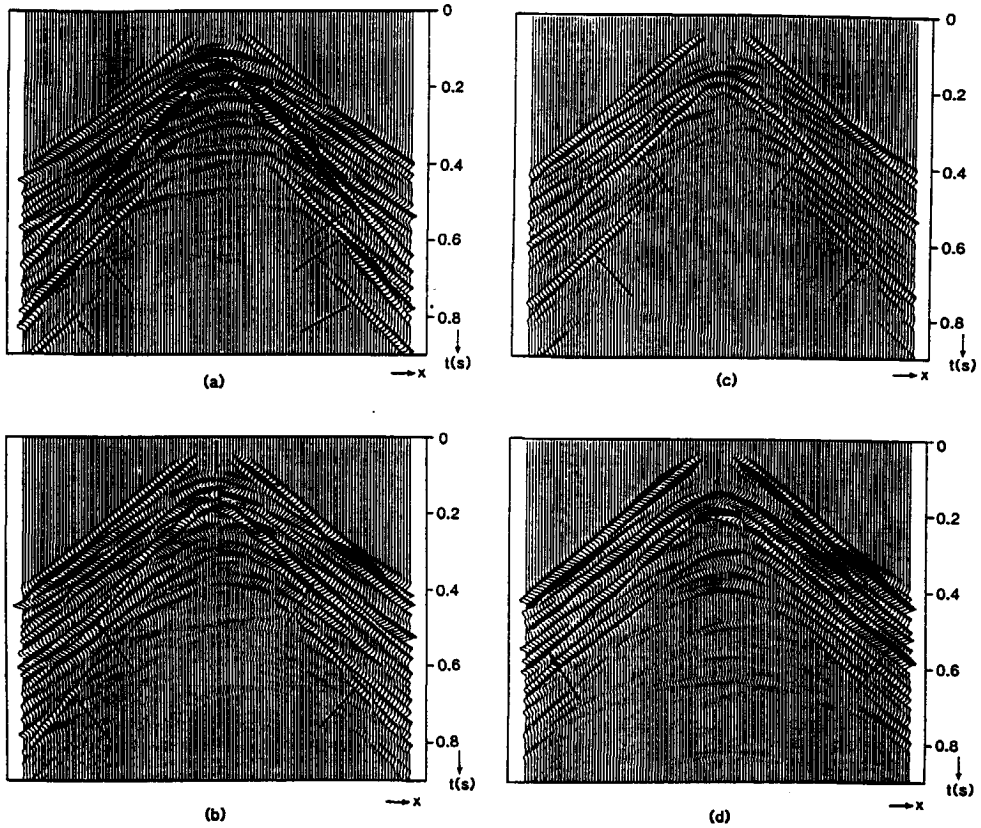

Figure 3.3.6

Multicomponent shot record of Figure 3.3.5 after removal of the ground-roll
a) pseudo P receiver-pseudo P source *c) pseudo P receiver-pseudo S_y source*
b) pseudo S_y receiver-pseudo P source *d) pseudo S_y receiver-pseudo S_y source*
The arrows indicate some events that would not be in the sections if instead of the pseudo P and S_y sources and detectors we had use the true ones.

These figures clearly illustrate that traction sources emit both P and S waves and that particle velocity detectors are both sensitive to incident P and S waves. The amplitude variations along the reflection curves is an illustration of the directivity of the sources and of the sensitivity of the particle velocity detectors to the direction of propagation.

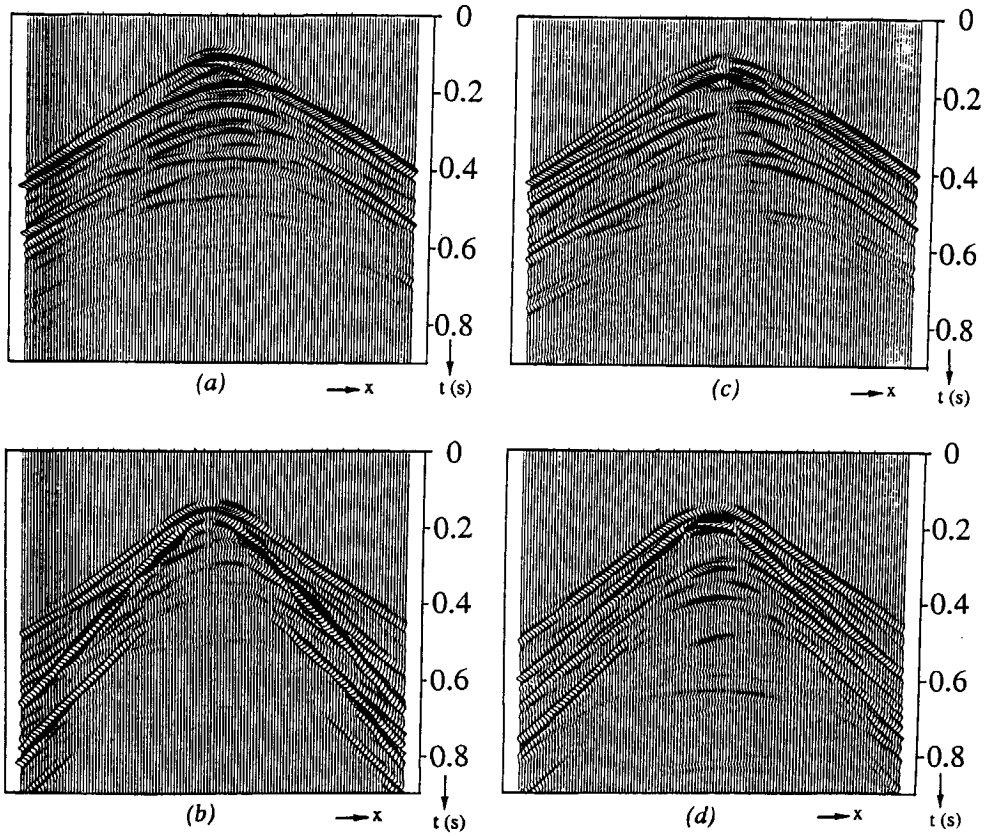

Figure 3.3.7

Multicomponent shot record of Figure 3.3.6 after decomposition at the receiver side into upgoing one-way P- and S_y- wave responses

a) true P receiver-pseudo P source

b) true S_y receiver-pseudo P source

c) true P receiver-pseudo S_y source

d) true S_y receiver-pseudo S_y source

These sections represent the data that would have been recorded if instead of the particle velocity detectors we had used detectors that only record upgoing P or upgoing S waves. The comparison of Figures 3.3.6 and 3.3.7 already shows how the decomposition at the receiver side simplifies the original seismic sections without loss of information.

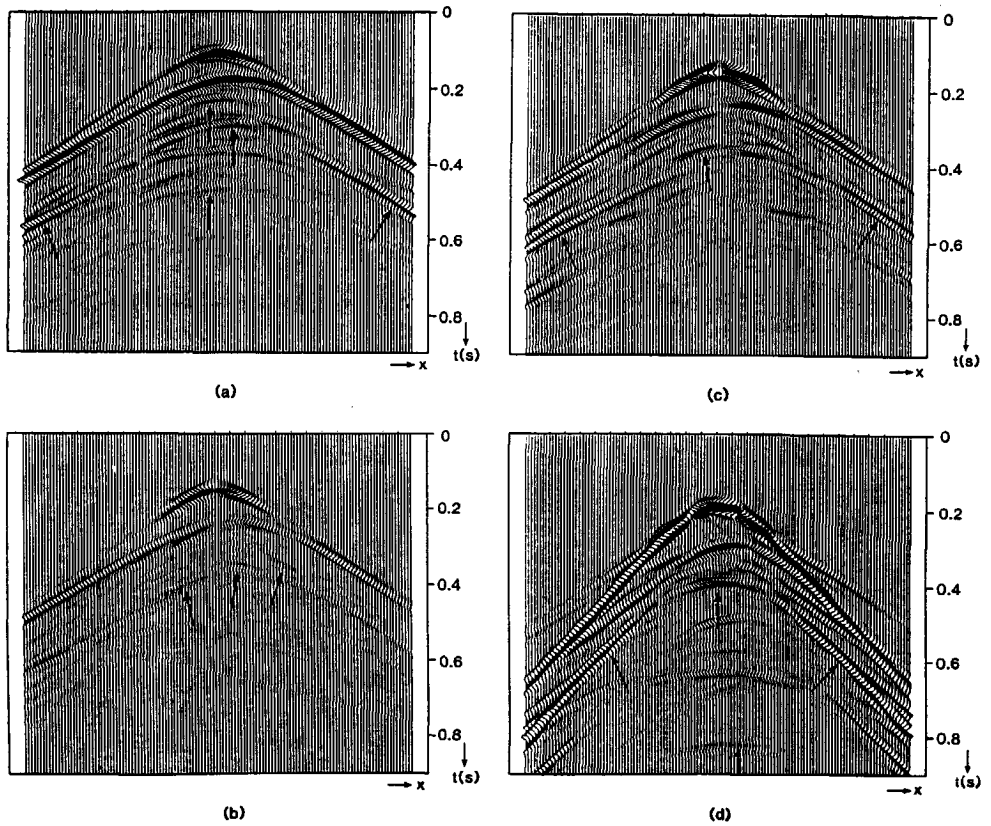

Figure 3.3.8

Multi component shot record after decomposition into one-way P- and Sy- wave responses, see Figure 3.3.2

a) true P receiver-true P source *c) true P receiver-true S_y source*

b) true S_y receiver-true P source *d) true S_y receiver-true S_y source*

The arrows indicate surface-related reflections and conversions.

These sections represent the previous data if instead of traction sources we had used pure downgoing P and S wave sources with a dipole directivity. When we compare these sections with the original ones (figure 3.3.6) we are aware of the importance of the sources and of the detectors on the data organization in the seismic sections. The decomposed sections already look simpler than the original ones, they can be further simplified (without loss of information) by removing the surface related multiples.

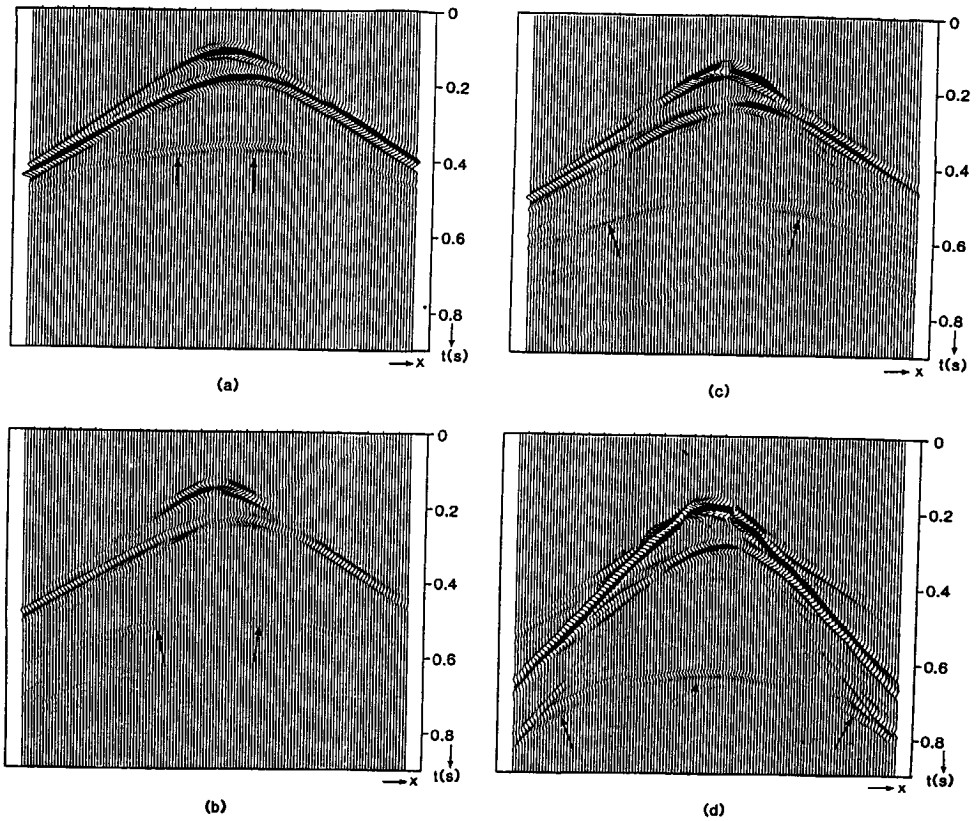

Figure 3.3.9

Multicomponent shot record, after elastic multiple elimination

a) true P receiver-true P source *c) true P receiver-true S_y source*

b) true S_y receiver-true P source *d) true S_y receiver-true S_y source*

The arrows indicate the response of the target reflectors below $z_t = 450m$

These seismic sections obtained after wavefield decomposition at the source and receiver side and after removal of the surface related multiples constitute the output of the surface related processing step in the DELPHI scheme. Starting from these sections further processing like migration and angle dependent imaging can be done in a scalar oriented way instead of the initial vector oriented way.

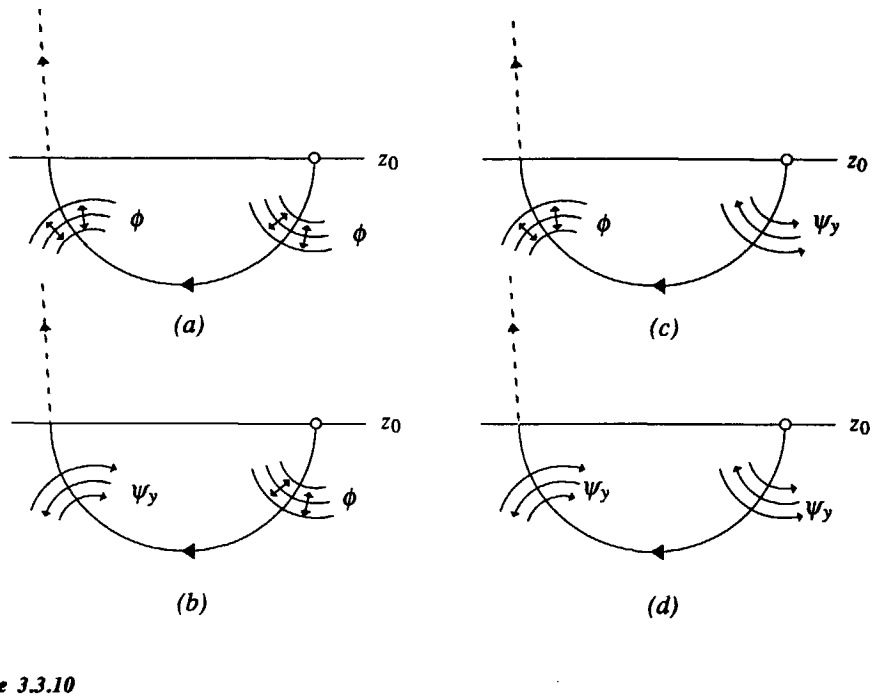

Figure 3.3.10

2D visualization of decomposed data at a reflection-free surface z_0 (after surface related elastic multiple elimination).

particle velocity field $\tilde{L}_1^-(z_0)\,\vec{\tilde{p}}^{\,-}(z_0)$, generated by the upgoing normal one-way wavefield, as well as the particle velocity field $\tilde{L}_1^+(z_0)\,\tilde{R}_{fr}^-(z_0)\,\vec{\tilde{p}}^{\,-}(z_0)$ generated by the downgoing reflected normal one-way wavefield.

Let us now describe in detail the receiver-composition operator for an isotropic medium. The first column of $\tilde{C}(z_0)$ contains the particle velocity vector $\vec{\tilde{v}}_p$, generated at the traction free surface z_O by an upgoing unit amplitude zero-phase plane P wave. Similarly the second and third column of $\tilde{C}(z_0)$ contain the particle velocity vectors $\vec{\tilde{v}}_{S1}$ and $\vec{\tilde{v}}_{S2}$, respectively generated by an upgoing unit amplitude zero-phase S_1 and S_2 plane wave. Using expression *(2.7.13d)* for the matrix $\tilde{M}_1^-(z_0)$,we have :

$$\begin{array}{cccc} & \vert\ v_x\ \vert\vert & v_y\ \vert\vert & v_z\ \vert \\ \vec{\tilde{v}}_p = [\tilde{C}_{11}, \tilde{C}_{21}, \tilde{C}_{31}]^T = \frac{\omega}{\mu}\frac{2k_{z,p}}{\Delta(k_r)} & [2k_xk_{z,s} & ,2k_yk_{z,s} & ,-(k_s^2-2k_r^2)]^T, \end{array} \qquad (3.4.2a)$$

$$\vec{\tilde{v}}_{Sv} = [\tilde{C}_{12}, \tilde{C}_{22}, \tilde{C}_{32}]^T = \frac{\omega}{\mu}\frac{2jk_{z,s}}{k_r\Delta(k_r)}[-k_x\,(k_s^2-2k_r^2)\,,\ -k_y\,(k_s^2-2k_r^2)\,,\ -2k_{z,p}k_r^2\,]^T, \qquad (3.4.2b)$$

$$\begin{array}{cccc} & \vert\ v_x\ \vert\vert & v_y\ \vert\vert & v_z\ \vert \\ \vec{\tilde{v}}_{Sh} = [\tilde{C}_{13}, \tilde{C}_{23}, \tilde{C}_{33}]^T = \frac{2\omega}{\mu}\frac{1}{k_s^2k_r} & [k_y & ,-k_x & ,0\ ]^T, \end{array} \qquad (3.4.2c)$$

with,

$$k_r^2 = k_x^2 + k_y^2 \,, \tag{3.4.2d}$$

and

$$\Delta(k_r) = 4k_{z,p}k_{z,s}k_r^2 + \left(k_s^2 - 2k_r^2\right)^2 \,. \tag{3.4.2e}$$

Looking at *(3.4.2)* we note that the particle velocity detectors are particularly sensitive to "upgoing" P and S_V plane wave when $\Delta(k_r)=0$. We recognize in $\Delta(k_r)$ the Rayleigh denominator, that vanishes for $k_r = \pm k_R$ with $k_R=\omega/c_r$, c_r being the Rayleigh wave propagating velocity. This explains one of the reasons why Rayleigh waves appear so strong compared to the body waves when the wavefield is recorded on the traction free surface by particle velocity detectors.

Remark: the scaling factors in front of expressions 3.4.2 depend on the definition of the P and S wave potentials.

To simplify the study of the sensitivity of the particle velocity detectors to the angle of incidence of the upgoing P and S plane waves, we restrict ourself to the two-dimensional situation. Then, we only have plane waves of the type $(k_x,k_y=0,\omega)$ with $k_x = \omega\, sin\theta_p/c_p$ for the P waves and $k_x = \omega\, sin\theta_s/c_s$ for the S waves. Choosing $k_r=k_x$, the following results are obtained:

$$\vec{\tilde{v}}_P = \frac{2c_p}{\mu}\left[\frac{sin2\theta_p}{\Delta_p(\theta_p)}\sqrt{\frac{c_p^2}{c_s^2} - sin^2\theta_p}\,,\quad 0\quad ,\, -\frac{cos\theta_p}{\Delta_p(\theta_p)}\left(\frac{c_p^2}{c_s^2} - 2sin^2\theta_p\right)\right]^T , \tag{3.4.3a}$$

$$\vec{\tilde{v}}_{SV} = \frac{-2jc_s}{\mu}\left[\frac{cos\theta_s\, cos2\theta_s}{\Delta_s(\theta_s)}\quad ,\quad 0\quad ,\quad \frac{sin2\theta_s}{\Delta_s(\theta_s)}\sqrt{\frac{c_s^2}{c_p^2} - sin^2\theta_s}\right]^T , \tag{3.4.3b}$$

$$\vec{\tilde{v}}_{Sh} = -\frac{2}{\rho\omega}[0\quad ,\quad 1\quad ,\quad 0]^T . \tag{3.4.3b}$$

$$\begin{array}{cccccc} | & v_x & \| & v_y & \| & v_z \end{array}$$

with,

$$\Delta_p(\theta_p) = 4sin^2\theta_p\, cos\theta_p\sqrt{\frac{c_p^2}{c_s^2} - sin^2\theta_p} + \left(\frac{c_p^2}{c_s^2} - 2sin^2\theta_p\right)^2 , \tag{3.4.3d}$$

$$\Delta_s(\theta_s) = 4sin^2\theta_s cos\theta_s\sqrt{\frac{c_s^2}{c_p^2} - sin^2\theta_s} + cos^2 2\theta_s \,, \tag{3.4.3e}$$

Expressions *(3.4.3)* establish that the particle velocities generated at the traction free surface depend on the angle of incidence of the incident plane waves and on the P and S wave velocity ratio (or equivalently on the Poisson ratio $\sigma = (r^2-2)/(2r^2-2)$ with $r = c_p/c_s$) of the near surface layer. This is contrary to *Sh* waves for which the generated particle velocities are independent of the angle of incidence and of the P and S wave velocity. From *(3.4.3ab)* we observe that for vertically propagating waves ($\theta_p=\theta_s=0$), the vertical particle velocity detector only records P waves (*pseudo P wave detector*) and the horizontal one only S waves (*pseudo S wave*

detector). When the upgoing plane wave has a non-zero angle of incidence, it will be recorded on both particle velocity detector components. In the case of a low velocity near surface layer (weathering), the rays are bended towards the vertical before reaching the surface, hence the *P* and *S* waves will then be naturally separated by the vertical and horizontal particle velocity detectors, see *Figure 3.4.1a*. In the case of a high velocity near surface layer (permafrost) the rays are bended away from the vertical before reaching the surface, hence the *P* and *S* waves are recorded by all the particle velocity components, see *Figure 3.4.1b*.

To get a good feeling of the effects induced by a traction free surface on the sensitivity of the particle velocity detectors, we can compare their sensitivity to upgoing *P* and *S* plane waves in the case they record the wavefield on a traction free or non-reflecting surfce, see *Figures 3.4.2*, *3.4.3* and *3.4.4*.

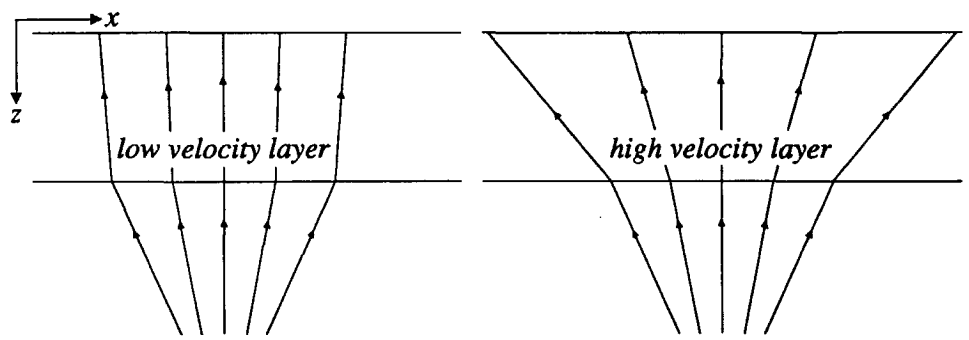

Figure 3.4.1

(a) In the case of a low velocity near surface layer (weathering), the rays are bended towards the vertical. The P and S waves are naturally separated by the vertical and horizontal particle velocity detectors.

(b) In the case of a high velocity near surface layer (permafrost), the rays are bended away from the vertical. The P and S waves are recorded by all the particle velocity detector components.

3.5 SENSITIVITY ANALYSIS OF THE DECOMPOSITION AT THE RECEIVER SIDE

To separate the normal one-way wavefield components from the particle velocity field we use the decomposition operator at the receiver side $[\tilde{C}(z_0)]^{-1}$. This operator depends on: the stiffness tensor (for the wave-type polarization vectors) and on the wave-type propagation velocities (for the dispersion relations) in the near surface. In this section we study the sensitivity of the decomposed upgoing normal one-way wavefield $\langle \vec{\tilde{p}}^{\cdot}(z_0) \rangle$ to errors made in

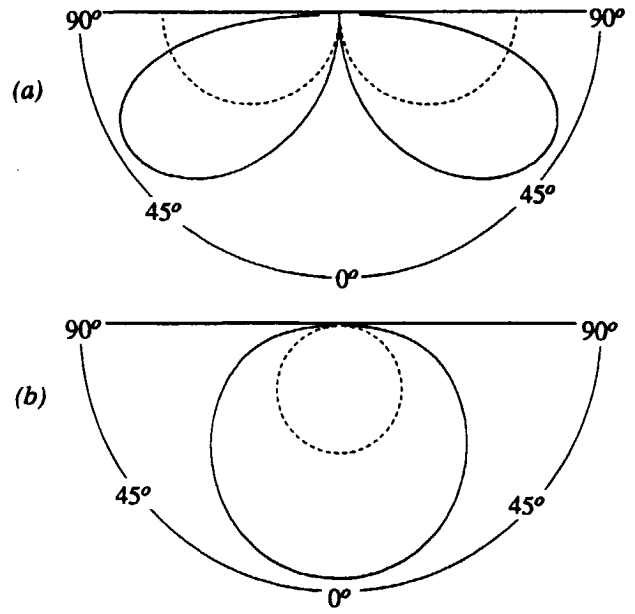

Figure 3.4.2

Sensitivity of the particle velocity detectors to upgoing P plane waves. Horizontal (a) and vertical (b) particle velocity amplitudes generated at a traction free surface (solid line) and at a non reflecting surface (dotted line). We used $c_P/c_S=2$.

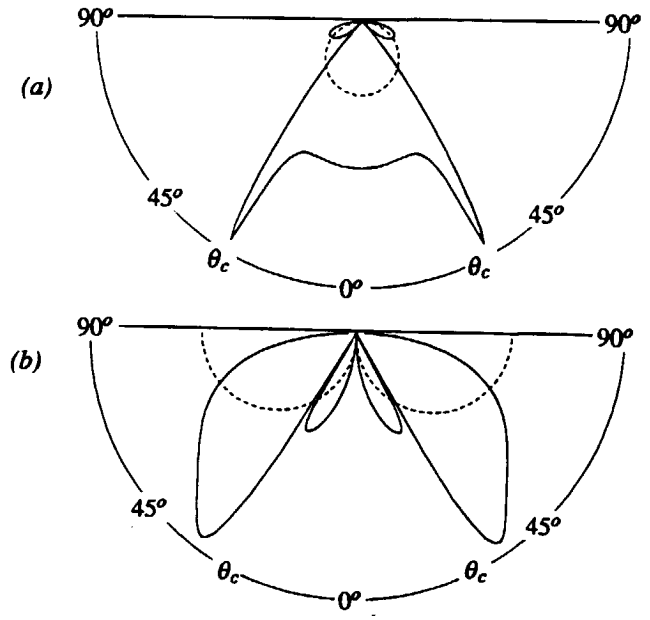

Figure 3.4.3

Sensitivity of the particle velocity detectors to upgoing S plane waves. Horizontal (a) and vertical (b) particle velocity amplitudes generated at a free surface (solid line) and at a non reflecting surface (dotted line). We used $c_P/c_S=2$.

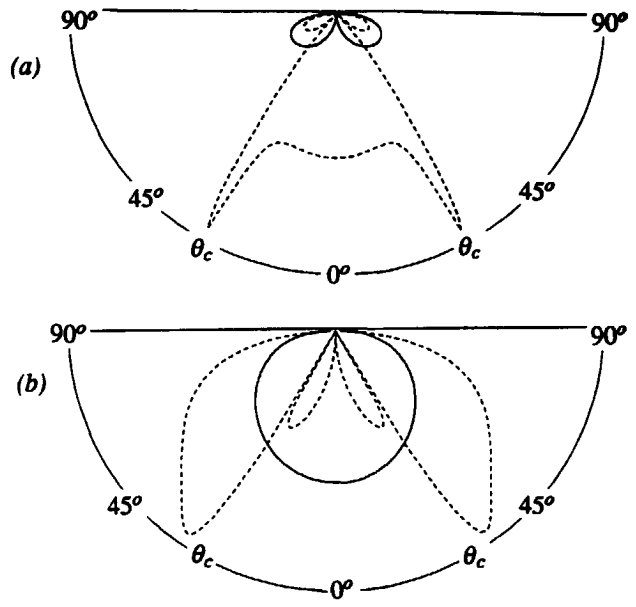

Figure 3.4.4

Comparison of the sensitivity of the particle velocity detectors at the free surface to upgoing P (solid line) and S (dotted line) plane wave. (a) Horizontal component, (b) vertical component. We used $c_P/c_S = 2$.

the input parameters. When the stiffness tensor and the wave-type propagating velocities are not properly estimated, we use an erroneous decomposition operator at the receiver side $\langle[\tilde{\boldsymbol{C}}(z_0)]^{-1}\rangle$. To obtain the true upgoing normal one-way wavefield vector $\vec{\tilde{p}}^{-}(z_0)$ we have to use the true decomposition operator at the receiver side $[\tilde{\boldsymbol{C}}(z_0)]^{-1}$.

Knowing that the two following equations hold :

$$\vec{\tilde{p}}^{-}(z_0) = [\tilde{\boldsymbol{C}}(z_0)]^{-1}\,\vec{\tilde{v}}(z_0)\,, \qquad (3.5.1a)$$

and

$$\langle\vec{\tilde{p}}^{-}(z_0)\rangle = \langle[\tilde{\boldsymbol{C}}(z_0)]^{-1}\rangle\,\vec{\tilde{v}}(z_0)\,, \qquad (3.5.1b)$$

we find the following relation between the estimated and the exact upgoing normal one-way wavefield:

$$\langle\vec{\tilde{p}}^{-}(z_0)\rangle = [\,\tilde{\boldsymbol{I}} + \tilde{\boldsymbol{E}}_r(z_0)\,]\,\vec{\tilde{p}}^{-}(z_0)\,, \qquad (3.5.1c)$$

with,

$$\tilde{\boldsymbol{E}}_r(z_0) = \langle[\tilde{\boldsymbol{C}}(z_0)]^{-1}\rangle\tilde{\boldsymbol{C}}(z_0) - \tilde{\boldsymbol{I}}\,. \qquad (3.5.1d)$$

In the case that no errors are made in the parameters estimation, $\widetilde{\boldsymbol{E}}_r(z_0)$ is zero. Otherwise the relative error matrix $\widetilde{\boldsymbol{E}}_r(z_0)$ is a full square matrix, which implies from *(3.5.1c)* that the upgoing normal one-way wavefield components are not properly separated from each other. An interesting question to address is the following: is it possible from the decomposed wavefield results to find a criterion that could inform us when the correct input elastic parameters have been used?. A possible criterion may be formulated as follows: when the correct parameters are used, the elements of the relative error matrix are zero. These zeroes have the effect of removing in each of the decomposed wave-type sections the two other undesired wave-types. The number of seismic events in each of the decomposed seismic sections is thus minimum when the decomposition parameters are correctly estimated. This may constitute an interesting criterion. The sensitivity of this criterion being then governed by the sensitivity of the off diagonal elements of the relative error matrix $\widetilde{\boldsymbol{E}}_r(z_0)$.

In an isotropic medium we see from expressions *(2.7.11i)* and *(2.7.13d)* that the S wave decomposition operator at the receiver side, only involves the S wave velocity, c_S. This implies that *the wavefield decomposition into S waves is independent of the P wave velocity.* This constitutes an important result. On the other hand, the P wavefield decomposition operator, depends both on the P and S wave propagation velocities. In *Figure (3.5.1a)* the amplitude of the P wave residuals in the decomposed S panel is represented for a set of k_x values going from 0, to the horizontal slowness of horizontally propagating P waves. For larger k_x values the P wavefield is evanescent. The sensitivity of the P wave suppression from the S panel, to errors made in the S wave velocity estimation $<c_S>$, is weak for moderate angles of incidence and increases for higher angles (far offset data). *Figure (3.5.1b)* represents the amplitude of the S wave residuals in the decomposed P panel, assuming a correct estimate of the S wave velocity. The function is represented for a set of k_x values going from *0* to the horizontal wavenumber of critical S waves (for larger k_x values, a low-pass filter is applied to the operator to avoid the operator instability for horizontally propagating P waves). From *Figure (3.5.1b)* we see that the sensitivity increases with the angle of incidence of the S waves.

Conclusion: *For moderate angles of incidence the decomposition is robust to the choice of c_P and c_S. An estimation of the P and S wave velocities of the near surface (based on the wavefield decomposition results) is possible if and only if we have incident P and S waves with high angles of incidence (far offset data). In this case the following algorithm is proposed: as the S wavefield decomposition only depends on the S wave velocity c_S, we first estimate it by minimizing the P wave residuals in the decomposed S panel. Once c_S is known, the P wave velocity c_P can be estimated by minimizing the S wave residuals in the decomposed P panel.*

We illustrate the discussion on simulated data. We consider an homogeneous isotropic medium (c_P *=3000m/s*, c_S*=1730m/s*, ρ*=1000kg/m*^{3}) bounded by a traction free surface at z_0. A buried vertically oriented body force source generates a wavefield recorded by horizontal and vertical

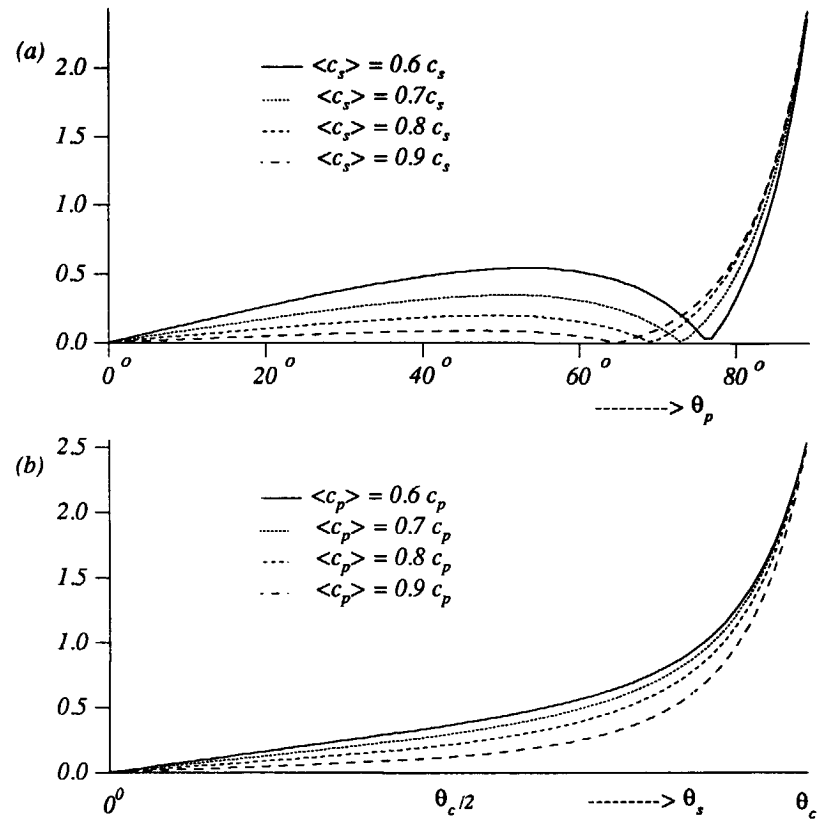

Figure 3.5.1

a) P wave residuals in the decomposed S panel as a function of the P wave angle of incidence θ_P. These residuals only depend on the accuracy of the S wave velocity estimation.

b) S wave residuals in the decomposed P panel as a function of the S wave angle of incidence θ_S (up to the citical angle θ_C). Here we assume that $<c_S>=c_S$.

particle velocity detectors at z_0, see *Figure 3.5.2*. *Figure 3.5.4* represents the decomposed *P* and *S* wavefields obtained with different values of the *P* and *S* wave velocity.

3.6 WAVEFIELD EMITTED BY SURFACE SEISMIC SOURCES

The source-composition operator $\left[\widetilde{D}(z_0)\right]^{-1}$enables to simulate at the surface a downgoing normal one-way source wavefield by combining three mutually perpendicularly oriented surface traction sources. Thus, the inverse of this operator enables to study the amplitude and phase of the downgoing normal one-way waves emitted by surface traction sources. For simplicity we consider an homogeneous near surface layer and we work in the wavenumber-frequency domain.

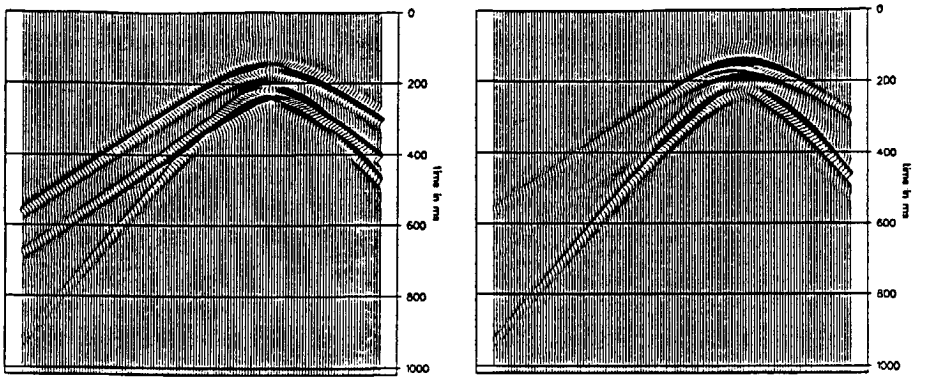

Figure 3.5.3

Horizontal (a) and vertical (b) particle velocities recorded at the traction free surface.

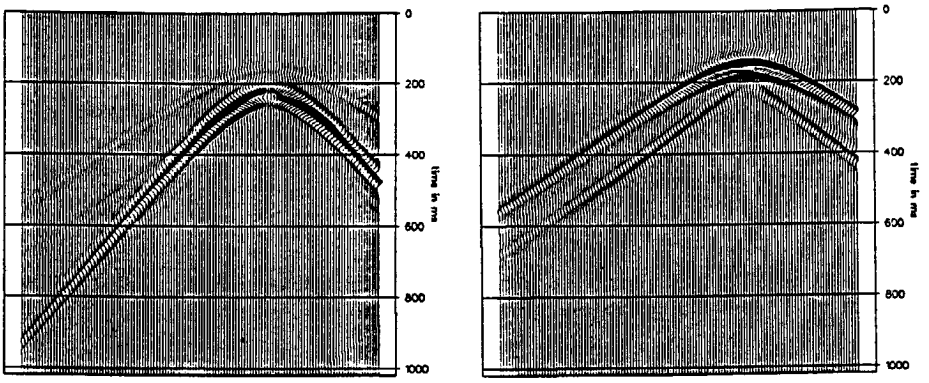

Figure 3.5.4a

Decomposed upgoing S (a) and P (b) wavefields obtained with $<c_S>=0.8\ c_S$ and $<c_P>=0.8\ c_P$.

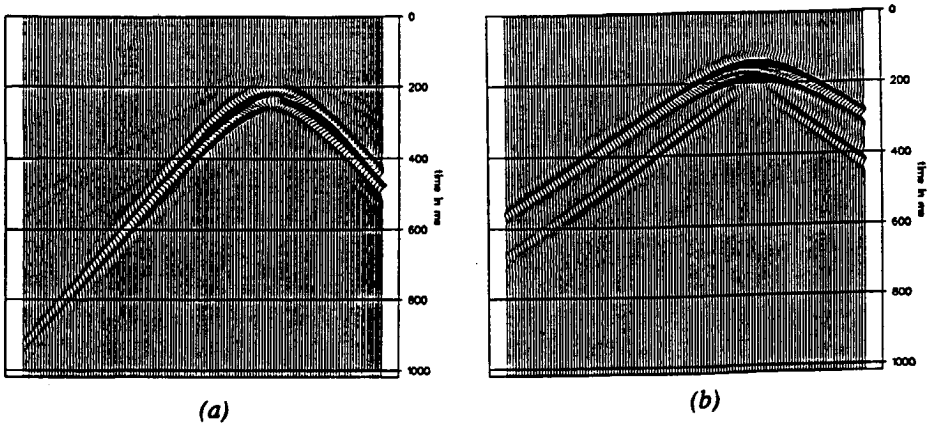

Figure 3.5.4b

Decomposed upgoing S (a) and P (b) wavefields obtained with $<c_S> = 0.9\ c_S$ and $<c_P>=0.8\ c_P$.

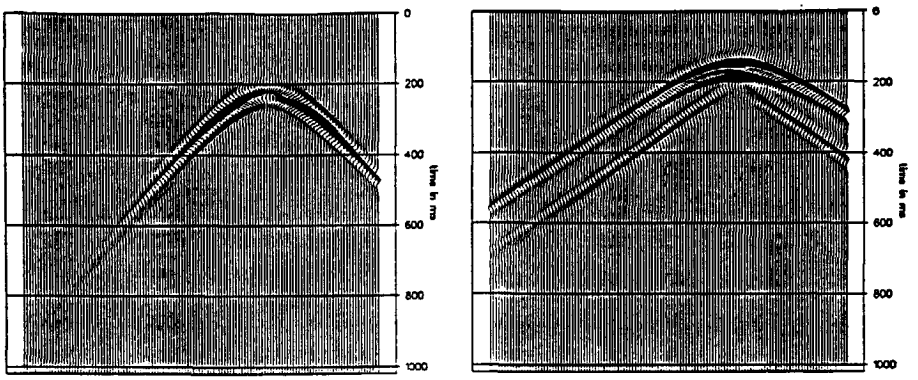

(a) (b)

Figure 3.5.4c

Decomposed upgoing S (a) and P (b) wavefields obtained with $<c_S> = c_S$ and $<c_P> = 0.8\ c_P$.

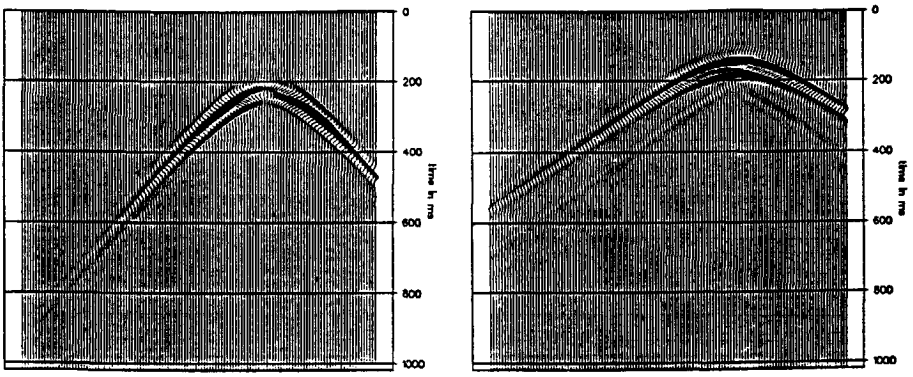

Figure 3.5.4d (a) (b)

Decomposed upgoing S (a) and P (b) wavefields obtained with $<c_S> = c_S$ and $<c_P> = 0.9\ c_P$.

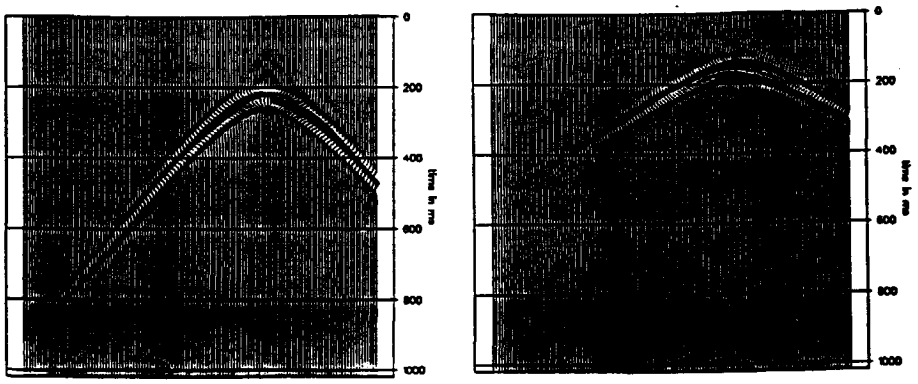

Figure 3.5.4e (a) (b)

Decomposed upgoing S (a) and P (b) wavefields obtained with $<c_S> = c_S$ and $<c_P> = c_P$.

In the wavenumber-frequency domain we have:

$$\vec{\tilde{p}}_s^{+}(z_0) = \tilde{\boldsymbol{D}}(z_0)\, \vec{\tilde{\tau}}_{z,s}(z_0)\ , \tag{3.6.1a}$$

with,

$$\tilde{\boldsymbol{D}}(z_0) = \left[\tilde{\boldsymbol{L}}_2^{+}(z_0)\right]^{-1}. \tag{3.6.1b}$$

The i^{th} column of $\tilde{\boldsymbol{D}}(z_0)$ contains the amplitude and phase of the downgoing normal one-way source wavefield $\vec{\tilde{p}}^{+}_{s,\tau_{iz}}$, emited by a unit traction source τ_{iz} applied at the earth surface z_0. In the case of an isotropic near surface layer we have (see *(2.7.13c)*):

$$\begin{array}{ccccc} & | \ P & || & S_V & ||S_h \ | \\ \vec{\tilde{p}}^{+}_{s,\tau_{xz}} = \left[\tilde{D}_{11}, \tilde{D}_{21}, \tilde{D}_{31}\right]^T = k_s^2 \Bigg[& -\dfrac{2k_x k_{z,s}}{\Delta(k_r)} & , \dfrac{jk_x(k_s^2-2k_r^2)}{\Delta(k_r)k_r} & , -\dfrac{k_y}{k_r k_{z,s}} \Bigg]^T , \end{array} \tag{3.6.2a}$$

$$\vec{\tilde{p}}^{+}_{s,\tau_{yz}} = \left[\tilde{D}_{12}, \tilde{D}_{22}, \tilde{D}_{32}\right]^T = k_s^2 \left[-\frac{2k_y k_{z,s}}{\Delta(k_r)} , \frac{jk_y(k_s^2-2k_r^2)}{\Delta(k_r)k_r} , \frac{k_x}{k_r k_{z,s}} \right]^T , \tag{3.6.2b}$$

$$\begin{array}{ccccc} & | \ P & || & S_V & ||S_h \ | \\ \vec{\tilde{p}}^{+}_{s,\tau_{zz}} = \left[\tilde{D}_{13}, \tilde{D}_{23}, \tilde{D}_{33}\right]^T = k_s^2 \Bigg[& -\dfrac{(k_s^2-2k_r^2)}{\Delta(k_r)} & , -\dfrac{2jk_r^2 k_{z,p}}{\Delta(k_r)k_r} & , \ 0 \ \Bigg]^T , \end{array} \tag{3.6.2c}$$

with,

$$k_r^2 = k_x^2 + k_y^2\ , \tag{3.6.2d}$$

and

$$\Delta(k_r) = 4k_{z,p}k_{z,s}k_r^2 + \left(k_s^2-2k_r^2\right)^2. \tag{3.6.2e}$$

Looking at *(3.6.2)* we note that the traction sources emit high amplitude "*downgoing*" evanescent *P* and *Sv* plane waves when $\Delta(k_r) = 0$ ($\Delta(k_r)$ Rayleigh denominator). This explains why Rayleigh waves appear so strongly when surface traction sources are used. A possibility to reduce the Rayleigh wave contribution consists then in burying the sources. Note that the Rayleigh wave phenomenon does not affect the *Sh* waves. To simplify the study of the amplitude and phase of the downgoing *P* and *S* waves generated at the surface by a unit traction source, we restrict ourselves to the two-dimensional situation. We then only have plane waves of the type $(k_x, k_y=0, \omega)$ with $k_x = \omega\, sin\theta_p/c_p$ for the downgoing *P* plane waves and $k_x = \omega\, sin\theta_s/c_s$ for the downgoing *S* plane waves. Choosing $k_r=k_x$, the following results are obtained:

$$\begin{array}{ccccc} & | \quad P & || & S_V & || \ S_h \ | \\ \vec{\tilde{p}}^{+}_{s,\tau_{xz}} = \Bigg[& -\dfrac{2c_p^2 sin\theta_p}{c_s^2\Delta(\theta_p)}\sqrt{\dfrac{c_p^2}{c_s^2} - sin^2\theta_p} & , \dfrac{jcos2\theta_s}{\Delta(\theta_s)} & , 0 \ \Bigg]^T , \end{array} \tag{3.6.3a}$$

$$\vec{\tilde{p}}^{+}_{s,\tau_{yz}} = \left[0 \qquad , 0 \qquad , \frac{\omega}{c_s cos\theta_s} \right]^T , \tag{3.6.3b}$$

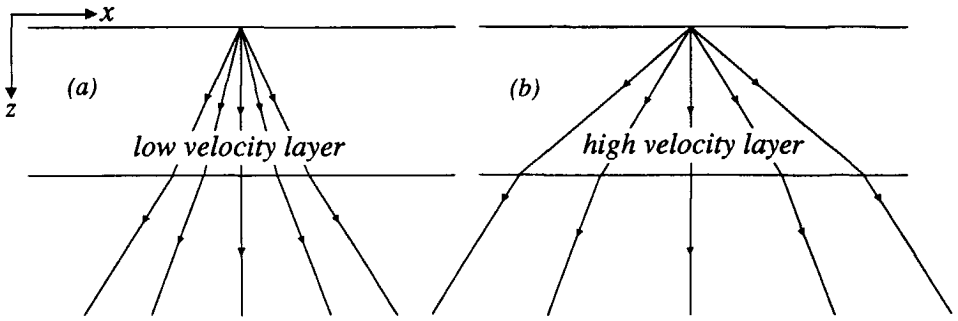

Figure 3.6.1

(a) In the case of a low velocity near surface layer, the rays are bended away from the vertical in the lower medium. For small offsets (small angles), the vertical traction source may then be considered as a P wave source and similarly the horizontal traction source as a S wave source.(b) In the case of a high velocity near surface layer, the rays are bended towards the vertical in the lower medium. In this case even for small offsets, the vertical and horizontal traction sources may no longer be considered as P and S wave sources.

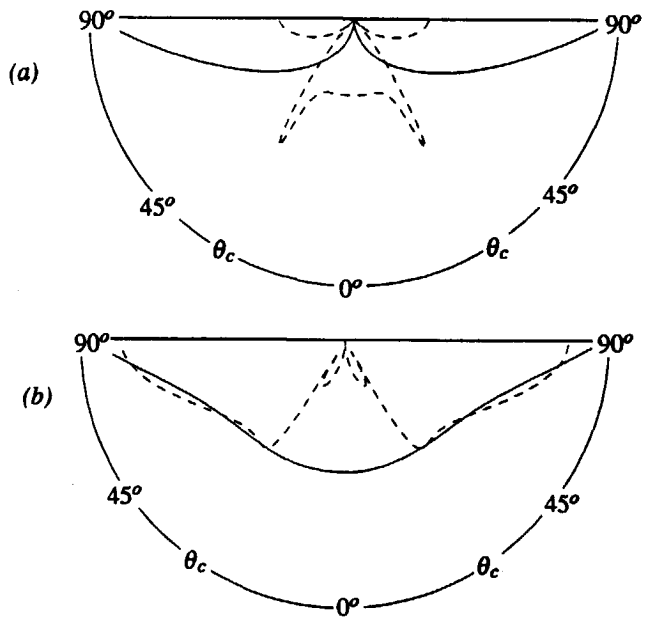

Figure 3.6.2

Amplitudes as a function of the emergence angle for the downgoing P (solid line) and S(dotted line) plane waves emitted by a horizontal (a) and vertical (b) traction source (cp/cs=2).

$$\vec{\tilde{p}}^{+}_{s,\tau_{zz}} = \left[-\frac{c_p^2}{c_s^2 \Delta(\theta_p)} \left(\frac{c_p^2}{c_s^2} - 2sin^2\theta_p \right) , -\frac{2jsin\theta_s}{\Delta(\theta_s)} \sqrt{\frac{c_s^2}{c_p^2} - sin^2\theta_s} , 0 \right]^T , \qquad (3.6.3c)$$

$$\| \quad P \quad \| \quad Sv \quad \| \quad Sh \quad \|$$

with,

$$\Delta_p(\theta_p) = 4sin^2\theta_p cos\theta_p \sqrt{\frac{c_p^2}{c_s^2} - sin^2\theta_p} + \left(\left(\frac{c_p^2}{c_s^2} \right) - 2sin^2\theta_p \right)^2 , \qquad (3.6.3d)$$

and

$$\Delta_s(\theta_s) = 4cos\theta_s sin^2\theta_s \sqrt{\frac{c_s^2}{c_p^2} - sin^2\theta_s} + (cos2\theta_s)^2 . \qquad (3.6.3e)$$

We observe that the amplitude and phase of the downgoing P and Sv plane waves generated by a surface traction source depend on the emergence angle θ as well as on the P and S wave velocity ratio (or equivalently on the Poisson ratio of the near surface layer). Expressions *(3.6.3)* indicate that vertical and horizontal unit traction sources emit both P and S waves. For vertically propagating plane waves ($\theta_p=\theta_s=0$), the vertical traction source only emits P waves (*pseudo P wave source*) and the horizontal traction source only S waves (*pseudo S wave source*). In the case of a low velocity near surface layer, the rays are bended away from the vertical in the lower medium, see *Figure 3.6.1a*. For small offsets (small angles) the vertical traction source may then be considered as a P wave source and, similarly, the horizontal traction source as a S wave source. In the case of a high velocity near surface layer the rays are bended towards the vertical in the lower medium, see *Figure 3.6.1b*. For small offsets the vertical and horizontal traction sources may no longer be considered respectively as P or S wave sources.

Figure 3.6.2 represents the amplitudes as a function of angle for the downgoing P (solid line) and S (dotted line) plane waves emitted by a horizontal *(a)* and vertical *(b)* traction source ($c_P/c_S=2$).

3.7 SENSITIVITY ANALYSIS OF THE DECOMPOSITION AT THE SOURCE SIDE

The traction distribution $\vec{\tilde{\tau}}_{z,s}(z_0)$ that must be applied at the earth's surface to simulate a downgoing source wavefield $\vec{\tilde{p}}^{+}_s(z_0)$, is contained in the composition operator at the source side $\left[\tilde{\boldsymbol{D}}(z_0)\right]^{-1}$. This operator depends on: the stiffness tensor and on the wave-type propagation velocities in the near surface. In this section we study the sensitivity of the simulated downgoing source wavefield $<\vec{\tilde{p}}^{+}_s(z_0)>$ to errors made in the input parameters.

When the stiffness tensor and the wave-type propagation velocities are not properly estimated, we use an erroneous decomposition at the source side $\left[<\widetilde{\boldsymbol{D}}(z_0)>\right]^{-1}$. Knowing that the two following equations hold:

$$\vec{\widetilde{p}}_s^{\,+}(z_0) = \widetilde{\boldsymbol{D}}(z_0)\, \vec{\vec{\tau}}_{z,s}(z_0)\,, \tag{3.7.1a}$$

and

$$<\vec{\widetilde{p}}_s^{\,+}(z_0)> = <\widetilde{\boldsymbol{D}}(z_0)>\, \vec{\vec{\tau}}_{z,s}(z_0)\,, \tag{3.7.1b}$$

we find the following relation between the effective downgoing normal source wavefield emitted in the subsurface $\vec{\widetilde{p}}_s^{\,+}(z_0)$ and the expected one $<\vec{\widetilde{p}}_s^{\,+}(z_0)>$:

$$\vec{\widetilde{p}}_s^{\,+}(z_0) = \left[\widetilde{\boldsymbol{I}} + \widetilde{\boldsymbol{E}}_s(z_0)\right] <\vec{\widetilde{p}}_s^{\,+}(z_0)>\,, \tag{3.7.1c}$$

with,

$$\widetilde{\boldsymbol{E}}_s(z_0) = \widetilde{\boldsymbol{D}}(z_0)\left[<\widetilde{\boldsymbol{D}}(z_0)>\right]^{-1} - \widetilde{\boldsymbol{I}}\,. \tag{3.7.1d}$$

In the case that no errors are made in the parameter estimation $\widetilde{\boldsymbol{E}}_s(z_0)$ equals zero. Otherwise the relative error matrix $\widetilde{\boldsymbol{E}}_s(z_0)$ is a full square matrix. Which implies from *(3.7.1c)* that if the expected source wavefield consists of only one wave-type the effective source wavefield will in fact be a mixture of the three wave-types.

The study of the sensitivity of the decomposition at the source side in an isotropic medium, is similar to the one previously developed for the decomposition at the receiver side. We will just mention that similarly to the decomposition at the receiver side the wavefield decomposition at the source side into *S* waves does not depend on the *P* wave velocity: the two last columns of the composition operator $\left[\widetilde{\boldsymbol{D}}(z_0)\right]^{-1} = \widetilde{\boldsymbol{L}}_2^{+}(z_0)$ do not involve the *P* wave velocity, see expressions *(2.7.11h)* and *(2.7.13c)*.

3.8 DECOMPOSITION OPERATORS IN THE SPACE-FREQUENCY DOMAIN

The decomposition at the receiver side in the wavenumber-frequency domain is satisfactory in the case of a large distribution of regularly spaced particle velocity detectors over a laterally homogeneous near surface layer. Except for this ideal situation we would rather work in the space-frequency domain; indeed this domain offers much more flexibility for the following situations:

- For a laterally inhomogeneous near surface layer, the decomposition operator is space dependent. It is adapted according to the elastic parameters at all surface locations where the wavefield has to be decomposed. This space dependency is easily taken into account in the

space-frequency domain.

- In the space-frequency domain the decomposition operators can take into account quite well all kinds of detector distributions. This domain is suited for wavefields that are irregularly sampled. This irregularity could come, for example, from the rejection of some noisy traces. An other advantage of this domain is that it is also easier to take into account the finite extent of the shot records, this aperture limitation being always the root of artefacts.

In this section we explain how we design the decomposition operators in the space-frequency domain, bearing in mind to make them as small as possible. This is not only to reduce the computational cost of the decomposition, but mainly to make the decomposition process as local as possible. *Local operators are well suited for laterally inhomogeneous near surface layers.*

In the space-frequency domain the decomposition operation is no more a scalar product but a convolutional product of the data with the decomposition operators. The problem of determining the space-frequency representation of an operator known in the wavenumber-frequency domain, is often met in geophysical techniques such as migration (Berkhout, 1985, Blacquière et al, 1989). To introduce the method that we use, we illustrate it for the two dimensional case, leaving us with a simplified notation (this method can be easily extended to the three dimensional case). We want to determine the expression of the convolutional operator, that, at a lateral position $x_0 = 0$, simulates the filter $F(k_x,\omega)$ for all the incident plane waves that may reach x_0, see *Figure 3.8.1*. As in the space domain the data are discretized we consider a discretized convolutional operator of M_2+M_1+1 complex points, contained in the vector $\vec{f}(\omega)$:

$$\vec{f}(\omega) = (f_{-M_2}(\omega), \dots , f_0(\omega), \dots , f_{M_1}(\omega))^T . \qquad (3.8.1a)$$

To determine the vector coefficients we proceed as follows: A unit plane wave of horizontal wavenumber k_x recorded at the M_2+M_1+1 lateral surface positions $x_{-M_2}, \dots , x_0 = 0, \dots , x_{M_1}$, leads to M_2+M_1+1 complex values $d(k_x, x_i, \omega)$, that can be written in a vector $\vec{d}(k_x,\omega)$ according to :

$$\vec{d}(k_x, \omega) = (d(k_x, x_{-M_2}, \omega), \dots ,d(k_x, x_0, \omega), \dots ,d(k_x, x_{M_1}, \omega))^T , \qquad (3.8.1b)$$

with,

$$d(k_x, x_i, \omega) = e^{-jk_x x_i} . \qquad (3.8.1c)$$

We would like that the vector product of the vector $\vec{f}(\omega)$with the data vector $\vec{d}(k_x,\omega)$leads to the filtered version $d_f(k_x, x_0, \omega)$ of $d(k_x, x_0, \omega)$, with:

$$d_f(k_x, x_0, \omega) = F(k_x, \omega)\, d(k_x, x_0, \omega) = F(k_x,\omega) . \qquad (3.8.1d)$$

The M_2+M_1+1 complex coefficients $f_i(\omega)$ must then verify :

$$e(k_x, \omega, \hat{f}(\omega)) = 0 , \qquad (3.8.2a)$$

with,

$$e(k_x, \omega, \hat{f}(\omega)) = \vec{d}^T(k_x, \omega)\, \hat{f}(\omega) - F(k_x, \omega) . \qquad (3.8.2b)$$

Working per frequency component equation *(3.8.2a)* must be verified for all k_x values such that $k_x \in [k_{xmin}, k_{xmax}]$, k_{xmin} and k_{xmax} depending on the horizontal wavenumbers of the plane waves that are expected to reach the lateral position x_0.

Introducing the error vector $\vec{e}(\omega, \hat{f}(\omega))$:

$$\vec{e}(\omega, \hat{f}(\omega)) = \left(e(k_{xmin}, \omega, \hat{f}(\omega)), \cdots\cdots, e(k_{xmax}, \omega, \hat{f}(\omega))\right)^T , \qquad (3.8.3a)$$

we have :

$$\vec{e}(\omega, \hat{f}(\omega)) = \boldsymbol{L}\, \hat{f}(\omega) - \vec{F}(\omega) , \qquad (3.8.3b)$$

with,

$$\boldsymbol{L} = \begin{pmatrix} \vec{d}^T(k_{xmin},\omega) \\ \vdots \\ \vec{d}^T(k_{xmax},\omega) \end{pmatrix}, \qquad (3.8.3c)$$

and

$$\vec{F}(\omega) = \begin{pmatrix} F(k_{xmin},\omega) \\ \vdots \\ F(k_{xmax},\omega) \end{pmatrix}. \qquad (3.8.3d)$$

The coefficients $f_i(\omega)$ are computed to minimize $S(\omega, \vec{a}(\omega))$:

$$S(\omega, \hat{f}(\omega)) = \vec{e}^H(\omega, \hat{f}(\omega))\, \boldsymbol{W}(\omega)\, \vec{e}(\omega, \hat{f}(\omega)) , \qquad (3.8.3e)$$

(H stands for Hermitian: conjugate transpose), with $\boldsymbol{W}(\omega)$ an hermitian positive definite diagonal matrix :

$$\boldsymbol{W}(\omega) = \begin{pmatrix} W(k_{xmin},\omega) & & 0 \\ & \ddots & \\ 0 & & W(k_{xmax},\omega) \end{pmatrix}. \qquad (3.8.3f)$$

The weight matrix $\boldsymbol{W}(\omega)$ is introduced to give more or less importance to the errors made for some plane waves. As $\boldsymbol{W}(\omega)$ is an hermitian positive definite matrix, expression *(3.8.3e)* can be rewritten as:

$$S(\omega, \hat{f}(\omega)) = \left[\boldsymbol{W}^{1/2}\vec{e}(\omega, \hat{f}(\omega))\right]^H \left[\boldsymbol{W}^{1/2}\vec{e}(\omega, \hat{f}(\omega))\right] \qquad (3.8.3g)$$

From the above expression we deduce that the operator $\hat{f}(\omega)$ that minimize *(3.8.3g)* is the least square solution of the linear system:

$$\boldsymbol{W}^{1/2}\left[\boldsymbol{L}\, \hat{f}(\omega) - \vec{F}(\omega)\right] = \vec{0} . \qquad (3.8.3h)$$

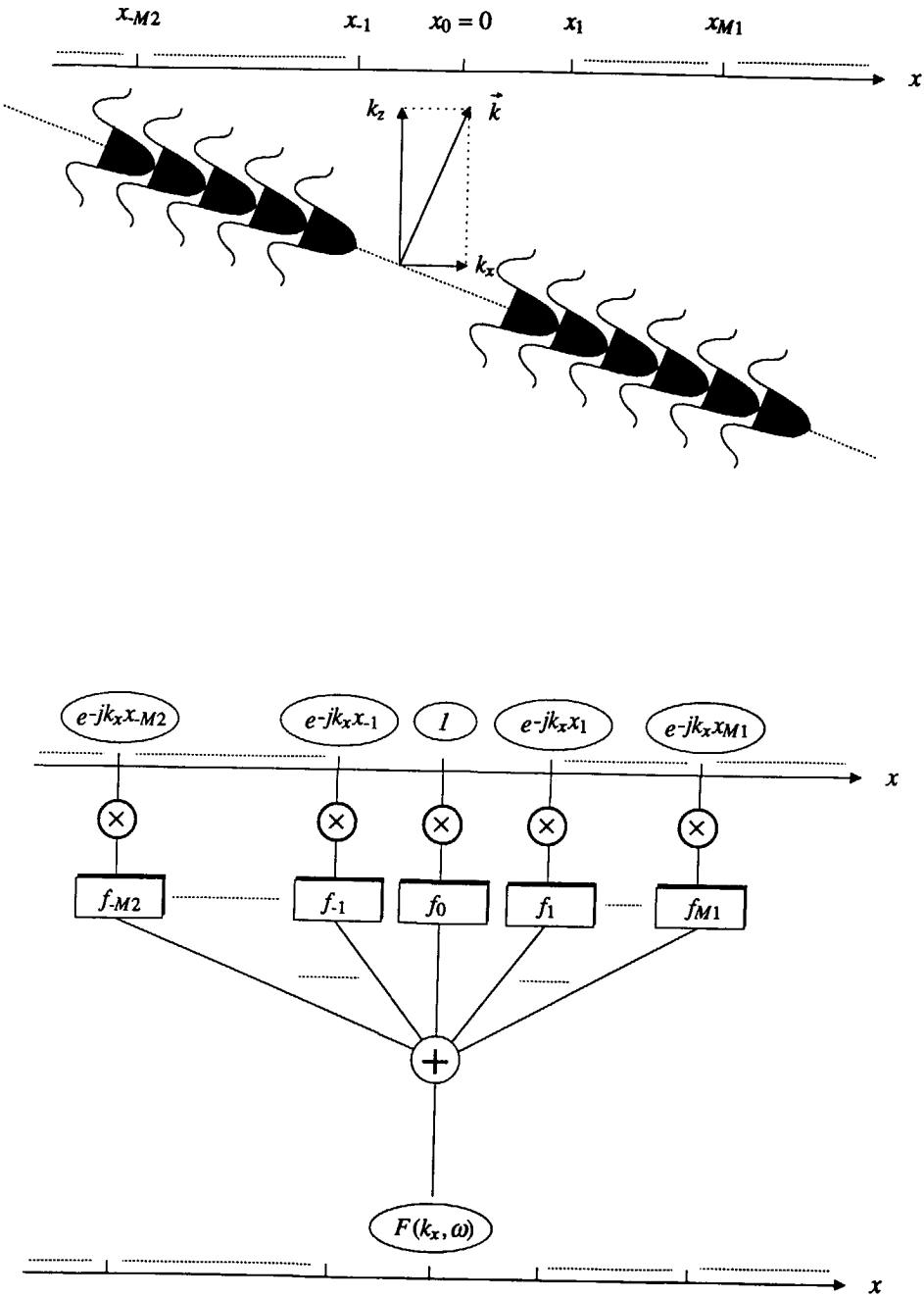

Figure 3.8.1

We want to determine the M2+M1+1 complex points of the convolutional operator that filters the plane waves of horizontal wavenumber k_x with the filter function $F(k_x,\omega)$.

The least square solution of *(3.8.4h)*, is a solution of the square linear system:

$$A(\omega)\,\vec{f}(\omega) = \vec{b}(\omega)\,, \qquad (3.8.4a)$$

with,

$$A(\omega) = L^H\,W(\omega)\,L\,, \qquad (3.8.4b)$$

$$A_{mn}(\omega) = \sum_{k_x = k_{xmin}}^{k_{xmax}} W(k_x,\omega)\; e^{jk_x(x_m - x_n)} \qquad m, n = -M_2, \cdots, M_1\,, \qquad (3.8.4c)$$

and

$$\vec{b}(\omega) = L^H W(\omega)\,\vec{F}(\omega)\,, \qquad (3.8.4d)$$

$$b_m(\omega) = \sum_{k_x = k_{xmin}}^{k_{xmax}} W(k_x,\omega)\,F(k_x,\omega)\; e^{jkx_m}\,. \qquad (3.8.4e)$$

Note that A is an Hermitian matrix, which has a Toeplitz structure if we can write $x_i = i\,\Delta x$, which is the case for a regularly sampled data set. When A has a Toeplitz structure the linear system *(3.8.4a)* can be efficiently solved using a Levinson type algorithm (Numerical Recipies, p47-52).

The linear system *(3.8.4a)* greatly simplifies for the following situation :
Consider a regularly sampled operator, with a sampling interval Δx. Choose $k_{xmin} = -k_{xnyq}$ and $k_{xmax} = k_{xnyq} - \Delta k_x$, k_{xnyq} being the spatial Nyquist wavenumber $(\pi/\Delta x)$ and Δk_x being the sampling interval in the horizontal wavenumber domain $\Delta k_x = 2\pi/N\Delta x$, with N an integer. Set the weight matrix $W(\omega)$ equal to the identity matrix. We then have:

$$f_i(\omega) = \frac{1}{N} \sum_{k_x = -k_{xNyq}}^{k_{xNyq} - \Delta k_x} F(k_x,\omega)\; e^{jk_x x_i} \qquad i = -M_2\,, \cdots, M_1 \qquad (3.8.5)$$

We recognize in solution *(3.8.5)* that for this special situation the convolutional decomposition operator $\vec{f}(\omega)$ can be obtained by truncating in the space domain the inverse Fourier transform of the filter $F(k_x,\omega)$ to M_2+M_1+1 points. Outside this particular situation the system *(3.8.4a)* has to be solved either with a Levinson type of algorithm for a regularly sampled operator, or with the Cholesky algorithm (A is a positive definite matrix) in the case of irregularly sampled data.

In practice the number of points per operator depends on the accuracy and stability conditions the operator must obey. We want the operator to be accurate over the spectral band corresponding to the data, and we want it to be stable outside this band (noise region). For the low frequencies the convolution operator determination is mainly concerned with stability conditions and for high frequencies the convolution operator determination is mainly concerned with accuracy conditions.

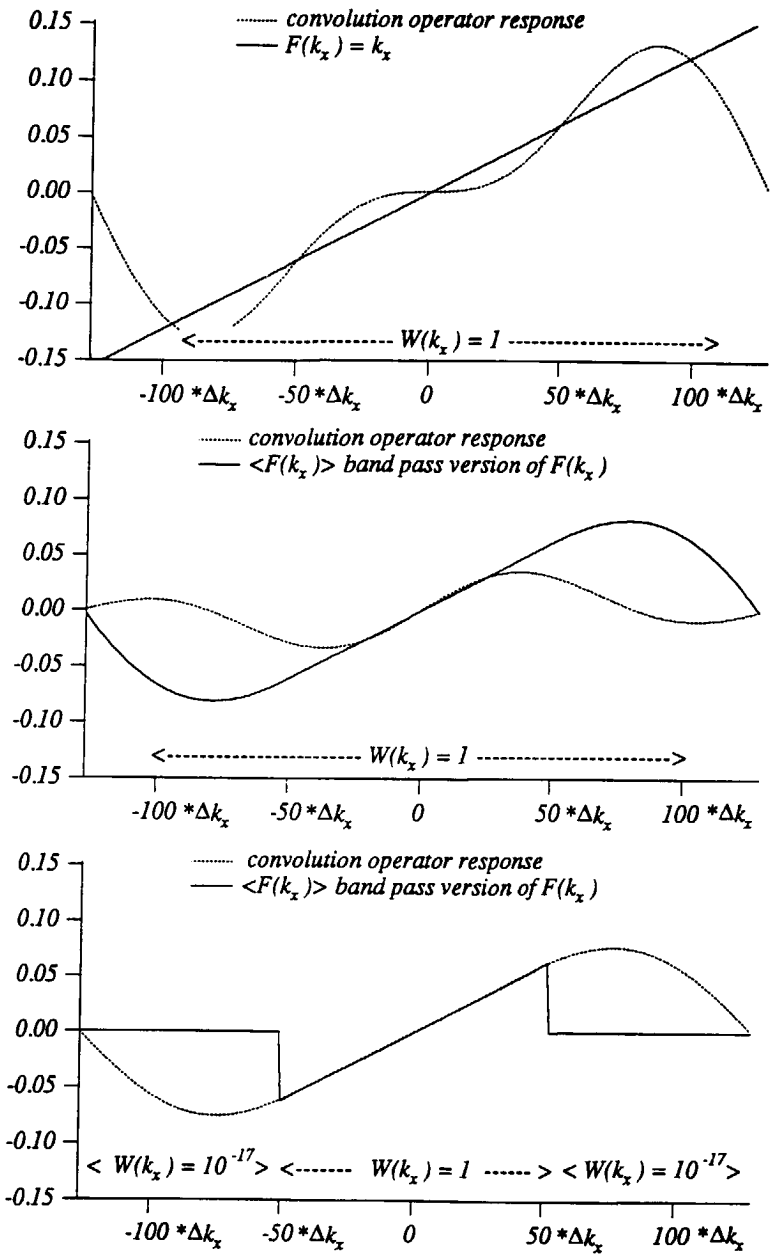

Figure 3.8.2

Convolutional operator response for different choices of $F(k_X)$ and $W(k_X)$ over the seismic bandwidth where the convolutional operator response has just to be stable.

Depending on the method used to compute the convolutional operator coefficients, the convolutional operator response will be more or less close to the filter $F(k_x)$ We illustrate this with an example. Consider the operator $F(k_x)=k_x$. We want the convolutional operator be accurate over the seismic band $k_x \in [-50\ \Delta k_x,\ 50\ \Delta k_x]$ with $\Delta k_x = 2\pi/(256\ \Delta x)$ and $\Delta x = 25\ m$ and be stable outside this band. We choose $M_2 = M_1 = 2$. We then have a five point convolutional operator. In *Figure 3.8.2* the convolutional operator response is displayed for different choices of $F(k_x)$ and $W(k_x)$ in the seismic band over which the operator has just to be stable. We see that the best choice consists in taking a low weight function and setting $F(k_x)$ to zero over the seismic band where the operator has just to be stable and by setting $F(k_x)=k_x$ with $W(k_x)=1$ over the seismic band where the operator response has to be close to $F(k_x)$.

To illustrate the possibility of doing a correct elastic wavefield decomposition at the receiver side in the space-frequency domain in the case of a laterally inhomogeneous near surface, we consider the simulated data set displayed in *Figure 3.8.3*. The model consists of a laterally inhomogeneous medium with two buried vertically oriented body force point sources. At the traction free surface, vertical and horizontal particle velocities are measured, see *Figures 3.8.3a,b*. *Figures 3.8.3c,d* represent the result of the P and S wavefield decomposition at the receiver side in the space-frequency domain. As can be seen the wavefield is correctly separated even around the discontinuity.

For the derivation of the decomposition operators at the source side in the space-frequency domain, we keep the same formalism as the one used for the decomposition operator at the receiver side. The equations stay the same, except for *(3.8.2c)* that must be rewritten as :

$$d(k_x, x_i, \omega) = e^{+jk_x x_i}\ , \qquad (3.8.6)$$

For the decomposition at the source side we do a plane wave front synthesis instead of a plane wave decomposition, this explains why the - sign is transformed into a + sign.

3.9 INFLUENCE OF NEAR SURFACE LAYERS ON THE RECORDED SEISMIC WAVEFIELD

In the case of one or more near surface layers we would like a decomposition operator at the receiver side that gives us the upgoing one-way wavefield at the top of the lower medium, see *Figure 3.9.1*, thus free of the influence of the near surface layer. To determine this operator we need to know the phenomena induced by such a near surface. We start this study for the simple case of a single near surface layer, first with a one-way approach to well see all the wave phenomena involved, then with a two-way approach which easily enables the extension of the previous results to the case of a multi-layer near surface medium. We will check that the two approaches give exactly the same solutions. For simplicity we consider laterally homogeneous near surface layers and the expressions are derived in the wavenumber-frequency domain.

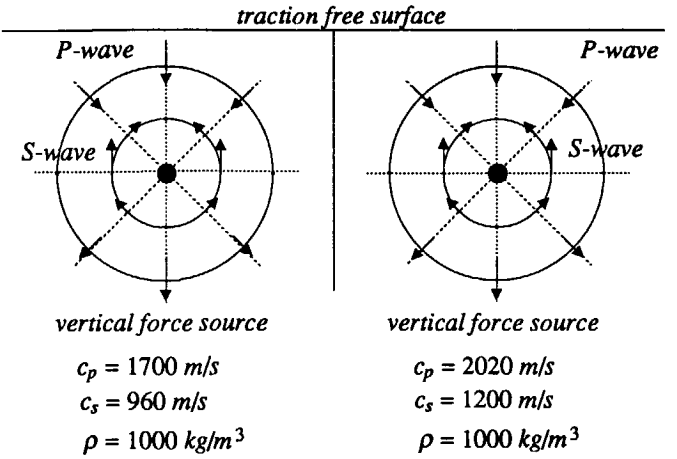

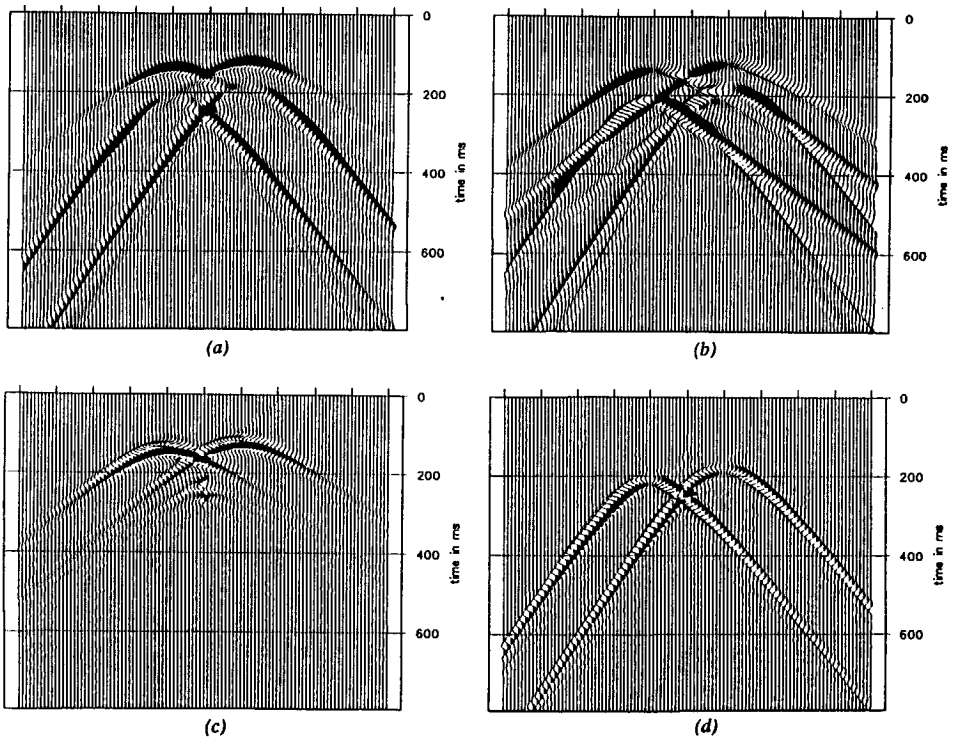

Figure 3.8.3

Example of wavefield decomposition in the space-frequency domain, with a laterally inhomogeneous near surface.

a) v_z *(vertical particle velocity)* *b)* v_x *(horizontal particle velocity)*

c) Φ^- *(the event at time t=250ms is an P - S conversion)* *c)* Ψ^-

One-way-approach

With this approach, we follow the propagation of an upgoing plane wave $\vec{\vec{p}}^{-}(z_1)$ (coming from the subsurfac), through the near surface layer, taking into account the transmission, reflection, conversion and propagation effects occuring along its path. *Figure 3.9.1* illustrates the different wave phenomena affecting the incident upgoing wave. We consider an *upper* layer characterized by the stiffness tensor $C_{ijkl,u}$ and the density ρ_u, overlying a *lower* medium characterized by the stiffness tensor $C_{ijkl,l}$ and the density ρ_l. The particle velocity $\vec{\vec{v}}(z_0)$ measured at the traction free surface, (i.e., $\vec{\vec{\tau}}_z(z_0) = \vec{0}$), is related to the upgoing wavefield $\vec{\vec{p}}^{-}(z_0)$ according to:

$$\vec{\vec{v}}(z_0) = \left[\widetilde{\boldsymbol{M}}^{-}_{1,u}\right]^{-1} \vec{\vec{p}}^{-}(z_0) \,. \qquad (3.9.1)$$

To relate $\vec{\vec{v}}(z_0)$ to $\vec{\vec{p}}^{-}(z_1)$, we need to know how $\vec{\vec{p}}^{-}(z_0)$ is related to $\vec{\vec{p}}^{-}(z_1)$. The relation is :

$$\vec{\vec{p}}^{-}(z_0) = (\widetilde{\boldsymbol{W}}^{-}(z_0,z_1)\widetilde{\boldsymbol{T}}^{-}(z_1) + \left[\widetilde{\boldsymbol{W}}^{-}(z_0,z_1)\widetilde{\boldsymbol{R}}^{+}(z_1)\widetilde{\boldsymbol{W}}^{+}(z_1,z_0)\widetilde{\boldsymbol{R}}^{-}(z_0)\right] \widetilde{\boldsymbol{W}}^{-}(z_0,z_1)\widetilde{\boldsymbol{T}}^{-}(z_1) + \left[\widetilde{\boldsymbol{W}}^{-}(z_0,z_1)\widetilde{\boldsymbol{R}}^{+}(z_1)\widetilde{\boldsymbol{W}}^{+}(z_1,z_0)\widetilde{\boldsymbol{R}}^{-}(z_0)\right]^2 \widetilde{\boldsymbol{W}}^{-}(z_0,z_1)\widetilde{\boldsymbol{T}}^{-}(z_1) + \cdots) \vec{\vec{p}}^{-}(z_1) \qquad (3.9.2a)$$

or equivalently,

$$\vec{\vec{p}}^{-}(z_0) = \left[\widetilde{\boldsymbol{I}} - \widetilde{\boldsymbol{W}}^{-}(z_0,z_1)\widetilde{\boldsymbol{R}}^{+}(z_1)\widetilde{\boldsymbol{W}}^{+}(z_1,z_0)\widetilde{\boldsymbol{R}}^{-}(z_0)\right]^{-1} \widetilde{\boldsymbol{W}}^{-}(z_0,z_1)\widetilde{\boldsymbol{T}}^{-}(z_1) \vec{\vec{p}}^{-}(z_1) \,. \qquad (3.9.2b)$$

The first term of the series in *(3.9.2a)* represents the primary response, taking into account the transmission effects $\widetilde{\boldsymbol{T}}^{-}(z_1)$ at the boundary z_1, as well as the wavefield propagation effects in the upper layer from z_1 to z_0, $\widetilde{\boldsymbol{W}}^{-}(z_0,z_1)$. The second term in the series accounts for the first order multiple : the primary wave is reflected at the surface z_0, propagates downward from z_0 to z_1, is reflected at z_1 and propagates upward to z_0. The $n+1^{st}$ term in the series accounts for the n^{th} order multiple. The combination of equation *(3.9.1)* with *(3.9.2b)* leads to the relation between $\vec{\vec{p}}^{-}(z_1)$ and $\vec{\vec{v}}(z_0)$:

$$\vec{\vec{v}}(z_0) = \left[\boldsymbol{M}^{-}_{1,u}\right]^{-1} \left[\widetilde{\boldsymbol{I}} - \widetilde{\boldsymbol{W}}^{-}(z_0,z_1)\widetilde{\boldsymbol{R}}^{+}(z_1)\widetilde{\boldsymbol{W}}^{+}(z_1,z_0)\widetilde{\boldsymbol{R}}^{-}(z_0)\right]^{-1} \widetilde{\boldsymbol{W}}^{-}(z_0,z_1)\widetilde{\boldsymbol{T}}^{-}(z_1) \vec{\vec{p}}^{-}(z_1) \,. \qquad (3.9.3a)$$

Note that the term $\left[\widetilde{\boldsymbol{I}} - \widetilde{\boldsymbol{W}}^{-}(z_0,z_1)\widetilde{\boldsymbol{R}}^{+}(z_1)\widetilde{\boldsymbol{W}}^{+}(z_1,z_0)\widetilde{\boldsymbol{R}}^{-}(z_0)\right]^{-1}$ is at the origin of a frequency dependent reverberation phenomenon.

The operator developed in *(3.9.3a)* describes the particle velocities generated at the traction free surface by an upgoing wavefield coming from the lower medium, taking into account all the near surface layer effects. The inverse of this operator is the decomposition operator at the receiver side we are looking for :

$$\vec{\vec{p}}^{-}(z_1) = \left[\widetilde{\boldsymbol{T}}^{-}(z_1)\right]^{-1} \left[\left[\widetilde{\boldsymbol{W}}^{-}(z_0,z_1)\right]^{-1} - \widetilde{\boldsymbol{R}}^{+}(z_1)\widetilde{\boldsymbol{W}}^{+}(z_1,z_0)\widetilde{\boldsymbol{R}}^{-}(z_0)\right] \boldsymbol{M}^{-}_{1,u} \vec{\vec{v}}(z_0) \,. \qquad (3.9.3b)$$

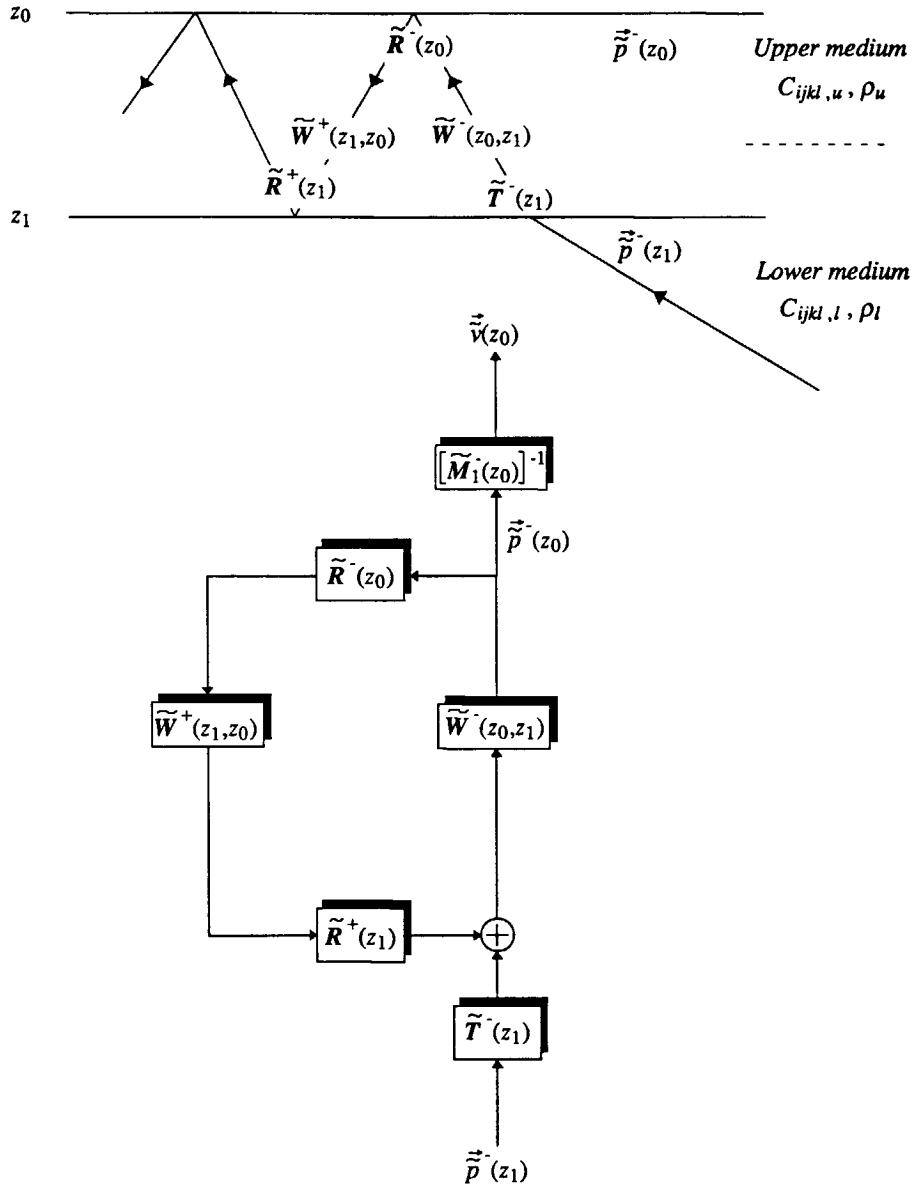

Figure 3.9.1

Near surface layers induce frequency dependent reverberation phenomena to the upgoing incident wavefield.

Two-way approach

This more straightforward approach can be easily extended to the case of a multi-layer near surface. The two-way approach can be described as follows: knowing the velocity and traction field at z_0, $\vec{\tilde{v}}(z_0)$ and $\vec{\tilde{\tau}}_z(z_0)$, we extrapolate them to z_1 using the two-way extrapolation operator $\tilde{U}(z_1,z_0)$:

$$\begin{pmatrix} \vec{\tilde{v}}(z_1) \\ \vec{\tilde{\tau}}_z(z_1) \end{pmatrix} = \tilde{U}(z_1, z_0) \begin{pmatrix} \vec{\tilde{v}}(z_0) \\ \vec{\tilde{\tau}}_z(z_0) \end{pmatrix}, \qquad (3.9.4a)$$

with,

$$\tilde{U}(z_1,z_0) = \tilde{L}_u \, \tilde{W}(z_1,z_0) \, \tilde{M}_u \,, \qquad (3.9.4b)$$

when the near surface layer is source free, which is the case in our derivation. Then, from the velocity and traction field at z_1, we can determine the up and downgoing one-way wavefields at the top of the lower medium with the decomposition operator $\tilde{M}_l$:

$$\begin{pmatrix} \vec{\tilde{p}}^{+}(z_1) \\ \vec{\tilde{p}}^{-}(z_1) \end{pmatrix} = \tilde{M}_l \begin{pmatrix} \vec{\tilde{v}}(z_1) \\ \vec{\tilde{\tau}}_z(z_1) \end{pmatrix} = \tilde{M}_l \, \tilde{U}(z_1, z_0) \begin{pmatrix} \vec{\tilde{v}}(z_0) \\ \vec{\tilde{\tau}}_z(z_0) \end{pmatrix}. \qquad (3.9.4c)$$

Taking into account that $\vec{\tilde{\tau}}_z(z_0) = \vec{0}$, we have :

$$\vec{\tilde{p}}^{-}(z_1) = \left(\left[\tilde{M}^{-}_{\alpha,l} \tilde{L}^{-}_{\alpha,u} \right] \left[\tilde{W}^{-}(z_0,z_1) \right]^{-1} \tilde{M}^{-}_{1,u} + \left[\tilde{M}^{-}_{\alpha,l} \tilde{L}^{+}_{\alpha,u} \right] \tilde{W}^{+}(z_1,z_0) \tilde{M}^{+}_{1,u} \right) \vec{\tilde{v}}(z_0) \,. \qquad (3.9.5a)$$

Using relations *(2.8.5c)*, *(2.8.6m)* and *(2.8.1f)* equation *(3.9.5a)* can be rewritten :

$$\vec{\tilde{p}}^{-}(z_1) = \left[\tilde{T}^{-}(z_1) \right]^{-1} \left[\left[\tilde{W}^{-}(z_0,z_1) \right]^{-1} - \tilde{R}^{+}(z_1) \tilde{W}^{+}(z_1,z_0) \tilde{R}^{-}(z_0) \right] M^{-}_{1,u} \vec{\tilde{v}}(z_0) \,, \qquad (3.9.5b)$$

As expected the two-way and one-way approaches lead to the same result.

This procedure can be extended to the case of a near surface medium consisting of a stack of horizontal homogeneous layers with interfaces at depths $z_1, z_2, \ldots, z_m$. To obtain the upgoing waves $\vec{\tilde{p}}^{-}(z_m)$ at the top of the lower medium from the measured particle velocities $\vec{\tilde{v}}(z_0)$ at the traction free surface, we first extrapolate the velocities and stresses from z_0 to z_m, using a cascaded combination of two-way extrapolation operators:

$$\begin{pmatrix} \vec{\tilde{v}}(z_m) \\ \vec{\tilde{\tau}}_z(z_m) \end{pmatrix} = \tilde{U}(z_m,z_{m-1}) \cdots \tilde{U}(z_1,z_0) \begin{pmatrix} \vec{\tilde{v}}(z_0) \\ \vec{0} \end{pmatrix}. \qquad (3.9.6a)$$

From the velocities and stresses at the top of the lower medium, we can determine the upgoing normal wavefield with the decomposition operator $\tilde{M}_l$:

$$\begin{pmatrix} \vec{\tilde{p}}^{+}(z_m) \\ \vec{\tilde{p}}^{-}(z_m) \end{pmatrix} = \tilde{M}_l \begin{pmatrix} \vec{\tilde{v}}(z_m) \\ \vec{\tilde{\tau}}_z(z_m) \end{pmatrix} = \tilde{M}_l \, \tilde{U}(z_m,z_{m-1}) \cdots \tilde{U}(z_1,z_0) \begin{pmatrix} \vec{\tilde{v}}(z_0) \\ \vec{0} \end{pmatrix}. \qquad (3.9.6b)$$

From which we deduce that:

$$\vec{\tilde{p}}^{-}(z_m) = [\boldsymbol{C}(z_m, z_0)]^{-1}\,\vec{\tilde{v}}(z_0)\,, \qquad (3.9.6c)$$

with $[\boldsymbol{C}(z_m, z_0)]^{-1}$ the lower left submatrix of the matrix product $\tilde{\boldsymbol{M}}_l\,\tilde{\boldsymbol{U}}(z_m,z_{m-1})\cdots\tilde{\boldsymbol{U}}(z_1,z_0)$.
In the case of an m layer near surface medium equation *(3.9.6c)* describes the decomposition operation at the receiver side that enables to obtain the upgoing wavefield $\vec{\tilde{p}}^{-}(z_m)$ at the top of the lower medium from the particle velocities $\vec{\tilde{v}}(z_0)$.
Going back to the case of a single near surface layer, it is interesting to know how the decomposition operator described in *(3.9.3b)* behaves when the upper layer thickness is small. Knowing that :

$$\lim_{(z_1-z_0)\to 0} \tilde{\boldsymbol{U}}(z_1,z_0) = \tilde{\boldsymbol{I}} \qquad (3.9.7a)$$

we then have :

$$\begin{pmatrix} \vec{\tilde{p}}^{+}(z_1) \\ \vec{\tilde{p}}^{-}(z_1) \end{pmatrix} \approx \tilde{\boldsymbol{M}}_l \begin{pmatrix} \vec{\tilde{v}}(z_0) \\ \vec{\tilde{\tau}}_z(z_0) \end{pmatrix} = \tilde{\boldsymbol{M}}_l \begin{pmatrix} \vec{\tilde{v}}(z_0) \\ \vec{0} \end{pmatrix}, \qquad (3.9.7b)$$

which implies that :

$$\vec{\tilde{p}}^{-}(z_1) = \tilde{\boldsymbol{M}}^{-}_{1,l}\,\vec{\tilde{v}}(z_0)\,. \qquad (3.9.7c)$$

We then conclude that in the case of a very thin near surface layer the decomposition operator at the receiver side that has to be used is the one of the **lower** medium $\tilde{\boldsymbol{M}}^{-}_{1,l}$ and not the one of the near surface layer $\tilde{\boldsymbol{M}}^{-}_{1,u}$. A layer can be considered as thin when the ratio of the layer thickness and the apparent vertical wavelength of the incident wave is small. This implies that:

- high frequency waves are more affected by the near surface layer than low frequency waves.
- *S* waves are more affected than *P* waves.

With simulated data we illustrate the influence of a thin low velocity near surface layer, as well as the effects of the dereverberation and decomposition operator at the receiver side *(3.9.3b)*. In *Figure 3.9.2* the thin layer model is displayed; traction sources are applied at the surface. *Figure 3.9.3* represents the vertical particle velocities recorded at the surface when a vertical traction source is applied. We can recognize the dispersion phenomena generated by the low velocity near surface layer. *Figure 3.9.4* represents the decomposed upgoing *P* wavefield without and with dereverberation. As can be seen the reverberation modifies the seismic wavelet. *Figure 3.9.5* represents the horizontal particle velocities recorded at the surface when a horizontal traction source is applied. We can recognize the dispersion phenomena that affect the seismic wavefield due to the presence of the low velocity near surface layer. *Figure 3.9.6* represents the decomposed upgoing *S* wavefield without and with dereverberation. The reverberation affects more the *S* wavefield than the *P* wavefield as the S wavelength is smaller than the *P* wavelength.

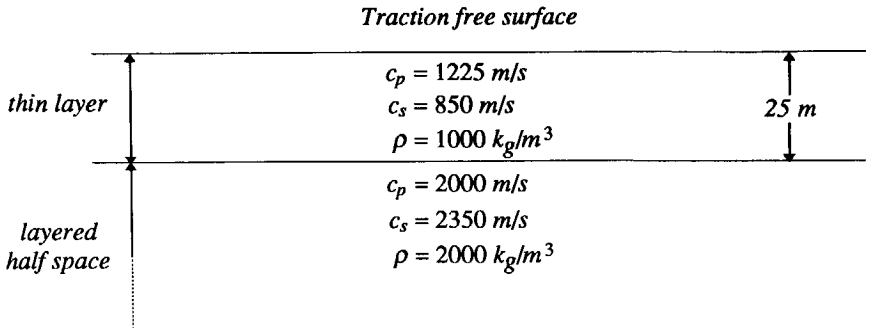

Figure 3.9.2

Thin low velocity near surface layer model

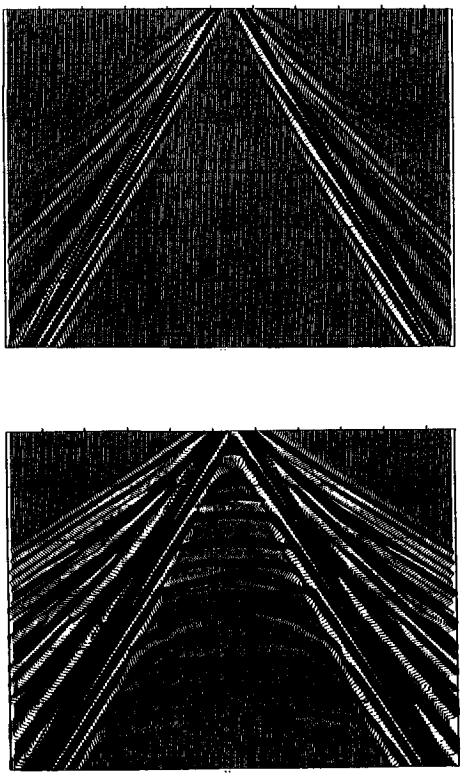

Figure 3.9.3

Vertical particle velocities recorded at the surface due to a vertical traction source

(a) 0 dB clipped (b) 40 dB clipped

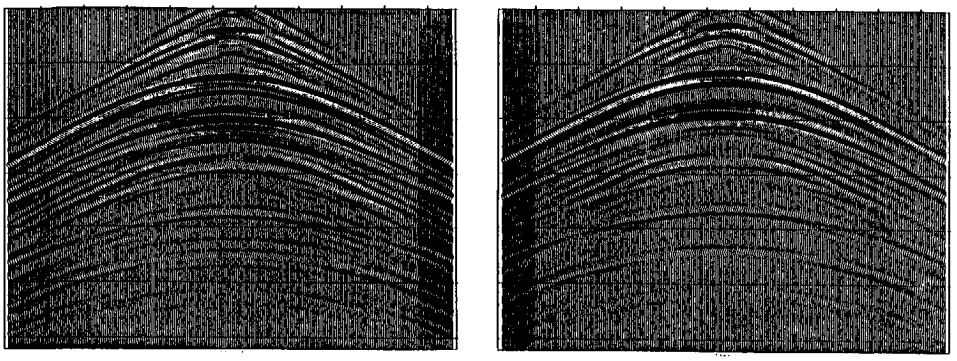

Figure 3.9.4

Decomposed upgoing P wavefield

(a) without dereverberation *(b) with dereverberation*

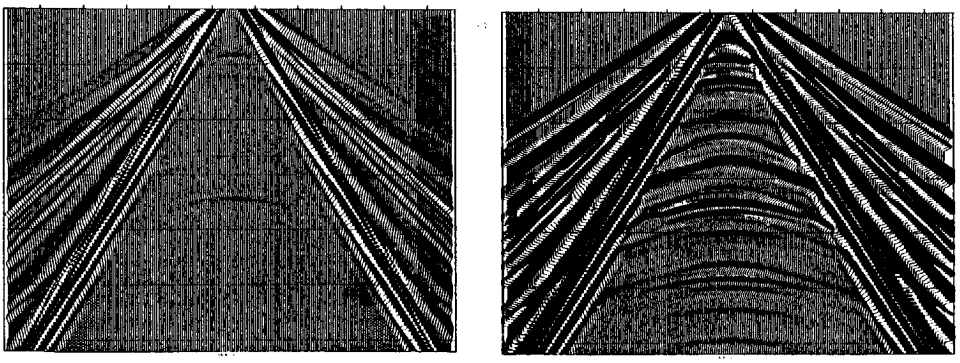

Figure 3.9.5

Horizontal particle velocities recorded at the surface due to a horizontal traction source

(a) 0 dB clipped *(b) 40 dB clipped*

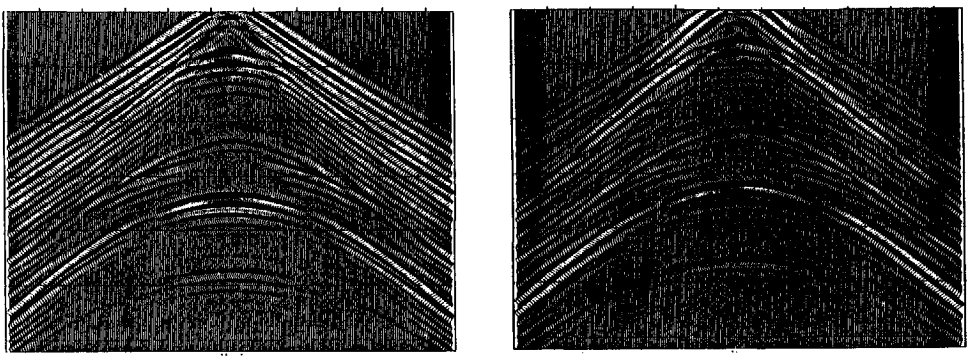

Figure 3.9.6

Decomposed upgoing S wavefield

(a) without dereverberation (b) with dereverberation

3.10 INFLUENCE OF NEAR SURFACE LAYERS ON THE SEISMIC SOURCE WAVEFIELD

The decomposition at the source side consists in simulating a pure downgoing normal source wavefield by combining several horizontal and vertical traction sources. The decomposition operator at the source side, that describes this traction distribution, is fully based on the expressions of the downgoing normal waves emitted by a traction source applied at the surface. These expressions involve the elastic parameters of the medium over which the traction is applied. In the case of one or more near surface layers we would like that the decomposition operator at the source side simulates a pure downgoing normal source wavefield in the lower medium and not in the near surface layers. To determine this operator we need to know what are the downgoing waves emitted in the lower medium due to a traction source applied at z_0. As for the previous study we start with the simple case of a single near surface layer, first with the one-way wave equations to see well all the wave phenomena involved, then with the two-way wave equation. This second approach enables to extend easily the results to the case of a multi-layer near surface medium.

One-way approach

With this approach, we follow the propagation of the downgoing plane source wave $\vec{\tilde{p}}_s^{+}(z_0)$

(emitted by a traction source $\vec{\tilde{\tau}}_{z,s}(z_0)$) through the near surface layer, to determine the transmitted downgoing waves $\vec{\tilde{p}}^{+}(z_1)$ in the lower medium. *Figure 3.10.1* illustrates the situation. The downgoing wave $\vec{\tilde{p}}_s^{+}(z_0)$ emitted by a traction source $\vec{\tilde{\tau}}_{z,s}(z_0)$ is given by :

$$\vec{\tilde{p}}_s^{+}(z_0) = \left[\tilde{L}_{2,u}^{+}\right]^{-1} \vec{\tilde{\tau}}_{z,s}(z_0) . \qquad (3.10.1)$$

To relate $\vec{\tilde{p}}^{+}(z_1)$ to $\vec{\tilde{\tau}}_{z,s}(z_0)$, we first need to know how $\vec{\tilde{p}}^{+}(z_1)$ is related to $\vec{\tilde{p}}_s^{+}(z_0)$. The relation is :

$$\vec{\tilde{p}}^{+}(z_1) = (\tilde{T}^{+}(z_1)\tilde{W}^{+}(z_1,z_0) + \tilde{T}^{+}(z_1)\left[\tilde{W}^{+}(z_1,z_0)\tilde{R}^{-}(z_0)\tilde{W}^{-}(z_0,z_1)\tilde{R}^{+}(z_1)\right]\tilde{W}^{+}(z_1,z_0) + \tilde{T}^{+}(z_1)\left[\tilde{W}^{+}(z_1,z_0)\tilde{R}^{-}(z_0)\tilde{W}^{-}(z_0,z_1)\tilde{R}^{+}(z_1)\right]^2 \tilde{W}^{+}(z_1,z_0) + \cdots) \vec{\tilde{p}}_s^{+}(z_0) \qquad (3.10.2a)$$

or equivalently,

$$\vec{\tilde{p}}^{+}(z_1) = \tilde{T}^{+}(z_1)\left[\tilde{I} - \tilde{W}^{+}(z_1,z_0)\tilde{R}^{-}(z_0)\tilde{W}^{-}(z_0,z_1)\tilde{R}^{+}(z_1)\right]^{-1} \tilde{W}^{+}(z_1,z_0)\, \vec{\tilde{p}}_s^{+}(z_0) . \qquad (3.10.2b)$$

The first term of the series *(3.10.2a)* describes the transmitted primary waves, taking into account the propagation effects in the upper layer to go from z_0 to z_1 and the transmission effects that affect the downgoing wavefield $\vec{\tilde{p}}^{+}(z_1)$ at the boundary z_1. The second term of the series accounts for the first order multiple :the primary waves are reflected at z_1, propagate upward to be reflected at the traction free surface z_0 and finally propagate downward from z_0 to z_1 to be transmitted into the lower medium. The $n+1^{st}$ term in the series accounts for the n^{th} order multiple.

The combination of equations *(3.10.1b)* and *(3.10.2b)* leads to the relation between $\vec{\tilde{p}}^{+}(z_1)$ and $\vec{\tilde{\tau}}_{z,s}(z_0)$:

$$\vec{\tilde{p}}^{+}(z_1) = \tilde{T}^{+}(z_1)\left[\tilde{I} - \tilde{W}^{+}(z_1,z_0)\tilde{R}^{-}(z_0)\tilde{W}^{-}(z_0,z_1)\tilde{R}^{+}(z_1)\right]^{-1} \tilde{W}^{+}(z_1,z_0)\left[\tilde{L}_{2,u}^{+}\right]^{-1} \vec{\tilde{\tau}}_{z,s}(z_0) . \qquad (3.10.3a)$$

It is interesting to note that the term $\left[\tilde{I} - \tilde{W}^{+}(z_1,z_0)\tilde{R}^{-}(z_0)\tilde{W}^{-}(z_0,z_1)\tilde{R}^{+}(z_1)\right]^{-1}$ is at the origin of a frequency dependent reverberation phenomenon. The operator developed in *(3.10.3a)* describes the downgoing waves emitted in the lower medium, generated by a surface traction source, taking into account all the near surface layer effects. The inverse of this operator is the composition operator at the source side that has to be used if we want to simulate a pure downgoing normal source wavefield in the lower medium:

$$\vec{\tilde{\tau}}_{z,s}(z_0) = \tilde{L}_{2,u}^{+}\left[\tilde{W}^{+}(z_0,z_1) - \tilde{R}^{-}(z_0)\tilde{W}^{-}(z_0,z_1)\tilde{R}^{+}(z_1)\right]\left(\tilde{T}^{+}(z_1)\right)^{-1} \vec{\tilde{p}}^{+}(z_1) . \qquad (3.10.3b)$$

Two-way approach

This more straightforward approach can be easily extended to the case of a multi-layer near surface. The two-way approach can be described as follows: knowing the upgoing and downgoing wavefields at z_1 in the lower medium $\vec{\tilde{p}}^{+}(z_1)$ and $\vec{\tilde{p}}^{-}(z_1)$, we can determine $\vec{\tilde{v}}(z_1)$ and $\vec{\tilde{\tau}}_z(z_1)$ using the composition operator $\tilde{L}_1$:

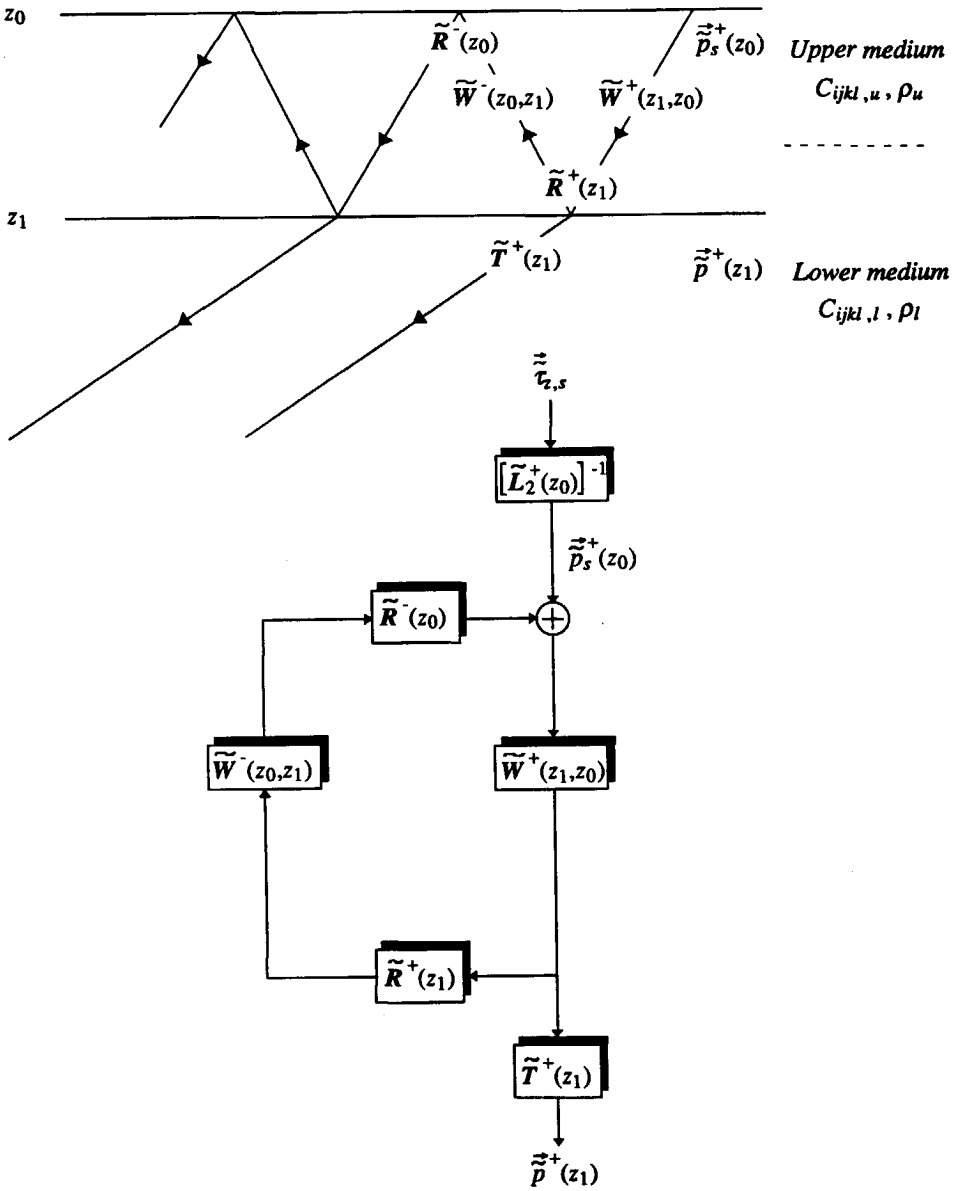

Figure 3.10.1

Downgoing source wavefields are affected by frequency dependent reverberation phenomena induced by the near surface layers.

$$\begin{pmatrix} \vec{\tilde{v}}(z_1) \\ \vec{\tilde{\tau}}_z(z_1) \end{pmatrix} = \tilde{L}_l \begin{pmatrix} \vec{\tilde{p}}^{+}(z_1) \\ \vec{0} \end{pmatrix}, \qquad (3.10.4a)$$

here we took into account that for a traction source applied at z_0 we only have downgoing waves in the lower medium (i.e $\vec{\tilde{p}}^{-}(z_1) = \vec{0}$).The velocity and traction wavefields can be extrapolated from z_1 to z_0 using the elastic two-way extrapolation operator $\tilde{U}(z_0, z_1)$:

$$\begin{pmatrix} \vec{\tilde{v}}(z_0) \\ \vec{\tilde{\tau}}_{z,s}(z_0) \end{pmatrix} = \tilde{U}(z_0, z_1) \begin{pmatrix} \vec{\tilde{v}}(z_1) \\ \vec{\tilde{\tau}}_z(z_1) \end{pmatrix} = \tilde{U}(z_0, z_1) \tilde{L}_l \begin{pmatrix} \vec{\tilde{p}}^{+}(z_1) \\ \vec{0} \end{pmatrix}, \qquad (3.10.4b)$$

with,

$$\tilde{U}(z_0, z_1) = \tilde{L}_u \, \tilde{W}(z_0, z_1) \, \tilde{M}_u \, . \qquad (3.10.4c)$$

We then have :

$$\vec{\tilde{\tau}}_{z,s}(z_0) = \left(\tilde{L}^{+}_{2,u} \tilde{W}^{+}(z_0,z_1) \left[\tilde{M}^{+}_{\alpha,u} \tilde{L}^{+}_{\alpha,l}\right] + \tilde{L}^{-}_{2,u} \tilde{W}^{-}(z_0,z_1) \left[\tilde{M}^{-}_{\alpha,u} \tilde{L}^{+}_{\alpha,l}\right]\right) \vec{\tilde{p}}^{+}(z_1) \, . \qquad (3.10.5a)$$

Using relations *(2.8.4e)*, *(2.8.1d)* and *(2.8.4f)* we obtain::

$$\vec{\tilde{\tau}}_{z,s}(z_0) = \tilde{L}^{+}_{2,u} \left[\tilde{W}^{+}(z_0,z_1) - \tilde{R}^{-}(z_0) \tilde{W}^{-}(z_0,z_1) \tilde{R}^{+}(z_1)\right] \left[\tilde{T}^{+}(z_1)\right]^{-1} \vec{\tilde{p}}^{+}(z_1) \, . \qquad (3.10.5b)$$

As expected the one-way and two-way approaches lead to the same result. The procedure can be extended to the case of a near surface medium consisting of a stack of horizontal layers with interfaces at depths $z_1, z_2, \ldots, z_m$. First from the upgoing and downgoing wavefields in the lower medium , $\vec{\tilde{p}}^{+}(z_m)$ and $\vec{\tilde{p}}^{-}(z_m) = \vec{0}$ we determine the associated particle velocities and tractions using the composition operator $\tilde{L}_l$:

$$\begin{pmatrix} \vec{\tilde{v}}(z_m) \\ \vec{\tilde{\tau}}_z(z_m) \end{pmatrix} = \tilde{L}_l \begin{pmatrix} \vec{\tilde{p}}^{+}(z_m) \\ \vec{0} \end{pmatrix}. \qquad (3.10.6a)$$

The velocity and traction wavefields are extrapolated from depth level z_m to the surface z_0 using a cascaded combination of two-way elastic extrapolation operators :

$$\begin{pmatrix} \vec{\tilde{v}}(z_0) \\ \vec{\tilde{\tau}}_{z,s}(z_0) \end{pmatrix} = \tilde{U}(z_0,z_1) \cdots \tilde{U}(z_{m-1},z_m) \begin{pmatrix} \vec{\tilde{v}}(z_m) \\ \vec{\tilde{\tau}}_z(z_m) \end{pmatrix} = \tilde{U}(z_0,z_1) \cdots \tilde{U}(z_{m-1},z_m) \tilde{L}_l \begin{pmatrix} \vec{\tilde{p}}^{+}(z_m) \\ \vec{0} \end{pmatrix}. \qquad (3.10.6b)$$

From which we deduce that :

$$\vec{\tilde{\tau}}_{z,s}(z_0) = \left[\tilde{D}(z_0,z_m)\right]^{-1} \vec{\tilde{p}}^{+}(z_m) \, , \qquad (3.10.6c)$$

$\left[\tilde{D}(z_0,z_m)\right]^{-1}$ being the lower left submatrix of the matrix product $\tilde{U}(z_0,z_1)..\tilde{U}(z_{m-1},z_m)\tilde{L}_l$. We deduce that in the case of an m layer near surface medium equation *(3.10.6c)* describes the decomposition operator at the source side that enables to simulate a downgoing normal source wavefield in the lower medium by combining several surface traction sources. This operator takes into account all the wave phenomena generated by the near surface layers.

Going back to the case of a single near surface layer, it is interesting to know how the decomposition operator at the source side *(3.10.5b)* behaves when the layer thickness becomes thinner and thinner. Following the same approach as for the decomposition at the receiver side we find that:

$$\vec{\vec{\tau}}_{z,s}(z_0) \approx \tilde{L}^{+}_{2,l}\,\vec{\vec{p}}^{\,+}(z_1)\,, \qquad (3.10.7)$$

We deduce that in the case of a thin near surface layer the decomposition operator at the source side that has to be used is the one of the lower medium $\tilde{L}^{+}_{2,l}$ and not the one of the near surface layer $\tilde{L}^{+}_{2,u}$.

APPENDIX 3A

MATRIX/VECTOR NOTATION FOR DISCRETIZED WAVEFIELDS

We review Berkhout's matrix notation, generalized for 2D and 3D applications. Consider a 2D wavefield, measured at a constant depth level as a function of lateral position and time, described by :

$$p(x, z_0, t) , \qquad (3A.1a)$$

where,

- p wavefield (for instance acoustic pressure),
- x lateral coordinate of the receivers,
- z_0 depth level of the acquisition surface,
- t time.

After a Fourier transformation from time to frequency, this wavefield is described by :

$$p(x, z_0, \omega) , \qquad (3A.1b)$$

where,

- p Fourier-transformed wavefield,
- ω circular frequency.

In the following we only consider the frequency-domain representation, that is, we assume that monochromatic wavefields $p(x, z_0, \omega_i)$ are available for a range of ω_i values. All these monochromatic wavefields can be treated independently. If we consider one frequency component ω_i only, then the discretized version of the wavefield can be represented by a vector, according to :

$$\vec{p}(z_0) = \begin{pmatrix} p\,(-K\,\Delta x,\, z_0,\, \omega_i) \\ \vdots \\ p\,(k\,\Delta x,\, z_0,\, \omega_i) \\ \vdots \\ p\,(K\,\Delta x,\, z_0,\, \omega_i) \end{pmatrix}, \qquad (3A.1c)$$

where Δx is the distance between the receivers.

For the seismic situation this vector may represent the (monochromatic) data in one common shot record. Let us now write this vector symbolically as :

$$\vec{p}(z_0) = \begin{pmatrix} p_{-K} \\ \vdots \\ p_k \\ \vdots \\ p_K \end{pmatrix} \begin{matrix} \downarrow \\ x_r \end{matrix}, \qquad (3A.2a)$$

where x_r denotes that the different elements in this vector correspond to the different lateral positions of the receivers. With this notation we can write the (monochromatic) data $p(x_r, x_s, z_0, \omega_i)$ of a 2D seismic survey symbolically as a matrix, according to :

$$\boldsymbol{P}(z_0) = \begin{pmatrix} & & \rightarrow x_s & & \\ p_{-K,\,-M} & \cdots & p_{-K,\,m} & \cdots & p_{-K,\,M} \\ \vdots & & \vdots & & \vdots \\ p_{k,\,-M} & \cdots & p_{k,\,m} & \cdots & p_{k,\,M} \\ \vdots & & \vdots & & \vdots \\ p_{K,\,-M} & \cdots & p_{K,m} & \cdots & p_{K,\,M} \end{pmatrix} \begin{matrix} \\ \downarrow \\ x_r \end{matrix}, \qquad (3A.2b)$$

where x_s denotes the different lateral positions of the sources. Each element $p_{k,m}$ correspond to a fixed lateral receiver coordinate $x_{r,k}$ and a fixed lateral source coordinate $x_{s,m}$. Each column (fixed x_s) in this data matrix represents one (monochromatic) common shot record; each row (fixed x_r) represents one common receiver record; the diagonal ($x_s = x_r$) represents zero-offset data and the anti-diagonal ($x_s = -x_r$) represents common midpoint data.

The (monochromatic) data $p(x_r, y_r, x_s, y_s, z_0, \omega_i)$ in a 3D seismic areal survey can also be represented by a matrix (Kinneging et al. 1989), according to :

$$\boldsymbol{P}(z_0) = \begin{pmatrix} & & \rightarrow y_s & & \\ \boldsymbol{P}_{-K,\,-M} & \cdots & \boldsymbol{P}_{-K,\,m} & \cdots & \boldsymbol{P}_{-K,\,M} \\ \vdots & & \vdots & & \vdots \\ \boldsymbol{P}_{k,\,-M} & \cdots & \boldsymbol{P}_{k,\,m} & \cdots & \boldsymbol{P}_{k,\,M} \\ \vdots & & \vdots & & \vdots \\ \boldsymbol{P}_{K,\,-M} & \cdots & \boldsymbol{P}_{K,m} & \cdots & \boldsymbol{P}_{K,\,M} \end{pmatrix} \begin{matrix} \\ \downarrow \\ y_r \end{matrix}, \qquad (3A.2c)$$

where y_r denotes the different cross-line positions of the receivers and where y_s denotes the different cross-line positions of the sources. Each submatrix $\boldsymbol{P}_{l,n}$ corresponds to a fixed cross-line receiver coordinate $y_{r,l}$ and a fixed cross-line source coordinate $y_{s,n}$. The elements in the sub-matrix itself are defined as in *(3A.2b)* (see *Figure 3A.1*). Note that each column (fixed

$x_S\, y_S$) of the total matrix $\boldsymbol{P}(z_0)$ represents one (monochromatic) common shot record and each row (fixed x_r, y_r) represents one common receiver record.

So far we considered the situation of single-component data. The data matrix for multi-component data contains 3×3 submatrices, each submatrix having a similar organization as the single component data matrix $\boldsymbol{P}(z_0)$, see for instance equation *(3.2.11c)*.

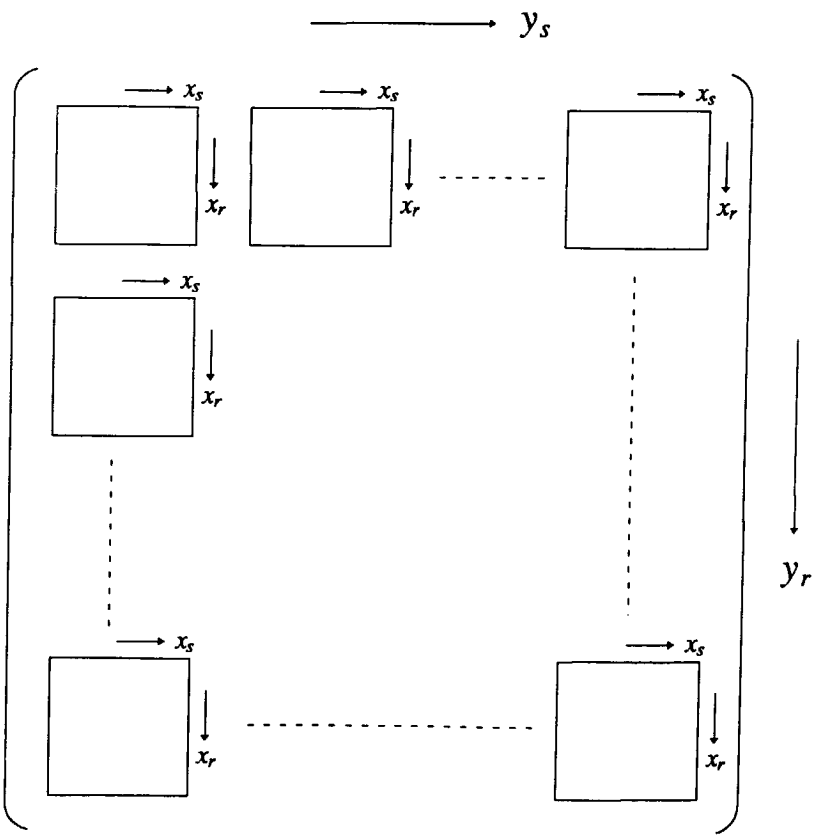

Figure 3A.1

Organization of the data matrix for a 3D seismic areal survey

CHAPTER 4

2D ACQUISITION OF 3D SEISMIC DATA

4.1 INTRODUCTION

Whenever the data acquisition is restricted to a multicomponent *line* survey rather than to an *areal* survey, we only get a 2D slice $(r,\theta=\theta_0,z=z_0,t)$ of the 3D seismic wavefield $(x,y,z=z_0,t)$, see *Figure 4.1.1* (r, radial distance, is used instead of x to point out that the wavefield is measured along a line of fixed azimuth θ_0). In this chapter we discuss under which conditions, the normal one-way wavefield decomposition can still be accurately achieved for such an acquisition geometry. As we will see it depends on the wavefield variations along the x and y directions. Only two types of wavefields can be well handled: wavefields that are constant along a direction (line source data) and wavefields with simple azimuthal symmetry. Apart from these two particular situations, two-way wavefields recorded along a line of detectors can not be uniquely decomposed into their normal one-way wavefields components.

4.2 LINE SOURCE DATA

In the hypothetical situation of a line source, the source function is constant along the line direction. Therefore, if the stiffness tensor $C_{ijkl}(x,y,z)$ and the density function $\rho(x,y,z)$ are constant functions along this direction, so will be the direct and reflected waves. For the example let us consider a line source oriented along the y-axis. As the wavefield is constant along the y- direction, the wavevectors of the plane waves that compose the elastic wavefield are of the type $(k_x, k_y=0, k_z)^T$. The plane-wave decomposition of the particle velocity vector

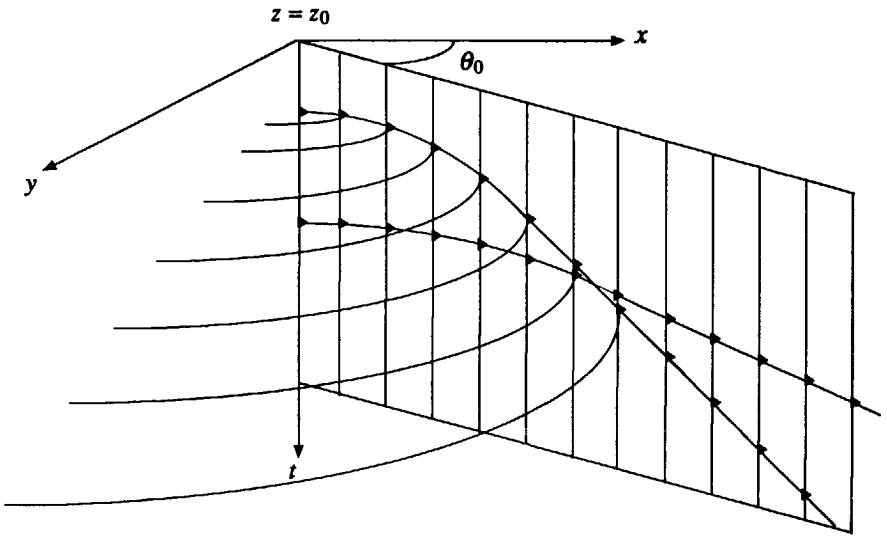

Figure 4.1.1

When the seismic wavefield is measured along a radius with azimuth angle θ_0, we only get a 2D slice ($r,\theta=\theta_0,z=z_0,t$) of the 3D seismic wavefield ($x,y,z=z_0,t$).

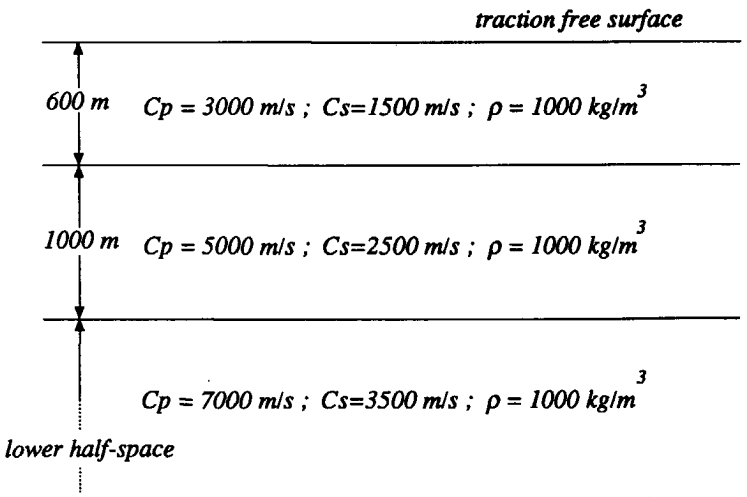

Figure 4.2.1

Model used to illustrate the difference in the seismic response between a line and a point source of vertical traction . In the following simulated data sets, the multiples and surface waves are ignored: they have not been modeled. The trace distance is 33m.

may then be done according to:

$$\begin{pmatrix} \tilde{v}_x(k_x, 0, z, \omega) \\ \tilde{v}_y(k_x, 0, z, \omega) \\ \tilde{v}_z(k_x, 0, z, \omega) \end{pmatrix} = \int_{-\infty}^{+\infty} \begin{bmatrix} e^{-jk_x x} & 0 & 0 \\ 0 & e^{-jk_x x} & 0 \\ 0 & 0 & e^{-jk_x x} \end{bmatrix}^H \begin{pmatrix} v_x(x, 0, z) \\ v_y(x, 0, z) \\ v_z(x, 0, z) \end{pmatrix} dx \,, \tag{4.2.1}$$

where H denotes Hermitian (transpose complex conjugate). A similar expression also holds for the traction components. The wavefield recorded along the x-direction at depth z_0, is enough to describe completely the wavefield over the whole surface $z=z_0$. The normal one-way wavefield decomposition is then possible. In the case that the subsurface stiffness tensor and/or the density are arbitrary functions of x, y and z, so will be the direct and reflected wavefields. The wavevectors $\vec{k} = (k_x, k_y, k_z)^T$ of the plane waves that compose the elastic wavefield may then have any direction. From the wavefield only recorded along the x-direction, it is then not possible to distinguish between plane waves with distinct k_y horizontal wavenumber. Consequently the wavefield decomposition into its normal one-way wavefield components can not be uniquely done.

To illustrate the difference between the wavefield emitted by a line source of vertical traction and a point source of vertical traction, we consider the simple model described in *Figure 4.2.1*. The seismic response (without multiples and surface waves) of this subsurface to a line source and to a point source is represented in *Figures 4.2.2* and *4.2.3*. Differences appear at near as well as at far offsets.

4.3 POINT SOURCE DATA

In reality the sources used in the field emit waves that have both a dependency along the x- and y- directions. Then, independently of the subsurface configuration, we can not assume any more that the elastic wavefield is constant along a direction. Wapenaar et al. (1992) propose to simulate the line source response of the subsurface from the point source response. They point out that a line source response is obtained from many point source responses by an integration along the source coordinate axis y_s, see *Figure 4.3.1*. The underlying assumption is that the point source responses are described by a linear wave equation. For a continuous distribution of point sources along the y_s-axis, the superposition principle may be mathematically formulated as :

$$\hat{p}(x_r, z_r; x_s, z_s; t) = \int_{-\infty}^{+\infty} p(x_r, y_r=0, z_r; x_s, y_s, z_s; t)\, dy_s \,, \tag{4.3.1}$$

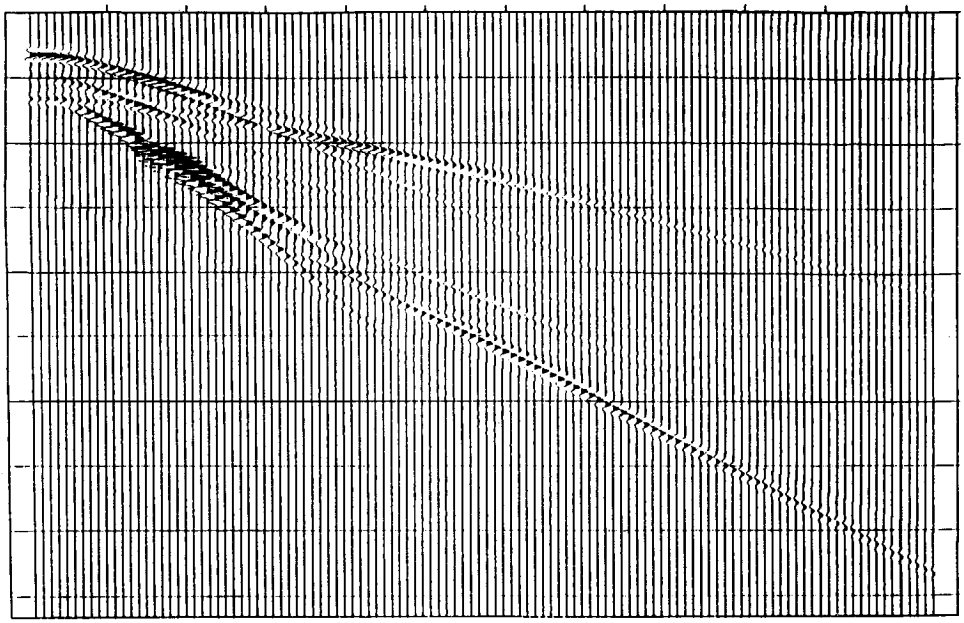

(a)

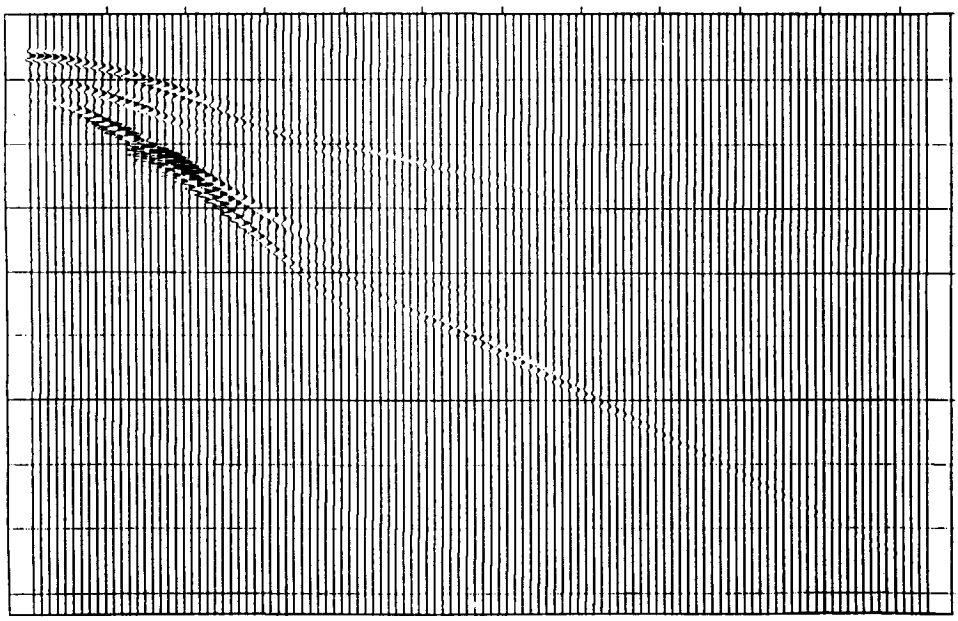

(b)

Figure 4.2.2

(a) vertical particle velocity component generated at the surface by a line source of vertical traction.

(b) vertical particle velocity component generated at the surface by a point source of vertical traction.

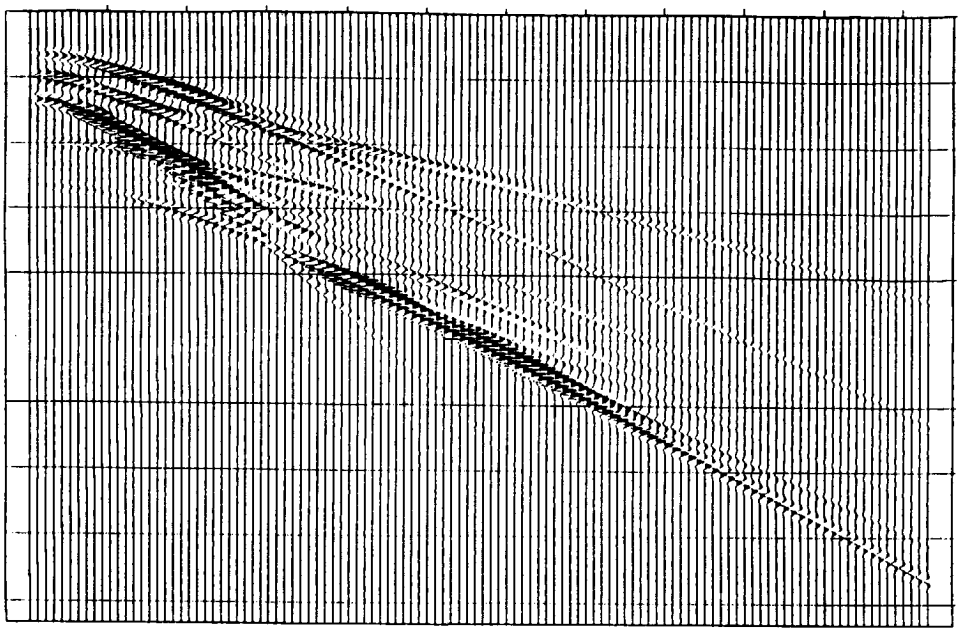

(a)

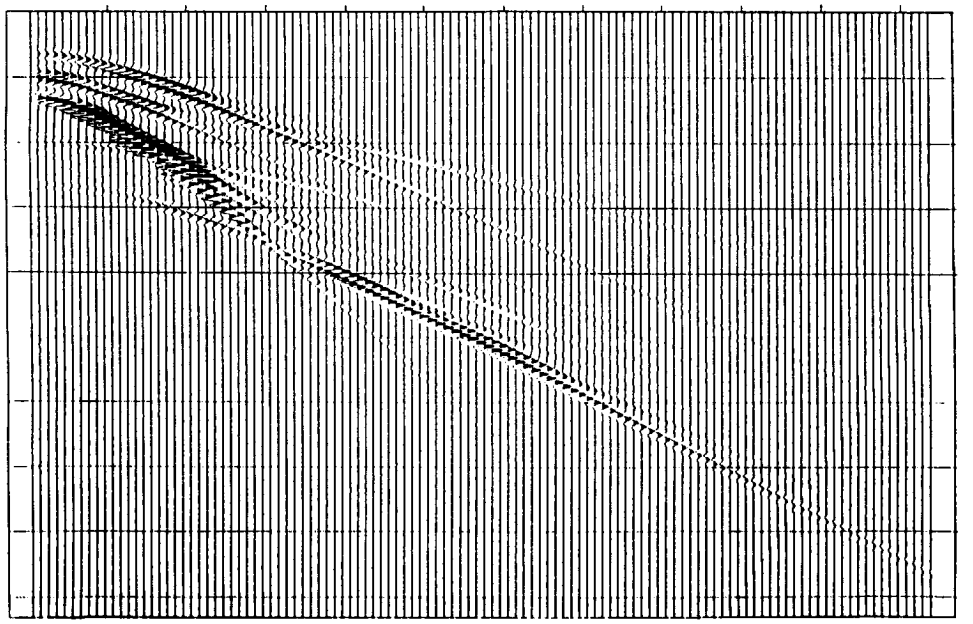

(b)

Figure 4.2.3

(a) horizontal particle velocity component generated at the surface by a line source of vertical traction.

(b) horizontal particle velocity component generated at the surface by a point source of vertical traction.

Here $p(x_r, y_r, z_r; x_s, y_s, z_s; t)$ is a point source response as a function of time (t) at receiver position (x_r, y_r, z_r) for a point source at (x_s, y_s, z_s) and $\hat{p}(x_r, z_r; x_s, z_s; t)$ is a line source response at receiver point (x_r, z_r) for a line source at (x_s, z_s). When the medium parameters are independent of the y_s- coordinate, the response of a point source at (x_s, y_s, z_s) is just a shifted version of the response of a point source at $(x_s, 0, z_s)$:

$$p(x_r, y_r, z_r; x_s, y_s, z_s; t) = p(x_r, y_r - y_s, z_r; x_s, 0, z_s; t) . \qquad (4.3.2)$$

Substitution in equation *(4.3.1)* yields :

$$\hat{p}(x_r, z_r; x_s, z_s; t) = \int_{-\infty}^{+\infty} p(x_r, -y_s, z_r; x_s, 0, z_s; t)\, dy_s , \qquad (4.3.3a)$$

or renaming the integration variable,

$$\hat{p}(x_r, z_r; x_s, z_s; t) = \int_{-\infty}^{+\infty} p(x_r, y_r, z_r; x_s, 0, z_s; t)\, dy_r . \qquad (4.3.3b)$$

The latter equation states that the line source response $\hat{p}(x_r, z_r; x_s, z_s; t)$ may be synthesized from a single point source response by carrying out an integration along the receiver coordinate y_r. The principle is visualized in *Figure 4.3.2*. Equation *(4.3.3b)* is not yet suited for practical situations where the response is often measured only for y_r=0. When the response satisfies certain symmetry properties in the x_r, y_r - plane, the integral *(4.3.3b)* along the receiver coordinate y_r may be replaced by an integral along the receiver coordinate x_r, as described by Wapenaar et al.(1992). The symmetry properties that make this procedure possible are verified for wavefields propagating in a laterally homogeneous medium, see section *4.5*. In the case of a moderate laterally inhomogeneous medium it is preferable to work per *CMP* (*C*ommon *M*id *P*oint) gather instead of per *CSP* (*C*ommon *S*hot *P*oint) gather. Once the point source response has been transformed into a line source response, the elastic wavefield can be decomposed with the 2-D version of the decomposition algorithm. Of course we must then be aware that we decompose the elastic wavefield generated by the simulated line source and no more the one generated by the original source.

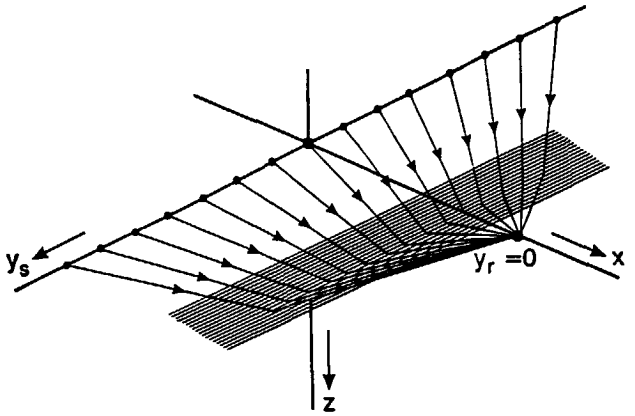

Figure 4.3.1

A line source response is obtained from many point source responses by integration along the source coordinate y_S.

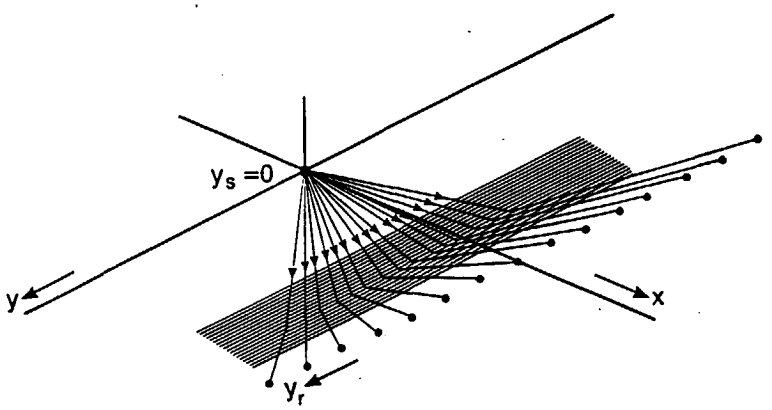

Figure 4.3.2

For any 2D inhomogeneous medium, a line source response may be obtained from one point source response by integration along the receiver coordinate y_r.

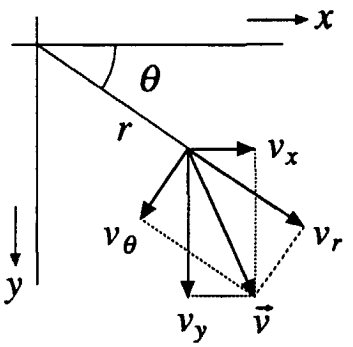

Figure 4.4.1

Plan view of the cartesian and cylindrical coordinate systems.

$v_r = v_x \cos\theta + v_y \sin\theta$, $v_\theta = - v_x \sin\theta + v_y \cos\theta$

4.4 CYLINDRICAL WAVE DECOMPOSITION OF 3D SEISMIC DATA

As explained in the previous section, a possibility to treat point source data consists in transforming the point source response into a line source response. In the case we want to preserve the point source amplitude behaviour, this transformation must be avoided. We leave the Cartesian coordinates *(x, y, z)* for the cylindrical coordinates *(r, θ, z)*, see *Figure 4.4.1*. The cylindrical coordinates are naturally adapted to the acquisition geometry we are dealing with. They enable to treat point source data without going through the line source transformation. A change of coordinates implies modifications in the transform domain introduced in chapter 2. Starting from the results established in 2.7, we show in Appendix 4A, how *cylindrical* waves (instead of plane waves) naturally appear in the seismic wavefield description when cylindrical coordinates are used. In this section we give, for an isotropic medium, the integral formulas that enable to transform the data from the space domain to the wavenumber domain and vice versa. In cylindrical coordinates, this data transformation corresponds to a cylindrical wave decomposition or composition of the data, depending on the direction of the transformation (forward or backward). The following expressions are exact for wavefields propagating in an isotropic laterally homogeneous medium. In the case of moderate lateral inhomogeneities, it is preferable to apply the transformations on *CMP* gathers rather then on *CSP* gathers.

In cylindrical coordinates, the forward transform of the particle velocity components from the space domain to the wavenumber domain reads (for all the derivations we refer to Appendix 4A, for the numerical aspects see Appendix 4B):

$$\begin{pmatrix} \tilde{v}_S^m(k_r,z,\omega) \\ \tilde{v}_T^m(k_r,z,\omega) \\ \tilde{v}_R^m(k_r,z,\omega) \end{pmatrix} = \frac{1}{2\pi} \int_0^{2\pi} \int_0^{+\infty} \begin{bmatrix} f_1^m(k_r r,\theta) & f_2^m(k_r r,\theta) & 0 \\ -f_2^m(k_r r,\theta) & f_1^m(k_r r,\theta) & 0 \\ 0 & 0 & f_3^m(k_r r,\theta) \end{bmatrix}^H \begin{pmatrix} v_r(r,\theta,z,\omega) \\ v_\theta(r,\theta,z,\omega) \\ v_z(r,\theta,z,\omega) \end{pmatrix} r dr d\theta \,, \tag{4.4.1a}$$

with,

$$f_1^m(k_r r,\theta) = g_1^m(k_r r)\, e^{jm\theta}\,; \quad g_1^m(k_r r) = \frac{j}{2}\left[J_{m-1}(k_r r) - J_{m+1}(k_r r)\right],$$

$$f_2^m(k_r r,\theta) = g_2^m(k_r r)\, e^{jm\theta}\,; \quad g_2^m(k_r r) = \frac{1}{2}\left[J_{m-1}(k_r r) + J_{m+1}(k_r r)\right],$$

$$f_3^m(k_r r,\theta) = J_m(k_r r)\, e^{jm\theta}\,.$$

The inverse transform from the wavenumber to the space domain reads:

$$\begin{pmatrix} v_r(r,\theta,z,\omega) \\ v_\theta(r,\theta,z,\omega) \\ v_z(r,\theta,z,\omega) \end{pmatrix} = \sum_{m=-\infty}^{+\infty} \int_0^{+\infty} \begin{bmatrix} f_1^m(k_r r,\theta) & f_2^m(k_r r,\theta) & 0 \\ -f_2^m(k_r r,\theta) & f_1^m(k_r r,\theta) & 0 \\ 0 & 0 & f_3^m(k_r r,\theta) \end{bmatrix} \begin{pmatrix} \tilde{v}_S^m(k_r,z,\omega) \\ \tilde{v}_T^m(k_r,z,\omega) \\ \tilde{v}_R^m(k_r,z,\omega) \end{pmatrix} k_r \, dk_r \, . \tag{4.4.1b}$$

Similar expressions are also valid for the traction components. The superscript m is an integer, it represents the azimuthal order of the cylindrical wave. The real k_r represents the horizontal wavenumber of the cylindrical wave. The cylindrical wave transformation matrices involved in expressions *(4.4.1ab)* are not diagonal, contrary to the plane wave transformation matrices. Consequently, to transform one of the horizontal components (radial or tangential), the other one has also to be used. It is interesting to note that under the far field approximation ($k_r r >> 1$), the transformation matrix can be well approximated by a diagonal matrix. Under the far field approximation we have:

$$f_1^m(k_r r,\theta) \approx j\, J_{m-1}(k_r r)\, e^{jm\theta} \tag{4.4.2a}$$

$$f_2^m(k_r r,\theta) \approx 0 \tag{4.4.2b}$$

The forward transform of the normal one-way wavefield components from the space to the wavenumber domain reads:

$$\begin{pmatrix} \tilde{\phi}^{\pm,m}(k_r,z,\omega) \\ \tilde{\psi}_s^{\pm,m}(k_r,z,\omega) \\ \tilde{\zeta}_s^{\pm,m}(k_r,z,\omega) \end{pmatrix} = \frac{1}{2\pi} \int_0^{2\pi} \int_0^{+\infty} \begin{bmatrix} f_3^m(k_r r,\theta) & 0 & 0 \\ 0 & f_3^m(k_r r,\theta) & 0 \\ 0 & 0 & f_3^m(k_r r,\theta) \end{bmatrix}^H \begin{pmatrix} \phi^{\pm}(r,\theta,z,\omega) \\ \psi_s^{\pm}(r,\theta,z,\omega) \\ \zeta_s^{\pm}(r,\theta,z,\omega) \end{pmatrix} r\, dr\, d\theta \, . \tag{4.4.3a}$$

The inverse transform of the normal one-way wavefield components from the space to the wavenumber domain reads:

$$\begin{pmatrix} \phi^{\pm}(r,\theta,z,\omega) \\ \psi_s^{\pm}(r,\theta,z,\omega) \\ \zeta_s^{\pm}(r,\theta,z,\omega) \end{pmatrix} = \sum_{m=-\infty}^{+\infty} \int_{-\infty}^{+\infty} \begin{bmatrix} f_3^m(k_r r,\theta) & 0 & 0 \\ 0 & f_3^m(k_r r,\theta) & 0 \\ 0 & 0 & f_3^m(k_r r,\theta) \end{bmatrix} \begin{pmatrix} \tilde{\phi}^{\pm,m}(k_r,z,\omega) \\ \tilde{\psi}_s^{\pm,m}(k_r,z,\omega) \\ \tilde{\zeta}_s^{\pm,m}(k_r,z,\omega) \end{pmatrix} k_r \, dk_r \, . \tag{4.4.3b}$$

The transformation matrices used for the normal one-way wavefield components are diagonal and are valid both for the near and far field terms.

Applying the cylindrical wave decomposition formulas to the two-way wavefield vectors, we obtain simple linear relations, similar to the ones developed in chapter 2, between the two-way and the normal one-way wavefield components. We have:

$$\begin{pmatrix} \vec{\tilde{v}}^{\,m} \\ \vec{\tilde{\tau}}_z^{\,m} \end{pmatrix} = \begin{pmatrix} \tilde{L}_1^{+} & \tilde{L}_1^{-} \\ \tilde{L}_2^{+} & \tilde{L}_2^{-} \end{pmatrix} \begin{pmatrix} \vec{\tilde{p}}^{\,+,m} \\ \vec{\tilde{p}}^{\,-,m} \end{pmatrix}, \tag{4.4.4a}$$

and its inverse,

$$\begin{pmatrix} \vec{\tilde{p}}^{\,+,m} \\ \vec{\tilde{p}}^{\,-,m} \end{pmatrix} = \begin{pmatrix} \tilde{M}_1^{+} & \tilde{M}_2^{+} \\ \tilde{M}_1^{-} & \tilde{M}_2^{-} \end{pmatrix} \begin{pmatrix} \vec{\tilde{v}}^{\,m} \\ \vec{\tilde{\tau}}_z^{\,m} \end{pmatrix}, \tag{4.4.4b}$$

with,

$\vec{\tilde{v}}^{\,m}$ the particle velocity vector :

$$\vec{\tilde{v}}^{\,m}(k_r,z,\omega) = \left(\tilde{v}_S^m(k_r,z,\omega),\, \tilde{v}_I^m(k_r,z,\omega),\, \tilde{v}_R^m(k_r,z,\omega)\right)^T, \tag{4.4.5a}$$

$\vec{\tilde{\tau}}_z^{\,m}$ the traction vector :

$$\vec{\tilde{\tau}}_z^{\,m}(k_r,z,\omega) = \left(\tilde{\tau}_{zS}^m(k_r,z,\omega),\, \tilde{\tau}_{zI}^m(k_r,z,\omega),\, \tilde{\tau}_{zR}^m(k_r,z,\omega)\right)^T, \tag{4.4.5b}$$

$\vec{\tilde{p}}^{\,+,m}$ the normal downgoing wavefield :

$$\vec{\tilde{p}}^{\,+,m}(k_r,z,\omega) = \left(\tilde{\phi}^{+,m}(k_r,z,\omega),\, \tilde{\psi}_s^{+,m}(k_r,z,\omega),\, \tilde{\zeta}_s^{+,m}(k_r,z,\omega)\right)^T, \tag{4.4.5c}$$

$\vec{\tilde{p}}^{\,-,m}$ the normal upgoing wavefield :

$$\vec{\tilde{p}}^{\,-,m}(k_r,z,\omega) = \left(\tilde{\phi}^{-,m}(k_r,z,\omega),\, \tilde{\psi}_s^{-,m}(k_r,z,\omega),\, \tilde{\zeta}_s^{-,m}(k_r,z,\omega)\right)^T, \tag{4.4.5d}$$

and

$$\tilde{L}_1^{\pm} = \frac{1}{\rho\omega}\begin{pmatrix} k_r & \pm jk_{z,s} & 0 \\ 0 & 0 & -1 \\ \pm k_{z,p} & -jk_r & 0 \end{pmatrix}, \tag{4.4.6a}$$

$$\tilde{L}_2^{\pm} = \frac{1}{k_s^2}\begin{pmatrix} \mp 2k_rk_{z,p} & -j(k_s^2-2k_r^2) & 0 \\ 0 & 0 & \pm k_{z,s} \\ (-k_s^2+2k_r^2) & \pm 2jk_rk_{z,s} & 0 \end{pmatrix}, \tag{4.4.6b}$$

$$\tilde{M}_1^{\pm} = \frac{\mu}{\omega}\begin{pmatrix} k_r & 0 & \pm\dfrac{(k_s^2-2k_r^2)}{2k_{z,p}} \\ \mp j\dfrac{(k_s^2-2k_r^2)}{2k_{z,s}} & 0 & +jk_r \\ 0 & -\dfrac{k_s^2}{2} & 0 \end{pmatrix}, \tag{4.4.6c}$$

$$\widetilde{M}_2^{\pm} = \frac{1}{2}\begin{pmatrix} \mp\frac{k_r}{k_{z,p}} & 0 & -1 \\ j & 0 & \mp\frac{jk_r}{k_{z,s}} \\ 0 & \pm\frac{k_s^2}{k_{z,s}} & 0 \end{pmatrix}. \qquad (4.4.6d)$$

The properties of the composition and decomposition matrices developed in chapters 2 and 3, stay valid here. Note that expressions *(4.4.6a-d)* can be deduced from expressions *(2.7.13b,c)* setting k_y to 0 and replacing k_x by k_r.

Expressions *(4.4.1a)* and *(4.4.3a)* make clear that the wavefield decomposition into cylindrical waves requires an integration over the azimuth angle θ, in order to separate the cylindrical waves of distinct azimuthal order m. In the case the seismic wavefield is only recorded along a line of detectors, that is, only for a given azimuth angle θ_0, the azimuthal integration can not be done. This has the consequence that the elastic wavefield decomposition into cylindrical waves can not be done uniquely, as we can not make the distinction between waves of distinct azimuthal behaviour. From the above remark we conclude that for such an acquisition geometry *the normal one-way wavefield decomposition is possible, if and only if the wavefield contains a unique type of known azimuthal symmetry.*

4.5 WAVEFIELD SYMMETRIES IN ISOTROPIC LATERALLY HOMOGENEOUS MEDIA

In this section, we show that when the subsurface is isotropic and laterally homogeneous, the elastic wavefield generated by traction point sources only contains one type of azimuthal symmetry.

Applying the change of variables:

$$k_x = k_r \cos\beta,\ k_y = k_r \sin\beta\,, \qquad (4.5.1a)$$

in expressions *(3.6.2)*, we obtain (in the wavenumber domain) the azimuthal behaviour as a function of β of the downgoing P, S_v and S_h monochromatic plane waves emitted by surface traction sources. From this, we can deduce in the space domain, the azimuthal behaviour as a function of θ of the downgoing emitted P and S waves. The azimuthal angle θ is defined according to:

$$x = r\cos\theta,\ y = r\sin\theta\,. \qquad (4.5.1b)$$

The azimuthal behaviour, in the space domain, of the downgoing P, Sv and Sh waves emitted by horizontal and vertical traction sources applied to the earth surface, is summarized in *table 4.5.1*.

	τ_{xz}	τ_{yz}	τ_{zz}
Φ^+	$cos\theta$	$sin\theta$	1
Ψ^+	$cos\theta$	$sin\theta$	1
ζ^+	$sin\theta$	$cos\theta$	0

(table 4.5.1)

From the azimuthal dependency of the downgoing emitted P and S, waves we can determine the azimuthal dependency of the radial (v_r, τ_{rz}), tangential $(v_\theta, \tau_{\theta z})$ and vertical (v_z, τ_{zz}) particle velocity and traction field. The following relations are obtained :

	τ_{xz}	τ_{yz}	τ_{zz}
v_r , τ_{rz}	$cos\theta$	$sin\theta$	1
v_z , τ_{zz}	$cos\theta$	$sin\theta$	1
v_θ , $\tau_{\theta z}$	$sin\theta$	$cos\theta$	0

(table 4.5.2)

table 4.5.2 illustrates well that the particle velocity and the vertical traction field generated by surface traction sources have a simple azimuthal dependency. In the case of a laterally homogeneous subsurface the azimuthal behaviour of the elastic wavefield is preserved during reflection and transmission at horizontal interfaces. This means that for such a medium the azimuthal dependency displayed in *table 4.5.2* does not only apply to the downgoing source wavefield but to all wave types (body and surface waves), at any depth level. Consequently the azimuthal dependency of the normal one-way wavefield displayed in *table 4.5.1*, does not only apply to the downgoing normal source wavefield but also to all upgoing and downgoing normal wavefields at any depth level.

To summarize we may say that the elastic wavefield, generated by surface traction point sources applied over an isotropic horizontally layered medium, only involves one type of azimuthal symmetry. This result can be extended to buried horizontal and vertical body force point - sources. Due to this simple situation, the integral over θ in equation *(4.4.1a)* can be computed analytically, meaning that it is possible to decompose such a seismic wavefield into its cylindrical wave components, even if it has only been recorded at a single azimuthal angle θ_0. In the following we give the expression of the cylindrical wave decomposition formulas that must be applied to the two-way wavefield vector $\vec{v}(r,\theta_0,z,\omega)$ generated by a surface traction source $(\tau_{iz}, i=x, y, z)$.

For a τ_{zz} traction source :

$$\vec{v}(r,\theta,z,\omega) = v_r(r,\theta_0,z,\omega)\,\vec{r} + v_z(r,\theta_0,z,\omega)\,\vec{z}\,, \qquad (4.5.3a)$$

from which we deduce that :

$$\vec{\tilde{v}}^{m}(k_r,z,\omega) = \vec{0} \text{ for } m \neq 0 , \tag{4.5.3b}$$

for the components of the vector $\vec{\tilde{v}}^{m}$ we refer to *(4.4.5a)* and, for $m=0$:

$$\begin{pmatrix} \tilde{v}_S^0(k_r,z,\omega) \\ \tilde{v}_T^0(k_r,z,\omega) \\ \tilde{v}_R^0(k_r,z,\omega) \end{pmatrix} = \int_0^{+\infty} \begin{bmatrix} -jJ_1(k_r r) & 0 & 0 \\ 0 & -jJ_1(k_r r) & 0 \\ 0 & 0 & J_0(k_r r) \end{bmatrix}^H \begin{pmatrix} v_r(r,\theta_0,z,\omega) \\ v_\theta(r,\theta_0,z,\omega) \\ v_z(r,\theta_0,z,\omega) \end{pmatrix} rdr . \tag{4.5.3c}$$

For a τ_{xz} traction source:

$$\vec{v}(r,\theta,z,\omega) = cos\ \theta \frac{v_r(r,\theta_0,z,\omega)}{cos\ \theta_0} \vec{r} + sin\ \theta \frac{v_\theta(r,\theta_0,z,\omega)}{sin\ \theta_0} \vec{\theta} + cos\ \theta \frac{v_z(r,\theta_0,z,\omega)}{cos\ \theta_0} \vec{z}, \tag{4.5.4a}$$

from which we deduce that :

$$\vec{\tilde{v}}^{m}(k_r,z,\omega) = \vec{0} \text{ for } m \neq \pm 1 , \tag{4.5.4b}$$

and, for m=±1:

$$\vec{\tilde{v}}^{(\pm 1)}(k_r,z,\omega) = \frac{1}{2} \int_0^{+\infty} \begin{bmatrix} g_1^1(k_r r) & g_2^1(k_r r) & 0 \\ \mp jg_2^1(k_r r) & \pm jg_1^1(k_r r) & 0 \\ 0 & 0 & \pm J_1(k_r r) \end{bmatrix}^H \begin{pmatrix} v_r(r,\theta_0,z,\omega)/cos\ \theta_0 \\ v_\theta(r,\theta_0,z,\omega)/sin\ \theta_0 \\ v_z(r,\theta_0,z,\omega)/cos\ \theta_0 \end{pmatrix} rdr . \tag{4.5.4c}$$

For a τ_{yz} traction source:

$$\vec{v}(r,\theta,z,\omega) = sin\ \theta \frac{v_r(r,\theta_0,z,\omega)}{sin\ \theta_0} \vec{r} + cos\ \theta \frac{v_\theta(r,\theta_0,z,\omega)}{cos\ \theta_0} \vec{\theta} + sin\ \theta \frac{v_z(r,\theta_0,z,\omega)}{sin\ \theta_0} \vec{z}, \tag{4.5.5a}$$

from which we deduce that :

$$\vec{\tilde{v}}^{m}(k_r,z,\omega) = \vec{0} \text{ for } m \neq \pm 1 , \tag{4.5.5b}$$

and, for m=±1:

$$\vec{\tilde{v}}^{(\pm 1)}(k_r,z,\omega) = \frac{1}{2} \int_0^{+\infty} \begin{bmatrix} \pm jg_1^1(k_r r) & \pm jg_2^1(k_r r) & 0 \\ -g_2^1(k_r r) & g_1^1(k_r r) & 0 \\ 0 & 0 & jJ_1(k_r r) \end{bmatrix}^H \begin{pmatrix} v_r(r,\theta_0,z,\omega)/sin\ \theta_0 \\ v_\theta(r,\theta_0,z,\omega)/cos\ \theta_0 \\ v_z(r,\theta_0,z,\omega)/sin\ \theta_0 \end{pmatrix} rdr . \tag{4.5.5c}$$

These expressions (also valid for the vertical traction field) look complicated, but they are valid both for the near- and the far-field. In Appendix 4A we see that the cylindrical wave decomposition formulas greatly simplify when we neglect the near-field terms. Under the far field approximation $(k_r r >> 1)$ the transformation matrix simplifies to a diagonal matrix. We have:

$$g_1^1(k_r r) \approx jJ_0(k_r r) \text{ and } g_2^1(k_r r) \approx 0. \qquad (4.5.6)$$

The above formulas show that the cylindrical wave decomposition of the two-way wavefield involves Hankel transformations of zero, first and second order. In the next section, we present how they can be efficiently computed. The transformation formulas involve divisions by $cos\ \theta_0$ and $sin\ \theta_0$, which are unstable for the following azimuth angles $\theta_0 = 0,\ \pi/2,\ \pi,\ 3\pi/2$. It is then advantageous to make use of the following relations:

$$\frac{v_r^{\tau_{xz}}(r,\theta_0,z,\omega)}{cos\ \theta_0} = \frac{v_r^{\tau_{yz}}(r,\theta_0,z,\omega)}{sin\ \theta_0}, \qquad (4.5.7a)$$

$$\frac{v_\theta^{\tau_{xz}}(r,\theta_0,z,\omega)}{sin\ \theta_0} = -\frac{v_\theta^{\tau_{yz}}(r,\theta_0,z,\omega)}{cos\ \theta_0}, \qquad (4.5.7b)$$

$$\frac{v_z^{\tau_{xz}}(r,\theta_0,z,\omega)}{cos\ \theta_0} = \frac{v_z^{\tau_{yz}}(r,\theta_0,z,\omega)}{sin\ \theta_0}, \qquad (4.5.7c)$$

where the notation $v_i^{\tau_{jz}}$ means i^{th} component of the particle velocity field generated by a τ_{jz} traction source.

Wavefield decomposition at the receiver side

Once the wavefield has been decomposed into cylindrical waves, it is possible to do a correct normal one-way wavefield decomposition at the receiver side with the decomposition operator $\left[\tilde{C}(z_0)\right]^{-1} = \tilde{M}_1^-(z_0)$. The decomposed wavefield can be transformed back to the space domain by applying an inverse Hankel transform, the order of the Bessel function depending on the source type:

for a τ_{zz} source, we have:

$$\begin{pmatrix} \phi^-(r,\theta,z,\omega) \\ \psi_s^-(r,\theta,z,\omega) \\ \zeta_s^-(r,\theta,z,\omega) \end{pmatrix} = \int_0^{+\infty} \begin{bmatrix} J_0(k_r r) & 0 & 0 \\ 0 & J_0(k_r r) & 0 \\ 0 & 0 & J_0(k_r r) \end{bmatrix} \begin{pmatrix} \tilde{\phi}^-(k_r,z,\omega) \\ \tilde{\psi}_s^-(k_r,z,\omega) \\ 0 \end{pmatrix} k_r dk_r . \qquad (4.5.8a)$$

For a τ_{xz} source, we have:

$$\begin{pmatrix} \phi^-(r,\theta,z,\omega) \\ \psi_s^-(r,\theta,z,\omega) \\ \zeta_s^-(r,\theta,z,\omega) \end{pmatrix} = \int_0^{+\infty} \begin{bmatrix} J_1(k_r r) & 0 & 0 \\ 0 & J_1(k_r r) & 0 \\ 0 & 0 & J_1(k_r r) \end{bmatrix} \begin{pmatrix} \cos\theta\, \tilde{\phi}^-(k_r,z,\omega) \\ \cos\theta\, \tilde{\psi}_s^-(k_r,z,\omega) \\ \sin\theta\, \tilde{\zeta}_s^-(k_r,z,\omega) \end{pmatrix} k_r dk_r \,. \tag{4.5.8b}$$

For a τ_{yz} source, we have:

$$\begin{pmatrix} \phi^-(r,\theta,z,\omega) \\ \psi_s^-(r,\theta,z,\omega) \\ \zeta_s^-(r,\theta,z,\omega) \end{pmatrix} = \int_0^{+\infty} \begin{bmatrix} J_1(k_r r) & 0 & 0 \\ 0 & J_1(k_r r) & 0 \\ 0 & 0 & J_1(k_r r) \end{bmatrix} \begin{pmatrix} \sin\theta\, \tilde{\phi}^-(k_r,z,\omega) \\ \sin\theta\, \tilde{\psi}_s^-(k_r,z,\omega) \\ \cos\theta\, \tilde{\zeta}_s^-(k_r,z,\omega) \end{pmatrix} k_r dk_r \,. \tag{4.5.9c}$$

For the illustration, we consider a 3D seismic wavefield measured at a traction free surface, for the azimuth angle $\theta_0=0$, see *Figure 4.5.1*. The subsurface consists of a number of isotropic laterally homogeneous layers. To generate the data we used a buried point source, that only emits P waves, without azimuthal dependency. *Figures 4.5.2a* and *4.5.3a* represent the decomposed P and S wavefields when the proper transforms are applied to the data. *Figures 4.5.2b* and *4.5.3b* represent the decomposed P and S wavefields, when the data are erroneously decomposed into plane waves instead of cylindrical waves. It is interesting to note that in both cases the P and S waves are well separated. The differences appear in the relative amplitude of the decomposed arrivals and in the wavelet phase.

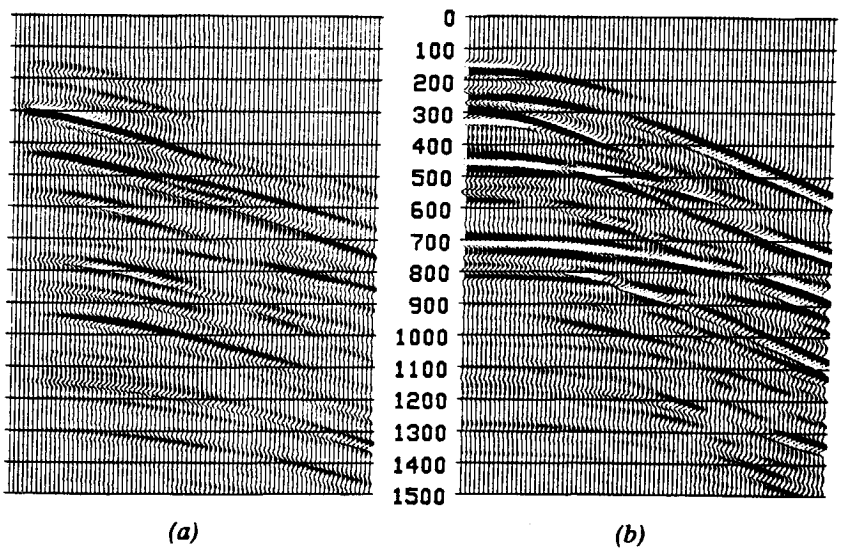

Figure 4.5.1

3D seismic wavefield measured at the traction free surface, for the azimuth angle $\theta_0 = 0$. trace interval: 20m. a) radial particle velocities b) vertical particle velocities.

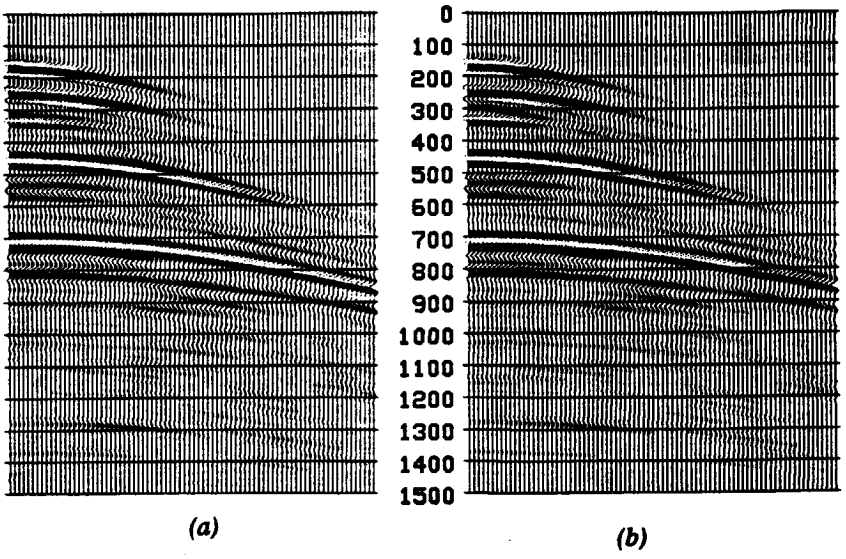

Figure 4.5.2

Decomposed P wavefield

a) with the appropriate cylindrical wave decomposition of the wavefield

b) with a plane wave decomposition of the wavefield.

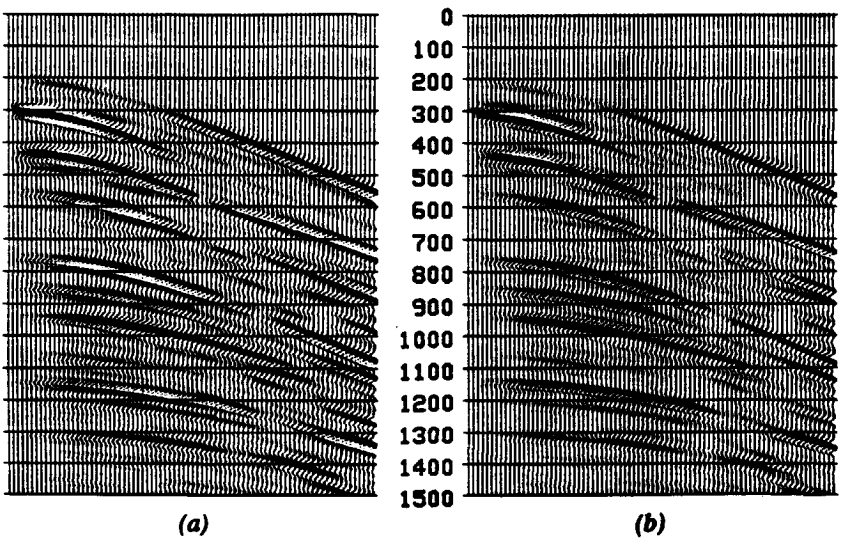

Figure 4.5.3

Decomposed S wavefield

a) with the appropriate cylindrical wave decomposition of the wavefield

b) with a plane wave decomposition of the wavefield

APPENDIX 4A

THE TRANSFORM DOMAIN IN CYLINDRICAL COORDINATES

In section 2.3 we have seen that when the wavefield is described with Cartesian coordinates, the transformation from the space to the wavenumber domain corresponds to a plane wave decomposition of the data. In this appendix, we assume the wavefield to be described with cylindrical coordinates. We show that within this system of coordinates the transformation from the space to the wavenumber domain corresponds to a cylindrical wave decomposition of the data.

In a homogeneous isotropic medium, the particle velocity vector can be described with the scalar potential ϕ (for the P waves) and the two potentials ψ and ζ (for the S_v and S_h waves). In the space-frequency domain the relation between the particle velocity vector and the three potentials reads:

$$\vec{v} = -\frac{1}{j\rho\omega}(\vec{\nabla}\phi - \vec{\nabla}\times\vec{\nabla}\times\vec{\psi} + \vec{\nabla}\times\vec{\zeta}), \qquad (4A.1a)$$

with,

$$\vec{\psi} = (0,0,\psi)^T \qquad (4A.1b)$$

and

$$\vec{\zeta} = (0,0,\zeta)^T. \qquad (4A.1c)$$

In a source free medium, the three potentials are solutions of the Helmholtz equations:

$$\nabla^2\phi + \frac{\omega^2}{c_p^2}\phi = 0, \qquad (4A.2a)$$

$$\nabla^2 \vec{\psi} + \frac{\omega^2}{c_s^2} \vec{\psi} = \vec{0}\,, \tag{4A.2b}$$

$$\nabla^2 \vec{\zeta} + \frac{\omega^2}{c_s^2} \vec{\zeta} = \vec{0}\,. \tag{4A.2c}$$

The method of separation of variables applied to the differential equations *(4A.2)* (see Goudet (1943)) establishes that the general solution is a superposition of cylindrical waves of the type:

$$\phi^m(k_r,r,\theta,z,\omega) = Y^m(k_r,r,\theta)\, \tilde{\phi}^m(k_r,z,\omega), \tag{4A.3a}$$

$$\psi^m(k_r,r,\theta,z,\omega) = Y^m(k_r,r,\theta)\, \tilde{\psi}^m(k_r,z,\omega), \tag{4A.3b}$$

$$\zeta^m(k_r,r,\theta,z,\omega) = Y^m(k_r,r,\theta)\, \tilde{\zeta}^m(k_r,z,\omega). \tag{4A.3c}$$

The horizontal wave function $Y^m(k_r,r,\theta)$ is defined as:

$$Y^m(k_r, r,\theta) = J_m(k_r r)\, e^{jm\theta}, \tag{4A.4}$$

with $J_m(k_r r)$ the m^{th} order Bessel function. The vertical wave functions $\tilde{\phi}^m(k_r,z,\omega)$, $\tilde{\psi}^m(k_r,z,\omega)$ and $\tilde{\zeta}^m(k_r,z,\omega)$ are defined according to:

$$\tilde{\phi}^m(k_r,z,\omega) = \tilde{\phi}^{+,m}(k_r,z,\omega) + \tilde{\phi}^{-,m}(k_r,z,\omega)\,, \tag{4A.5a}$$

with,

$$\tilde{\phi}^{\pm,m}(k_r,z,\omega) = \tilde{\phi}_0^{\pm,m}(k_r,\omega) e^{\mp jk_{z,p}z}, \tag{4A.5b}$$

$$\tilde{\psi}^m(k_r,z,\omega) = \tilde{\psi}^{+,m}(k_r,z,\omega) + \tilde{\psi}^{-,m}(k_r,z,\omega)\,, \tag{4A.5c}$$

with,

$$\tilde{\psi}^{\pm,m}(k_r,z,\omega) = \tilde{\psi}_0^{\pm,m}(k_r,\omega) e^{\mp jk_{z,s}z}, \tag{4A.5d}$$

and

$$\tilde{\zeta}^m(k_r,z,\omega) = \tilde{\zeta}^{+,m}(k_r,z,\omega) + \tilde{\zeta}^{-,m}(k_r,z,\omega)\,, \tag{4A.5e}$$

with,

$$\tilde{\zeta}^{\pm,m}(k_r,z,\omega) = \tilde{\zeta}_0^{\pm,m}(k_r,\omega) e^{\mp jk_{z,s}z}, \tag{4A.5f}$$

For the *P* waves the vertical wavenumber $k_{z,p}$ reads:

$$k_{z,p}^2 = \frac{\omega^2}{c_p^2} - k_r^2, \tag{4A.6a}$$

similarly, for the *S* waves the vertical wavenumber $k_{z,s}$ reads:

$$k_{z,s}^2 = \frac{\omega^2}{c_s^2} - k_r^2, \tag{4A.6b}$$

The azimuthal dependency of the cylindrical wave is described by $e^{jm\theta}$. As we must have $e^{jm\theta} = e^{jm(\theta+2\pi)}$ for any angle θ, the azimuthal order m must be an integer. The radial amplitude behaviour of such a wave is determined by the m^{th} order Bessel function $J_m(k_r r)$,

with k_r the horizontal wavenumber. Note that a cylindrical wave is fully determined by its azimuthal order and its horizontal wavenumber. The wave splitting in expressions *(4A.5)* corresponds to a decomposition of the compressional and shear wavefield in an upgoing *(-)* and downgoing *(+)* part. $\tilde{\phi}^{\pm,m}(k_r,z,\omega)$, $\tilde{\psi}^{\pm,m}(k_r,z,\omega)$ and $\tilde{\zeta}^{\pm,m}(k_r,z,\omega)$ are the normal one-way wavefield components of the cylindrical wave of azimuthal order m and of horizontal wavenumber k_r.

The combination of all the possible cylindrical P waves leads to the solution of equation *(4A.2a)*. We have:

$$\phi(r,\theta,z,\omega) = \sum_{m=-\infty}^{+\infty} \int_0^{+\infty} \phi^m(k_r,r,\theta,z,\omega)\, k_r dk_r. \qquad (4A.7a)$$

or equivalently,

$$\phi(r,\theta,z,\omega) = \sum_{m=-\infty}^{+\infty} \int_0^{+\infty} \tilde{\phi}^m(k_r,z,\omega)\, J_m(k_r r)\, e^{jm\theta}\, k_r dk_r. \qquad (4A.7b)$$

To decompose the P wavefield from the space to the wavenumber domain, we must be able to separate the cylindrical waves of distinct azimuthal order m and of distinct wavenumber k_r. This can be done according to:

$$\tilde{\phi}^m(k_r, z, \omega) = \frac{1}{2\pi} \int_0^{2\pi} \int_0^{+\infty} \phi(r, \theta, z, \omega) \left[J_m(k_r r)\, e^{jm\theta}\right]^* r dr\, d\theta, \qquad (4A.8)$$

where * denotes complex conjugate. Similar expressions are obtained for $\tilde{\psi}^m(k_r,z,\omega)$ and $\tilde{\zeta}^m(k_r,z,\omega)$.

Solutions of the type *(4A.7)* mean that in a homogeneous isotropic medium any P or S wavefield is the result of a cylindrical wave composition. In *Figure 4A.1*, the radial and time variations of a cylindrical wave of fixed horizontal wavenumber k_r and of fixed frequency ω is shown for the azimuth angle $\theta=0$, for different azimuthal orders m.

From expression *(4A.3)* it is possible using expression *(4A.1a)* and the constitutive relation, to derive the particle velocity as well as the traction field generated by a P and/or S cylindrical wave. Knowing that the gradient and the curl of the horizontal wave functions are often used, we introduce the following vectors:

$$\vec{S}^m(k_r,r,\theta) = \frac{j}{k_r} \vec{\nabla} Y^m(k_r,r,\theta) = g_1^m(k_r r)\, e^{jm\theta}\, \vec{r} - g_2^m(k_r r)\, e^{jm\theta}\, \vec{\theta}, \qquad (4A.9a)$$

$$\vec{T}^m(k_r,r,\theta) = -\frac{j}{k} \vec{\nabla} \times (0,0,Y^m(k_r,r,\theta))^T = g_2^m(k_r r)\, e^{jm\theta}\, \vec{r} + g_1^m(k_r r)\, e^{jm\theta}\, \vec{\theta}, \qquad (4A.9b)$$

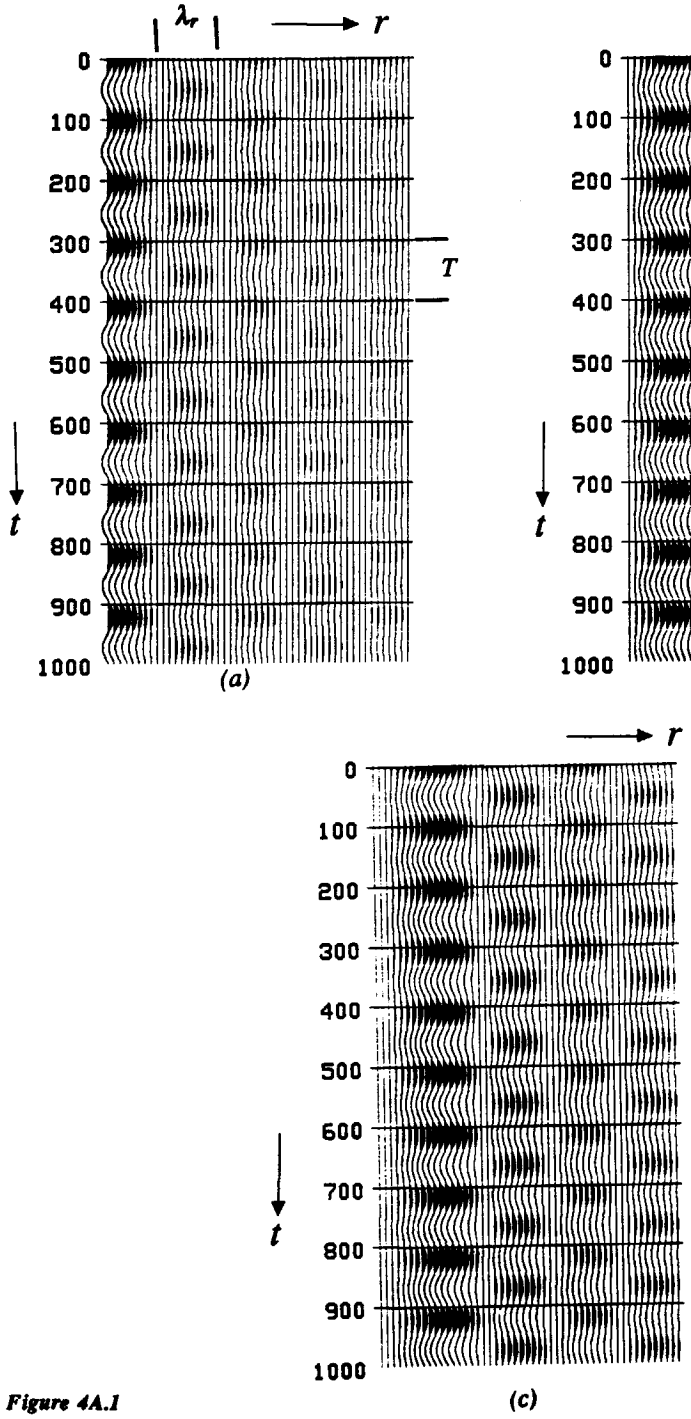

Figure 4A.1

Radial and time variations of a cylindrical wave of horizontal wavenumber $k_r = 2\pi/\lambda_r$ ($\lambda_r=30\Delta r$, $\Delta r=33m$) and of fixed circular frequency $\omega = 2\pi/T$ ($T=0.1s$). The variations are displayed for the azimuth $\theta=0$, for different azimuthal order m.a) m=0, b) m=1, c) m=2.

$$\vec{R}^m(k_r,r,\theta) = Y^m(k_r,r,\theta)\ \vec{z} = J_m(k_r r)\, ejm\theta\ \vec{z}, \tag{4A.9c}$$

with,

$$g_1^m(k_r r) = \frac{j}{2}\left[J_{m-1}(k_r r) - J_{m+1}(k_r r)\right], \tag{4A.9d}$$

$$g_2^m(k_r r) = \frac{1}{2}\left[J_{m-1}(k_r r) + J_{m+1}(k_r r)\right]. \tag{4A.9e}$$

The following expressions are obtained for the particle and traction field:

$$\vec{v}^m(k_r,r,\theta,z,\omega) = \tilde{v}_S^m(k_r,z,\omega)\,\vec{S}^m(k_r,r,\theta) + \tilde{v}_T^m(k_r,z,\omega)\,\vec{T}^m(k_r,r,\theta) + \tilde{v}_R^m(k_r,z,\omega)\,\vec{R}^m(k_r,r,\theta), \tag{4A.10a}$$

$$\vec{\tau}_z^m(k_r,r,\theta,z,\omega) = \tilde{\tau}_{z,S}^m(k_r,z,\omega)\,\vec{S}^m(k_r,r,\theta) + \tilde{\tau}_{z,T}^m(k_r,z,\omega)\,\vec{T}^m(k_r,r,\theta) + \tilde{\tau}_{z,R}^m(k_r,z,\omega)\,\vec{R}^m(k_r,r,\theta), \tag{4A.10b}$$

with :

$$\tilde{v}_S^m = \frac{1}{\rho\omega}\left[k_r\,(\tilde{\phi}^{+,m} + \tilde{\phi}^{-,m}) + jk_{z,s}\,(\tilde{\psi}_s^{+,m} - \tilde{\psi}_s^{-,m})\right], \tag{4A.11a}$$

$$\tilde{v}_T^m = -\frac{1}{\rho\omega}\left[\tilde{\zeta}_s^{+,m} + \tilde{\zeta}_s^{-,m}\right], \tag{4A.11b}$$

$$\tilde{v}_R^m = \frac{1}{\rho\omega}\left[k_{z,p}\,(\tilde{\phi}^{+,m} - \tilde{\phi}^{-,m}) - jk_r\,(\tilde{\psi}_s^{+,m} + \tilde{\psi}_s^{-,m})\right], \tag{4A.11c}$$

$$\tilde{\tau}_{zS}^m = \frac{1}{k_s^2}\left[-2k_r k_{z,p}\,(\tilde{\phi}^{+,m} - \tilde{\phi}^{-,m}) - j(k_s^2 - 2k_r^2)(\tilde{\psi}_s^{+,m} + \tilde{\psi}_s^{-,m})\right], \tag{4A.11d}$$

$$\tilde{\tau}_{zT}^m = \frac{k_{z,s}}{k_s^2}\left[\tilde{\zeta}_s^{+,m} - \tilde{\zeta}_s^{-,m}\right], \tag{4A.11e}$$

$$\tilde{\tau}_{zR}^m = \frac{1}{k_s^2}\left[(-k_s^2 + 2k_r^2)\,(\tilde{\phi}^{+,m} + \tilde{\phi}^{-,m}) + 2jk_r k_{z,s}(\tilde{\psi}_s^{+,m} - \tilde{\psi}_s^{-,m})\right]. \tag{4A.11f}$$

with,

$$\tilde{\psi}_s^{\pm,m} = k_r\,\tilde{\psi}^{\pm,m} \text{ and } \tilde{\zeta}_s^{\pm,m} = k_r\,\tilde{\zeta}^{\pm,m}. \tag{4.4.11g}$$

The combination of all the possible P and S cylindrical waves leads to the expression of the two-way wavefield vectors $\vec{v}$ and $\vec{\tau}_z$ in the space-frequency domain:

$$\begin{pmatrix} v_r(r,\theta,z,\omega) \\ v_\theta(r,\theta,z,\omega) \\ v_z(r,\theta,z,\omega) \end{pmatrix} = \sum_{m=-\infty}^{+\infty} \int_0^{+\infty} \left[C(k_r r,\theta)\right] \begin{pmatrix} \tilde{v}_S^m(k_r,z,\omega) \\ \tilde{v}_T^m(k_r,z,\omega) \\ \tilde{v}_R^m(k_r,z,\omega) \end{pmatrix} k_r\, dk_r, \tag{4A.12a}$$

with,

$$C(k_r r,\theta) = \begin{bmatrix} g_1^m(k_r r)\, ejm\theta & g_2^m(k_r r)\, ejm\theta & 0 \\ -g_2^m(k_r r)\, ejm\theta & g_1^m(k_r r)\, ejm\theta & 0 \\ 0 & 0 & J_m(k_r r)\, ejm\theta \end{bmatrix}. \tag{4A.12b}$$

The azimuthal functions $e^{jm\theta}$ for different m being orthogonal to each other, the two-way wavefield decomposition into cylindrical waves of distinct azimuthal order can thus be easily done. The wavefield decomposition into cylindrical waves of distinct k_r values is more complicated as the Bessel functions of distinct index m are not orthogonal to each other. We must find a suited change of coordinates which transform the matrix $\boldsymbol{C}(k_r r,\theta)$ into a diagonal matrix, with a unique type of Bessel function on its diagonal.

Expression *(4A.12a)* can be rewritten:

$$\boldsymbol{A}\begin{pmatrix} v_r(r,\theta,z,\omega) \\ v_\theta(r,\theta,z,\omega) \\ v_z(r,\theta,z,\omega) \end{pmatrix} = \sum_{m=-\infty}^{+\infty} \int_0^{+\infty} \left[\boldsymbol{A}\boldsymbol{C}(k_r r,\theta)\,\boldsymbol{B}^{-1}\right] \boldsymbol{B} \begin{pmatrix} \tilde{v}_S^m(k_r,z,\omega) \\ \tilde{v}_T^m(k_r,z,\omega) \\ \tilde{v}_R^m(k_r,z,\omega) \end{pmatrix} k_r\, dk_r \,. \qquad (4A.13a)$$

By choosing,

$$\boldsymbol{A} = \begin{pmatrix} 1 & -j & 0 \\ 1 & j & 0 \\ 0 & 0 & 1 \end{pmatrix} \text{ and } \boldsymbol{B} = \begin{pmatrix} j & 1 & 0 \\ -j & 1 & 0 \\ 0 & 0 & 1 \end{pmatrix}, \qquad (4A.13b)$$

we have,

$$\boldsymbol{A}\,\boldsymbol{C}(k_r r,\theta)\,\boldsymbol{B} = \begin{bmatrix} J_{m-1}(k_r r)\, e^{jm\theta} & 0 & 0 \\ 0 & J_{m+1}(k_r r)\, e^{jm\theta} & 0 \\ 0 & 0 & J_m(k_r r)\, e^{jm\theta} \end{bmatrix}. \qquad (4A.13c)$$

Now, we can easily invert expression (4A.13a), from which we deduce the expression of the transformation formulas that have to be used to do a proper cylindrical wave decomposition of the two-way vector wavefield. We finally find that:

$$\begin{pmatrix} \tilde{v}_S^m(k_r,z,\omega) \\ \tilde{v}_T^m(k_r,z,\omega) \\ \tilde{v}_R^m(k_r,z,\omega) \end{pmatrix} = \frac{1}{2\pi} \int_0^{2\pi} \int_0^{+\infty} \left[\boldsymbol{C}(k_r r,\theta)\right]^{H} \begin{pmatrix} v_r(r,\theta,z,\omega) \\ v_\theta(r,\theta,z,\omega) \\ v_z(r,\theta,z,\omega) \end{pmatrix} r\, d_r d_\theta \,, \qquad (4A.14)$$

where H hands for Hermitian (transpose complex conjugate), expression (4A.14) is also valid for the traction vector. The cylindrical transformation matrices involved in expressions *(4A.12a)* and *(4A.14)* are not diagonal, contrary to the plane wave transformation matrices. Consequently, to transform one of the horizontal component (radial or tangential), the other one has also to be used. It is interesting to note, that under the far field approximation $(k_r r >> 1)$ the matrix $\boldsymbol{C}(k_r r,\theta)$ can be well approximated by a diagonal matrix. Under the far field approximation, we have:

$$g_1^m(k_r r) \approx j\, J_{m-1}(k_r r) \text{ and } g_2^m(k_r r) \approx 0. \qquad (4A.15)$$

A final interesting point to note is: as the operator that enables to decompose the elastic wavefield in cylindrical waves is the transpose complex conjugate of the operator that enables to

compose all the cylindrical waves, the vectors $\vec{S}^m(k_r,r,\theta)$, $\vec{T}^m(k_r,r,\theta)$ and $\vec{R}^m(k_r,r,\theta)$ are orthogonal to each other and each of them satisfies an orthogonality relation of the form:

$$\int_0^{2\pi}\int_0^{+\infty} \vec{S}^m(k_r,r,\theta)\cdot\left[\vec{S}^{m'}(k_r',r,\theta)\right]^* r\,dr\,d\theta = 2\pi\,\delta_{mm'}\frac{\delta(k_r-k_r')}{\sqrt{k_r\,k_r'}}. \qquad (4A.16)$$

Equality *(4A.16)* is also verified by $\vec{T}^m(k_r,r,\theta)$ and $\vec{R}^m(k_r,r,\theta)$.

APPENDIX 4B

NUMERICAL IMPLEMENTATION OF THE HANKEL TRANSFORM

In the previous section we have seen that the 3D elastic wavefield decomposition into cylindrical waves involves integrals of the type :

$$\tilde{v}(k_r) = \int_0^{+\infty} v(r)\, J_n(k_r r)\, r\, dr \,. \qquad (4B.1a)$$

Such a transformation is called a forward Hankel transform of order n. The inverse Hankel transform of order n is defined according to:

$$v(r) = \int_0^{+\infty} \tilde{v}(k_r)\, J_n(k_r r)\, k_r\, dk_r \,. \qquad (4B.1b)$$

A direct numerical evaluation of expressions *(4B.1)* is possible but computationnaly expensive. An efficient scheme to compute the zero order Hankel transform, named *Fourier transform* plus *square root filter*, has been presented by Fokkema et al.(1992). In this section we review their method and extend it to higher order transforms. We also propose a different formulation, which has a clear physical meaning.

4B.1 FOURIER TRANSFORM plus SQUARE ROOT FILTER method

From Goudet (1943, page 35) we have the following expression for the n^{th} order Hankel function $J_n(k_r r)$:

$$J_n(k_r r) = \frac{(-j)^n}{2\pi} \int_0^{2\pi} e^{jk_r r \cos\beta} \cos(n\beta)\, d\beta \,. \qquad (4B.2a)$$

When we introduce the above expression in *(4B.1a)* and we do the following change of variables $k_x = k_r \cos\beta$ and a change in the order of integrations, we find that *(4B.1a)* can be rewritten as:

using,

$$\cos(n\beta) = \sum_{p=0}^{int(n/2)} (-1)^p C_n^{2p} (\cos\beta)^{n-2p} (\sin\beta)^{2p} \quad \text{with } C_n^{2p} = \frac{n!}{(2p)!(n-2p)!} \,,$$

we get,

$$\tilde{v}(k_r) = \frac{(j)^{-n}}{\pi k_r^{\,n}} \sum_{p=0}^{int(n/2)} (-1)^p C_n^{2p} \int_0^{k_r} \tilde{f}_{n,p}(k_r,k_x)\, \tilde{u}(k_x)\, dk_x \,,$$

$$\tilde{v}(0) = 0 \qquad \text{for } n \neq 0 \,,$$

$$\tilde{v}(0) = \frac{1}{2}\tilde{u}(0) \quad \text{for } n=0, \qquad (4B.3a)$$

with,

$$\tilde{f}_{n,p}(k_r,k_x) = k_x^{n-2p} \left(\sqrt{k_r^2 - k_x^2}\right)^{2p-1} \,, \qquad (4B.3b)$$

and

$$\tilde{u}(k_x) = \int_{-\infty}^{+\infty} v(r)\, |r|\, e^{jk_x r}\, dr \,. \qquad (4B.3c)$$

To derive these expressions we used the property that $v(r)$ is an even function of r when n is an even integer, and an odd function of r when n is an odd integer ($v(-r) = (-1)^n v(r)$). Expression *(4B.3a)* states that the Hankel transform *(4B.1a)* can be efficiently evaluated by firstly computing $\tilde{u}(k_x)$, i.e., the Fourier transform of $v(r)|r|$ (FFT routines can be used for this purpose), followed by a square root filter of $\tilde{u}(k_x)$ with $\tilde{f}_{n,p}(k_r, k_x)$, see *Figure (4B.1a)* The lateral filter $\tilde{f}_{n,p}(k_r, k_x)$ is data independent. It can be computed in advance and be used for different data sets.

To derive the inverse Hankel transform, expressions *(4B.3)* can again be used, we have just to change the name of the variables and of the functions according to :

$$\begin{aligned} k_r &\rightarrow r \,, \\ k_x &\rightarrow x \,, \\ r &\rightarrow k_r \,, \\ \tilde{v}(k_r) &\rightarrow v(r) \,, \end{aligned}$$

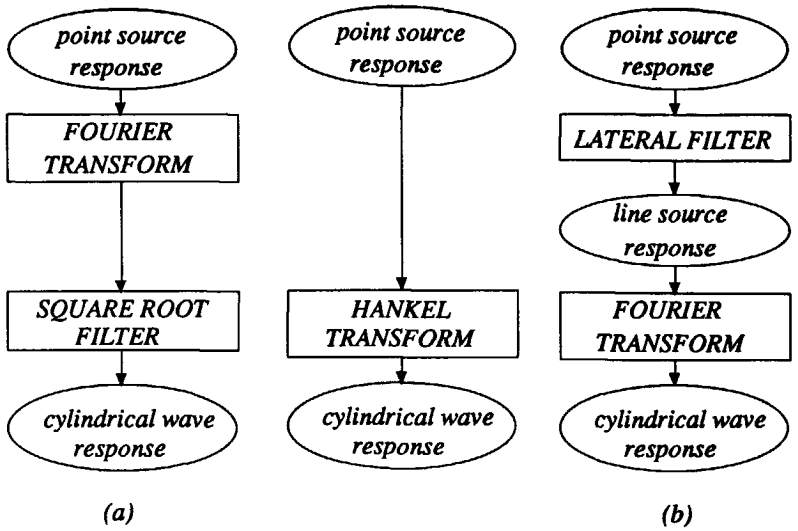

Figure 4B.1

(a) The Hankel transform can be split into two operations: a Fourier transform followed by a square root filter.

(b) Alternatively, the Hankel transform can be split in two operations: a lateral filtering which transforms the point source response into a line source response, followed by a Fourier transform which does the plane wave decomposition of the line source response.

$$\begin{aligned} v(r) &\rightarrow \tilde{v}(k_r) \ , \\ \tilde{u}(k_x) &\rightarrow u(x) \ . \end{aligned} \qquad (4B.4)$$

Due to the term k_r^{-n} in *(4B.3a)* some numerical problems may arise when $k_r^{-n} << 1$ (for small k_r values and/or high order transforms). It is also important to point out that in the case of discretized data recorded at a finite aperture, the Fourier transform of $v(r)\,|r|$ may generate artefacts due to the first and higher order derivative discontinuities at the origin (the derivative discontinuities are introduced by the multiplication of $v(r)$ with $|r|$).

4B.2 LATERAL FILTERING plus FOURIER TRANSFORM method

Here we propose to compute the Hankel transform with the following sequence of steps: first we introduce $\hat{v}(x)$ as the inverse Fourier transform of $\tilde{v}(k_r)$:

$$\hat{v}(x) = \frac{1}{2\pi} \int_{-\infty}^{+\infty} \tilde{v}(k_r)\, e^{-jk_r x}\, dk_r \ . \qquad (4B.5a)$$

In the above expression we substitue for $\tilde{v}(k_r)$ the expression *(4B.1a)* and we change the order of integrations. We find that:

$$\hat{v}(x) = \int_0^{+\infty} v(r)\, f_n(r, x)\, dr \,, \qquad (4B.5b)$$

with,

$$f_n(r, x) = \frac{r}{2\pi} \int_{-\infty}^{+\infty} J_n(k_r r)\, e^{-jk_r x}\, dk_r \,. \qquad (4B.5c)$$

From *(4B.5b)* we see that $\hat{v}(x)$, the inverse Fourier transform of $\tilde{v}(k_r)$ can be obtained by lateral filteringing $v(r)$ with $f_n(r, x)$. The lateral filter $f_n(r, x)$ is data independent, it can be computed in advance and be used for different data sets. Once $\hat{v}(x)$ is known, we can easily obtain $\tilde{v}(k_r)$ from the forward Fourier transform of $\hat{v}(x)$, see *Figure (4B.1b)*. We have:

$$\tilde{v}(k_r) = \int_{-\infty}^{+\infty} \hat{v}(x)\, e^{jk_r x}\, dx \,. \qquad (4B.5d)$$

The forward Fourier transform can be efficiently computed using FFT routines. *With this formulation, the lateral filtering has a clear physical meaning: it transforms the point source response into a line source response, see also section 4.3.* The forward Fourier transform corresponds then to a plane wave decomposition of the line source response.

To determine the expression of $f_n(r, x)$ we have to calculate the forward Fourier transform of the n^{th} order order Hankel function. We start from expression *(4B.2a)* and we apply the following change of variable :

$$r \cos\beta = x \,. \qquad (4B.6a)$$

Taking into account that :

$$\cos n\beta = \sum_{p=0}^{int(n/2)} (-1)^p\, C_n^{2p}\, (\cos\beta)^{n-2p}\, (\sin\beta)^{2p} \,, \qquad (4B.6b)$$

we find that :

$$J_n(k_r r) = \int_{-r}^{r} g_n(x,r)\, e^{jk_r x}\, dx \,, \qquad (4B.6c)$$

with,

$$g_n(x, r) = \frac{(-j)^n}{\pi r^n} \sum_{p=0}^{int(n/2)} (-1)^p\, C_n^{2p}\, x^{n-2p} \left(\sqrt{r^2 - x^2}\right)^{2p-1} \,. \qquad (4B.6d)$$

From which we deduce that :

$$f_n(r,x) = \frac{r}{2\pi} \int_{-\infty}^{+\infty} J_n(k_r r)\, e^{-jk_r x}\, dk_r = 0 \qquad \text{when } |r| < |x| \ , \tag{4B.7a}$$

$$f_n(r,x) = \frac{r}{2\pi} \int_{-\infty}^{+\infty} J_n(k_r r)\, e^{-jk_r x}\, dk_r = r\, g_n(x,r) \qquad \text{when } |r| \geq |x| \ . \tag{4B.7b}$$

Expression *(4B.5b)* can then be rewritten according to :

$$\hat{v}(x) = \frac{(-j)^n}{\pi} \sum_{p=0}^{int(n/2)} (-1)^p\, C_n^{2p}\, x^{n-2p} \int_{|x|}^{+\infty} \frac{(\sqrt{r^2-x^2})^{2p-1}}{r^{n-1}}\, v(r)\, dr \ . \tag{4B.8}$$

To compute the inverse Hankel transform, expression *(4B.8)* stays valid, we just have to change the name of the variables and of the functions according to :

$$\begin{aligned} r &\rightarrow k_r \ , \\ x &\rightarrow k_x \ , \\ k_r &\rightarrow r \ , \\ v(r) &\rightarrow \tilde{v}(k_r) \ , \\ \tilde{v}(k_r) &\rightarrow v(r) \ , \\ u(x) &\rightarrow \tilde{u}(k_x) \ . \end{aligned} \tag{4B.9}$$

With this formulation we see that the lateral data filtering *(4B.8)* involves an integration from a given offset to infinity. Due to the finite aperture of the data some artefacts may arise from the integral truncation. It can be overcome by slightly tapering the far offset data. Nevertheless we must be aware that even if the upper boundary of the integral goes to infinity, the main contribution comes from the lower boundary. Which means that the finite aperture of the data will mainly affect the transformation of the far offset data.

4B.3 NUMERICAL EVALUATION OF THE LATERAL FILTERING

The Hankel transform can be obtained from the combination of a lateral filtering and of a Fourier transform. For the Fourier transform we can use efficient FFT routines everywhere available, for the lateral filtering we develop our own algorithm. In this paragraph we study the numerical evaluation of the square root filter *(4B.3a)* and of the lateral filtering *(4B.8)* for the

zero, first and second order Hankel transforms. We follow a similar approach as Fokkema et al. (1992)

For the **FFT** plus **square root filter** method we approximate equation *(4B.3a)* by :

$$\tilde{v}(k_r) \approx \sum_{m=0}^{M(k_r)-1} \int_{m\,\Delta k_x}^{(m+1)\Delta k_x} \tilde{u}^m(k_x)\, h_n(k_r,k_x)\, dk_x \,, \qquad (4B.10a)$$

where,

$$M(k_r) = k_r/\Delta k_x \,, \qquad (4B.10b)$$

and

$$h_n(k_r,k_x) = \frac{(-j)^{-n}}{\pi k_r^n} \sum_{p=0}^{int(n/2)} (-1)^p\, C_n^{2p}\, k_x^{n-2p} \left(\sqrt{k_r^2 - k_x^2}\right)^{2p-1} . \qquad (4B.10c)$$

Δk_x is the wavenumber discretization interval and $\tilde{u}^m(k_x)$ is a polynomial representation of $\tilde{u}(k_x)$ on the interval $m\Delta k_x \le k_x < (m+1)\Delta k_x$, hence :

$$\tilde{u}^m(k_x) = A_0^m + k_x A_1^m + k_x^2 A_2^m + \cdots . \qquad (4B.11a)$$

In practice accurate results are obtained by using the first two terms only, with :

$$A_0^m = (m+1)\, \tilde{u}(m\Delta k_x) - m\, \tilde{u}((m+1)\Delta k_x) \,, \qquad (4B.11b)$$

and

$$A_1^m = \frac{\tilde{u}((m+1)\Delta k_x) - \tilde{u}(m\Delta k_x)}{\Delta k_x} . \qquad (4B.11c)$$

Thus equation *(4B.10a)* can be rewritten as :

$$\tilde{v}(k_r) \approx \sum_{m=0}^{M(k_r)-1} \left[I_{0,n}^m(k_r) A_0^m + I_{1,n}^m(k_r) A_1^m \right] , \qquad (4B.12a)$$

where,

$$I_{0,n}^m(k_r) = \int_{m\Delta k_x}^{(m+1)\Delta k_x} h_n(k_r, k_x)\, dk_x \,, \qquad (4B.12b)$$

and

$$I_{1,n}^m(k_r) = \int_{m\Delta k_x}^{(m+1)\Delta k_x} k_x\, h_n(k_r, k_x)\, dk_x . \qquad (4B.12c)$$

To be more efficient on vector computers, we rewrite expression *(4B.12a)* as :

$$\tilde{v}(k_r) \approx \sum_{m=0}^{M(k_r)} \tilde{u}(m\Delta k_x)\, F_n^m(k_r)\,, \qquad (4B.12d)$$

with,

$$F_n^0(k_r) = I_{0,n}^0(k_r) - \frac{I_{1,n}^0(k_r)}{\Delta k_x}\,,$$

$$F_n^m(k_r) = (m+1)I_{0,n}^m(k_r) - \frac{I_{1,n}^m(k_r)}{\Delta k_x} - \left((m-1)I_{0,n}^{m-1}(k_r) - \frac{I_{1,n}^{m-1}(k_r)}{\Delta k_x}\right),\ m = 1,\cdots, M(k_r)-1$$

$$F_n^{M(k_r)}(k_r) = -(M(k_r)-1)I_{0,n}^{M(k_r)-1}(k_r) + \frac{I_{1,n}^{M(k_r)-1}(k_r)}{\Delta k_x} \qquad (4B.12e)$$

As the filter coefficients are data independent they can be computed in advance and stored in a table. Simplifying any further lateral filtering to a simple vector operation see *(4B.12d)*. The table coefficients can be efficiently computed using this type of algorithm :

$I_{0new} = 0$
$I_{1new} = 0$
DO $m = 0, M(k_r)-1$
  $I_{0old} = I_{0new}$
  $I_{1old} = I_{1new}$
  $I_{0new} = I_{0,n}^m(k_r)$
  $I_{1new} = I_{1,n}^m(k_r)/\Delta k_x$
  $F_n^m = (m+1)\, I_{0new} - I_{1new} - (\,(m-1)\, I_{0old} - I_{1old}\,)$
ENDDO
$F_n^{M(k)} = -(M(k)-1)\, I_{0new} + I_{1new}$

Now we give the expression of $h_n(k_r,k_x)$, $I_{0,n}^m(k_r)$ and $I_{1,n}^m(k_r)$ for the zero, first and second order Hankel transforms.

Zero order Hankel transform : $n = 0$

$$h_0(k_r, k_x) = \frac{1}{\pi}\frac{1}{\sqrt{k_r^2 - k_x^2}}\,, \qquad (4B.13a)$$

$$I_{0,0}^m(k_r) = \frac{1}{\pi}\int_{m\Delta k_x}^{(m+1)\Delta k_x} \frac{dk_x}{\sqrt{k_r^2 - k_x^2}} = \frac{1}{\pi}\, \arcsin\left(\frac{k_x}{k_r}\right)\Big|_{m\Delta k_x}^{(m+1)\Delta k_x}\,, \qquad (4B.13b)$$

$$I_{1,0}^m(k_r) = \frac{1}{\pi}\int_{m\Delta k_x}^{(m+1)\Delta k_x} \frac{k_x}{\sqrt{k_r^2 - k_x^2}}\, dk_x = -\frac{1}{\pi}\sqrt{k_r^2 - k_x^2}\,\Big|_{m\Delta k_x}^{(m+1)\Delta k_x}\,. \qquad (4B.13c)$$

First order Hankel transform : n=1

$$h_1(k_r, k_x) = \frac{-j}{\pi k_r} \frac{k_x}{\sqrt{k_r^2 - k_x^2}}, \qquad (4B.14a)$$

$$I_{0,1}^{m}(k_r) = \frac{-j}{\pi k_r} \int_{m\Delta k_x}^{(m+1)\Delta k_x} \frac{k_x}{\sqrt{k_r^2 - k_x^2}}\, dk_x = \frac{j}{\pi k_r} \sqrt{k_r^2 - k_x^2}\,\Big|_{m\Delta k_x}^{(m+1)\Delta k_x}, \qquad (4B.14b)$$

$$I_{1,1}^{m}(k_r) = \frac{-j}{\pi k_r} \int_{m\Delta k_x}^{(m+1)\Delta k_x} \frac{k_x^2}{\sqrt{k_r^2 - k_x^2}}\, dk_x = \frac{j}{2\pi k} \left[k_x \sqrt{k_r^2 - k_x^2} - k_r^2 \arcsin\left(\frac{k_x}{k_r}\right) \right]\Big|_{m\Delta k_x}^{(m+1)\Delta k_x}. \qquad (4B.14c)$$

Second order Hankel transform : n=2

$$h_2(k_r, k_x) = \frac{1}{\pi k_r^2} \frac{k_r^2 - 2k_x^2}{\sqrt{k_r^2 - k_x^2}}, \qquad (4B.15a)$$

$$I_{0,2}^{m}(k_r) = \frac{1}{\pi k_r^2} \int_{m\Delta k_x}^{(m+1)\Delta k_x} \frac{k_r^2 - 2k_x^2}{\sqrt{k_r^2 - k_x^2}}\, dk_x = \frac{1}{\pi k_r^2}\, k_x \sqrt{k_r^2 - k_x^2}\,\Big|_{m\Delta k_x}^{(m+1)\Delta k_x}, \qquad (4B.15b)$$

$$I_{1,2}^{m}(k_r) = \frac{1}{\pi k_r^2} \int_{m\Delta k_x}^{(m+1)\Delta k_x} \frac{k_x \left(k_r^2 - 2k_x^2\right)}{\sqrt{k_r^2 - k_x^2}}\, dk_x = \frac{1}{3\pi} \left(\frac{2k_x^2}{k_r^2} + 1 \right) \sqrt{k_r^2 - k_x^2}\,\Big|_{m\Delta k_x}^{(m+1)\Delta k_x}, \qquad (4B.15c)$$

For the **lateral filtering** plus **FFT** method we approximate equations *(4B.8)* by :

$$\hat{v}(x) \approx \sum_{m\,=\,M(x)}^{Mmax-1} \int_{m\,\Delta r}^{(m+1)\Delta r} v^m(r)\, h_n(x, r)\, dr, \qquad (4B.16a)$$

where,

$$M(x) = |x|/\Delta r, \qquad (4B.16b)$$

$$Mmax = |offsetmax|/\Delta r. \qquad (4B.16c)$$

and

$$h_n(x, r) = \frac{(-j)^n}{\pi} \sum_{p\,=\,0}^{int(n/2)} (-1)^p\, C_n^{2p}\, x^{\,n-2p}\, r^{1-n} \left(\sqrt{r^2 - x^2}\right)^{2p-1}. \qquad (4B.16d)$$

Δr is the spatial discretization interval, *offsetmax* the largest offset available in the data set and $v^m(r)$ is a polynomial representation of $v(r)$ on the interval $m\Delta r \le r < (m+1)\Delta r$, hence :

$$v^m(r) = A_0^m + r\,A_1^m + r^2\,A_2^m + \cdots . \qquad (4B.17a)$$

In practice accurate results are obtained by using the first two terms only, with :

$$A_0^m = (m+1)\,v\,(m\Delta r) - m\,v\,((m+1)\Delta r)\,, \qquad (4B.17b)$$

and

$$A_1^m = \frac{v((m+1)\Delta r) - v(m\Delta r)}{\Delta r}\,. \qquad (4B.17c)$$

Thus equation *(4B.16a)* can be rewritten as :

$$\hat{v}(x) \approx \sum_{m=M(x)}^{Mmax-1} \left[I_{0,n}^m(x)A_0^m + I_{1,n}^m(x)A_1^m\right], \qquad (4B.18a)$$

where,

$$I_{0,n}^m(x) = \int_{m\Delta r}^{(m+1)\Delta r} h_n(x, r)\,dr\,, \qquad (4B.18b)$$

and

$$I_{1,n}^m(x) = \int_{m\Delta r}^{(m+1)\Delta r} r\,h_n(x, r)\,dr\,. \qquad (4B.18c)$$

To be more efficient on vector computers, we rewrite expression *(4B.18a)* as :

$$\hat{v}(x) = \sum_{m=M(x)}^{Mmax} v(m\Delta r)\,F_n^m(x)\,, \qquad (4B.18d)$$

with,

$$F_n^{M(x)}(x) = I_{0,n}^{M(x)}(x) - \frac{I_{1,n}^{M(x)}(x)}{\Delta r}\,,$$

$$F_n^m(x) = (m+1)I_{0,n}^m(x) - \frac{I_{1,n}^m(x)}{\Delta r} - \left((m-1)I_{0,n}^{m-1}(x) - \frac{I_{1,n}^{m-1}(x)}{\Delta r}\right),\ m = M(x)+1, \cdots, Mmax-1$$

$$F_n^{Mmax}(x) = -\,(Mmax-1)I_{0,n}^{Mmax-1}(x) + \frac{I_{1,n}^{Mmax-1}(x)}{\Delta r} \qquad (4B.18e)$$

As the filter coefficients are data independent they can be computed in advance, stored in a table. Simplifying any further lateral filtering to a simple vector operation see *(4B.18d)*. The coefficient table can be efficiently computed by using this type of algorithm :

$I_{0new} = 0$
$I_{1new} = 0$
$DO\ m = M(x), Mmax\text{-}1$
$\quad I_{0old} = I_{0new}$
$\quad I_{1old} = I_{1new}$
$\quad I_{0new} = I^m_{0,n}(x)$
$\quad I_{1new} = I^m_{1,n}(x)/\Delta r$
$\quad F^m_n = (m+1)\, I_{0new} - I_{1new} - (\,(m-1)\, I_{0old} - I_{1old}\,)$
$ENDDO$
$F^{Mmax}_n = -(Mmax-1)\, I_{0new} + I_{1new}$

Now we give the expression of $h_n(x, r)$, $I^m_{0,n}(x)$ and $I^m_{1,n}(x)$ for the zero, first and second order Hankel transforms.

Zero order Hankel transform : n= 0

$$h_0(x, r) = \frac{1}{\pi} \frac{r}{\sqrt{r^2\text{-}x^2}}, \qquad (4B.19a)$$

$$I^m_{0,0}(x) = \frac{1}{\pi} \int_{m\Delta r}^{(m+1)\Delta r} \frac{r}{\sqrt{r^2\text{-}x^2}}\, dr = \frac{1}{\pi} \sqrt{r^2\text{-}x^2}\,\Big|_{m\Delta r}^{(m+1)\Delta r}, \qquad (4B.19b)$$

$$I^m_{1,0}(x) = \frac{1}{\pi} \int_{m\Delta r}^{(m+1)\Delta r} \frac{r^2}{\sqrt{r^2\text{-}x^2}}\, dr = \frac{1}{2\pi} \left[r \sqrt{r^2\text{-}x^2} + x^2 \ln(r + \sqrt{r^2\text{-}x^2}) \right] \Big|_{m\Delta r}^{(m+1)\Delta r}, \qquad (4B.19c)$$

First order Hankel transform : n=1

$$h_1(x, r) = -\frac{j}{\pi} \frac{x}{\sqrt{r^2\text{-}x^2}}, \qquad (4B.20a)$$

$$I^m_{0,1}(x) = -\frac{jx}{\pi} \int_{m\Delta r}^{(m+1)\Delta r} \frac{1}{\sqrt{r^2\text{-}x^2}}\, dr = -2jx\ \ln(r + \sqrt{r^2\text{-}x^2})\,\Big|_{m\Delta r}^{(m+1)\Delta r}, \qquad (4B.20b)$$

$$I^m_{1,1}(x) = -\frac{jx}{\pi} \int_{m\Delta r}^{(m+1)\Delta r} \frac{r}{\sqrt{r^2\text{-}x^2}}\, dr = -\frac{jx}{\pi} \sqrt{r^2\text{-}x^2}\,\Big|_{m\Delta r}^{(m+1)\Delta r}, \qquad (4B.20c)$$

Second order Hankel transform : n=2

$$h_2(x, r) = \frac{1}{\pi} \frac{r^2\text{-}2x^2}{r \sqrt{r^2\text{-}x^2}}, \qquad (4B.21a)$$

$$I^m_{0,2}(x) = \frac{1}{\pi}\int_{m\Delta r}^{(m+1)\Delta r} \frac{r^2-2x^2}{r\sqrt{r^2-x^2}}\,dr = \frac{1}{\pi}\left[\sqrt{r^2-x^2} - 2x\arccos\left(\frac{x}{r}\right)\right]\Big|_{m\Delta r}^{(m+1)\Delta r}, \qquad (4B.21b)$$

$$I^m_{1,2}(x) = \frac{1}{\pi}\int_{m\Delta r}^{(m+1)\Delta r} \frac{r^2-2x^2}{\sqrt{r^2-x^2}}\,dr = \frac{1}{2\pi}\left[r\sqrt{r^2-x^2} - 3x^2\ln\left(r+\sqrt{r^2-x^2}\right)\right]\Big|_{m\Delta r}^{(m+1)\Delta r}, \qquad (4B.21c)$$

CHAPTER 5

WAVEFIELD DECOMPOSITION OF VSP DATA

5.1 INTRODUCTION

The data acquisition along a borehole, the so called VSP technique, is another type of acquisition geometry often used. The source can be located at the surface or can be buried; the particle velocity detectors (clamped along the VSP borehole), measure the particle velocities of the elastic waves that cross the borehole. In this chapter, we show how the normal one-way components of the elastic wavefield can be deduced from the measured particle velocities. Due to the differences in the acquisition geometry and in the boundary conditions at the receiver side, the decomposition operator for VSP data is different from the one used for surface data. We first derive the operator expression for a homogeneous medium. But due to the strong vertical velocity variations that may occur along the borehole, we will put our attention to the derivation of short local operators in the space domain.

5.2 VSP SURVEY DESCRIPTION

The acquisition geometry for VSP experiments is schematically described in *Figure 5.2.1*. The elastic wavefield generated by a surface or buried source, propagates into the subsurface and is recorded by multi-component particle velocity detectors clamped along the borehole. The (z,t) seismic sections contain: direct, reflected and converted waves. Depending on the vertical distance (z_d) of the receivers to the source and depending on the source-borehole offset (r_b), the moveout of the seismic events will more or less deviate from the linear moveout of vertically propagating waves. For the extreme case of vertically propagating waves, the normal one-way

wave components can be separated in the vertical wavenumber-frequency domain by apparent vertical velocity filtering. This technique only holds for detectors for which r_b/z_d is small. Note that velocity filtering does not yield the normal one-way wave amplitudes but their associated horizontal or vertical particle velocity components. For most common surveys, however, the waves do not propagate vertically; most often, the normal one-way wavefields overlap each other in the vertical wavenumber-frequency domain and can not be separated with a simple F-K_z fan filter. That is why it is necessary to develop a more advanced filter, not only based on the moveout but also on the polarization of the incident waves.

5.3 TWO-WAY AND NORMAL ONE-WAY WAVEFIELD RELATIONS FOR VSP DATA

Similarly to what has been done for surface seismic data, the decomposition operators presented here are based on the linear relations that exist in the wavenumber-frequency domain between the two-way and the normal one-way wavefield components. We start the derivation of the decomposition operator for the special case of a 2D seismic wavefield propagating in a homogeneous medium. A 2D seismic wavefield is a wavefield without dependency along a certain direction, e.g. the y- direction. This situation corresponds to the use of line sources parallel to the y- axis, over or in a medium whose stiffness tensor and density function do not depend on the y- coordinate. Such a wavefield is only composed of plane waves with wave-vectors $\vec{k}$ of the type: $\vec{k} = (k_x, k_y=0, k_z)^T$. As $k_y=0$, the square of the horizontal wavenumber of any normal one-way plane wave can be deduced from its vertical wavenumber k_z using the dispersion relation :

$$k_x^2 + k_z^2 = \frac{\omega^2}{c^2}, \qquad (5.3.1)$$

with c, the propagation velocity of the wave. To transform the two-way wavefield component f (particle velocity or stress measured along the borehole) from the space(z)-time(t) domain to the vertical wavenumber-frequency domain, we make use of the 2D spatial and temporal Fourier transform :

$$\tilde{f}(k_z, \omega) = \int_{-\infty}^{+\infty}\int f(z, t)\, e^{-j(\omega t - k_z z)}\, dz\, dt, \qquad (5.3.2a)$$

the inverse transform being defined as :

$$f(z, t) = \frac{1}{2\pi^2} Real\left\{\int_0^{+\infty}\left[\int_{-\infty}^{+\infty} \tilde{f}(k_z, \omega)\, e^{j(\omega t - k_z z)}\, dk_z\right] d\omega\right\}. \qquad (5.3.2b)$$

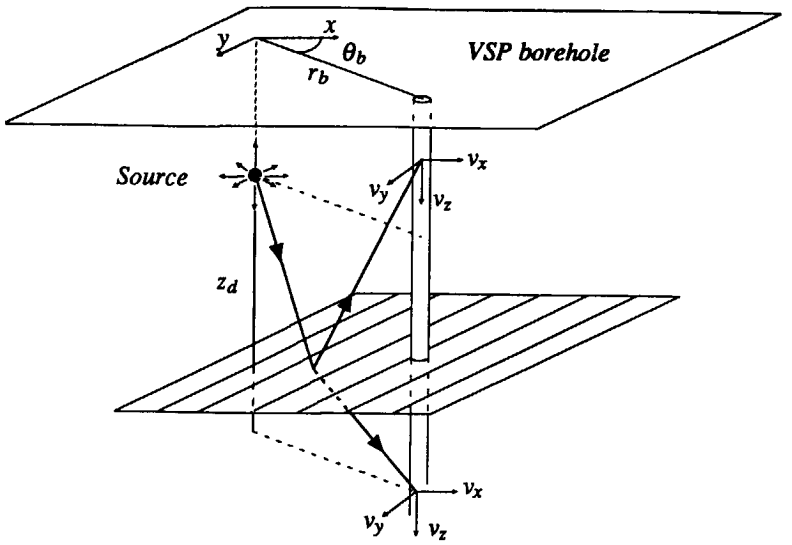

Figure 5.2.1

Schematic representation of a VSP acquisition geometry, (r_b) borehole offset, (z_d) depth of a detector relative to the source position.

In the vertical wavenumber-frequency domain, using a similar approach as the one used in chapter 2, it is possible to find a linear relation between the two-way and the normal one-way wavefield components. There is a composition operator $\tilde{L}$, which relates the normal one-way wavefield components to the two-way components:

$$\begin{pmatrix} \vec{\tilde{v}} \\ \vec{\tilde{\tau}}_x \end{pmatrix} = \begin{pmatrix} \tilde{L}_1^+ & \tilde{L}_1^- \\ \tilde{L}_2^+ & \tilde{L}_2^- \end{pmatrix} \begin{pmatrix} \vec{\tilde{p}}^+ \\ \vec{\tilde{p}}^- \end{pmatrix}. \qquad (5.3.3a)$$

The columns of the operator $\tilde{L}_1^{\pm}$ contain the polarization vectors of the normal one-way waves of vertical wavenumber k_z, that propagate in the source-borehole (+) and in the borehole-source (-) direction. The inverse of the composition operator, constitutes the decomposition operator $\tilde{M}$ which relates the two-way components to the normal one-way components:

$$\begin{pmatrix} \vec{\tilde{p}}^+ \\ \vec{\tilde{p}}^- \end{pmatrix} = \begin{pmatrix} \tilde{M}_1^+ & \tilde{M}_2^+ \\ \tilde{M}_1^- & \tilde{M}_2^- \end{pmatrix} \begin{pmatrix} \vec{\tilde{v}} \\ \vec{\tilde{\tau}}_x \end{pmatrix}. \qquad (5.3.3b)$$

Hence, $\vec{\tilde{v}}$ is the particle velocity vector :

$$\vec{\tilde{v}}(k_z, \omega) = \left(\tilde{v}_x(k_z, \omega), \tilde{v}_y(k_z, \omega), \tilde{v}_z(k_z, \omega)\right)^T, \qquad (5.3.3c)$$

and $\vec{\tilde{\tau}}_x$ is the traction vector:

$$\vec{\tilde{\tau}}_x(k_z, \omega) = \left(\tilde{\tau}_{xx}(k_z, \omega), \tilde{\tau}_{yx}(k_z, \omega), \tilde{\tau}_{zx}(k_z, \omega)\right)^T. \qquad (5.3.3d)$$

The vector $\vec{\tilde{p}}^{+}$ contains the amplitude of the three normal waves propagating in the source-borehole direction and $\vec{\tilde{p}}^{-}$ contains the amplitude of the normal waves propagating in the borehole-source direction. In an isotropic medium, 2D P and S_V wavefields only affect the x and z components. Thus we only consider two components particle velocity and traction vectors and 4×4 composition and decomposition operators. We have:

$$\tilde{L}_1^{\pm} = \frac{1}{\rho\omega}\begin{pmatrix} \pm k_{x,p} & -k_z \\ k_z & \pm k_{x,s} \end{pmatrix}, \tag{5.3.4a}$$

$$\tilde{L}_2^{\pm} = \frac{1}{k_s^2}\begin{pmatrix} -(k_s^2-2k_z^2) & \pm 2k_{x,s}k_z \\ \mp 2k_{x,p}k_z & -(k_s^2-2k_z^2) \end{pmatrix}, \tag{5.3.4b}$$

$$\tilde{M}_1^{\pm} = \frac{\mu}{2\omega}\begin{pmatrix} \pm\dfrac{(k_s^2-2k_z^2)}{2k_{x,p}} & k_z \\ -k_z & \pm\dfrac{(k_s^2-2k_z^2)}{2k_{x,s}} \end{pmatrix}, \tag{5.3.4c}$$

$$\tilde{M}_2^{\pm} = \frac{1}{2}\begin{pmatrix} -1 & \mp\dfrac{k_z}{k_{x,p}} \\ \pm\dfrac{k_z}{k_{x,s}} & -1 \end{pmatrix}, \tag{5.3.4d}$$

with,

$$k_{x,p}^2 = \frac{\omega^2}{c_p^2} - k_z^2 , \tag{5.3.4e}$$

and

$$k_{x,s}^2 = \frac{\omega^2}{c_s^2} - k_z^2 . \tag{5.3.4f}$$

These expressions developed for 2D wavefields remain valid, under the far field approximation, for any 3D wavefields propagating in a laterally homogeneous medium. Expressions *(5.3.3a)* and *(5.3.3b)*, constitute the basic relations that will be used to determine the expression of the decomposition operator at the receiver side for VSP data.

5.4 WAVEFIELD DECOMPOSITION OF VSP DATA AT THE RECEIVER SIDE

In the (hypothetical) case that velocities as well as stresses are measured along the borehole, the operator $\tilde{M}$ in *(5.3.3b)* constitutes the decomposition operator at the receiver side. This operator is unstable for vertically propagating P and S waves, as for such waves $k_{x,p}= 0$ and $k_{x,s}= 0$. This instability arises from the impossibility to split vertically propagating waves into source-borehole or borehole-source propagating waves. A way to overcome this instability is to decompose the elastic wavefield into normal waves without splitting them into (+) or (-) wave-types, according to :

$$\vec{\tilde{p}} = \vec{\tilde{p}}^{+} + \vec{\tilde{p}}^{-} = \left[\tilde{M}_1^{+} + \tilde{M}_1^{-}\right]\vec{\tilde{v}} + \left[\tilde{M}_2^{+} + \tilde{M}_2^{-}\right]\vec{\tilde{\tau}}_x \,, \qquad (5.4.1a)$$

with, for the isotropic case :

$$\tilde{M}_1^{+} + \tilde{M}_1^{-} = \frac{\mu}{\omega} k_z \begin{pmatrix} 0 & 1 \\ -1 & 0 \end{pmatrix}, \qquad (5.4.1b)$$

$$\tilde{M}_2^{+} + \tilde{M}_2^{-} = -\begin{pmatrix} 1 & 0 \\ 0 & 1 \end{pmatrix}. \qquad (5.4.1c)$$

As can be seen from expressions *(5.4.1)*, we then have stable decomposition operators. To determine the *P* wavefield ($\tilde{\phi} = \tilde{\phi}^{+} + \tilde{\phi}^{-}$) we only need to know $\tilde{v}_z$ and $\tilde{\tau}_{xx}$. Similarly to determine the *S* wavefield ($\tilde{\psi} = \tilde{\psi}^{+} + \tilde{\psi}^{-}$) we only need to know $\tilde{v}_x$ and $\tilde{\tau}_{zx}$.

Unfortunately, in VSP surveys the stress measurements are not available along the well. We only measure the particle velocities, thus it is not possible to recover both the $\vec{\tilde{p}}^{+}$ and $\vec{\tilde{p}}^{-}$ waves. The situation could be solved if we knew one of the two, say $\vec{\tilde{p}}^{-}$. Then from *(5.3.3a)* we can determine the other one, according to :

$$\vec{\tilde{p}}^{+} = \left[\tilde{L}_1^{+}\right]^{-1}\left[\vec{\tilde{v}} - \tilde{L}_1^{-}\vec{\tilde{p}}^{-}\right]. \qquad (5.4.2a)$$

For the situation depicted in *Figure 5.2.1* we can assume that at the well $\vec{\tilde{p}}^{-} = \vec{0}$. This assumption is realistic for two main reasons :

- Except in the case of a complicated subsurface, all the waves emitted by the source reach the detectors as $\vec{\tilde{p}}^{+}$ waves (especially when the borehole offset r_b is large).

- Since the diameter of the well is small compared to the wavelength of the incident body waves, its effect on any incident wavefield $\vec{\tilde{p}}^{+}$ can be neglected.Similarly to surface waves in Chapter 3, here we assume that the particle velocities associated to the tube waves have been removed from the total particle velocity field.

Under the assumption $\vec{\tilde{p}}^{-} = \vec{0}$,we have :

$$\vec{\tilde{p}}^{+} = \left[\tilde{L}_1^{+}\right]^{-1}\vec{\tilde{v}}. \qquad (5.4.2b)$$

The aforegoing leads to the decomposition operator at the receiver side in the case we only measure the particle velocities along the borehole.

5.5 THE DECOMPOSITION OPERATOR AT THE RECEIVER SIDE IN THE SPECTRAL DOMAIN

In the previous section we saw that the decomposition operator at the receiver side reads:

$$\left[\tilde{L}_1^+\right]^{-1} = \frac{\rho\omega}{k_z^2 + k_{x,p}k_{x,s}} \begin{pmatrix} k_{x,s} & k_z \\ -k_z & k_{x,p} \end{pmatrix}. \qquad (5.5.1)$$

Figure 5.5.1 represents the real and imaginary part of the operator components as a function of k_z. Expression $\Delta(k_z) = k_z^2 + k_{x,p}k_{x,s}$ does not vanish for real k_z values, the decomposition operator at the receiver side is then stable for all incident plane waves. The operator components are either symmetric or antisymmetric functions of k_z . It is important to point out that the operator has discontinuous first and higher order derivatives at $k_z = k_p$ and $k_z = k_s$. These two wavenumber values correspond to vertically propagating *P* and *S* waves. In the next section we will see that these discontinuities are difficult to handle when we want to design short decomposition convolutional operators in the space-frequency domain.

The decomposition operator at the receiver side requires the knowledge of both the *P* and *S* wave velocities along the VSP borehole. In the case we use an erroneous estimate $<c_p>$ and $<c_s>$ of the true *P* and *S* wave velocity, as well as an erroneous estimate$<\rho>$ of the density, it is possible to quantify the error made on the decomposed wavefield $<\vec{\tilde{p}}^+>$, by relating it to the true one, $\vec{\tilde{p}}^+$.

Knowing that the two following equations hold :

$$\vec{\tilde{p}}^+ = \left[\tilde{L}_1^+\right]^{-1} \vec{\tilde{v}}, \qquad (5.5.2a)$$

and

$$<\vec{\tilde{p}}^+> = \left[<\tilde{L}_1^+>\right]^{-1} \vec{\tilde{v}}, \qquad (5.5.2b)$$

we have the following relation between the estimated and the exact normal one-way wavefield:

$$<\vec{\tilde{p}}^+> = \left[\tilde{I} + \tilde{E}_R\right]\vec{\tilde{p}}^+, \qquad (5.5.2c)$$

with,

$$\tilde{E}_R = \left[<\tilde{L}_1^+>\right]^{-1} \tilde{L}_1^+ - \tilde{I}. \qquad (5.5.2d)$$

In the case no errors are made in the parameters estimation $\tilde{E}_R = 0$. Otherwise, the relative error matrix $\tilde{E}_R$ is a full square matrix. Which implies from *(5.5.2c)* that the normal one-way wavefield components are not well separated from each other. Just by looking at expression *(5.5.1)* we may say that in the case where the shear wave velocity is correctly estimated, the *P* wavefield will be well separated from the total wavefield. Its amplitude will be correct if and only if the compressional wave velocity has been correctly estimated as well. Due to the k_z dependency of the scaling factor, the decomposed P panel in the space-time domain may be

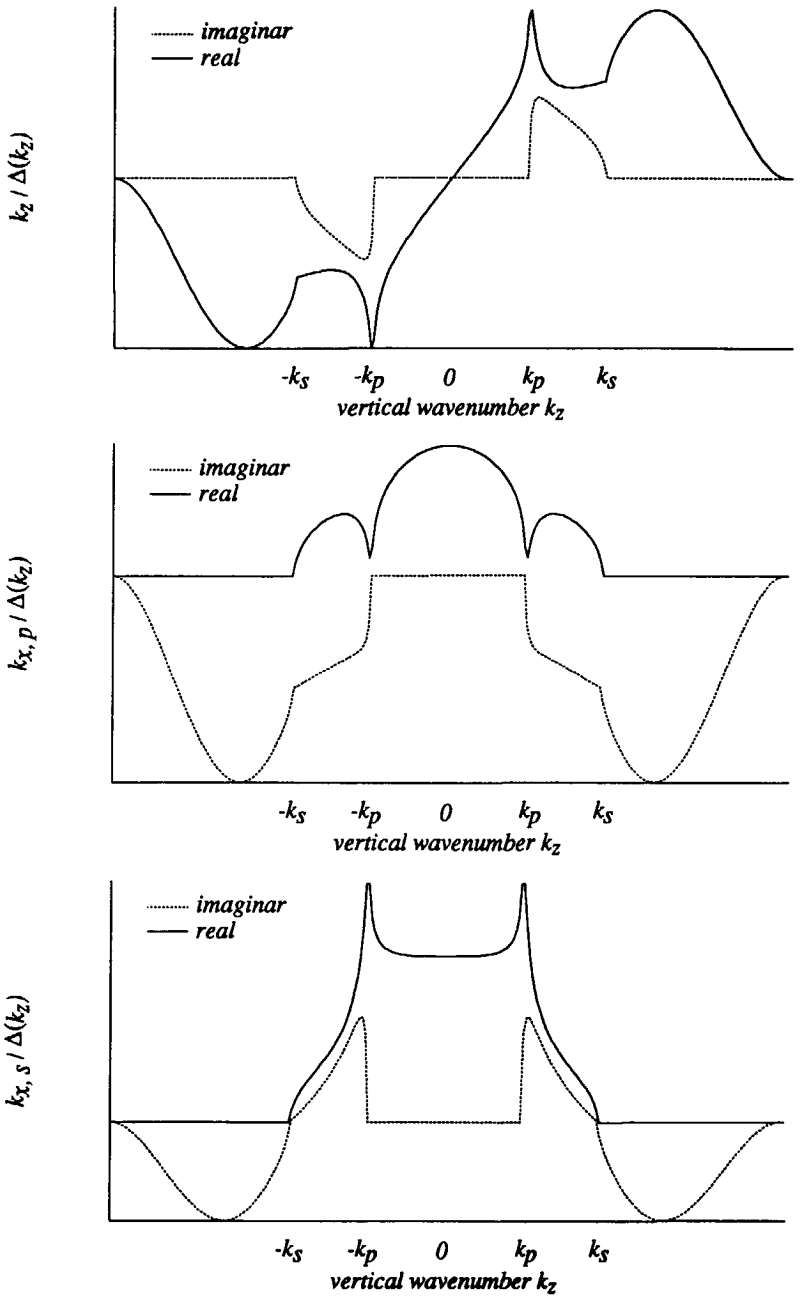

Figure 5.5.1

Real and Imaginary part of the decomposition operator components in the spectral domain

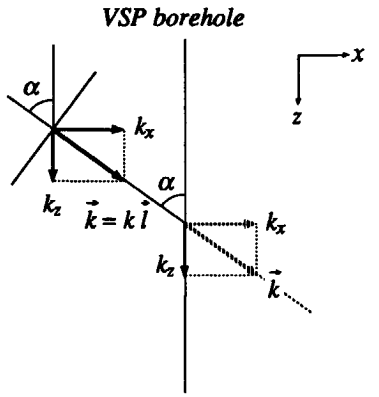

Figure 5.5.2

When the wavefield is recorded along the VSP borehole, we only have access to the vertical wavenumber k_z of the incident plane waves. To determine their direction of propagation $\hat{l}$ or equivalently their angle of incidence α, we have to determine their horizontal wavenumber k_x.

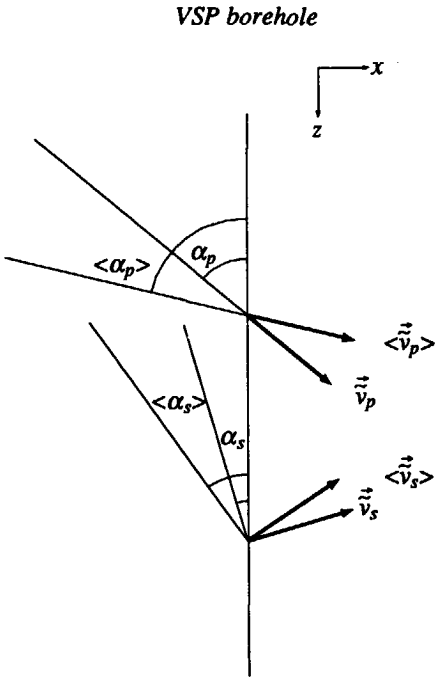

Figure 5.5.3

An incorrect estimation of the wave-type phase velocity leads to an incorrect estimation of the angle of incidence of the incident plane waves. The wave-type polarization vector is then not correctly estimated.

seriously deteriorated when c_p is not well estimated. Similar remarks hold for the decomposed S panel.

The physics behind the wavefield decomposition of VSP data is simpler than the one involved in the wavefield decomposition of surface data, as the recording site does not interfer with the incident waves. We can then give a simple physical understanding of the sensitivity of the method to its input parameters. Let us consider a plane wave propagating in the source-borehole direction, see *Figure 5.5.2*. To be able to decompose the incident elastic wavefield, we implicitly need to know its direction of propagation. Indeed, from the direction of propagation ($\hat{l}$), we can determine the polarization vectors, so the columns of $\tilde{L}_1^+$, of the three wave-types that can propagate along this direction, thus the particle velocity field can be decomposed according to *(5.4.2b)*. The wavefield being recorded along the VSP borehole, we can only determine the vertical wavenumber k_z of the incident plane wave. To be able to determine its direction of propagation, or equivalently its angle of incidence α, we have to know the horizontal wavenumber k_x ($tg\alpha = k_x/k_z$). For a given wave-type, k_x may be deduced from the dispersion relations. As these relations involve the wave-type propagation velocity, an incorrect estimate $<c>$ of the true velocity c leads to an erroneous estimate $<\alpha>$ of α. From this development we may then say that: *the sensitivity of the decomposition at the receiver side depends on the sensitivity of the wave-type polarization vectors to the direction of propagation and to the stiffness tensor. As in an isotropic medium the wave-type polarization vectors only depend on the direction of propagation, the wavefield decomposition will be more robust for isotropic than for an anisotropic medium.*

For the illustration, we consider an isotropic medium and a wave-type with propagation velocity c. We have:

$$k_x = \sqrt{\frac{\omega^2}{c^2} - k_z^2} \ . \qquad (5.5.3)$$

If we use for the phase velocity $<c>$ instead of c, the following relations hold between α and $<\alpha>$:

$$k_z = \frac{cos\ (<\alpha>)}{<c>} = \frac{cos\ (\alpha)}{c} \ . \qquad (5.5.4)$$

From expression *(5.5.4)* we deduce that an underestimation (overestimation) of the phase velocity implies an overestimation (underestimation) of the angle of incidence. It is then preferable to underestimate the velocity then to overestimate it, in order to avoid that propagating waves are interpreted as evanescent waves. In *Figure (5.5.4)* the difference $<\alpha>-\alpha$ is represented as a function of α for different ratios $<c>/c$. The error made on the angle of incidence decreases for increasing angle α. As in an isotropic medium the errors made on the estimate of the polarization vectors directly depend on the error made on the angle of incidence of the plane wave, see *Figure 5.5.3*, we may say that: *the sensitivity of the decomposition at the receiver side to errors made in the phase velocity estimation decreases with the source-borehole offset (r_b). Figure 5.5.5* represents the amplitude of the P wave residuals in the decomposed S panel, as well as the amplitude of the S wave residuals in the decomposed P

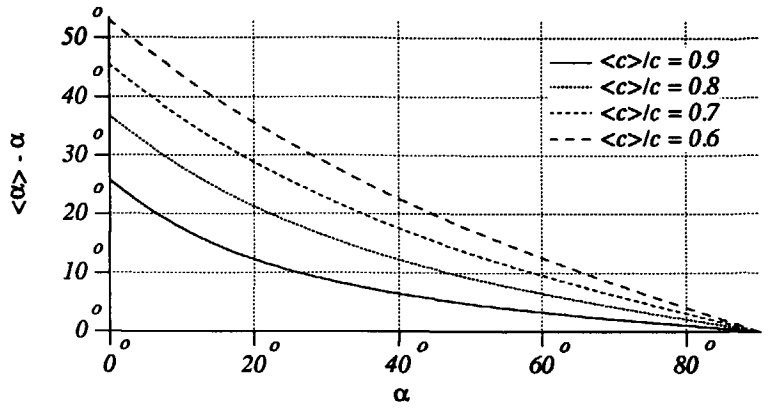

Figure 5.5.4

This graph represents the error <α>-α made on the estimation of the angle of incidence, as a function of α, for four relative velocity error <c>/c.

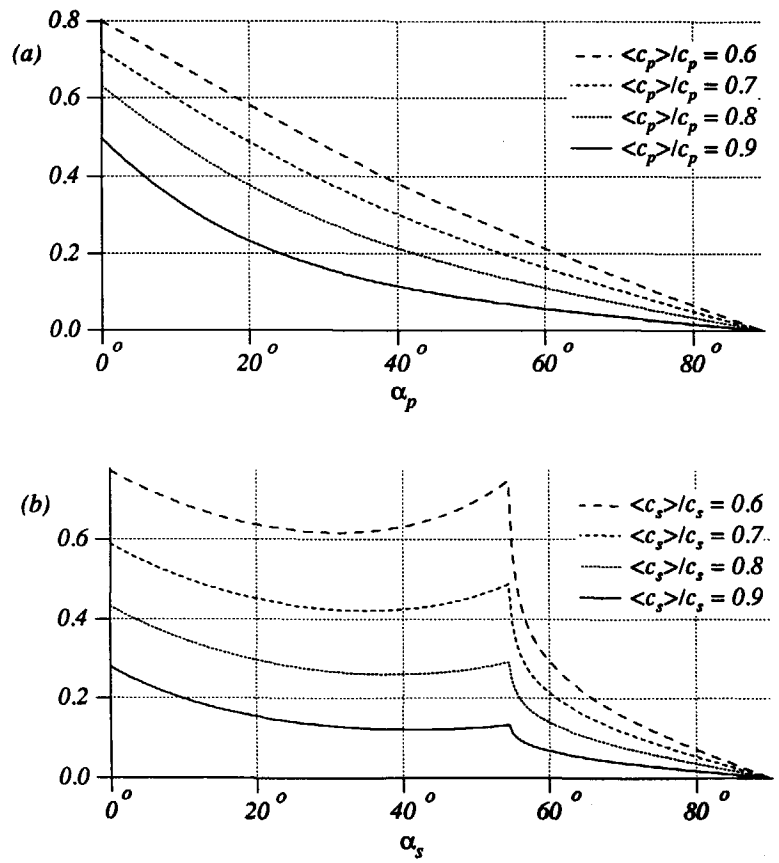

Figure 5.5.5

(a) P wave residuals in the decomposed S panel when $c_p/c_s=\sqrt{3}$ and $<c_s> = c_s$

(b) S wave residuals in the decomposed P panel when $c_p/c_s=\sqrt{3}$ and $<c_p> = c_p$

panel, for several relative errors made in the P and S wave propagating velocities. This Figure well illustrates that the quality of the separation increases with the angle. Hence, *the sensitivity of the decomposition at the receiver side of VSP data to its input parameters, decreases with the source-borehole offset (r_b).*

In section *5.4* we have seen that the decomposition operator at the receiver side has been derived under the assumption that we only have waves propagating in the source-borehole direction ($\vec{\tilde{p}}^{-} = \vec{0}$). In the case the subsurface is not laterally homogeneous, reflected P and S waves propagating in the borehole-source direction may be recorded by the particle velocity detectors. It is then interesting to know how such waves will be decomposed, see *Figure 5.5.6.* We have:

$$\vec{\tilde{v}} = \tilde{L}_1^{+}\vec{\tilde{p}}^{+} + \tilde{L}_1^{-}\vec{\tilde{p}}^{-} . \qquad (5.5.6a)$$

The decomposition operator at the receiver side *(5.4.2b)* applied to the particle velocity field *(5.5.6a)*, leads to:

$$<\vec{\tilde{p}}^{+}> = \vec{\tilde{p}}^{+} + \left[\tilde{L}_1^{+}\right]^{-1}\tilde{L}_1^{-}\vec{\tilde{p}}^{-} , \qquad (5.5.6b)$$

with,

$$\left[\tilde{L}_1^{+}\right]^{-1}\tilde{L}_1^{-} = \frac{1}{cos(\alpha_p - \alpha_s)}\begin{pmatrix} cos(\alpha_p + \alpha_s) & sin(2\alpha_s) \\ -sin(2\alpha_s) & cos(\alpha_p + \alpha_s) \end{pmatrix}, \qquad (5.5.6c)$$

and

$$k_z = \frac{cos(\alpha_p)}{c_p} = \frac{cos(\alpha_s)}{c_s} . \qquad (5.5.6d)$$

As the matrix product $\left[\tilde{L}_1^{+}\right]^{-1}\tilde{L}_1^{-}$ is not diagonal, P waves propagating in the borehole-source direction *(-)* will be interpreted as a combination of P and S waves propagating in the source-borehole direction *(+)*. A similar remark can be made for the S waves propagating in the borehole-source direction. *Figure 5.5.7* represents the amplitude of the P waves ($\tilde{\Phi}^{-}$) in the decomposed S panel ($\tilde{\psi}^{+}$)and the amplitude of the S waves ($\tilde{\psi}^{-}$) in the decomposed P panel ($\tilde{\Phi}^{+}$).

5.6 THE DECOMPOSITION OPERATOR IN THE SPACE-FREQUENCY DOMAIN

The wavefield decomposition at the receiver side in the wavenumber-frequency domain, suits well for a large distribution of regularly spaced particle velocity detectors in homogeneous medium. Outside this ideal situation we would rather work in the space-frequency domain; indeed this domain offers much more flexibility for the following situations :

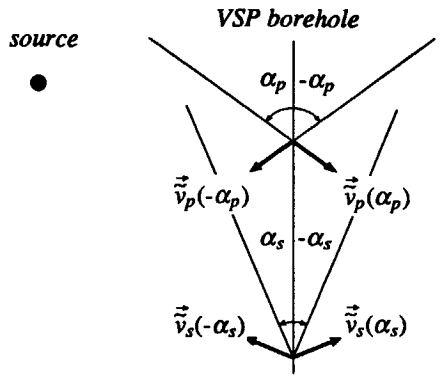

Figure 5.5.6

Due to the assumptions made for the derivation of the decomposition operator at the receiver side, P waves that propagate in the borehole-source direction (-) will be interpreted as a combination of P and S waves propagating in the source-borehole direction (+). A similar remark can be made for the S waves.

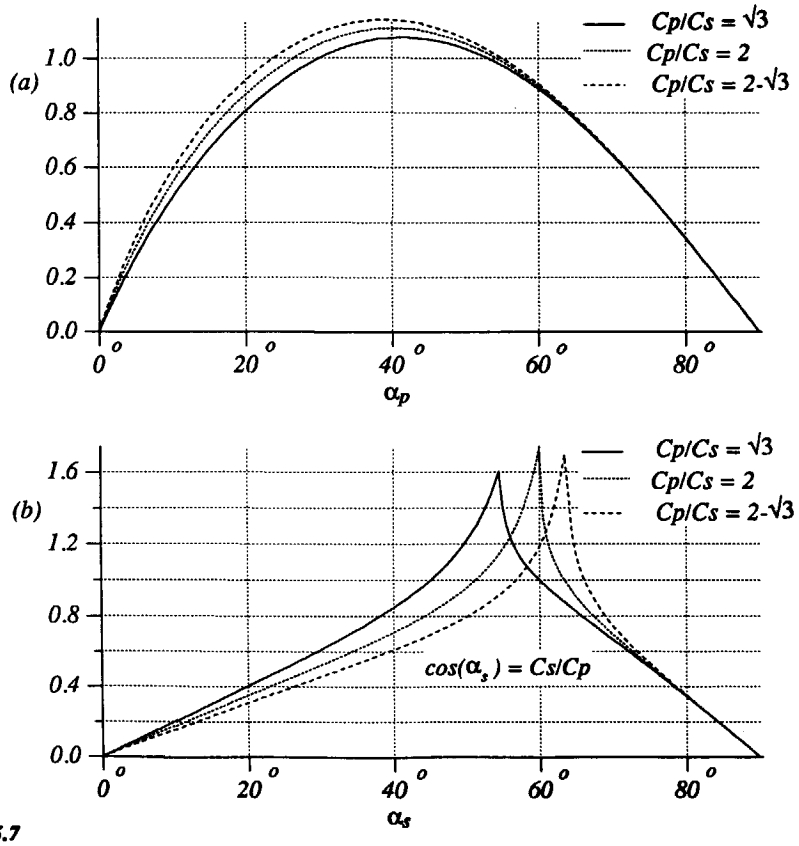

Figure 5.5.7

(a) $\tilde{\Phi}^-$ *residuals in* $\tilde{\Psi}^+$

(b) $\tilde{\Psi}^-$ *residuals in* $\tilde{\Phi}^+$

- When the borehole crosses a vertically inhomogeneous medium, the decomposition operator is space dependent. It has to be adapted to the elastic parameters at all depth levels where the wavefield has to be decomposed. This space dependency is easily taken into account in the space-frequency domain.

- In the space-frequency domain the decomposition operators can take into account quite well all kinds of detector distributions. This domain suits well then for wavefields that are irregularly sampled. An other advantage of this domain is that it is also easier to take into account the finite vertical aperture of the survey.

To determine the M_1+M_2+1 complex points of the discretized convolutional operator that simulates in the space-frequency domain one of the four decomposition operators $\tilde{F}(k_z,\omega)$ (previously developed in the vertical wavenumber-frequency domain), we use the same method as the one developed in section *(3.8)*. We find that for one frequency component, the M_1+M_2+1 complex operator points contained in the filter vector $\vec{f}$,

$$\vec{f} = (f_{-M_2}(\omega), \cdots, f_0(\omega), \cdots, f_{M_1}(\omega))^T , \qquad (5.6.1a)$$

are solutions of the linear system :

$$A(\omega)\,\vec{f}(\omega) = \vec{b}(\omega) , \qquad (5.6.1b)$$

with,

$$A_{mn}(\omega) = \sum_{k_z = k_{zmin}}^{k_z = k_{zmax}} W(k_z,\omega)\, e^{jk_z(z_m - z_n)} , \quad m,n = -M_2, \ldots, M_1 \qquad (5.6.1c)$$

and

$$b_m(\omega) = \sum_{k_z = k_{zmin}}^{k_z = k_{zmax}} W(k_z,\omega)\, \tilde{F}(k_z,\omega)\, e^{jk_z z_m} . \qquad (5.6.1d)$$

Where $W(k_z,\omega)$ is a weight function and k_{zmin}, k_{zmax} depend on the vertical wavenumbers of the plane waves that are expected to reach the vertical position z_0. Due to the derivative discontinuities at $k_z = k_p$ and $k_z = k_s$, the decomposition operator in the space domain will be long if we want to include these values in the seismic band over which the operator has to be accurate. When the data does not contain vertically propagating P and S waves, the convolutional operator length greatly reduce by allowing the operator not to be accurate for these spectral waves. Conclusion: *The wavefield decomposition of VSP data with convolutional operators is more suited for VSP surveys with source-borehole offset than without offset.*

To illustrate the wavefield decomposition in the space-frequency domain we first consider simulated data. The subsurface model consists of three horizontal layers overlaying a homogeneous lower half space. The physical properties and the thickness of the three layers are :

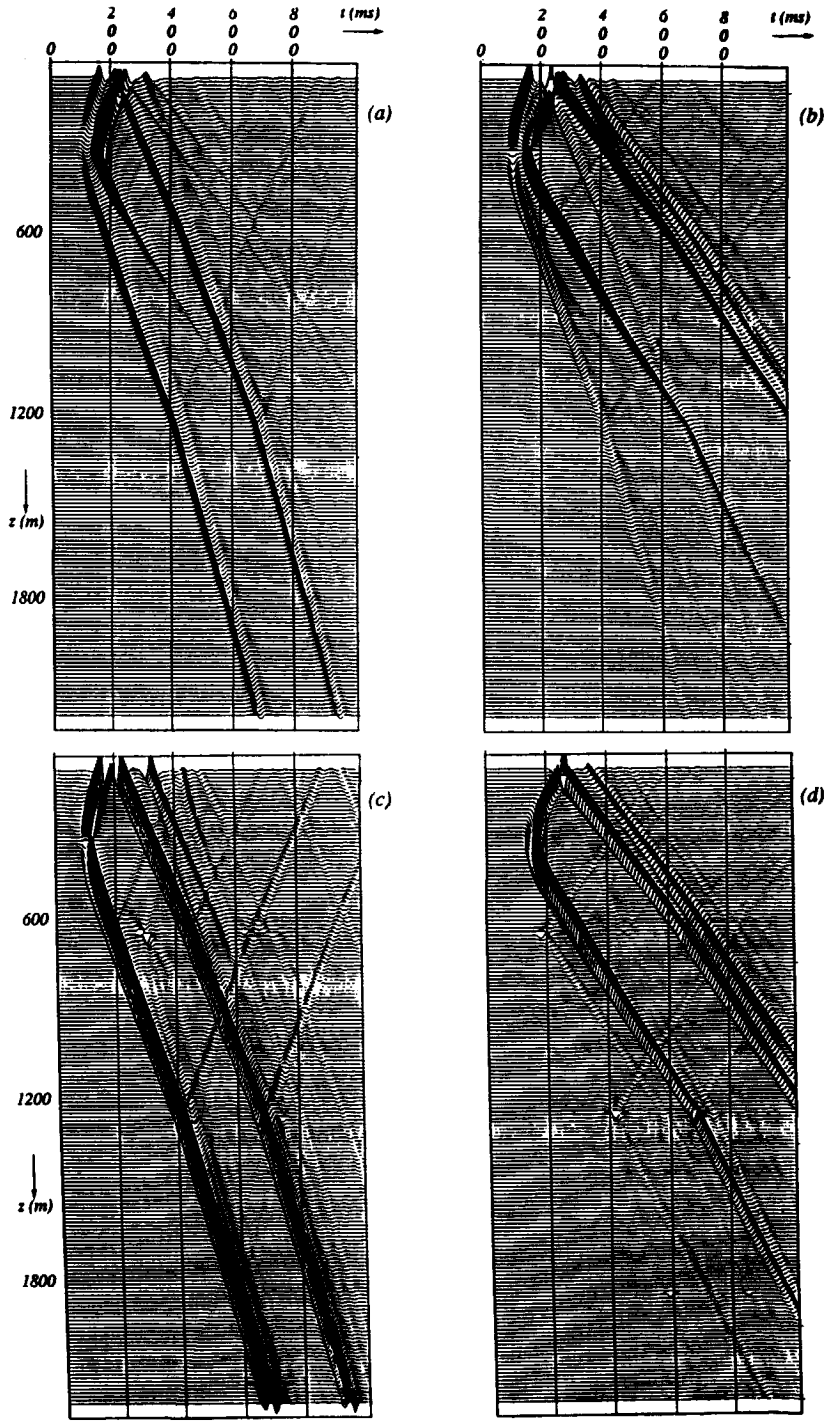

Figure 5.6.1

(a) vertical particle velocity, (b) horizontal particle velocity, (c) decomposed P wavefield 10dB clipped, (d) decomposed S wavefield 10dB clipped.

$c_{p1} = 2249\ m/s, c_{s1} = 1300\ m/s, \rho_1 = 1\ g/cm^3, \Delta z = 600\ m;$
$c_{p2} = 2595\ m/s, c_{s2} = 1500\ m/s, \rho_2 = 1\ g/cm^3, \Delta z = 600\ m;$
$c_{p3} = 3460\ m/s, c_{s3} = 2000\ m/s, \rho_3 = 1\ g/cm^3, \Delta z = 600\ m;$
$c_{p4} = 3700\ m/s, c_{s4} = 2000\ m/s, \rho_4 = 1\ g/cm^3.$

The VSP borehole is at a distance r_b=*150 m* from the source. The source consists of a vertical force buried at a depth of *300 m*. The detector spacing is *2* meters and the time sampling is *4 ms*. *Figures 5.6.1a,b* represent the vertical and horizontal particle velocities simulated with a 2D finite difference modeling program; *Figures 5.6.1c,d* represent the decomposed *P* and *S* wavefields, 7 points convolutional operators have been used. We can note the excellent normal one-way wavefield separation for a wide range of incident angles.

Now we present an example of wavefield decomposition of real VSP data. The data provided by the Compagnie Générale de Géophysique (CGG) have been shot in the Paris basin.

The data were recorded with the following parameters:

detector spacing	:	*10 (m)*
first detector	:	*220 (m)*
last detector	:	*1810 (m)*
borehole offset	:	*650 (m)*
sample interval	:	*2 (ms)*
frequency content	:	*10 - 80 (Hz)*

Figures 5.6.2a,b represent the horizontal and vertical particle velocity components recorded along the well. We used 5 points convolutional operators and the following depth model for the wavefield decomposition:

layer	*depth (m)*	c_p *(m/s)*	c_S *(m/s)*
1	*220*	*2690*	*1237*
2	*280*	*2815*	*1427*
3	*425*	*3075*	*1563*
4	*528*	*3343*	*1731*
5	*640*	*2771*	*1298*
6	*737*	*2417*	*1029*
7	*795*	*2650*	*1231*
8	*901*	*2600*	*1180*
9	*1005*	*3548*	*1686*
10	*1115*	*3862*	*2124*
11	*1227*	*3486*	*1570*
12	*1349*	*3320*	*1762*
13	*1432*	*4930*	*2620*
14	*1580*	*4080*	*2155*
15	*1733*	*3400*	*1688*

As can be seen on the original sections, *P* and *S* wave energy is recorded both on the horizontal and vertical particle velocity components. At small depths (*200-600m*), the data are mainly composed of refracted horizontally propagating *P* and *S* waves. We can also notice the presence of upgoing reflected waves (with small angles of incidence) coming from the deeper layers. This part of the data will enable to test if our decomposition operators can correctly treat *P* and *S* waves of the same apparent vertical velocity. In this case the separation is only based on the difference of polarization of the two wave types. This part of the data is also interesting to check if we can treat a wide range of angles of incidence. From the reflector at depth *1000m* a lot of wave reflections and conversions occur, because here the medium contains strong vertical velocity variations. It will enable to test if the local decomposition operators can handle a complex medium. One can see from the horizontal and vertical particle velocity sections the effect of the sensitivity of the particle velocity detectors to the angle of incidence of the waves. It is interesting to check if these effects are removed on the decomposed sections. The result of the decomposition, *Figures 5.6.3a,b*, is considered to be impressive. The following comments can be made: the strong downgoing direct *P* wave has been completely removed in the decomposed *S* section. The effects of the detector directivity has been removed and the continuity of the *P* and *S* waves is much better on the decomposed section than on the particle velocity sections. We can also note that all the dips have been correctly treated, and that the spatial resolution of the decomposed *S* section is high (even in the highly inhomogeneous part of the medium around *1000m).*

In conclusion, the VSP real data example indicates that *the decomposition operators effectively separate P- and S- waves in a true amplitude sense, also under complex field conditions (many overlapping events, similar apparent velocities, fast medium velocity variations).*

Remark:

The decomposition convolutional operator is well suited to decompose a seismic wavefield composed of a wide range of plane waves. Indeed, the convolutional operator is not designed to fit the theoretical operator exactly but in a least squares sense. By allowing a small error in the operator response for the plane waves of interest, a larger number of plane waves (larger than the number of operator points) may be satisfactory treated. In the case that the data can be well approximated as the sum of a small finite number of plane waves, an other decomposition approach is preferrable to treat in an exact manner the few plane waves contained in the data. For the illustration, let us consider a small offset VSP survey. At any depth level the seismic wavefield can be well approximated by the sum of two downgoing (*P* and *S*) and two upgoing (*P* and *S*) plane waves. From the relation between the amplitude, the angle of incidence of the normal wave-types and the particle velocities *(5.3.3a)*, it is possible using an inversion algorithm to determine these two parameters for each of the four incident plane waves. Such a scheme has been developed and illustrated by Esmersoy (1990) and Leaney (1990). With this method it is even possible to determine the *P* and *S* wave propagating velocities at the depth level where the wavefield is decomposed and to correctly treat plane waves propagating in the borehole-source direction. Unfortunately, the method requires a pre-interpretation step.

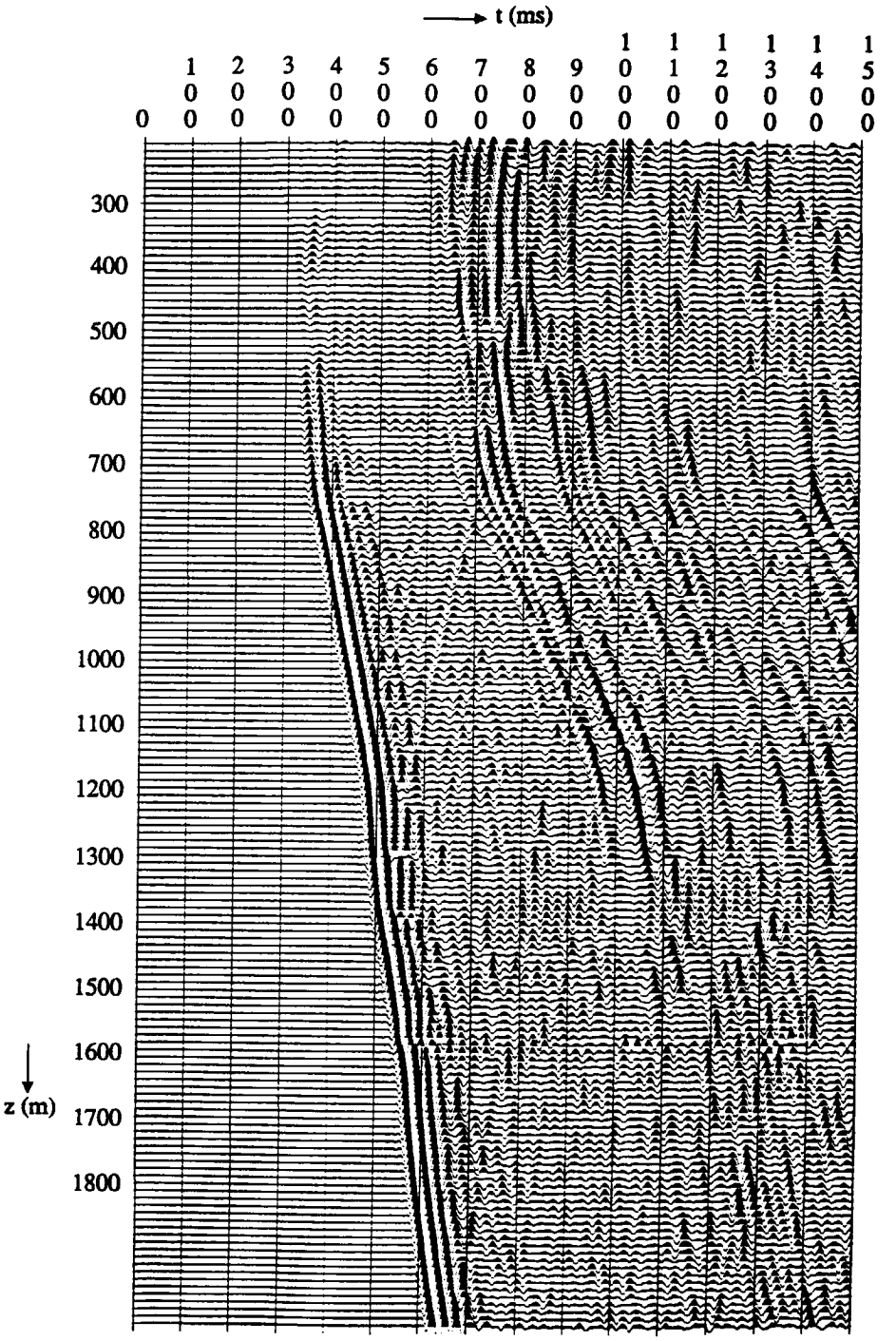

Figure 5.6.2

(a) vertical particle velocity

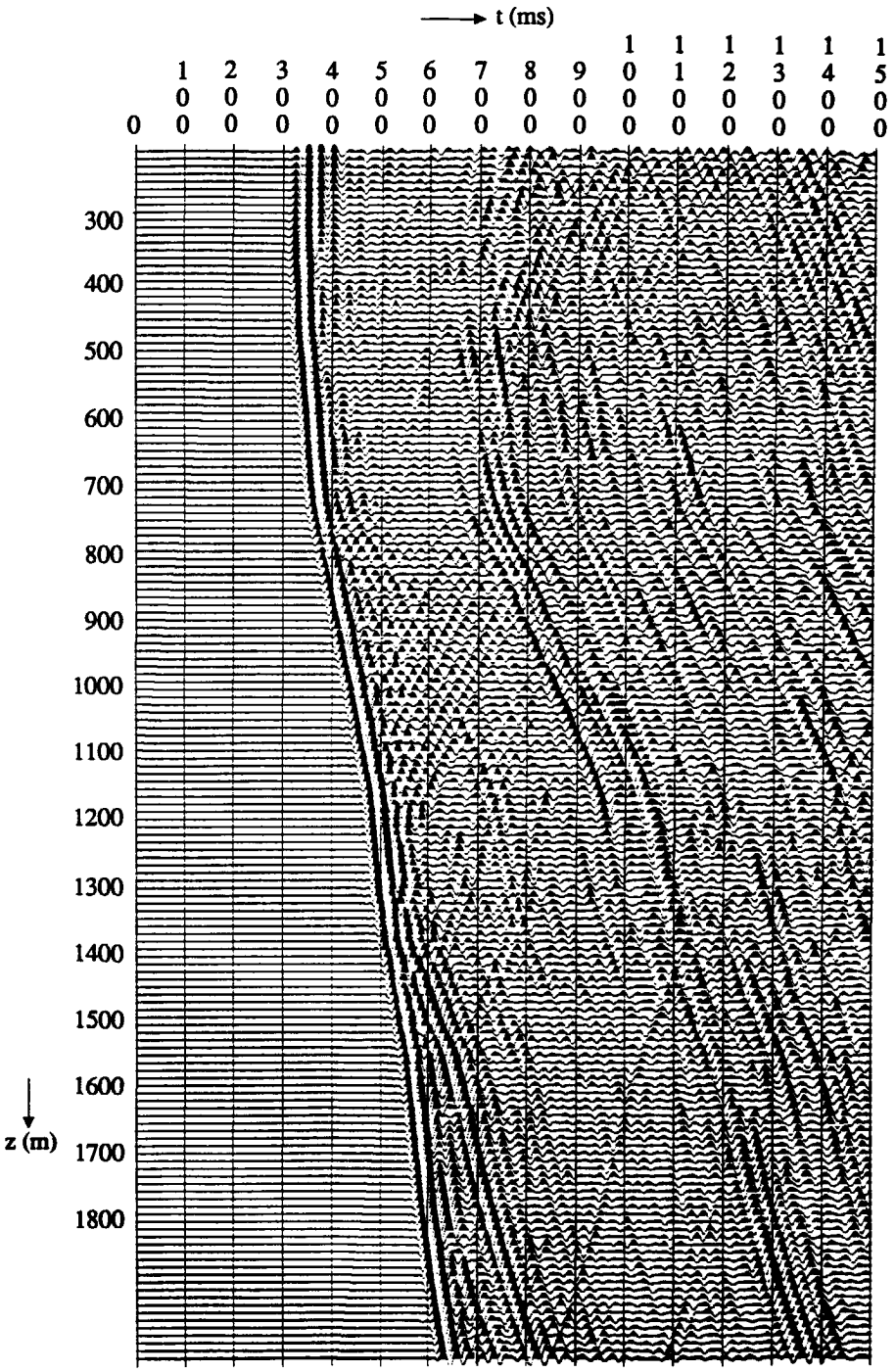

Figure 5.6.2

(b) horizontal particle velocity

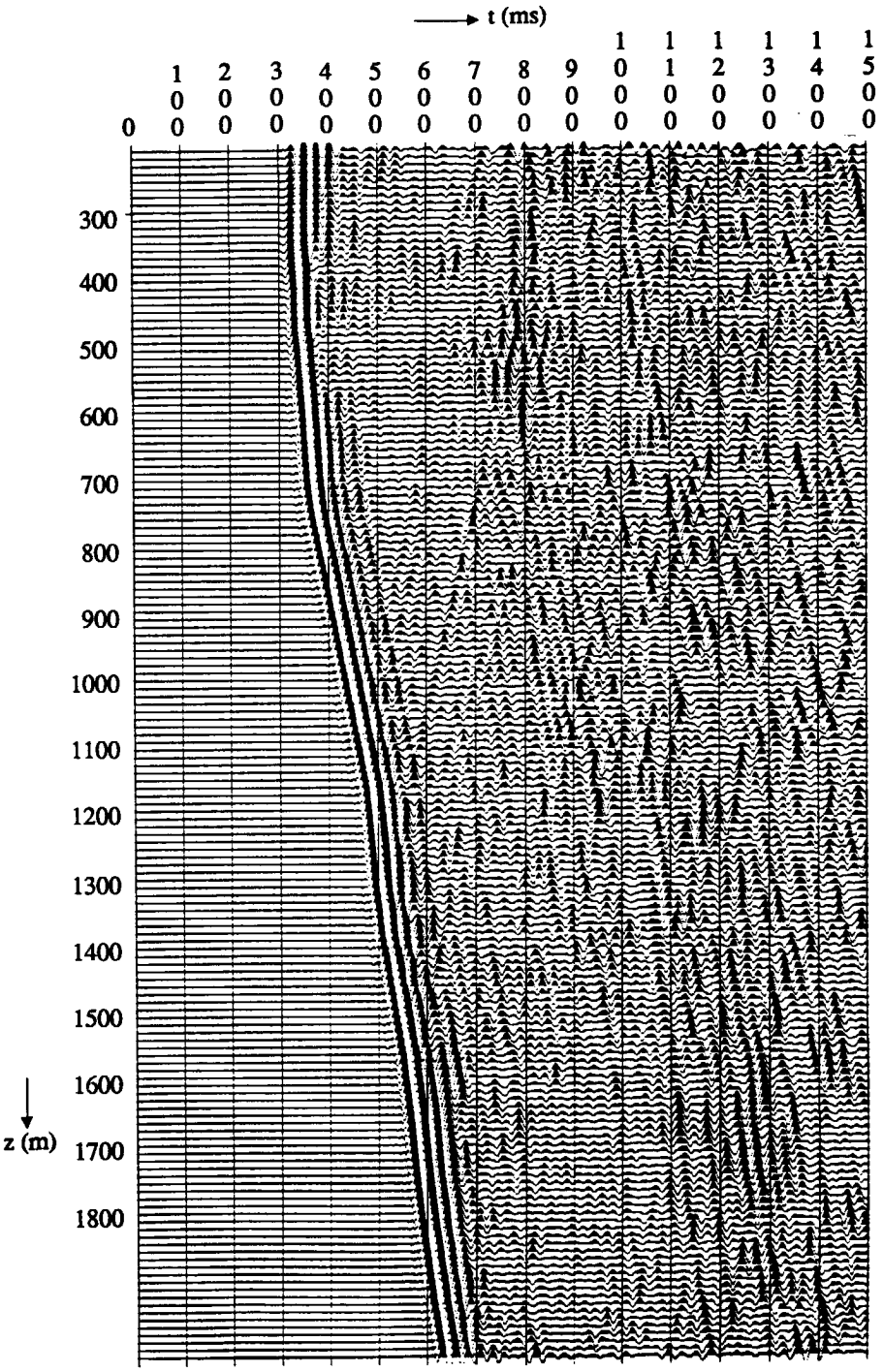

Figure 5.6.3

(a) decomposed P wavefield

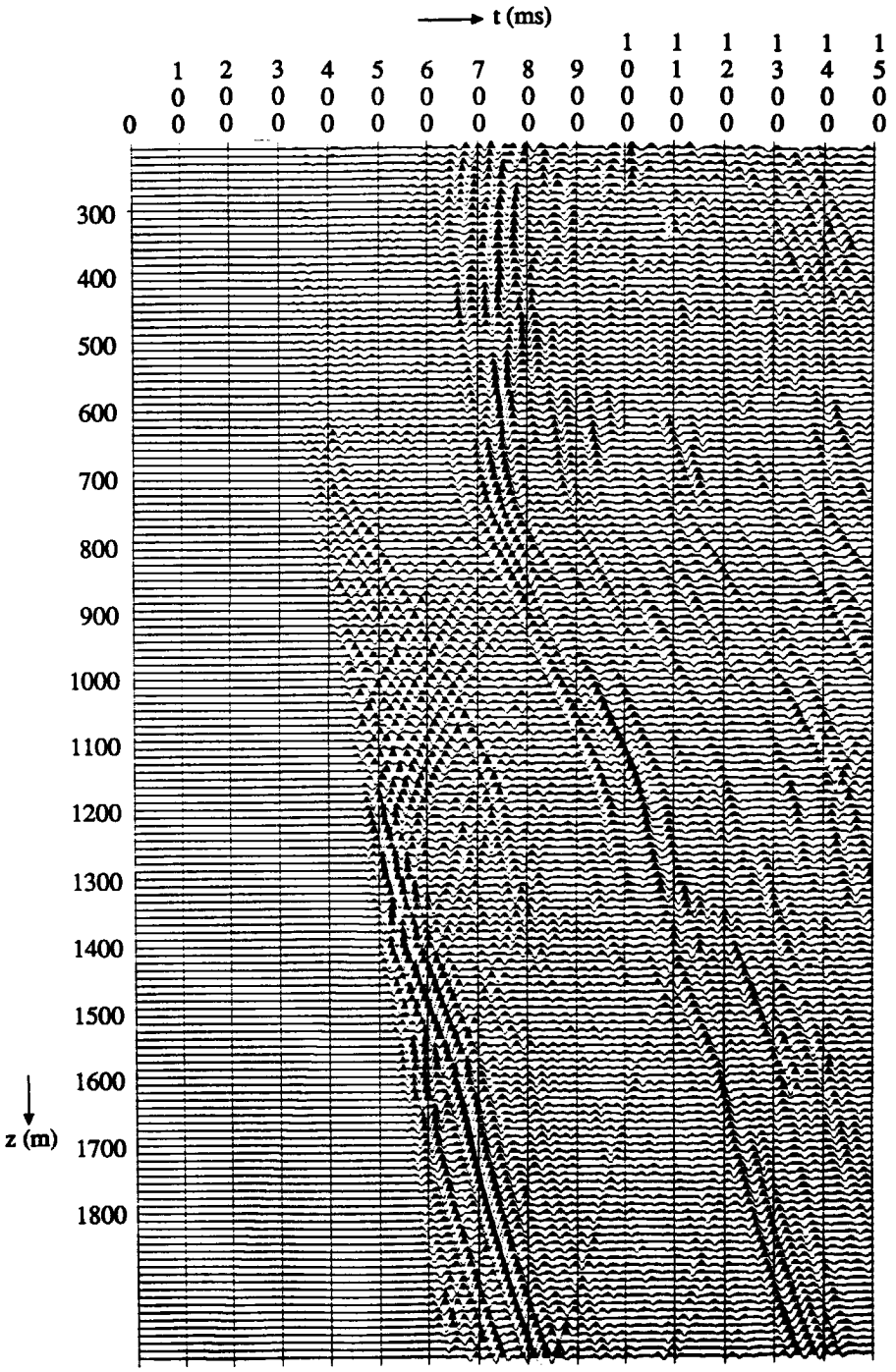

Figure 5.6.3

(b) decomposed S wavefield

CONCLUSIONS

In this thesis, we have defined elastic wavefield decomposition as a transformation of a two-way vector wavefield representation into a one-way scalar wavefield representation. Starting from this definition and using the relations between the two-way and normal one-way wavefield components, we have developed a general formalism for the wavefield decomposition of elastic waves.
For surface seismic data the following topics have been addressed

1) 2D *and* 3D

The elastic wavefield decomposition has been derived for 2D and 3D seismic wavefields (chapters 2 and 3). For 3D seismic wavefields recorded along one direction only, we have developed the proper cylindrical wave decomposition formulas, that enable to apply an exact wavefield decomposition when the subsurface is horizontally layered (chapter 4).

2) Isotropic *and* anisotropic

In isotropic media we separate the compressional (P) and shear (S) waves. In anisotropic media the decomposition operators separate the three normal modes of propagation that compose the total wavefield (chapter 2).

3) Lateral variations

For laterally variant media, the wavefield is decomposed in the space-frequency domain by means of convolutions. Special attention has been put in the derivation of short convolutional operators that act locally (chapter 3).

4) Wavefield decomposition at the detector *and* source side

We decompose the wavefield recorded by the detectors as well as the wavefield emitted by the sources (chapter 3).

5) Extra wavefield information

The decomposition operators are designed in such a way that any extra information about the wavefield can be easily included. It enables the decomposition of extrapolated wavefields (chapter 3)

6) Sensitivity analysis

We showed that for isotropic media the sensitivity of the wavefield decomposition algorithm to the P and S wave velocity of the near surface increase with the angles of incidence. We also studied the effect of the traction free surface on the sensitivity of the decomposition process (chapter 3).

Our experience with surface land data is yet small. However, from our limited experience we may conclude that proper-preprocessing (statics, coupling) prior to decomposition is a pre-requisite. In the case of a low velocity near surface medium the wavetype separation is largely made by the horizontal and vertical component sources/receivers.

The same topics have been addressed for VSP data (chapter 5). Due to the strong vertical velocity variations that may occur along the VSP well, the wavefield decomposition has to be done in the space-frequency domain. If the data can be well fitted by few plane waves (by e.g. two downgoing, two upgoing) it is preferrable to do a parametric wavefield decomposition as proposed by Leaney (1990). If the data is complex it is preferrable to do the wavefield decomposition by means of convolutional products (this thesis, chapter 3).

As the convolutional operators play an important part in wavefield decomposition, it is interesting to continue their development. For instance, the weighting function, as introduced in section 3.8 for the computation of the operators in the space-frequency domain, is defined in a very simple manner. An improvement will be obtained by updating the weighting function in an iterative way (one or two iterations).

REFERENCES

ACHENBACH, J.D., 1987. *Wave propagation in elastic solids:* North Holland Publ. Co.

AKI, K., and RICHARDS, P.G., 1980. *Quantitative seismology*: W.H. Freeman and Co.

BAETEN, G.J.M., 1989. *Theoritecal and practical aspects of the vibroseis method.* Ph.D. thesis, Delft University of Technology.

BERESFORD-SMITH, G. and RANGO, R. 1989. Suppression of ground roll by windowing in two domains. *First Break* **7**, 55-63.

BERKHOUT, A.J. 1982. *Seismic Migration: Imaging of acoustic energy by wave field extrapolation. A. Theoritecal aspects.* Elsevier Science Publishing Co.

BERKHOUT, A.J and WAPENAAR, C.P.A. 1988. Delft Philosophy on inversion of elastic data. 58th SEG meeting, Anaheim, U.S.A., Expanded Abstracts, 831-833.

BLACQUIÈRE, G., DEBEYE, H.W.J., WAPENAAR, C.P.A. and BERKHOUT, A.J. 1989. Three dimensional table-driven migration. *Geophysical Prospecting* **37**, 925-958.

CLIET, C. and DUBESSET, M., 1984. Three component recordings: interest for land seismic source study. *Institut Français du Pétrole, Ref 32 748.*

DANKBAAR, J.W.M., 1985. Separation of P- and S- waves. *Geophysical prospecting* **33**, 970-986.

DEVANEY, A.J. and ORISTAGLIO, M.L., 1986. A plane wave decomposition for elastic wavefields applied to the separation of P-waves and S-waves in vector seismic data. Short note, *Geophysics* **51**, 419-423.

ESMERSOY C., 1990. Inversion of P and SV waves from multi-component offset vertical seismic profiles: *Geophysics* **55**, p. 39-50.

FOKKEMA, J.T., VAN DEN BERG, P.M., and VISSINGA, M., 1992. On the computation of Radon transforms of seismic data. *Journal of Seismic exploration* **1**, 93-105.

GOUDET G., 1943. *Les Fonctions de Bessel et leurs applications en physique.* Ecole normale supérieure (publications des laboratoire de physique): Masson et C^{ie}, éditeurs.

KELLY, K.R., WARD, R.W., TREITEL, S. and ALFORD, R.M. 1976. Synthetic seismograms: a finite difference approach. *Geophysics* **41**, 2-27.

KINNEGING, N.A., BUDEJICKY, V., WAPENAAR, C.P.A. and BERKHOUT, A.J. 1989. Efficient 2D and 3D shot record redatuming. *Geophysical Prospecting* **37**, 493-530.

LEANEY, W.S., 1990. Parametric wavefield decomposition and applications: 60th SEG meeting, San Francisco, Expanded Abstract p1097-1099.

McMECHAN, G.A. and SUN, R. 1991. Depth filtering of first breaks and ground roll: *Geophysics* **56**, 390-396.

MUSGRAVE, M.P.J., 1970. *Crystal Acoustics, introduction to the study of elastic waves and vibrations in crystals*: Holden-Day.

PRESS, W.H., FLANNERY, B.P., TEUKOLSKY, S.A. and VETTERLING, W.T. *Numerical Recipes, The art of Scientific Computing*: Cambrige University Press.

URSIN, B., 1983. Review of elastic and electromagnetic wave propagation in horizontally layered media: *Geophysics* **48**, p. 1063-1081.

VERSCHUUR, E.,1991. *Surface related multiple elimination, an inversion approach.* Ph.D. thesis, Delft University of Technology.

WAPENAAR, C.P.A. and BERKHOUT, A.J., 1989. *Elastic wavefield extrapolation*: Advances in exploration Geophysics 2, Elsevier.

WAPENAAR, C.P.A and HAIMÉ, G.C, 1990. Elastic extrapolation of primary seismic P- and S-waves. *Geophysical prospecting* **38**, 23-60.

WAPENAAR, C.P.A., HERRMANN, P., VERSCHUUR, D.J. and BERKHOUT, A.J. 1990. Decomposition of multicomponent seismic data into primary P- and S- wave responses. *Geophysical Prospecting* **38**, 633-661.

WAPENAAR C.P.A, VERSCHUUR, D.J., HERRMANN, P.,1992. Amplitude pre-processing of single- and multi-component 2D seismic data: submitted to Geophysics.

WOODHOUSE, J.H., 1974. Surface waves in a laterally varying layered structure: *Geophys. J.R. astr. Soc.***37**, 461-490.

SUMMARY

To determine the geological *structure* of the subsurface, single component seismic surveys are generally sufficient. When we are interested in the type of materials that constitute the embedded layers, we have to determine their elastic (and preferably also their lithologic) properties. This can be done by illuminating the subsurface materials with different wave-types and to analyse the subsurface responses for each wave-type (DELPHI approach).

To analyse the total seismic subsurface response, the reflected wavefields have to be recorded by *multi-component* detectors. To determine the subsurface response for each wave-type, we have to use *multi-component* sources as well.

The image of the subsurface is obtained from the recorded data after a series of processing steps. We propose data decomposition *prior* to image related processing. This data decomposition step separates *P* and *S* waves at the surface.

In this thesis we present a general formalism for the decomposition per wave-type at the source as well as at the receiver side, both in surface and borehole seismics. For the *decomposition at the receiver side* we have formulated the relation between the quantity measured by the detectors (particle velocities) and the amplitudes of the three incident wave-types (see Chapter 2). For the *decomposition at the source side* we have formulated the relation between the emitted source quantity and the amplitudes of the three emitted wave-types (see Chapter 2). From these relations we can determine the expression of the decomposition operator at the receiver side; it enables us to separate the three wave-types reaching the detectors. Similarly, we can also determine the expression of the decomposition operator at the source side; it enables us to separate from the seismic earth response the part due to the different wave-types emitted by the sources (see Chapter 3). For reasons of stability and uniqueness we prefer the *multi-channel* approach to the single-channel approach, resulting in a spatial convolutional process to be applied to the source and receiver gathers. The decomposition operators depend on the

elastic parameters of the medium at the source and receiver side. As these parameters are generally not known during data acquisition, it is essential to do the decomposition numerically (in a data adaptive way) in the processing center. Hence, wavefield decomposition should not be done in the field.

Using the matrix notation, the operations involved in the decomposition are very similar to the operations involved in one extrapolation step of pre-stack depth migration, the wavefield extrapolation operators at the source and at the receiver side being replaced by the wavefield decomposition operators at the source and receiver side (see Chapter 3). Similar as in prestack migration, if the elastic medium is homogeneous at the source and receiver side the decomposition can be applied in the wavenumber-frequency domain. For inhomogeneous media the wavefield decomposition has to be done in the space-frequency domain. Contrary to pre-stack migration, we do not need a subsurface model but only a model of the elastic medium around the sources and receivers. It is important to note that in the case we are not interested in applying the proposed decomposition at the actual source and receiver locations, all the tools presented in this work can still be used to decompose the elastic wavefield away from the sources and receivers, after wavefield extrapolation. In the DELPHI project it has been shown, however, that decomposition should be carried out prior to extrapolation.

Low velocity near surface layers automatically realize wavefield separation at the source and receiver side. Therefore for surface seismics, the result of the wavefield decomposition will be most effective for high velocity near surface material. Generally, the near surface is unconsolidated, leading to poor quality data affected by problems of changes in coupling between adjacent sources and/or detectors, problems of statics and problems of absorption. Under such conditions pre-processing prior to decomposition is a pre-requisite.

In borehole seismics the particle velocity detectors are situated below the surface. The embedded layers are well consolidated and the coupling of the detectors to the borehole is well solved nowadays. These advantages make convolutional wavefield decomposition at the receiver side very effective for VSP surveys.

SAMENVATTING

Voor de bepaling van de geologische *struktuur* van de ondergrond kan in het algemeen volstaan worden met seismische gegevens welke zijn verkregen met éénkomponents-bronnen en –ontvangers. Wanneer het bovendien van belang is om de materiaaltypen van de verschillende lagen te bepalen, dan zullen hun elastische (en bij voorkeur ook hun lithologische) eigenschappen bepaald moeten worden. Dit kan gerealiseerd worden door de lagen in de ondergrond met verschillende typen golven te belichten en door de respons van de ondergrond voor ieder golftype te analyseren (de DELPHI methode).

Om de totale seismische respons van de ondergrond te analyseren zullen de gereflekteerde golfvelden met *multikomponenten*-ontvangers geregistreerd moeten worden. Om de respons voor ieder golftype te bepalen zullen bovendien multikomponenten-bronnen gebruikt moeten worden.

De afbeelding van de ondergrond wordt verkregen door de geregistreerde data een aantal processen te laten ondergaan. Wij stellen voor om data-decompositie toe te passen *voorafgaand* aan de afbeeldingsgerichte processen. Deze data-decompositie scheidt de P- en de S-golven aan het oppervlak.

In dit proefschrift presenteren we een algemeen formalisme voor de decompositie per golftype zowel aan de bronzijde als aan de ontvangerzijde (zowel voor oppervlakte- als voor boorput-seismiek). Voor de *decompositie aan de ontvangerzijde* hebben we een relatie geformuleerd tussen de door de ontvangers geregistreerde grootheid (deeltjessnelheid) enerzijds en de amplituden van de drie invallende golftypen anderzijds (zie Hoofdstuk 2). Voor de decompositie aan de bronzijde hebben we de relatie geformuleerd tussen de brongrootheid enerzijds (traktie) en de amplituden van de drie uitgezonden golftypen anderzijds (zie Hoofdstuk 2). Uitgaande van deze relaties is het mogelijk om de uitdrukking te bepalen van de decompositie-operator aan de ontvangerzijde: deze stelt ons in staat om de drie golftypen te scheiden welke bij de ontvangers arriveren. Evenzo zijn we in staat om de uitdrukking te bepalen van de decomposite-operator aan de bronzijde: deze stelt ons in staat om de respons van de ondergrond te scheiden

naar de drie door de bronnen uitgezonden golftypen (zie Hoofdstuk 3). Op grond van stabiliteit en uniekheid geven we de voorkeur aan een *multikanaals*-proces boven een éénkanaals-proces. Dit leidt tot een spatieel convolutieproces langs de bronnen en langs de ontvangers. De decompositie-operatoren zijn afhankelijk van de elastische eigenschappen van het medium ter plaatse van de bronnen en ontvangers. Aangezien deze parameters in het algemeen nog niet bekend zijn tijdens de data-acquisitie, is het essentieel om de decompositie numeriek te verrichten (data-adaptief) in het dataverwerkingscentrum. Golfvelddecompositie moet dus *niet* in het veld verricht worden.

Door gebruik te maken van een matrixnotatie vertonen de bij de decompositie betrokken operaties grote overeenkomst met de operaties welke bij één extrapolatiestap in dieptemigratie voor stack toegepast worden. Hierbij spelen de decompositie-operatoren aan de bron- en ontvangerzijde dezelfde rol bij de decompositie als de extrapolatie-operatoren aan de bron- en ontvangerzijde bij migratie (zie Hoofdstuk 3). Evenals migratie voor stack kan het decompositieproces in het golfgetal-frequentiedomein worden uitgevoerd wanneer het medium geen variaties vertoont aan de bronzijde en aan de ontvangerzijde. Voor inhomogene media echter moet het decompositieproces in het plaats-frequentiedomein worden uitgevoerd. In tegenstelling tot migratie, is bij decompositie geen model van de gehele ondergrond vereist, doch slechts een model van het elastische medium ter plaatse van de bronnen en de ontvangers. Het is belangrijk op te merken dat indien men niet geïnteresseerd is om het voorgestelde decompositieproces uit te voeren ter plaatse van de bronnen en ontvangers, al de in dit werk gepresenteerde gereedschappen ook gebruikt kunnen worden om het elastische golfveld te decomponeren op andere plaatsen in de ondergrond, *na* golfveldextrapolatie. In het DELPHI project is echter aangetoond dat decompositie bij voorkeur vóór het extrapolatieproces dient te worden uitgevoerd. Wanneer de oppervlaktelaag een lage golfpropagatiesnelheid heeft, wordt automatisch een golfvelddecompositie verkregen aan de bronzijde en aan de ontvangerzijde. Daarom zal bij oppervlakteseismiek het decompositieproces het meest effektief zijn wanneer de oppervlaktelaag een hoge golfpropagatiesnelheid bezit. In het algemeen is de oppervlaktelaag ongeconsolideerd, hetgeen leidt tot een lage kwaliteit van de data, nog versterkt door problemen t.g.v. de veranderingen van de koppeling van opeenvolgende bronnen en/of ontvangers, problemen met statische variaties en absorptie. Onder zulke omstandigheden zijn voorbewerkingen van de data noodzakelijk alvorens tot decompositie wordt overgegaan.

Bij boorputseismiek zijn de deeltjessnelheiddetectoren onder het oppervlak gesitueerd. De omliggende lagen zijn goed geconsolideerd en het probleem van de koppeling van de detectoren met de boorputwand is opgelost. Deze voordelen maken golfvelddecompositie d.m.v. deconvolutie langs de ontvangers in een boorput zeer effectief.

CURRICULUM VITAE

Name	: Herrmann, Philippe, Charles
Born	: January 14, 1964
Nationality	: French

EDUCATION

1979 - 1981	: Lycée Camille Sée (Colmar)
1982-1983	: DEUG A (Mulhouse)
1984	: Strasbourg University
1985-1987	: Ecole et Observatoire de Physique du Globe de Strasbourg
1988	: Military service
1989 - 1991	: Delft University of Technology

EMPLOYEMENT

1992	: Geophysicist at CGG